NATIONAL TECHNICAL UNIVERSITY OF ATHENS

SCHOOL OF CIVIL ENGINEERING

DEPARTMENT OF STRUCTURAL ENGINEERING

INSTITUTE OF STRUCTURAL ANALYSIS & ANTISEISMIC RESEARCH

Limit Load and Deformation Analysis for Frame Structures with Mathematical Programming

DOCTORAL DISSERTATION

for the title of Doctor of Philosophy in Engineering submitted in the School of Civil Engineering, National Technical University of Athens

Marina-Myrto S. Manola

Diploma in Civil Engineering N.T.U.A.

Master of Science in Civil Engineering N.T.U.A.

ATHENS 2015

European Union
European Social Fund

OPERATIONAL PROGRAMME
EDUCATION AND LIFELONG LEARNING
investing in knowledge society
MINISTRY OF EDUCATION & RELIGIOUS AFFAIRS
MANAGING AUTHORITY

NSRF 2007-2013
programme for development
EUROPEAN SOCIAL FUND

Co-financed by Greece and the European Union

ΕΘΝΙΚΟ ΜΕΤΣΟΒΙΟ ΠΟΛΥΤΕΧΝΕΙΟ

ΣΧΟΛΗ ΠΟΛΙΤΙΚΩΝ ΜΗΧΑΝΙΚΩΝ

ΤΟΜΕΑΣ ΔΟΜΟΣΤΑΤΙΚΗΣ

ΕΡΓΑΣΤΗΡΙΟ ΣΤΑΤΙΚΗΣ ΚΑΙ ΑΝΤΙΣΕΙΣΜΙΚΩΝ ΕΡΕΥΝΩΝ

Οριακή και Παραμορφωσιακή Ανάλυση Πλαισιωτών Κατασκευών με Χρήση Μεθόδων Μαθηματικού Προγραμματισμού

ΔΙΔΑΚΤΟΡΙΚΗ ΔΙΑΤΡΙΒΗ

για τον Επιστημονικό Τίτλο της Διδάκτορος Μηχανικού υποβληθείσα στη Σχολή Πολιτικών Μηχανικών του Εθνικού Μετσόβιου Πολυτεχνείου

Μαρίνα-Μυρτώ Σ. Μανωλά

Διπλωματούχος Πολιτικός Μηχανικός Ε.Μ.Π.

Μεταπτυχιακό Δίπλωμα Ειδίκευσης Ε.Μ.Π.

ΑΘΗΝΑ 2015

Ευρωπαϊκή Ένωση
Ευρωπαϊκό Κοινωνικό Ταμείο

ΕΠΙΧΕΙΡΗΣΙΑΚΟ ΠΡΟΓΡΑΜΜΑ
ΕΚΠΑΙΔΕΥΣΗ ΚΑΙ ΔΙΑ ΒΙΟΥ ΜΑΘΗΣΗ
επένδυση στην κοινωνία της γνώσης
ΥΠΟΥΡΓΕΙΟ ΠΑΙΔΕΙΑΣ ΚΑΙ ΘΡΗΣΚΕΥΜΑΤΩΝ
ΕΙΔΙΚΗ ΥΠΗΡΕΣΙΑ ΔΙΑΧΕΙΡΙΣΗΣ

ΕΣΠΑ 2007-2013
πρόγραμμα για την ανάπτυξη
ΕΥΡΩΠΑΪΚΟ ΚΟΙΝΩΝΙΚΟ ΤΑΜΕΙΟ

Με τη συγχρηματοδότηση της Ελλάδας και της Ευρωπαϊκής Ένωσης

NATIONAL TECHNICAL UNIVERSITY OF ATHENS
SCHOOL OF CIVIL ENGINEERING
DEPARTMENT OF STRUCTURAL ENGINEERING
INSTITUTE OF STRUCTURAL ANALYSIS & ANTISEISMIC RESEARCH

Limit Load and Deformation Analysis for Frame Structures with Mathematical Programming

DOCTORAL DISSERTATION

Marina-Myrto S. Manola

Supervisor **:** Vlasis K. Koumousis
Professor N.T.U.A.

Examined and approved by the committee:

.....	.....	.....
Vlasis Koumousis	Evangelos Sapountzakis	Panagiotis Tsopelas
Professor N.T.U.A.	Professor N.T.U.A.	Associate Professor N.T.U.A.

.....	.....	.....	.....
Manolis Papadrakakis	Christos Bisbos	Ioannis Vayas	Nikolaos Lagaros
Professor N.T.U.A.	Professor A.U.Th.	Professor N.T.U.A.	Assistant Professor N.T.U.A.

ATHENS 2015

……

Marina-Myrto S. Manola

Civil Engineer N.T.U.A., M.Sc.

This research has been co-financed by the European Union (European Social Fund – ESF) and Greek national funds through the Operational Program "Education and Lifelong Learning" of the National Strategic Reference Framework (NSRF) - Research Funding Program: Heracleitus II. Investing in knowledge society through the European Social Fund.

To my parents

ABSTRACT

This thesis concerns the determination of the ultimate structural state using mathematical programming techniques. Its main objective is to highlight the inner structure and drawbacks of the existing methods and to propose new approaches that improve and enhance their performance. The ultimate load and state of a structure is determined by solving an optimization problem that is based on the piecewise linearization of yield condition and constitutive laws. For rigid-perfectly plastic behavior, limit analysis is formulated as a Linear Programming (LP) problem expressing both the static and kinematic theorem. Incorporation of deformation constraints and/or softening behavior leads to the formulation of an optimization problem that aims at the maximization of the load factor subjected to equilibrium, compatibility, yield and complementarity constraints. Due to the disjunctive nature of the latter, the problem becomes nonsmooth, nonconvex and numerical unstable. Thus, a penalty function formulation is used to reformulate it to a nonlinear programming (NLP) problem, the size of which is strictly related to the discretization of the yield surface and the constitutive laws. In this work, the main research objectives revolve around the expression of yield condition and the incorporation of hardening/softening behavior in a more efficient way. Therefore, yield condition is expressed following three different schemes: i) a convex hull formulation, ii) a cone identification approach and iii) a local linearization technique. According to the convex hull formulation, yield condition is given in the form of a linear combination of the vectors corresponding to all vertices that define the a priori linearized yield hypersurface. The cone identification approach is based on the fact that for every cross section and at each optimization iteration only one yield constraint is potentially or truly activated and thus only one yield constraint is required. Extending this concept for the local linearization technique, the critical hyperplane for each cross section is not a priori defined, but it is determined at each optimization iteration for every stress point by locally linearizing the yield surface. In addition, multi-linear and nonlinear hardening/softening structural behavior is embedded efficiently without affecting the size of the problem. The herein proposed approaches uncouple the size of the problem from the linearization of the yield surface and constitutive laws, reducing accordingly the size of the complementarity condition that is the source of numerical difficulties for the solution of the problem. Numerical results of plane and 3D steel frames prove the computational advantages of the proposed formulations for multi-component interaction and multi-linear or nonlinear structural behavior. The main conclusions of this dissertation may constitute the central points of future research concerning limit analysis not only in the field of structural engineering, but also in fracture and soil mechanics applications.

Key Words: limit analysis, mathematical programming, complementarity conditions, stress resultant interaction, holonomic behavior

Acknowledgements

This dissertation is the capping stone of a five-year effort that wouldn't have been completed without several people's contribution. First of all, I would like to express my sincere gratitude to Vlasis Koumousis, the supervisor, the professor, the scientist, the instructor and, most of all, the person, for his insightful comments and guidance and his constant support and encouragement all along. Without his persistent help, none of these would have been possible. I would also like to thank Professor Evangelos Sapountzakis and Associate Professor Panagiotis Tsopelas for serving on my doctoral advisory committee and for their illuminating comments. My sincere gratitude also goes to Professor Manolis Papadrakakis, Professor Christos Bisbos, Professor Ioannis Vayas and Assistant Professor Nikolaos Lagaros for serving on my doctoral examination committee and for their constructive comments which enriched this dissertation. Special thanks to Dr. Manolis Chatzis, Associate Professor in Engineering Science at the University of Oxford, for being the "abettor" of this scientific matchmaking and for his insightful comments and suggestions. My gratitude also goes to Argyris Moysidis, ph.d. candidate at N.T.U.A., for his illuminating views and constructive advice. Moreover, I would like to thank my brother, Iakovos, for being always so near no matter how far. I also owe a very important debt to my officemates Savvas Triantafyllou, Ilias Gkimousis, Lefteris Asiminas, Michalis Roussis, Christos Sofianos, Ioannis Dikaros, Andreas Kampitsis, Vasilis Tsipiras, Ioannis Tsiptsis and Amalia Argyridi for sharing our worries and our thoughts and for making the working environment so pleasant, warm and friendly. Special thanks to Christos Dimou and Aristotelis Charalampakis for their constructive criticism and friendly advice. Furthermore, I am particularly grateful to my dearest friends Angeliki, Fivos, Vasilis, Katerina, Chris and Tsip for their support and encouragement and for reminding me that life consists of so many other things. I would also like to thank my friends Dimos, Christos, Mary, Dionisia, Lena, Stevi, Christos, Nikos, Stavros, Michalis and Panagiotis for making the trip so much easier and delightful. Last but not least, I would like to express my gratitude to my parents for their love, patience and constant support throughout my life.

Marina-Myrto Manola

Οριακή και Παραμορφωσιακή Ανάλυση Πλαισιωτών Κατασκευών με Μαθηματικό Προγραμματισμό

Πίνακας Περιεχομένων Εκτενούς Περίληψης

I. Εισαγωγή

Η ανάλυση των κατασκευών κατέχει κεντρικό ρόλο στο πεδίο επιστήμης του μηχανικού, καθώς αποτελεί ένα δυνατό εργαλείο για έναν ασφαλή και οικονομικό σχεδιασμό. Πληθώρα μεθόδων έχουν προταθεί, οι περισσότερες εκ των οποίων παρακολουθούν ολόκληρη την ανελαστική συμπεριφορά της κατασκευής μέχρι την κατάρρευση. Ωστόσο, η οριακή κατάσταση και το φορτίο που αντιστοιχεί σε αυτήν, τα οποία είναι πρωταρχικού ενδιαφέροντος, μπορούν να προσδιοριστούν απευθείας μέσω μεθόδων οριακής ανάλυσης.

Η οριακή ανάλυση, η οποία βασίζεται στην παραδοχή της τελείως πλαστικής συμπεριφοράς, έχει αποτελέσει τον ακρογωνιαίο λίθο της ελαστοπλαστικής ανάλυσης. Η θεωρία του μαθηματικού προγραμματισμού, από την άλλη πλευρά, βασίζεται στον άμεσο προσδιορισμό μιας βέλτιστης λύσης ικανοποιώντας κάποιους μαθηματικούς περιορισμούς. Ο συνδυασμός της οριακής ανάλυσης με τον μαθηματικό προγραμματισμό οδήγησε στον προσδιορισμό της τελικής κατάστασης μιας κατασκευής ακολουθώντας ένα μαθηματικό δρόμο. Στην κατεύθυνση αυτήν,

έχει προταθεί πλήθος μεθόδων μαθηματικού προγραμματισμού για την ανάλυση των κατασκευών, οι οποίες σχετίζονται με τους νόμους υλικού (παρουσία ή μη χαλάρωσης (softening)), με τη συμπεριφορά της κατασκευής (ολονομική ή μη ολονομική), τον τρόπο προσέγγισης της επιφάνειας διαρροής και την επιλογή της αντικειμενικής συνάρτησης.

Η οριακή ανάλυση για γραμμικοποιημένα κριτήρια διαρροής και τελείως πλαστική συμπεριφορά μπορεί να διατυπωθεί ως ένα πρόβλημα γραμμικού προγραμματισμού εκφράζοντας το στατικό και κινηματικό θεώρημα. Η άνθιση του γραμμικού προγραμματισμού (Kantorovich 1940, Dantzig 1947) έδωσε ώθηση στη χρήση τεχνικών μαθηματικού προγραμματισμού για την ανάλυση των κατασκευών. Οι Charnes και Greenberg (1951) ήταν οι πρώτοι που εφάρμοσαν το γραμμικό προγραμματισμό για την ανάλυση ράβδων κι έκτοτε έχει σημειωθεί σημαντική πρόοδος σε αυτό το πεδίο. Ο Maier και η ερευνητική του ομάδα (1967,1977, 2002,2003) επέκτειναν τη θεώρηση αυτή συμπεριλαμβάνοντας κράτυνση/χαλάρωση για ολονομική και μη-ολονομική συμπεριφορά. Το κεντρικό σημείο της διατύπωσης αυτών των προβλημάτων έγκειται στη γραμμικοποίηση των κριτηρίων διαρροής και των νόμων του υλικού, η οποία επιτρέπει τη γραμμική έκφρασή τους. Η ενσωμάτωση περιορισμών παραμορφώσεων ή/και η θεώρηση χαλάρωσης (softening) απαιτούν την παρουσία ενός περιορισμού συμπληρωματικότητας, ο οποίος αποκλείει την ταυτόχρονη ενεργοποίηση της πλαστικοποίησης με περιθώρια αντοχής. Η φύση του περιορισμού αυτού είναι διακριτή και αποτελεί την κύρια πηγή αριθμητικής αστάθειας του προβλήματος. Για αυτόν τον λόγο, πληθώρα τεχνικών μαθηματικού προγραμματισμού έχουν προταθεί, όπως iterative Linear Programming, Quadratic και Parametric Quadratic Programming, Restricted Basis Linear Programming, Linear και Parametric Linear Complementarity προσεγγίσεις, Mathematical Programming with Equilibrium Constraints (MPEC) (Maier et al. 1977,1979, Tangaramvong and Tin-Loi 2007). Επίσης, έχουν προταθεί διάφορες μέθοδοι που "χειρίζονται" κατάλληλα τη συνθήκη συμπληρωματικότητας μετατρέποντας το πρόβλημα σε ένα μη γραμμικού προγραμματισμού (Fukushima and Lin 2004).

Η πλειονότητα των προσεγγίσεων που αναφέρθηκαν βασίζεται στην εκ των προτέρων γραμμικοποίηση των κριτηρίων διαρροής και νόμων υλικού συνδέοντας το μέγεθος του προβλήματος με τη διακριτοποίηση. Η συνθήκη διαρροής διατυπώνεται υπολογίζοντας τα περιθώρια αντοχής για κάθε κρίσιμη διατομή και για όλα τα πιθανά υπερεπίπεδα της διακριτοποιημένης επιφάνειας διαρροής. Αυτό ορίζει ένα

μονοδιάστατο διάνυσμα περιθωρίων αντοχής για κάθε κρίσιμη διατομή με μέγεθος, που εξαρτάται από τον αριθμό των υπερεπιπέδων της υπερεπιφάνειας διαρροής. Επίσης, ο ίδιος αριθμός πλαστικών πολλαπλασιαστών απαιτείται για την έκφραση όλων των δυνατών πλαστικών παραμορφώσεων, αυξάνοντας το μέγεθος της συνθήκης συμπληρωματικότητας. Αυτή η διαδικασία γεννά περιττή πληροφορία αυξάνοντας με απαγορευτικό τρόπο το μέγεθος του προβλήματος, ειδικά για περιπτώσεις προβλημάτων μεγάλης κλίμακας και/ή πυκνής διακριτοποίησης της υπερεπιφάνειας διαρροής.

Σκοπός της παρούσης διατριβής είναι 1) η μείωση του μεγέθους του προβλήματος αποσυνδέοντας το από τη διακριτοποίηση της επιφάνειας διαρροής και των καταστατικών νόμων υλικού, 2) η μείωση του μεγέθους της συνθήκης συμπληρωματικότητας, η οποία είναι η πηγή αριθμητικής αστάθειας του προβλήματος, 3) η αποτελεσματική ενσωμάτωση πολυγραμμικών ή μη-γραμμικών καταστατικών νόμων υλικού, χωρίς να επηρεάζεται το μέγεθος του προβλήματος και 4) η εφαρμογή των προτεινόμενων προσεγγίσεων σε επίπεδα και τρισδιάστατα πλαίσια και ο έλεγχος της υπολογιστικής αποτελεσματικότητάς τους συγκρινόμενης με την εκείνη της υπάρχουσας μεθοδολογίας. Τα προβλήματα που αναπτύσσονται στην παρούσα εργασία αφορούν ολονομική συμπεριφορά και ανάλογα με τη θεώρηση των καταστατικών νόμων υλικού και την προσέγγιση της επιφάνειας διαρροής, διακρίνονται οι ακόλουθες περιπτώσεις: i) Τελείως πλαστική συμπεριφορά και γραμμικοποιημένη επιφάνεια διαρροής, ii) Γραμμικοποιημένη συμπεριφορά κράτυνσης/χαλάρωσης και γραμμικοποιημένη επιφάνεια διαρροής, iii) Γραμμικοποιημένη συμπεριφορά κράτυνσης/χαλάρωσης και μη γραμμική επιφάνεια διαρροής και iv) Μη γραμμική συμπεριφορά κράτυνσης/χαλάρωσης και μη γραμμική επιφάνεια διαρροής.

II. Οριακή ανάλυση επίπεδων πλαισίων με Γραμμικό Προγραμματισμό

Η οριακή ανάλυση υπό τη θεώρηση τελείως πλαστικής συμπεριφοράς μπορεί να μορφωθεί ως ένα πρόβλημα γραμμικού προγραμματισμού αξιοποιώντας το στατικό και κινηματικό θεώρημα. Τα επίπεδα πλαίσια θεωρούνται ότι αποτελούνται από πρισματικά μέλη, που υπόκεινται μόνο σε επικόμβιες φορτίσεις για λόγους απλότητας. Η πλαστική συμπεριφορά θεωρείται ότι εμφανίζεται σε προεπιλεγμένες θέσεις, οι οποίες αποτελούν τα άκρα κάθε μέλους. Η ισορροπία αφορά στην

απαραμόρφωτη κατάσταση και τα κριτήρια διαρροής είναι a priori γραμμικοποιημένα. Υιοθετείται η μητρωική διατύπωση, τα μητρώα συμβολίζονται με κεφαλαία και έντονα γράμματα, ενώ τα διανύσματα με μικρά και έντονα γράμματα. Κάθε πλαίσιο αποτελείται από n_{el} μέλη, έχει n_f βαθμούς ελευθερίας, ενώ d είναι ο αριθμός των εντατικών μεγεθών που αλληλεπιδρούν, h είναι ο αριθμός των γραμμών/επιπέδων διαρροής και n_v είναι ο αριθμός των κορυφών της γραμμικοποιημένης επιφάνειας διαρροής.

Η οριακή ανάλυση, βασιζόμενη στο στατικό θεώρημα, περιλαμβάνει περιορισμούς ισορροπίας και διαρροής. Η συνθήκη διαρροής μπορεί να εκφραστεί με δυο τρόπους: i) ως ένα σύνολο γραμμικών ανισοτήτων, οι οποίες εκφράζουν γεωμετρικά την τομή ενός πεπερασμένου αριθμού ημιχώρων και επιπέδων και ii) ως ένα κυρτό πολύεδρο (convex hull) ενός σταθερού αριθμού κορυφών. Το κυρτό πολύεδρο (convex hull) ενός συνόλου σημείων C είναι ο χώρος που περικλείεται από το πολύεδρο που περιλαμβάνει όλα τα σημεία. Η μαθηματική έκφραση του κυρτού πολύεδρου (convex hull or convex envelope) ενός συνόλου σημείων C είναι το μικρότερο κυρτό σύνολο, το οποίο περιλαμβάνει το C και εκφράζεται ως (Boyd and Vandenberghe 2009) :

$$\textbf{\textit{conv}}\, C = \left\{\theta_1 x_1 + \ldots + \theta_n x_n \mid x_i \in C, \quad \theta_i \geq 0,\ i = 1 \ldots n, \quad \theta_1 + \ldots + \theta_n = 1\right\} \quad (1)$$

όπου θ_i είναι μη αρνητικοί συντελεστές και $x_1, \ldots, x_n$ είναι τα σημεία-κορυφές.

Κάθε διάνυσμα εντατικής κατάστασης $\boldsymbol{s}_d$ εκφράζεται ως ο γραμμικός συνδυασμός όλων των διανυσμάτων, που αντιστοιχούν στις κορυφές του πολύεδρου διαρροής, με την προϋπόθεση το άθροισμα των μη αρνητικών παραμέτρων $\theta_i,\ i = 1 \ldots n_v$ να ισούται με 1. Για την περίπτωση δισδιάστατης αλληλεπίδρασης, διακρίνονται οι περιπτώσεις που φαίνονται στο Σχ.1 b,c,d. Αν το σημείο εντατικής κατάστασης βρίσκεται στην ελαστική περιοχή, τότε ενεργοποιούνται όλα τα θ_i (Σχ. 1b). Στην περίπτωση που η διατομή έχει διαρρεύσει, το αντίστοιχο διάνυσμα εντατικής κατάστασης εκφράζεται ως γραμμικός συνδυασμός των διανυσμάτων των κορυφών του ενεργοποιημένου επιπέδου διαρροής (Σχ. 1c). Για την ειδική περίπτωση, που ένα μόνο θ_i είναι ίσο με τη μονάδα και όλα τα υπόλοιπα παραμένουν μηδενικά, τότε το σημείο εντατικής κατάστασης ταυτίζεται με την αντίστοιχη κορυφή του πολυέδρου διαρροής.

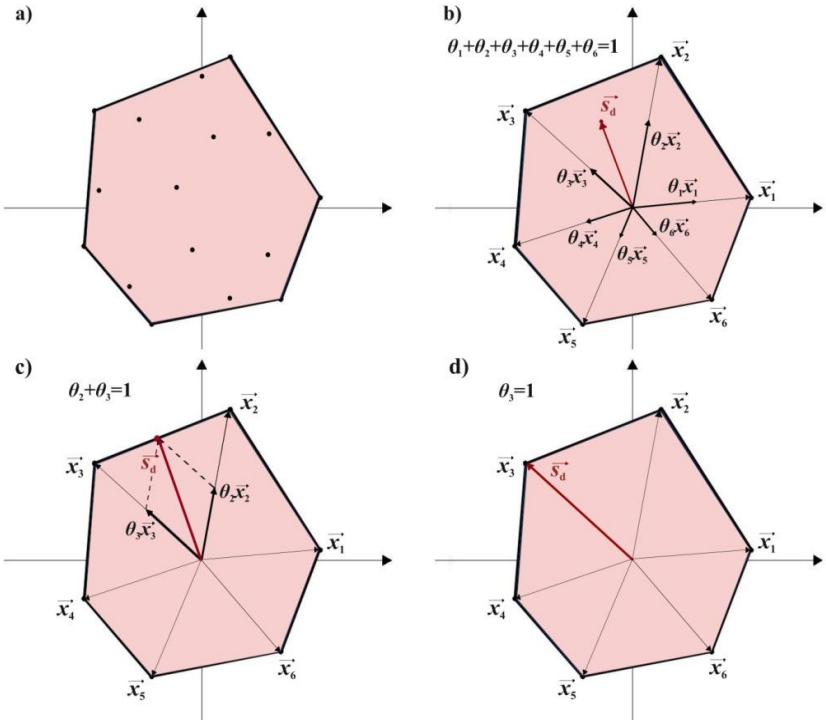

Σχ. 1: Θεώρηση κυρτού πολύεδρου (convex hull) για διάνυσμα εντατικής κατάστασης.

Σκοπός της οριακής ανάλυσης είναι ο προσδιορισμός του οριακού φορτίου μιας κατασκευής. Με βάση τη στατική προσέγγιση, η οποία περιλαμβάνει περιορισμούς ισορροπίας και διαρροής, μορφώνεται το ακόλουθο πρόβλημα γραμμικού προγραμματισμού:

$$\begin{aligned} &\textit{maximize} && \alpha \\ &\textit{subject to} && \boldsymbol{B}\cdot\boldsymbol{s}-a\cdot\boldsymbol{f}=\boldsymbol{f}_d && n_f \textit{ constraints} \\ & && \boldsymbol{N}^T\cdot\boldsymbol{s}\le\boldsymbol{r} && 2h\,n_{el} \textit{ constraints} \\ & && \boldsymbol{s}:\textit{unrestricted}, a\ge 0 \end{aligned} \tag{2}$$

όπου οι μεταβλητές σχεδιασμού είναι τα ανεξάρτητα εντατικά μεγέθη $\boldsymbol{s}$ και ο συντελεστής φόρτισης α. Η πρώτη ισότητα αντιπροσωπεύει την ισορροπία, όπου $\boldsymbol{B}$ είναι το $(n_f \times 3n_{el})$ μητρώο ισορροπίας της κατασκευής, $\boldsymbol{s}$ είναι το $(3n_{el} \times 1)$ διάνυσμα των ανεξάρτητων εντατικών μεγεθών όλων των μελών (θεωρούνται τρία εντατικά μεγέθη ανεξάρτητα σε κάθε μέλος: η αξονική δύναμη και η καμπτική ροπή του κόμβου αρχής και η καμπτική ροπή κόμβου τέλους), a είναι ο συντελεστής φόρτισης, $\boldsymbol{f}$ είναι το $(n_f \times 1)$ διάνυσμα των επικόμβιων φορτίσεων και $\boldsymbol{f}_d$ είναι το $(n_f \times 1)$ διάνυσμα των σταθερών επικόμβιων φορτίσεων. Οι ανισοτικοί περιορισμοί εκφράζουν τη συνθήκη διαρροής, όπου $\boldsymbol{N}$ είναι το $(3n_{el} \times 2hn_{el})$ μητρώο όλων των κάθετων-στα επίπεδα διαρροής-διανυσμάτων και $\boldsymbol{r}$ είναι το $(2hn_{el} \times 1)$ διάνυσμα, το

οποίο περικλείει τα όρια διαρροής, που αντιστοιχούν σε όλα τα επίπεδα διαρροής. Για την περίπτωση αλληλεπίδρασης αξονικής δύναμης-καμπτικής ροπής (NM) ισχύει ότι h=8, ενώ για την περίπτωση αλληλεπίδρασης αξονικής-τέμνουσας δύναμης-καμπτικής ροπής ισχύει ότι $h=32$.

Η διατύπωση του προβλήματος οριακής ανάλυσης χρησιμοποιώντας τη θεώρηση του κυρτού πολυέδρου (convex hull) δίδεται ως εξής:

$$\begin{aligned} &\textit{maximize} && \alpha \\ &\textit{subject to} && \boldsymbol{B}\cdot\boldsymbol{s} - a\cdot\boldsymbol{f} = \boldsymbol{f}_d && n_f \textit{ constraints} \\ & && \boldsymbol{T}\cdot\boldsymbol{s} - \boldsymbol{C}\cdot\boldsymbol{\theta} = \boldsymbol{0} && 2dn_{el} \textit{ constraints} \\ & && \boldsymbol{I}_{eq}\cdot\boldsymbol{\theta} = \boldsymbol{1} && 2n_{el} \textit{ constraints} \\ & && \boldsymbol{s}: \textit{unrestricted}, \boldsymbol{\theta} \geq \boldsymbol{0} \ , a \geq 0 \end{aligned} \tag{3}$$

όπου οι μεταβλητές σχεδιασμού είναι τα ανεξάρτητα εντατικά μεγέθη όλων των μελών $\boldsymbol{s}$, οι μη αρνητικές παράμετροι $\boldsymbol{\theta}$ και ο συντελεστής φόρτισης α. Το πρώτο σετ περιορισμών αντιπροσωπεύει την ισορροπία, το δεύτερο και τρίτο σετ εκφράζουν τη συνθήκη διαρροής χρησιμοποιώντας τη θεώρηση του κυρτού πολυέδρου (convex hull), όπου $\boldsymbol{T}$ είναι το ($2dn_{el}\times 3n_{el}$) μητρώο που περιλαμβάνει τις τιμές διαρροής των εντατικών μεγεθών, $\boldsymbol{C}$ είναι το ($2dn_{el}\times 2n_v n_{el}$) μητρώο που περιλαμβάνει τις συντεταγμένες των κορυφών όλων των επιπέδων διαρροής για όλες τις κρίσιμες διατομές της κατασκευής, $\boldsymbol{\theta}$ είναι το ($2n_v n_{el}\times 1$) διάνυσμα που περιλαμβάνει τους μη αρνητικούς συντελεστές θ_i όλων των διανυσμάτων που αντιστοιχούν στις n_v κορυφές για όλα τα μέλη και $\boldsymbol{I_{eq}}$ είναι το ($2nel\times 2n_v n_{el}$) μητρώο, το οποίο αθροίζει τα αντίστοιχα θ_i για κάθε διατομή. Για την περίπτωση αλληλεπίδρασης αξονικής δύναμης-καμπτικής ροπής (NM) ισχύει ότι $d=2$ και $h=n_v$=8, ενώ για την περίπτωση αλληλεπίδρασης αξονικής-τέμνουσας δύναμης-καμπτικής ροπής ισχύει ότι $d=3$, $h=32$ and $n_v=18$.

Η θεώρηση κυρτού πολυέδρου (convex hull) εκφράζει τη συνθήκη διαρροής με αυστηρούς ισοτικούς περιορισμούς, ο αριθμός των οποίων είναι ανεξάρτητος από τον αριθμό των γραμμών/επιπέδων, που χρησιμοποιούνται για την προσέγγιση της επιφάνειας διαρροής. Ο αριθμός των μεταβλητών, ωστόσο, αυξάνεται συγκρινόμενος με εκείνον της υφιστάμενης θεώρησης, αφού εισάγονται οι παράμετροι θ_i. Αξίζει να σημειωθεί ότι γενικά ένας επιπρόσθετος περιορισμός απαιτεί πολύ περισσότερη υπολογιστή προσπάθεια σε σχέση με μια επιπρόσθετη μεταβλητή. Ωστόσο, αυτό είναι μόνο ενδεικτικό για την υπολογιστική αποτελεσματικότητα της προτεινόμενης θεώρησης κυρτού πολυέδρου (convex hull), αφού ο αριθμός των μεταβλητών που

εισάγονται διαφέρει από τον αριθμό μείωσης των περιορισμών. Για την περίπτωση τρισδιάστατης αλληλεπίδρασης, ο αριθμός των κορυφών n_v είναι σημαντικά μικρότερος σε σχέση με τον αριθμό των επιπέδων h κι ως εκ τούτου η θεώρηση κυρτού πολυέδρου (convex hull) γίνεται υπολογιστικά πλεονεκτικότερη για την έκφραση της συνθήκης διαρροής.

Οι διατυπώσεις των προβλημάτων γραμμικού προγραμματισμού (2) και (3) εφαρμόζονται σε κώδικα Matlab για την ανάλυση μεταλλικών κατασκευών με τελείως πλαστική συμπεριφορά. Ο επιλύτης που επιλέγεται είναι η *linprog*, κατάλληλη για προβλήματα γραμμικού προγραμματισμού. Στόχος είναι η σύγκριση των δύο εκφράσεων του γραμμικοποιημένου κριτηρίου διαρροής και η διερεύνηση της επιρροής της αλληλεπίδρασης των εντατικών μεγεθών στο οριακό φορτίο. Εξετάζονται τρεις περιπτώσεις : Case (a): καθαρή κάμψη, Case (b): αλληλεπίδραση αξονικής δύναμης-καμπτικής ροπής με 1) με ανισοτικούς περιορισμούς και 2) θεώρηση κυρτού πολυέδρου (convex hull) και Case (c): αλληλεπίδραση αξονικής-τέμνουσας δύναμης-καμπτικής ροπής με 1) με ανισοτικούς περιορισμούς και 2) θεώρηση κυρτού πολυέδρου (convex hull). Για την πρώτη περίπτωση η διατύπωση του προβλήματος απλοποιείται, αφού οι περιορισμοί διαρροής εκφράζονται με άνω και κάτω όρια για τιμές των ροπών κάμψης (δεν απαιτείται το μητρώο $\boldsymbol{N}$). όλες οι αναλύσεις διεξήχθησαν σε υπολογιστή με Core Duo Quad CPU και 4GB RAM και τα αποτελέσματα παρουσιάζονται ακολούθως με βάση την κλασική κι όχι τη μητρωική σύμβαση προσήμων.

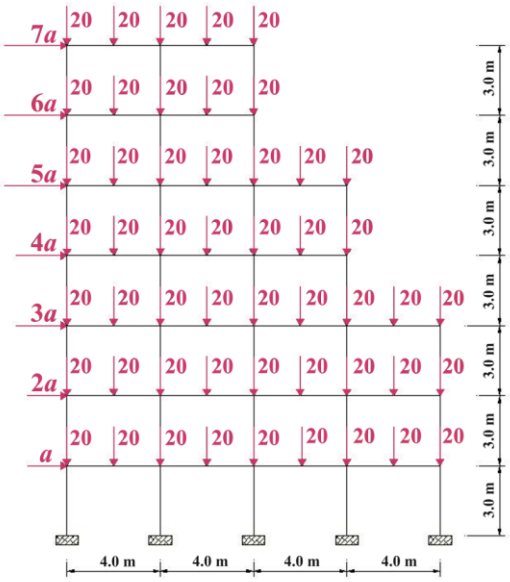

Σχ. 2: Επίπεδο πλαίσιο με πλευρική και κατακόρυφη φόρτιση.

Το παράδειγμα αφορά σε ένα 6-όροφο πλαίσιο 4 ανοιγμάτων, όπως φαίνεται στο Σχ.2. και αποτελείται από 73 μέλη, 56 κόμβους και 153 βαθμούς ελευθερίας. Ο χάλυβας είναι S235 με μέτρο ελαστικότητας $E=2\times10^{8}$ kN/m^2. Οι διατομές των υποστυλωμάτων έχουν τα ακόλουθα χαρακτηριστικά: $A=197.5\times10^{-4}$ m^2, $I=86970\times10^{-8}$ m^4, $s_{1y}=4641.3$ kN, $v_y=1013.24$ kN, $s_{2y}=928.02$ kNm, $s_{3y}=928.02$ kNm, ενώ οι διατομές των δοκών: $A=84.46\times10^{-4}$ m^2, $I=23130\times10^{-8}$ m^4, $s_{1y}=1984$ kN, $v_y=579.22$ kN, $s_{2y}=307.15$ kNm, $s_{3y}=307.15$ kNm.

Πίνακας 1. Αποτελέσματα όλων των αναλύσεων.

Cases	Καθαρή Κάμψη (a)	NM αλληλεπίδραση (b_1)	NM αλληλεπίδραση Convex Hull (b_2)	NQM αλληλεπίδραση (c_1)	NQM αλληλεπίδραση Convex Hull (c_2)
αριθμός μεταβλητών n_{var}	220	220	1388	220	2848
αριθμός ισοτικών περιορισμών n_{eq}	153	153	591	153	737
αριθμός ανισοτικών περιορισμών n_{inq}	—	1168	—	4672	—
φορτικός συντελεστής a (kN)	43.26	40.92	40.92	36.29	36.29
αριθμός πλαστικών αρθρώσεων	49	51	51	52	52
συνολικός υπολογιστικός χρόνος (s)	0.41	0.94	0.91	15.59	1.23
υπολογιστικός χρόνος μόνο για τη βελτιστοποίηση (s)	0.39	0.87	0.83	2.21	0.98

Τα αποτελέσματα παρουσιάζονται στον Πίνακα 1. Διαπιστώνεται ότι η αλληλεπίδραση εντατικών μεγεθών αντιστοιχεί σε μικρότερους φορτικούς συντελεστές σε σχέση με την περίπτωση της καθαρής κάμψης. Τα αποτελέσματα της θεώρησης κυρτού πολυέδρου (convex hull-cases (b_2) and (c_2)) είναι τα ίδια (οι τιμές των μεταβλητών και οι μηχανισμοί κατάρρευσης) με εκείνα των περιπτώσεων (b_1) και (c_1). Ωστόσο, η υφιστάμενη θεώρηση συγκρινόμενη με εκείνη του κυρτού πολυέδρου (convex hull) απαιτεί περισσότερο υπολογιστικό χρόνο, δηλαδή 1.03 φορές για την περίπτωση (b) και 12.67 φορές για την περίπτωση (c). Όσον αφορά στο χρόνο της διαδικασίας βελτιστοποίησης, οι αντίστοιχες τιμές είναι 1.05 και 2.26 φορές. Η αλληλεπίδραση των εντατικών μεγεθών επιδρά, επίσης, στους μηχανισμούς κατάρρευσης (αριθμό και κατανομή πλαστικών αρθρώσεων). Για την περίπτωση καθαρής κάμψης σχηματίζονται λιγότερες πλαστικές αρθρώσεις, οι οποίες εξαντλούν τα περιθώρια αντοχής τους λόγω κάμψης, όπως φαίνεται στο Σχ. 3b. Οι οριακές καταστάσεις του πλαισίου για τις περιπτώσεις (b) και (c) παρουσιάζονται στα Σχ. 4a

και 5a. Ο ρόλος της καμπρικής ροπής είναι κυρίαρχος σε όλες τις περιπτώσεις. Ωστόσο, η επιρροή της αξονικής δύναμης είναι προφανής στις διατομές των υποστυλωμάτων, οι οποίες διαρρέουν υπό συνδυασμένη δράση των εντατικών μεγεθών (Σχ. 4b και 6a), ενώ οι ίδιες διατομές παραμένουν στην ελαστική περιοχή για την περίπτωση της καθαρής κάμψης (Σχ. 3b). Επιπροσθέτως, η επίδραση της τέμνουσας δύναμης για κάποιες διατομές δοκών και υποστυλωμάτων είναι πιο έντονη σε σχέση με εκείνη της αξονικής δύναμης, όπως φαίνεται στο Σχ. 65b.

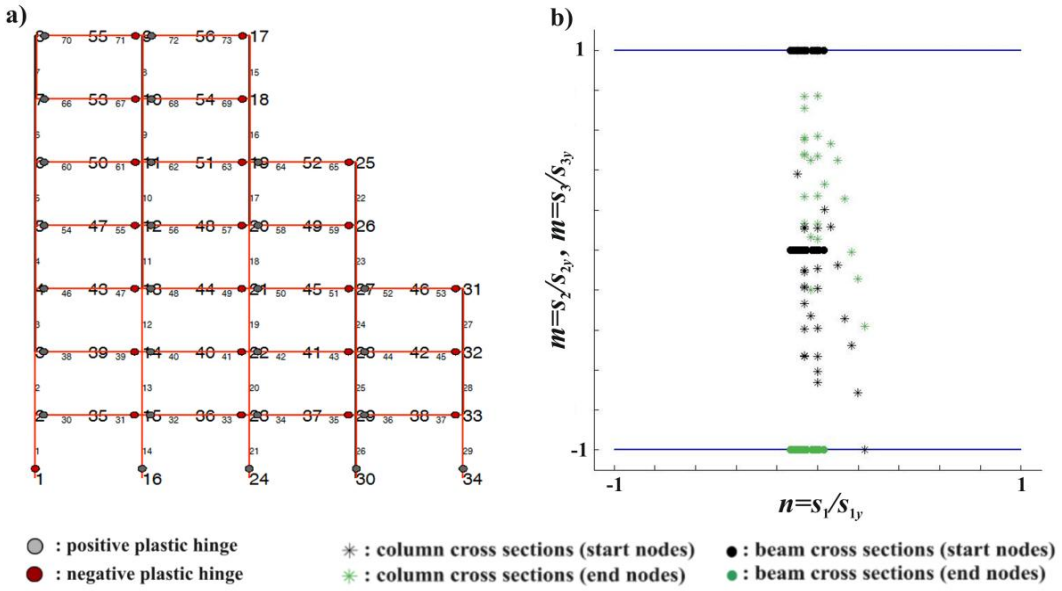

Σχ. 3: a) *Οριακή κατάσταση και b) διάγραμμα αλληλεπίδρασης για καθαρή κάμψη.*

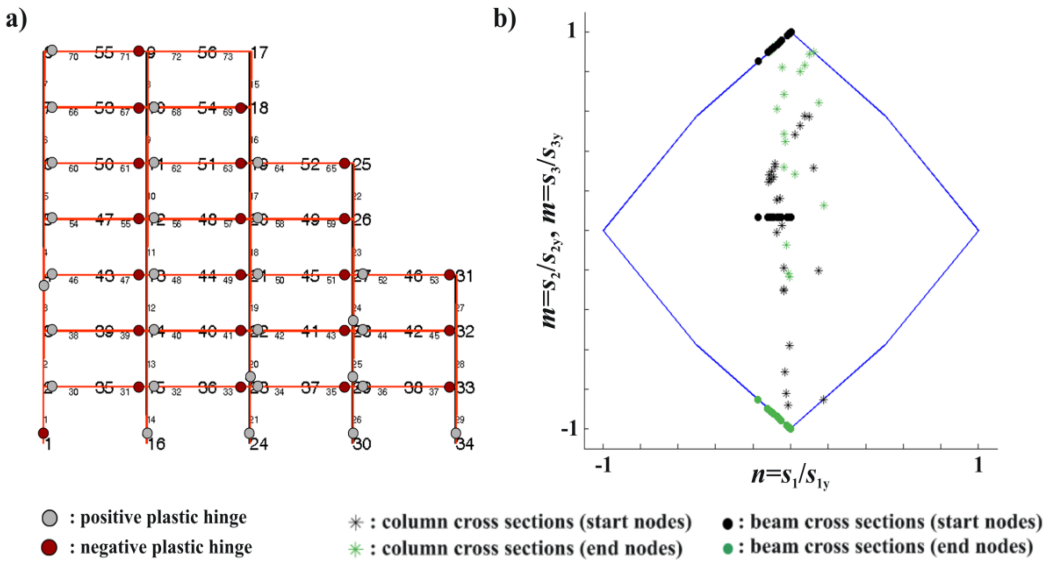

Σχ. 4: a) *Οριακή κατάσταση και b) διάγραμμα αλληλεπίδρασης για ΝΜ αλληλεπίδραση.*

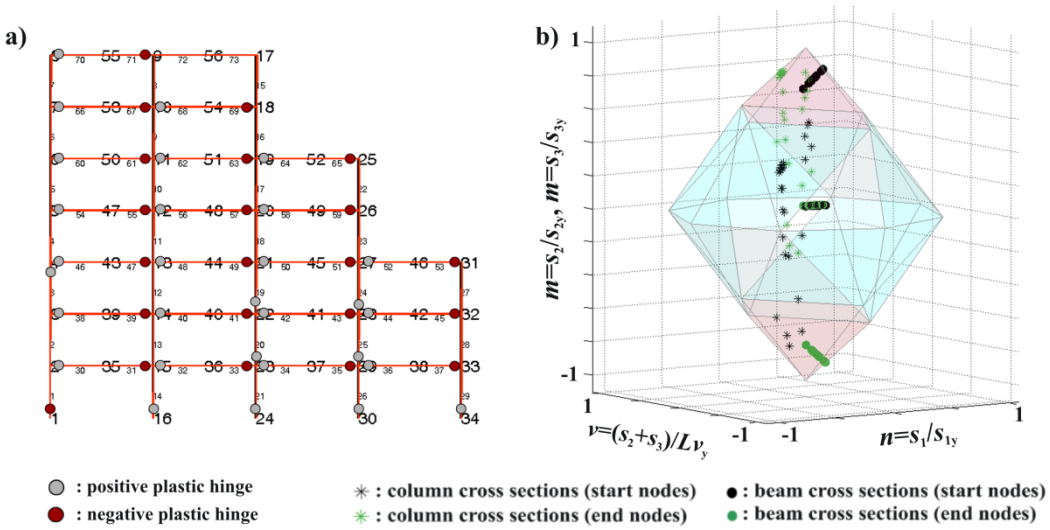

Σχ. 5: a) *Οριακή κατάσταση και b) διάγραμμα αλληλεπίδρασης για NQM αλληλεπίδραση.*

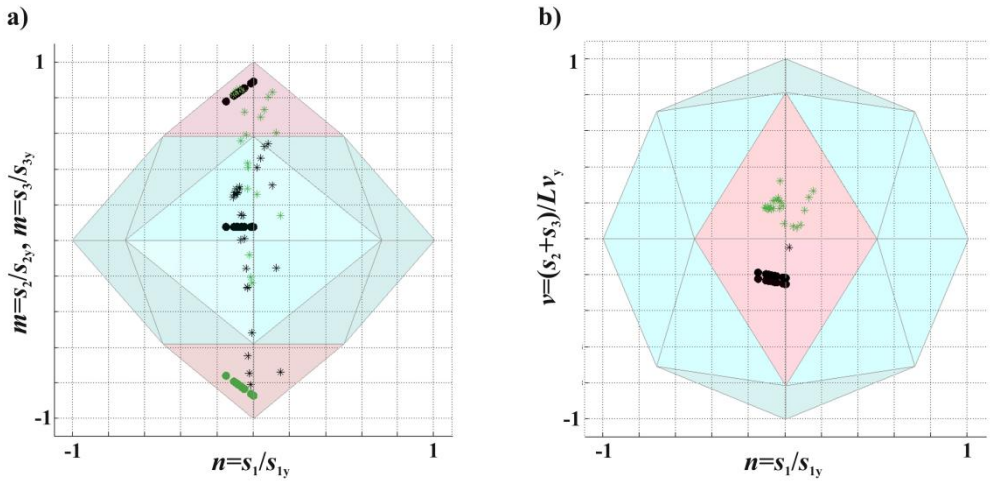

Σχ. 6: Όψεις του διαγράμματος αλληλεπίδρασης NQM.

III. Οριακή και παραμορφωσιακή ανάλυση επίπεδων πλαισίων με μαθηματικό προγραμματισμό

Το πρόβλημα της ελαστοπλαστικής ανάλυσης, υπό ολονομική θεώρηση και για γραμμικοποιημένες επιφάνειες διαρροής, γραμμικοποιημένους νόμους υλικού και ισοτροπική κράτυνση/χαλάρωση, διατυπώνεται στη γενική περίπτωση από τις ακόλουθες σχέσεις:

$$\left.\begin{aligned} \boldsymbol{B}\cdot\boldsymbol{s} &= a\cdot\boldsymbol{f}+\boldsymbol{f}_d && \textit{Equilibrium}\\ \boldsymbol{q} &= \boldsymbol{B}^T\cdot\boldsymbol{u} && \textit{Compatibility}\\ \boldsymbol{q} &= \boldsymbol{e}+\boldsymbol{p}=\boldsymbol{S}^{-1}\cdot\boldsymbol{s}+\boldsymbol{N}\cdot\mathbf{z} && \textit{Strain additivity}\\ \boldsymbol{w} &= -\boldsymbol{N}^T\cdot\boldsymbol{s}+\boldsymbol{r}'\geq\mathbf{0} && \textit{Yielding}\\ \boldsymbol{w}^T\cdot\mathbf{z} &= \mathbf{0},\quad \mathbf{z}\geq\mathbf{0} && \textit{Complementarity} \end{aligned}\right\} \qquad (4)$$

Η πρώτη σχέση αφορά στην ισορροπία του φορέα κι έχει οριστεί στη σχέση (2). Η δεύτερη σχέση αφορά στο συμβιβαστό των παραμορφώσεων και εμπεριέχει το διάνυσμα παραμορφώσεων $\boldsymbol{q}$ και το διάνυσμα επικόμβιων μετακινήσεων $\boldsymbol{u}$. Η τρίτη σχέση εκφράζει τη συνολική παραμόρφωση $\boldsymbol{q}$ ως άθροισμα των ελαστικών $\boldsymbol{e}$ και πλαστικών παραμορφώσεων $\boldsymbol{p}$, όπου $\boldsymbol{S}$ είναι το μητρώο που περιλαμβάνει διαγωνίως τα μητρώα ακαμψίας όλων των μελών, $\boldsymbol{N}$ είναι το μητρώο που περιλαμβάνει τα κάθετα -στις επιφάνειες διαρροής- διανύσματα και $\mathbf{z}$ είναι το διάνυσμα όλων των πλαστικών πολλαπλασιαστών. Η τέταρτη σχέση αφορά στη συνθήκη διαρροής, η οποία εκφράζεται μέσω των περιθωρίων αντοχής κάθε διατομής. Το $\boldsymbol{w}$ είναι το διάνυσμα που περιλαμβάνει τα περιθώρια αντοχής και $\boldsymbol{r}'$ είναι το διάνυσμα που περιλαμβάνει τα μεγεθυμένα/συρρικνωμένα όρια αντοχής, που αντιστοιχούν σε κάθε επίπεδο διαρροής λόγω κράτυνσης/χαλάρωσης αντίστοιχα. Η τελευταία συνθήκη εκφράζει τη συνθήκη συμπληρωματικότητας, η οποία επιβάλλει ότι δεν δύναται να υπάρξει ταυτόχρονη παρουσία πλαστικής παραμόρφωσης ($\mathbf{z}>\mathbf{0}$) με περιθώρια αντοχών ($\boldsymbol{w}>\mathbf{0}$).

Στην οριακή ανάλυση το ενδιαφέρον εστιάζεται στον απευθείας προσδιορισμό της τελικής κατάστασης. Χρησιμοποιώντας τεχνικές μαθηματικού προγραμματισμού και λαμβάνοντας υπόψιν τις σχέσεις που περιγράφουν το ολονομικό πρόβλημα (4), μορφώνεται το ακόλουθο πρόβλημα βελτιστοποίησης:

$$\left.\begin{array}{ll} \text{maximize} & a \\ \text{subject to} & \boldsymbol{B}\cdot\boldsymbol{s}-a\cdot\boldsymbol{f}=\boldsymbol{f}_d \\ & \boldsymbol{S}^{-1}\cdot\boldsymbol{s}-\boldsymbol{B}^T\cdot\boldsymbol{u}+\boldsymbol{N}\cdot\mathbf{z}=\mathbf{0} \\ & \boldsymbol{w}=-\boldsymbol{N}^T\cdot\boldsymbol{s}+\boldsymbol{r}'\geq\mathbf{0} \\ & \boldsymbol{w}^T\cdot\mathbf{z}=\mathbf{0} \\ & \mathbf{0}\leq\mathbf{z}\leq\mathbf{z}_u \\ & \boldsymbol{u}_l\leq\boldsymbol{u}\leq\boldsymbol{u}_u \end{array}\right\} \quad (5)$$

Το παραπάνω πρόβλημα βελτιστοποίησης έχει ως μεταβλητές σχεδιασμού τα εντατικά μεγέθη $\boldsymbol{s}$, τις μετακινήσεις $\boldsymbol{u}$, τους πλαστικούς πολλαπλασιαστές $\mathbf{z}$ και το φορτικό συντελεστή a. Στόχος είναι η μεγιστοποίηση του φορτίου ικανοποιώντας περιορισμούς ισορροπίας, συμβιβαστού των παραμορφώσεων, διαρροής, συμπληρωματικότητας και κάτω και άνω ορίων παραμορφώσεων ($\mathbf{0},\mathbf{z}_u$) και μετακινήσεων ($\boldsymbol{u}_l,\boldsymbol{u}_u$). Η παρουσία της συνθήκης συμπληρωματικότητας μετατρέπει το πρόβλημα σε μη-κυρτό και αριθμητικά ασταθές. Αυτού του είδους τα προβλήματα είναι γνωστά ως προβλήματα Μαθηματικού Προγραμματισμού με Περιορισμούς

Ισορροπίας (Mathematical Programming with Equilibrium Constraints (MPEC) problem) (Luo et al. 1996). Διάφορες μέθοδοι έχουν προταθεί που μετατρέπουν το πρόβλημα αυτό σε πρόβλημα μη γραμμικού προγραμματισμού (Fukushima and Lin 2004). Στην παρούσα εργασία υιοθετείται η μέθοδος "ποινής" (penalty function approach), σύμφωνα με την οποία η συνθήκη συμπληρωματικότητας μεταφέρεται στην αντικειμενική συνάρτηση και πολλαπλασιάζεται με μια παράμετρο. Οι τιμές της παραμέτρου αυξάνονται "πιέζοντας" τη συνθήκη συμπληρωματικότητας σε μηδενικές τιμές. Η διατύπωση αυτού του προβλήματος είναι ως εξής:

$$\left.\begin{array}{ll} \text{maximize} & a-\rho\cdot\boldsymbol{w}^T\cdot\mathbf{z} \\ \text{subject to} & \boldsymbol{B}\cdot\boldsymbol{s}-a\cdot\boldsymbol{f}=\boldsymbol{f}_d \\ & \boldsymbol{S}^{-1}\cdot\boldsymbol{s}-\boldsymbol{B}^T\cdot\boldsymbol{u}+\boldsymbol{N}\cdot\mathbf{z}=\mathbf{0} \\ & \boldsymbol{w}=-\boldsymbol{N}^T\cdot\boldsymbol{s}+\boldsymbol{r}'\geq\mathbf{0} \\ & \mathbf{0}\leq\mathbf{z}\leq\mathbf{z}_u \\ & \boldsymbol{u}_l\leq\boldsymbol{u}\leq\boldsymbol{u}_u \end{array}\right\} \quad (6)$$

Η παραπάνω διατύπωση, όπως προαναφέρθηκε βασίζεται στη γραμμικοποίηση του κριτηρίου διαρροής και στους γραμμικοποιημένους νόμους υλικού κι ως εκ τούτου το μέγεθος των μητρώων εξαρτάται από τη διακριτοποίηση. Για προβλήματα μεγάλης κλίμακας ή/και για πυκνές διακριτοποιήσεις, η εφαρμογή αυτής της διατύπωσης μπορεί να γίνει απαγορευτική. Σκοπός αυτής της εργασίας είναι η μείωση του μεγέθους και της πολυπλοκότητας του προβλήματος. Πιο συγκεκριμένα, η προσέγγιση που προτείνεται αφορά στην απλοποίηση του προβλήματος σε τρία επίπεδα: στην εκτίμηση των περιθωρίων αντοχής, στην αποτελεσματική ενσωμάτωση καταστατικών νόμων και στο μειωμένο μέγεθος της συνθήκης συμπληρωματικότητας. Οι παρεμβάσεις που προτείνονται αφορούν στη συνθήκη διαρροής και βασίζονται στη λογική του ότι κάθε διατομή σε κάθε επανάληψη της διαδικασίας βελτιστοποίησης στοχεύει σε ή ενεργοποιεί ένα μόνο επίπεδο διαρροής. Συνεπώς, μόνον ένας περιορισμός είναι εν δυνάμει ενεργός ή ενεργοποιείται για κάθε διατομή, ενώ οι περιορισμοί που αντιστοιχούν στα υπόλοιπα επίπεδα διαρροής είναι περιττοί. Στην παρούσα εργασία η συνθήκη διαρροής μορφώνεται ακολουθώντας την προαναφερθείσα λογική του ενός "κρίσιμου" επιπέδου για κάθε διατομή με δυο τρόπους: i) θεωρώντας γραμμικοποίηση της επιφάνειας διαρροής a priori και ii) εφαρμόζοντας τη γραμμικοποίηση τοπικά (η μη γραμμικότητα της επιφάνειας διαρροής διατηρείται).

i) ***Γραμμικοποίηση της επιφάνειας διαρροής a priori***

Στην περίπτωση που η επιφάνεια διαρροής έχει γραμμικοποιηθεί εκ των προτέρων, προτείνεται μια διαδικασία αναγνώρισης του "κρίσιμου κώνου" (cone identification), μέσα στον οποίο βρίσκεται κάθε σημείο εντατικής κατάστασης. Στο Σχ. 7 απεικονίζεται η διαδικασία για την περίπτωση δισδιάστατης αλληλεπίδρασης. Ενώνοντας τις κορυφές του πολυγώνου διαρροής με την αρχή των αξόνων, δημιουργείται ένας αριθμός τομέων-κώνων, που καλύπτουν όλο το διάγραμμα αλληλεπίδρασης. Κάθε διάνυσμα έντασης, που αντιστοιχεί σε κάθε διατομή, σχετίζεται με ένα μόνον κώνο. Η διαδικασία αναγνώρισης του "κρίσιμου κώνου" είναι απλή και βασίζεται σε μια λογική ταξινόμησης. Καταρχάς, οι κορυφές του πολυγώνου διαρροής και το διάνυσμα έντασης εκφράζονται σε πολικές συντεταγμένες. Οι αντιωρολογιακές γωνίες θ_i που αντιστοιχούν σε όλες τις κορυφές ταξινομούνται σε αύξουσα σειρά και κατόπιν, εντοπίζεται ο κώνος i μέσα στον οποίο βρίσκεται η γωνία θ_s του διανύσματος έντασης από τη σχέση: $\theta_i < \theta_s \le \theta_{i+1}$ με $\theta_{last} = \theta_1 + 2\pi$. Αυτή η απλή διαδικασία εφαρμόζεται σε κάθε επανάληψη της διαδικασίας βελτιστοποίησης για τον προσδιορισμό των κρίσιμων κώνων και των αντίστοιχων γραμμών διαρροής όλων των διατομών. Έχοντας την πληροφορία της κρίσιμης γραμμής διαρροής για κάθε διατομή, μορφώνεται ένας και μόνον ένας περιορισμός για τη διατομή αυτή.

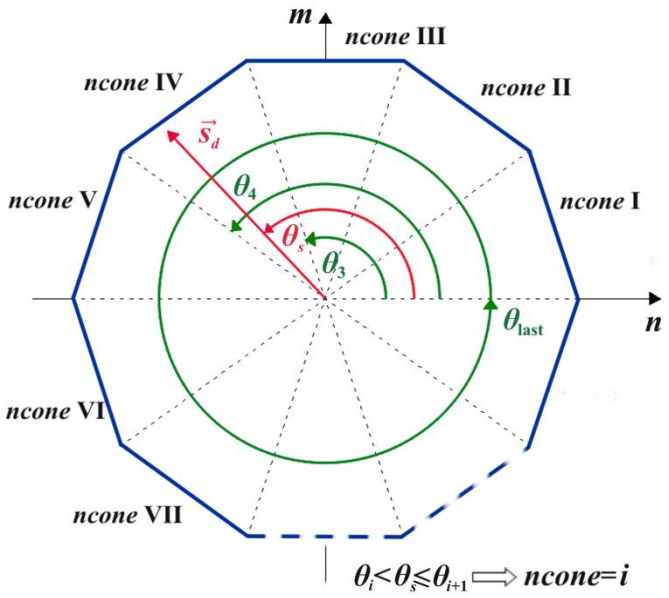

Σχ. 7: Εντοπισμός κρίσιμου κώνου για δισδιάστατη αλληλεπίδραση.

Για την περίπτωση της τρισδιάστατης αλληλεπίδρασης, η επιφάνεια διαρροής προσεγγίζεται με επίπεδα τρίγωνα, οι κορυφές των οποίων (V_1, V_2, V_3) μαζί με την αρχή των αξόνων (V_4) σχηματίζουν έναν κώνο-τετράεδρο (Σχ. 8).

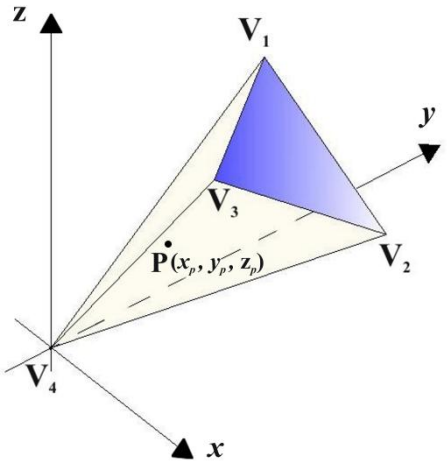

Σχ. 8: Εντοπισμός κρίσιμου κώνου για τρισδιάστατη αλληλεπίδραση.

Κάθε σημείο εντατικής κατάστασης ανήκει σε έναν μόνο κώνο-τετράεδρο και στοχεύει ή ενεργοποιεί το αντίστοιχο επίπεδο διαρροής. Για κάθε σημείο P με συντεταγμένες (x_p,y_p,z_p) και για τις κορυφές του τετράεδρου $V_1(x_1,y_1,z_1)$, $V_2(x_2,y_2,z_2)$, $V_3(x_3,y_3,z_3)$ και V_4 (0,0,0), ισχύει ότι το σημείο P βρίσκεται εντός του τετράεδρου, αν οι ακόλουθες ορίζουσες έχουν το ίδιο πρόσημο:

$$D_0 = \begin{vmatrix} x_1 & y_1 & z_1 & 1 \\ x_2 & y_2 & z_2 & 1 \\ x_3 & y_3 & z_3 & 1 \\ 0 & 0 & 0 & 1 \end{vmatrix}, \quad D_1 = \begin{vmatrix} x_p & y_p & z_p & 1 \\ x_2 & y_2 & z_2 & 1 \\ x_3 & y_3 & z_3 & 1 \\ 0 & 0 & 0 & 1 \end{vmatrix}, \quad D_2 = \begin{vmatrix} x_1 & y_1 & z_1 & 1 \\ x_p & y_p & z_p & 1 \\ x_3 & y_3 & z_3 & 1 \\ 0 & 0 & 0 & 1 \end{vmatrix},$$

$$D_3 = \begin{vmatrix} x_1 & y_1 & z_1 & 1 \\ x_2 & y_2 & z_2 & 1 \\ x_p & y_p & z_p & 1 \\ 0 & 0 & 0 & 1 \end{vmatrix}, \quad D_4 = \begin{vmatrix} x_1 & y_1 & z_1 & 1 \\ x_2 & y_2 & z_2 & 1 \\ x_3 & y_3 & z_3 & 1 \\ x_p & y_p & z_p & 1 \end{vmatrix} \tag{7}$$

Η σύγκριση των προσήμων των D_i και D_0 συνιστά έναν έλεγχο του αν το σημείο P και η κορυφή V_i βρίσκονται στην ίδια μεριά του επιπέδου i (δηλαδή του επιπέδου που σχηματίζεται από τα άλλα τρία σημεία εκτός του V_i). Αν το σημείο P βρίσκεται εντός των τεσσάρων επιπέδων, τότε το σημείο βρίσκεται εντός του τετράεδρου. Αν το πρόσημο οποιασδήποτε ορίζουσας D_i διαφέρει από εκείνο της D_0, τότε το σημείο P είναι εκτός του ορίου i, ενώ αν κάποια ορίζουσα ισούται με το μηδέν, τότε το σημείο

P βρίσκεται πάνω στο επίπεδο *i*. Η προαναφερθείσα διαδικασία αποτελεί τη βάση για τον εντοπισμό του κρίσιμου επιπέδου διαρροής για κάθε διατομή σε κάθε επανάληψη της διαδικασίας βελτιστοποίησης. Για την αποφυγή ψαξίματος όλων των πιθανών κώνων, ακολουθείται μια τεχνική εξάλειψης (pruning technique) των επτά από τους οχτώ υποχώρους που σχηματίζονται από τους άξονες, με βάση τις συντεταγμένες κάθε σημείου *P*. Κατόπιν, υπολογίζονται οι ορίζουσες των τετράεδρων μόνο του συγκεκριμένου υποχώρου, εντοπίζεται το κρίσιμο τετράεδρο και κατ'επέκτασιν το κρίσιμο επίπεδο διαρροής.

ii) *Γραμμικοποίηση της επιφάνειας διαρροής τοπικά*

Επεκτείνοντας τη λογική του εντοπισμού του κρίσιμου κώνου, μπορεί να διατηρηθεί η μη γραμμικότητα της επιφάνειας διαρροής και να εφαρμοστεί η γραμμικοποίησή της τοπικά για κάθε σημείο εντατικής κατάστασης. Τα επίπεδα διαρροής, δηλαδή, δεν είναι προσδιορισμένα εκ προοιμίου, αλλά ορίζονται για κάθε σημείο σε κάθε επανάληψη της διαδικασίας βελτιστοποίησης.

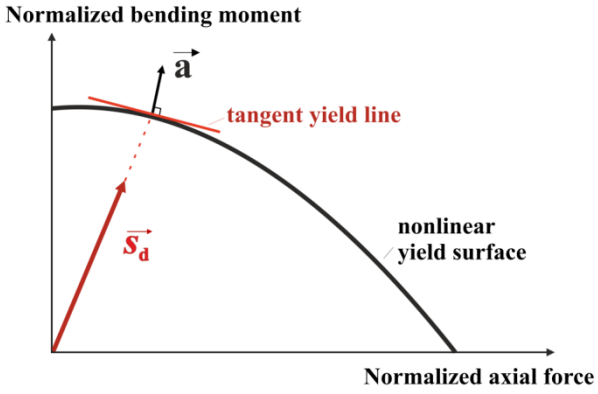

Σχ. 9: Τοπική γραμμικοποίηση της επιφάνειας διαρροής.

Η διαδικασία που ακολουθείται απεικονίζεται στο Σχ. 9 και είναι η εξής: καταρχάς, προσδιορίζεται το σημείο τομής του διανύσματος εντατικής κατάστασης με την επιφάνεια διαρροής και κατόπιν, ορίζεται το εφαπτόμενο-σε αυτό το σημείο-επίπεδο, καθώς και το κάθετο διάνυσμα του επιπέδου. Το διάνυσμα έντασης προβάλλεται στη διεύθυνση του κάθετου διανύσματος και η προβολή αυτή συγκρίνεται με την απόσταση του εφαπτομενικού επιπέδου από την αρχή των αξόνων. Κατ'αυτόν τον τρόπο, για κάθε διατομή μορφώνεται ένας περιορισμός διαρροής και οι διαστάσεις του μητρώου $\boldsymbol{N}$ και των διανυσμάτων $\boldsymbol{w}$ και $\boldsymbol{r'}$ είναι ακριβώς οι ίδιες με εκείνες, που προκύπτουν από τη θεώρηση εντοπισμού του κρίσιμου κώνου. Σημειώνεται ότι στο Σχ. 9 παρουσιάζεται η εφαρμογή της μεθόδου για δισδιάστατο κριτήριο διαρροής,

αλλά η προτεινόμενη μέθοδος είναι γενική και μπορεί να εφαρμοστεί για αλληλεπίδραση *d* εντατικών μεγεθών.

Στην παρούσα εργασία ενσωματώνεται, επίσης, ισοτροπική συμπεριφορά κράτυνσης/χαλάρωσης (hardening/softening) ακολουθώντας: i) πολυγραμμικούς και ii) μη γραμμικούς νόμους υλικού. Η ισότροπη συμπεριφορά συνίσταται στο ότι η επιφάνεια διαρροής διογκώνεται/συρρικνώνεται, χωρίς να αλλάζει το σχήμα της. Παρόλο που αυτή η θεώρηση για τη χαλάρωση (softening) θεωρείται απλοποιητική, για ολονομική συμπεριφορά και υπό την επίδραση μονοτονικώς αυξανόμενου φορτίου είναι αρκετά ακριβής (Tangaramvong&Tin-Loi 2008, Tin-Loi&Pang 1993).

i) *Πολυγραμμική συμπεριφορά κράτυνσης/χαλάρωσης (hardening/softening)*

Σε κάθε διατομή μ αντιστοιχεί ένας πλαστικός πολλαπλασιαστής z_μ, η μη μηδενική τιμή του οποίου σηματοδοτεί ότι η συγκεκριμένη διατομή έχει πλαστικοποιηθεί $(z_\mu \neq 0)$. Με βάση αυτήν την τιμή του πλαστικού πολλαπλασιαστή, εντοπίζεται το αντίστοιχο τμήμα n_s κράτυνσης/χαλάρωσης για κάθε διατομή, το οποίο προσδιορίζει το αντίστοιχο επίπεδο έντασης (Σχ. 10). Κατ'αυτόν τον τρόπο, τα μητρώα κράτυνσης σχηματίζονται για κάθε διατομή και στη συνέχεια για όλη την κατασκευή. Σκοπός είναι ο υπολογισμός του πλαστικού μέρους των συνδυασμένων δράσεων για όλες τις διατομές χρησιμοποιώντας μια γραμμική σχέση της μορφής $\boldsymbol{H}\cdot\mathbf{z}+\boldsymbol{c}$. Σε αυτή τη σχέση, το $\boldsymbol{H}$ είναι το διαγώνιο μητρώο κράτυνσης με διαστάσεις $(2n_{el}\times 2n_{el})$, $\mathbf{z}$ είναι το $(2n_{el}\times 1)$ διάνυσμα όλων των πλαστικών πολλαπλασιαστών και $\boldsymbol{c}$ το $(2n_{el}\times 1)$ διάνυσμα, το οποίο εκφράζει συσσωρευτικά την προηγηθείσα πλαστική συμπεριφορά. Για κάθε διατομή μ $(\mu = 1,2...2n_{el})$ που ακολουθεί πολυγραμμική συμπεριφορά κράτυνσης/χαλάρωσης με συνολικό αριθμό τμημάτων ℓ, οι σχέσεις που προσδιορίζουν τις μη μηδενικές τιμές των μητρώων κράτυνσης είναι οι ακόλουθες:

$$H(\mu,\mu) = \tau \cdot h_{n_s} \qquad \mu = 1...2n_{el},\ \ n_s = 1...\ell \tag{8}$$

$$c(\mu,1) = \begin{cases} 0, & for\ \ n_s = 1,\ \ \mu = 1...2n_{el} \\ \tau \cdot \sum_{i=2}^{n_s} (h_{i-1} - h_i) \cdot z_{i-1}, & for\ n_s \geq 2,\ i = 2,3,...,n_s,\ \mu = 1...2n_{el} \end{cases} \tag{9}$$

όπου λ_i είναι ο συντελεστής μεγέθυνσης/συρρίκνωσης του ορίου διαρροής ($\lambda_0 = 1$) και z_i είναι η τιμή του αντίστοιχου πλαστικού πολλαπλασιαστή στο τέλος του

τμήματος i ($z_0=0$) και $h_i=(\lambda_i-\lambda_{i-1})s_{2y}/(z_i-z_{i-1})$ είναι η κλίση των τμημάτων κράτυνσης/χαλάρωσης έχουσα διαστάσεις ροπής. Σημειώνεται ότι για τις διατομές, οι οποίες βρίσκονται στην ελαστική περιοχή, ο πλαστικός πολλαπλασιαστής και οι συντελεστές κράτυνσης είναι μηδενικοί. Επιπροσθέτως, για το πρώτο τμήμα κράτυνσης ισχύει ότι $c(\mu,1)=0$, αφού δεν υπάρχει προγενέστερη πλαστική συμπεριφορά. Αυτό σημαίνει ότι το μητρώο κράτυνσης $\boldsymbol{H}$ εκφράζει το μέτρο κράτυνσης/χαλάρωσης, που αντιστοιχεί στο εντοπισμένο τμήμα, ενώ το μητρώο $\boldsymbol{c}$ αντιστοιχεί στη συνολική προηγηθείσα πλαστική συμπεριφορά. Συνεπώς, η συνθήκη διαρροής για την κατασκευή συνολικά εκφράζεται ως εξής:

$$\boldsymbol{w}=-\boldsymbol{N}^T\cdot\boldsymbol{s}+\boldsymbol{r}'\geq\boldsymbol{0} \quad \text{and} \quad \boldsymbol{r}'=\boldsymbol{r}+\boldsymbol{H}\cdot\mathbf{z}+\boldsymbol{c} \tag{10}$$

όπου $\boldsymbol{r}'$ είναι το $(2n_{el}\times 1)$ διάνυσμα που περιλαμβάνει τα μεγεθυμένα/συρρικνωμένα όρια διαρροής και $\boldsymbol{r}$ είναι το $(2n_{el}\times 1)$ διάνυσμα που περιλαμβάνει τα αρχικά όρια διαρροής.

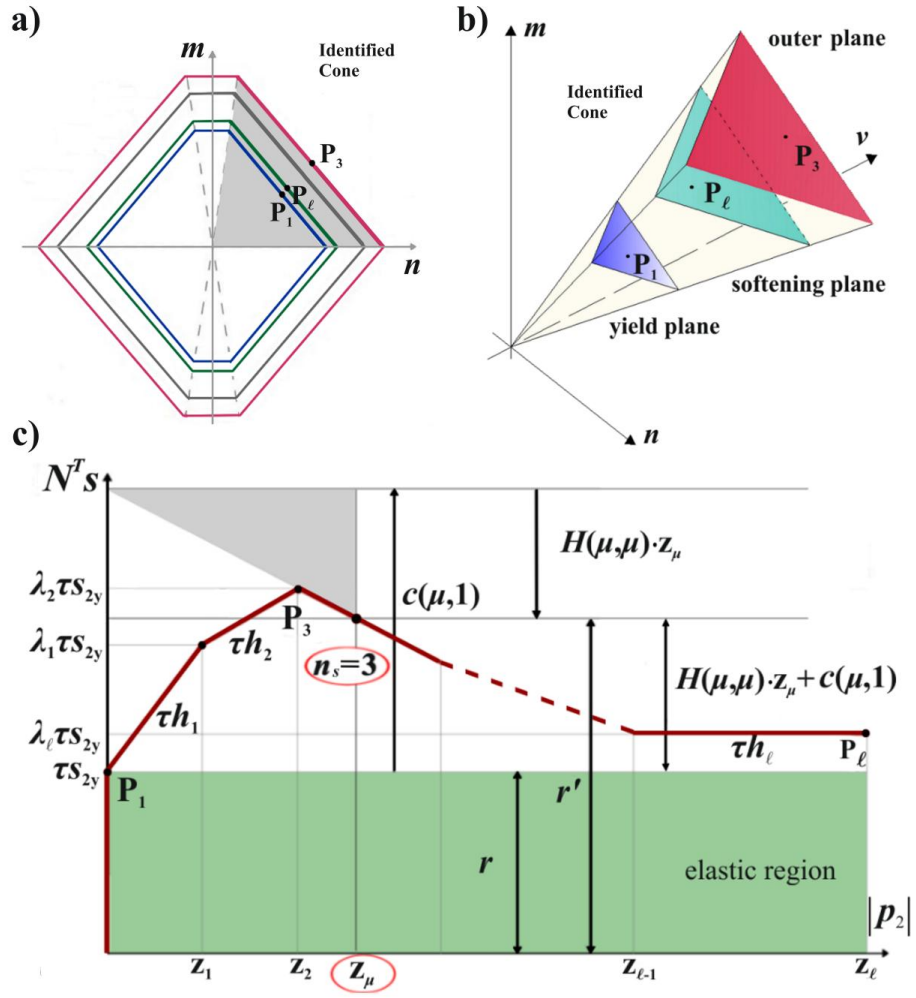

Σχ. 10: Ισοτροπική κράτυνση/χαλάρωση για α)δισδιάστατη και b)τρισδιάστατη αλληλεπίδραση και c)πολυγραμμική συμπεριφορά ενός σημείου εντατικής κατάστασης.

ii) ***Μη γραμμική συμπεριφορά κράτυνσης/χαλάρωσης (hardening/softening)***

Η μη γραμμική συμπεριφορά μπορεί να προσδιοριστεί βάσει κάποιων πειραματικών δεδομένων, τα οποία προσεγγίζονται με μια καμπύλη. Έχοντας, λοιπόν, πειραματικά δεδομένα, που αφορούν στην αξονική δύναμη σε συνάρτηση με την αξονική πλαστική παραμόρφωση και στην καμπτική ροπή σε συνάρτηση με την πλαστική στροφή, προσδιορίζονται οι αντίστοιχες μη-γραμμικές καμπύλες. Κατόπιν, οι καμπύλες αυτές συνδυάζονται με μια αναλογία που υπαγορεύεται από τους συντελεστές του κάθετου-στο επίπεδο διαρροής-διανύσματος και εν τέλει προκύπτει μία καμπύλη, που αφορά στη συνδυασμένη δράση των εντατικών μεγεθών συναρτήσει της πλαστικής στροφής. Ένας πλαστικός πολλαπλασιαστής z_μ αντιστοιχίζεται σε μια διατομή μ σε κάθε επανάληψη της διαδικασίας βελτιστοποίησης, η μη-μηδενική τιμή του οποίου σηματοδοτεί ότι η διατομή βρίσκεται στην πλαστική περιοχή. Έχοντας την αναλυτική έκφραση της μη-γραμμικής συμπεριφοράς κράτυνσης/χαλάρωσης και γνωρίζοντας την τιμή του πλαστικού πολλαπλασιαστή, μπορεί να υπολογιστεί απευθείας από την τεταγμένη του σημείου της καμπύλης το μεγεθυμένο/συρρικνωμένο όριο διαρροής r'_μ που αντιστοιχεί στη διατομή (Σχ. 11). Η συνθήκη διαρροής για την κατασκευή συνολικά δίδεται όπως και στη σχέση (10), με το $\boldsymbol{r}'$ να υπολογίζεται κατευθείαν από την καμπύλη συμπεριφοράς.

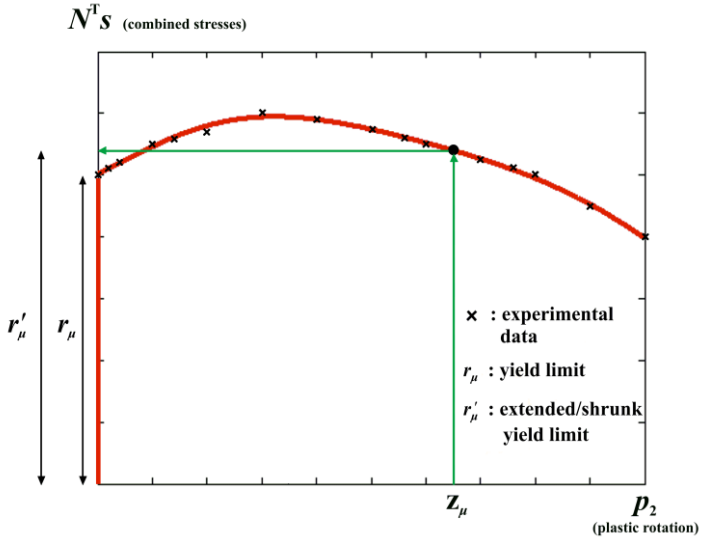

Σχ. 11:Μη γραμμική συμπεριφορά κράτυνσης/χαλάρωσης.

Το πρόβλημα που δίδεται από τη σχέση (6), καθώς και οι προτεινόμενες θεωρήσεις για τη συνθήκη διαρροής και για τους νόμους κράτυνσης/χαλάρωσης

(softening), εφαρμόζονται σε κώδικα Matlab. Επιλέγεται ο επιλύτης *fmincon* (κατάλληλος για μη γραμμικά προβλήματα ελαχιστοποίησης πολλών μεταβλητών με περιορισμούς) και η interior-point μέθοδος για τη διαδικασία της βελτιστοποίησης. Οι περιπτώσεις που εξετάζονται είναι οι ακόλουθες:

- Case (a): **NM** αλληλεπίδραση με :
    1. Γραμμικοποιημένοι καταστατικοί νόμοι και συνθήκη διαρροής.
    2. Γραμμικοποιημένοι καταστατικοί νόμοι και μη γραμμική συνθήκη διαρροής.
    3. Μη γραμμικοί καταστατικοί νόμοι και συνθήκη διαρροής.
- Case (b): **NQM** αλληλεπίδραση με:
    1. Γραμμικοποιημένοι καταστατικοί νόμοι και συνθήκη διαρροής.
    2. Γραμμικοποιημένοι καταστατικοί νόμοι και μη γραμμική συνθήκη διαρροής.
    3. Μη γραμμικοί καταστατικοί νόμοι και συνθήκη διαρροής.

Για τις παραπάνω περιπτώσεις αναλύεται το πλαίσιο του σχήματος 12, το οποίο αποτελείται από 30 μέλη, 21 κόμβους και 54 βαθμούς ελευθερίας. Η κατηγορία χάλυβα είναι S235 με μέτρο ελαστικότητας $E = 2\times10^8\ kN/m^2$. Για τις διατομές των υποστυλωμάτων ισχύει $A=112.5\times10^{-4}\ m^2$, $I=18260\times10^{-8}\ m^4$, $s_{1y}=2643.75kN$, $v_y=505.41kN$, $s_{2y}=s_{3y}=325kNm$, ενώ για τις διατομές των δοκών $A=28.48\times10^{-4}\ m^2$, $I=1943\times10^{-8}\ m^4$, $s_{1y}=669.28kN$, $v_y=189.89kN$, $s_{2y}=s_{3y}=51.84kNm$. Η αντίστοιχη πολυγραμμική συμπεριφορά φαίνεται στο Σχ. 13a και εξαρτάται από τις παραμέτρους κάθε διατομής. Πιο συγκεκριμένα, για τα υποστυλώματα ισχύει $h_1=6500kNm$ $z_1=0.005$ $\lambda_1=1.1$, $h_2=3250kNm$ $z_2=0.015$ $\lambda_2=1.20$, $h_3=-5200kNm$ $z_3=0.04$ $\lambda_3=0.8$, $h_4=10^{-6}kNm$ $z_4=0.05$ $\lambda_4=0.8$, ενώ για τις δοκούς $h_1=518.4kNm$ $z_1=0.005$ $\lambda_1=1.05$, $h_2=259.2kNm$ $z_2=0.015$ $\lambda_2=1.10$, $h_3=-777.6kNm$ $z_3=0.035$ $\lambda_3=0.80$, $h_4=10^{-6}kNm$ $z_4=0.04$ $\lambda_4=0.80$. Η μη γραμμική συμπεριφορά των υποστυλωμάτων και των δοκών απεικονίζεται στο Σχ. 13b χρησιμοποιώντας μια πολυωνυμική συνάρτηση $4^{ου}$ βαθμού (Πίνακας 2). Οι τιμές των z_4 αποτελούν τα άνω όρια για τις διατομές των υποστυλωμάτων και των δοκών. Το άνω όριο για όλες τις μετατοπίσεις είναι $u_u = 1$ και το κάτω όριο $u_l = -1$. Η παράμετρος ποινής ρ αυξάνεται σε κάθε κύκλο της διαδικασίας βελτιστοποίησης με βάση τη σχέση $\rho=10\rho$, έως ότου η επιθυμητή σύγκλιση επιτευχθεί ($w^T z \le 10^{-5}$).

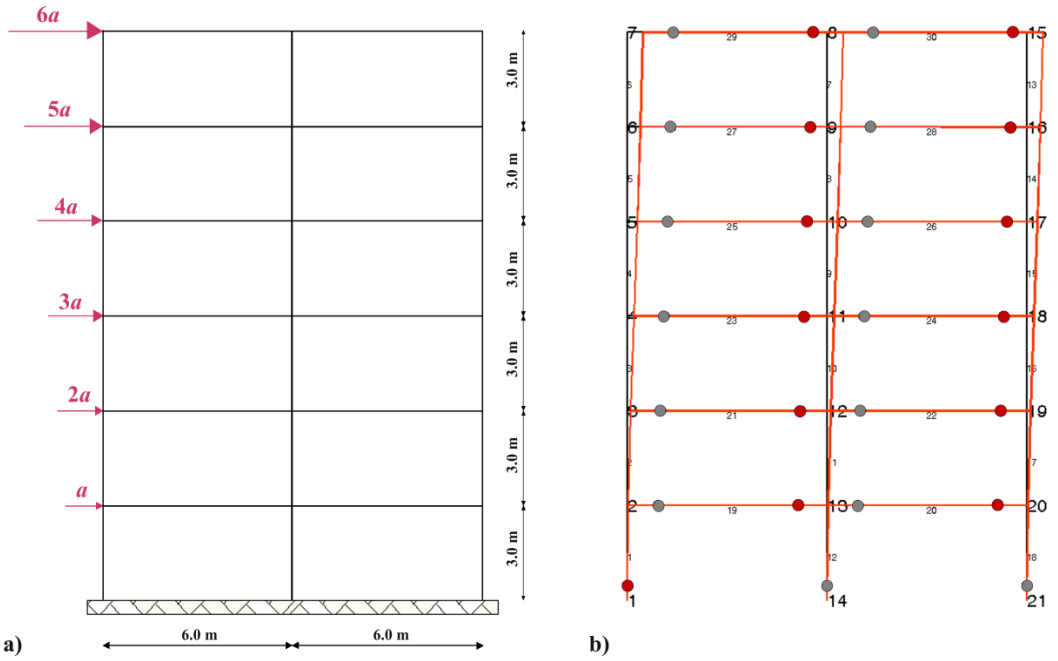

Σχ. 12: a) Επίπεδο μεταλλικό πλαίσιο και b) μηχανισμός κατάρρευσης για όλες τις περιπτώσεις.

Πίνακας 2: Εξισώσεις πολυωνυμικών γραμμών της μη-γραμμικής συμπεριφοράς.

x	0.00	0.001	0.002	0.005	0.007	0.01	0.015	0.020	0.025	0.028	0.030	0.035	0.038	0.040	0.045	0.050
f(x)	1.00	1.02	1.04	1.10	1.14	1.18	1.20	1.18	1.15	1.12	1.10	1.05	1.02	1.00	0.90	0.80
Polynomial line for column cross sections								$f(x) = p_1 \cdot x^4 + p_2 \cdot x^3 + p_3 \cdot x^2 + p_4 \cdot x + p_5$ $p_1 = -2.495 \cdot 10^5,\ p_2 = 3.077 \cdot 10^4,\ p_3 = -1624,\ p_4 = 31.66,\ p_5 = 0.9901$								
x	0.00	0.0005	0.001	0.005	0.008	0.015	0.017	0.019	0.020	0.021	0.023	0.025	0.028	0.030	0.035	0.050
f(x)	1.00	1.01	1.03	1.05	1.08	1.10	1.09	1.07	1.05	1.02	1.00	0.95	0.90	0.87	0.83	0.80
Polynomial line for beam cross sections								$f(x) = p_1 \cdot x^4 + p_2 \cdot x^3 + p_3 \cdot x^2 + p_4 \cdot x + p_5$ $p_1 = 2.38 \cdot 10^5,\ p_2 = -4310,\ p_3 = -827,\ p_4 = 18.24,\ p_5 = 0.9998$								

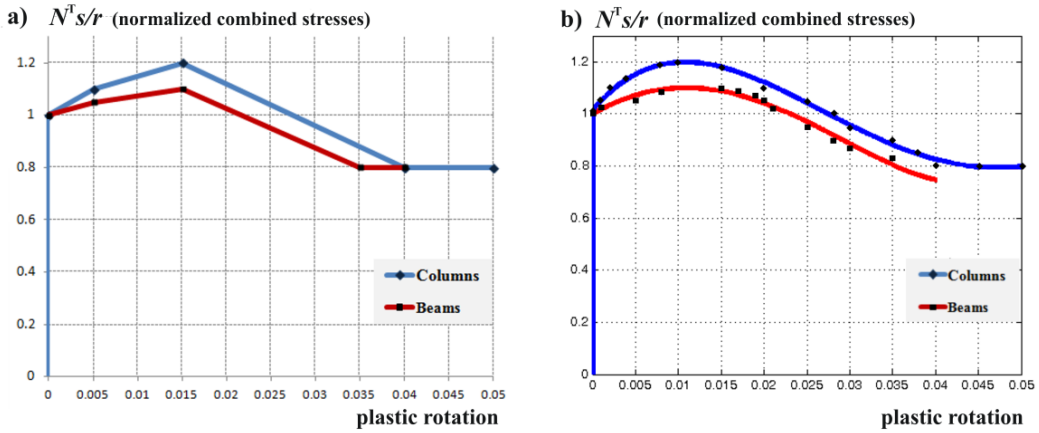

Σχ. 13: a) Πολυγραμμική και b) μη γραμμική συμπεριφορά κράτυνσης/χαλάρωσης.

Τα αποτελέσματα των αναλύσεων παρουσιάζονται στον Πίνακα 3. Οι φορτικοί συντελεστές είναι μεγαλύτεροι και για τις δυο περιπτώσεις μη γραμμικής αλληλεπίδρασης, συγκρινόμενοι με τη γραμμικοποιημένη θεώρηση. Επιπλέον, η επίδραση της τέμνουσας δύναμης είναι εμφανής στη μείωση του φορτίου κατάρρευσης. Η μόρφωση των πλαστικών αρθρώσεων (αριθμός και κατανομή τους στην κατασκευή) είναι η ίδια για όλες τις περιπτώσεις (Σχ. 12 b), αλλά διαφορετικές εντατικές καταστάσεις αντιστοιχούν σε κάθε περίπτωση. Τα αντίστοιχα διαγράμματα αλληλεπίδρασης φαίνονται στα Σχ. 14 και 15. Οι διατομές εντείνονται κυρίως λόγω κάμψης, με κάποιες διατομές να βρίσκονται στον κλάδο χαλάρωσης (softening). Η επίδραση της αξονικής δύναμης παρατηρείται στις δοκούς λόγω της πλευρικής φόρτισης (Σχ. 14 και *n-m* διαγράμματα του Σχ. 15), ενώ η επίδραση της τέμνουσας δύναμης είναι εμφανής και πιο έντονη από εκείνη της αξονικής δύναμης στις διατομές δοκών και υποστυλωμάτων (*v-m* διαγράμματα του Σχ. 15).

Πίνακας 3: Αποτελέσματα αναλύσεων για όλες τις περιπτώσεις.

Cases	**Case (a_1)**	**Case (a_2)**	**Case (a_3)**	**Case (b_1)**	**Case (b_2)**	**Case (b_3)**
number of variables n_{var}	**205**					
number of equality constraints n_{eq}	**144**					
number of inequality constraints n_{inq}	**60**					
maximum load factor a (kN)	**8.24**	**8.28**	**8.35**	**7.90**	**8.25**	**8.31**
number of plastic hinges	**27**	**27**	**27**	**27**	**27**	**27**
total computational time (s)	**18.82**	**483.61**	**542.47**	**825.10**	**536.51**	**715.52**
number of iterations	**59**	**80**	**84**	**102**	**83**	**95**
complementarity condition $w^T z$	**7.35E-12**	**1.84E-10**	**4.56E-11**	**1.82E-10**	**9.40E-13**	**1.50E-12**
initial values of ρ	**10**	**10**	**10**	**10^5**	**100**	**10**

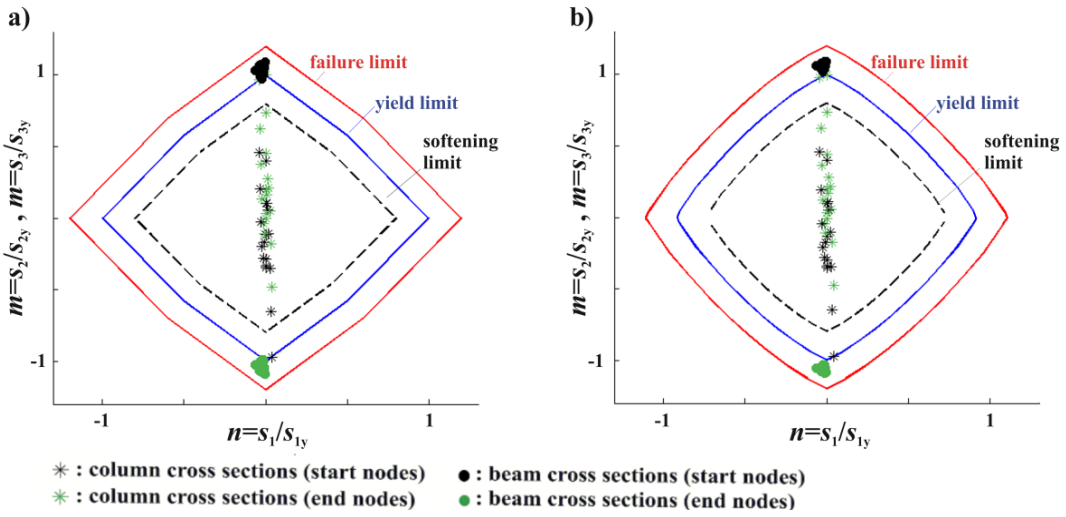

Σχ. 14: Διαγράμματα NM αλληλεπίδρασης για a) case (a_1) και b) case (a_3).

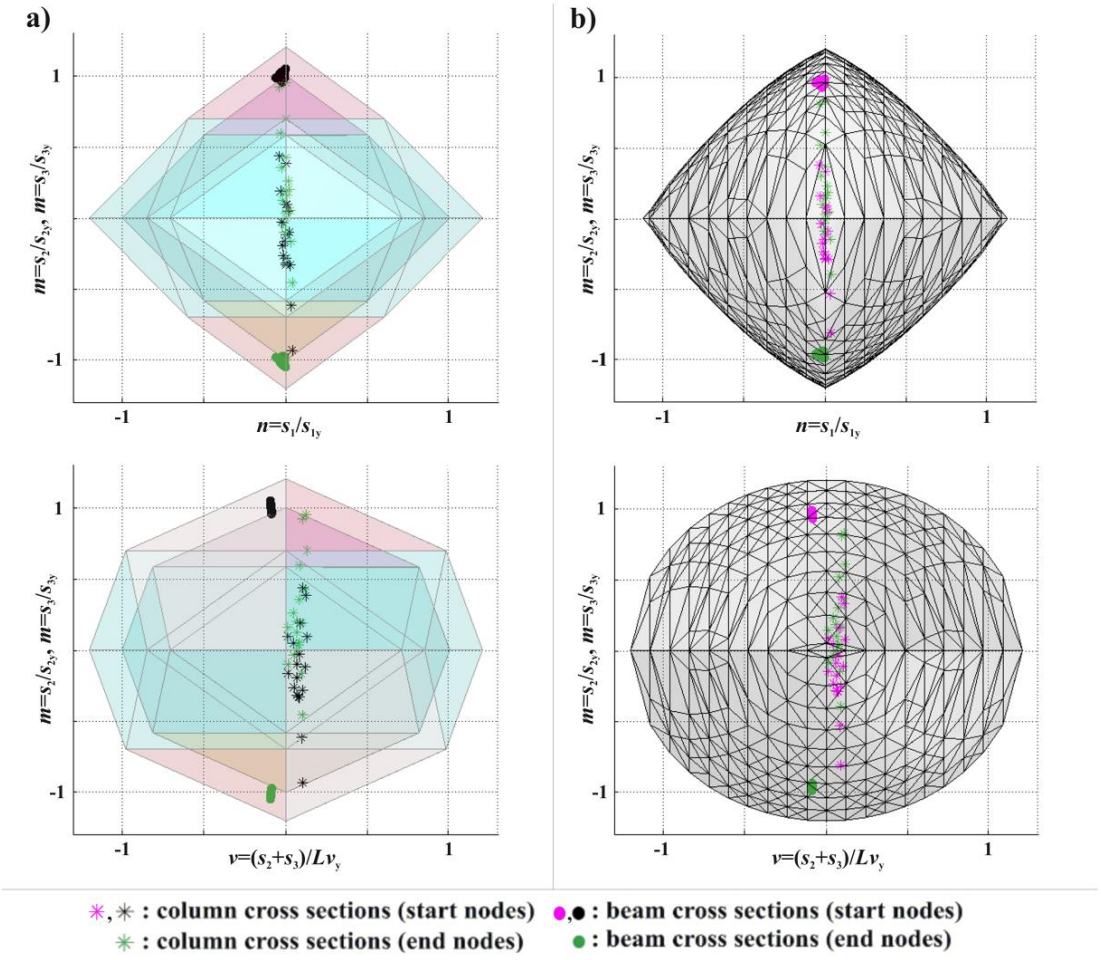

Σχ.15: Διαγράμματα NQM αλληλεπίδρασης για a) case (b_1) και b) case (b_3).

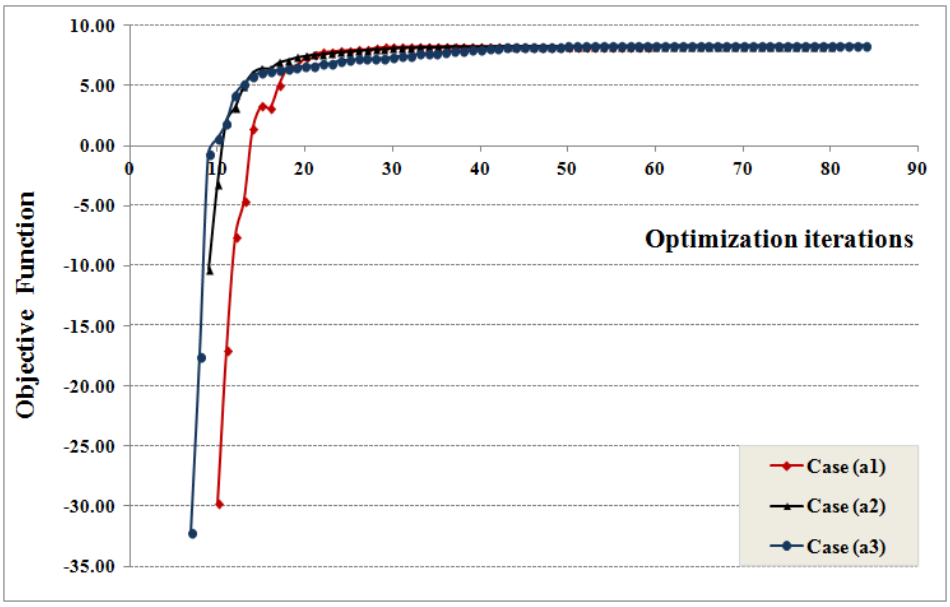

Σχ. 16: Εξέλιξη της διαδικασίας βελτιστοποίησης για NM αλληλεπίδραση.

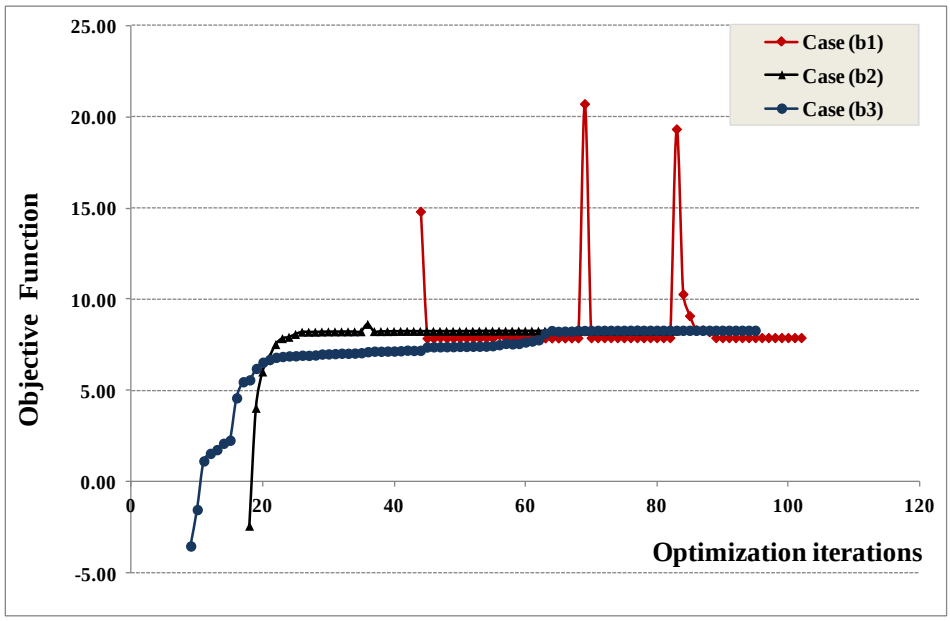

Σχ. 17: Εξέλιξη της διαδικασίας βελτιστοποίησης για NQM αλληλεπίδραση.

Η υπολογιστική επίδοση του αλγορίθμου για NM και NQM αλληλεπίδραση παρουσιάζεται στα Σχ. 16 και 17 αντίστοιχα, παραλείποντας τις αρχικές επαναλήψεις. Παρατηρείται ότι για NM αλληλεπίδραση ο αλγόριθμος για όλες τις περιπτώσεις φαίνεται να ακολουθεί περίπου το ίδιο μαθηματικό μονοπάτι. Ωστόσο, οι μη γραμμικές περιπτώσεις (a_2) και (a_3) απαιτούν περισσότερες επαναλήψεις και κατ'επέκτασιν περισσότερο υπολογιστικό χρόνο συγκρινόμενες με την περίπτωση της γραμμικοποίησης (a_1). Για την περίπτωση της NQM αλληλεπίδρασης, η διαδικασία

βελτιστοποίησης για τις περιπτώσεις (b_2) και (b_3) απαιτεί λιγότερες επαναλήψεις (83 και 95 επαναλήψεις έναντι 102) συγκρινόμενες με την περίπτωση (b_1) και λιγότερο υπολογιστικό χρόνο (536.51s και 715.52s έναντι 825.10s). Αυτό οφείλεται στο γεγονός ότι η διαδικασία εύρεσης του κρίσιμου κώνου για την περίπτωση της τρισδιάστατης αλληλεπίδρασης απαιτεί περισσότερο χρόνο σε σχέση τη διαδικασία τοπικής γραμμικοποίησης της επιφάνειας διαρροής. Οι έντονες κορυφές που παρουσιάζονται για την περίπτωση (b_1) οφείλονται στον όρο της συνθήκης συμπληρωματικότητας, ο οποίος πολλαπλασιάζεται με την παράμετρο ποινής στην αντικειμενική συνάρτηση. Το διάνυσμα των αγνώστων $\boldsymbol{s}$ και $\mathbf{z}$ καθορίζουν ένα γινόμενο $\boldsymbol{w}^T\mathbf{z}$, το οποίο αποκλίνει ελάχιστα από το μηδέν, αλλά αυτή η απόκλιση μεγεθύνεται από την παράμετρο ποινής ρ, επηρεάζοντας σημαντικά την τιμή της αντικειμενικής συνάρτησης.

IV. Οριακή και παραμορφωσιακή ανάλυση τρισδιάστατων πλαισίων με μαθηματικό προγραμματισμό

Η οριακή και παραμορφωσιακή ανάλυση μιας κατασκευής ως ένα πρόβλημα βελτιστοποίησης δίδεται από τις παρακάτω σχέσεις::

$$\left.\begin{array}{lcl} \text{maximize} & a-\rho\cdot\boldsymbol{w}^T\cdot\mathbf{z} & (i) \\ \text{subject to} & \boldsymbol{B}\cdot\boldsymbol{s}-a\cdot\boldsymbol{f}=\boldsymbol{f}_d & (ii) \\ & \boldsymbol{S}^{-1}\cdot\boldsymbol{s}+\boldsymbol{N}\cdot\mathbf{z}-\boldsymbol{B}^T\cdot\boldsymbol{u}=\mathbf{0} & (iii) \\ & \boldsymbol{w}=-\boldsymbol{N}^T\cdot\boldsymbol{s}+\boldsymbol{r}'\geq\mathbf{0} & (iv) \\ & \mathbf{0}\leq\mathbf{z}\leq\mathbf{z}_u & (v) \\ & \boldsymbol{u}_l\leq\boldsymbol{u}\leq\boldsymbol{u}_u & (vi) \end{array}\right\} \quad (11)$$

όπου τα διανύσματα και τα μητρώα για την ανάλυση τρισδιάστατων πλαισίων διαφοροποιούνται ως προς τις διαστάσεις σε σχέση με εκείνα, που χρησιμοποιούνται για τα επίπεδα πλαίσια. Η αντικειμενική συνάρτηση που περιγράφεται από την εξίσωση (11.*i*) περιλαμβάνει το φορτικό συντελεστή a και τη συνθήκη συμπληρωματικότητας $\boldsymbol{w}^T\mathbf{z}$ πολλαπλασιασμένη με μια παράμετρο ποινής ρ. Η ισορροπία για ολόκληρη την κατασκευή (θεωρώντας διπλά συμμετρικές διατομές για τα μέλη) δίδεται από την εξίσωση (11.*ii*), όπου $\boldsymbol{B}$ είναι το ($12n_{el}\times 6n_{el}$) μητρώο ισορροπίας της κατασκευής, $\boldsymbol{s}$ είναι το ($6n_{el}\times 1$) διάνυσμα των ανεξάρτητων εντατικών μεγεθών όλων των μελών, a είναι φορτικός συντελεστής, $\boldsymbol{f}$ είναι το ($n_f\times 1$) διάνυσμα των επικόμβιων δράσεων στο καθολικό σύστημα και $\boldsymbol{f}_d$ είναι το ($n_f\times 1$) διάνυσμα των σταθερών επικόμβιων δράσεων στο καθολικό σύστημα. Η εξίσωση

(11.*iii*) εκφράζει τη συνθήκη συμβιβαστού των παραμορφώσεων για την κατασκευή, όπου $\boldsymbol{S}$ είναι το ($6n_{el}\times 6n_{el}$) μητρώο που περιλαμβάνει διαγωνίως τα μητρώα ακαμψίας $\boldsymbol{S}^i$ όλων των μελών, $\boldsymbol{N}$ είναι το ($6n_{el}\times 2n_{el}$) μητρώο που περιλαμβάνει όλα τα κάθετα-στα εντοπισμένα επίπεδα διαρροής-διανύσματα, $\mathbf{z}$ είναι το ($2n_{el}\times 1$) διάνυσμα των πλαστικών πολλαπλασιαστών και $\boldsymbol{u}$ το ($6n_{el}\times 1$) διάνυσμα των αντίστοιχων επικόμβιων μετακινήσεων. Η σχέση (11.*iv*) περιγράφει με όρους περιθωρίων αντοχής $\boldsymbol{w}$ τον περιορισμό που τίθεται από τη συνθήκη διαρροής, η οποία μπορεί να εκφραστεί είτε εκ προοιμίου γραμμικοποιώντας την είτε εφαρμόζοντας την γραμμικοποίηση τοπικά. Επιπλέον, πολυγραμμικοί ή μη-γραμμικοί νόμοι συμπεριφοράς μπορούν να ενσωματωθούν μέσω του υπολογισμού των διευρυμένων/συρρικνωμένων ορίων διαρροής $\boldsymbol{r}'$.

Το πρόβλημα που διατυπώνεται από τη σχέση (11) εφαρμόζεται σε κώδικα Matlab και εξετάζεται η αλληλεπίδραση αξονικής δύναμης-διαξονικής κάμψης (NM_yM_z) για τις εξής περιπτώσεις: Case (a): γραμμικοποιημένη συνθήκη διαρροής και τελείως πλαστική συμπεριφορά, Case (b): γραμμικοποιημένη συνθήκη διαρροής και νόμοι υλικού-Εντοπισμός κρίσιμου κώνου, Case (c): μη-γραμμική συνθήκη διαρροής (η γραμμικοποίηση εφαρμόζεται τοπικά) και πολυγραμμικοί νόμοι υλικού, Case (d): μη-γραμμική συνθήκη διαρροής (η γραμμικοποίηση εφαρμόζεται τοπικά) και μη-γραμμικοί νόμοι υλικού. Το κριτήριο διαρροής που υιοθετείται είναι εκείνο του Gendy-Saleeb (1992).

Το τρισδιάστατο πλαίσιο που παρουσιάζεται στο Σχ. 18 υποβάλλεται σε μεταβλητό φορτίο κατά άξονα X και σταθερό κατά τον άξονα Y και Z. Για τη διακριτοποίηση του φορέα χρησιμοποιήθηκαν 26 μέλη, 18 κόμβοι και 72 βαθμοί ελευθερίας. Ο χάλυβας είναι κατηγορίας S235 και έχει μέτρο ελαστικότητας $E=2\times 10^8$ kN/m^2. Για όλες τις διατομές υποστυλωμάτων θεωρείται $A=159\times 10^{-4}m^2$, $I=45070\times 10^{-8}m^4$ (ισχυρός άξονας), $I=8564\times 10^{-8}m^4$ (ασθενής άξονας), $I=189\times 10^{-8}m^4$ (στρεπτική), $s_{1y}=3736.5kN$, $s_{2y}=301.6\ kNm$, $s_{3y}=s_{5y}=205.1\ kNm$, $s_{4y}=s_{6y}=602.1kNm$, ενώ για τις διατομές δοκών έχουμε $A=53.81\times 10^{-4}m^2$, $I=8356\times 10^{-8}m^4$ (ισχυρός άξονας), $I=603.8\times 10^{-8}m^4$ (ασθενής άξονας), $I=20.12\times 10^{-8}m^4$ (στρεπτική), $s_{1y}=1264.5\ kN$, $s_{2y}=65.3\ kNm$, $s_{3y}=s_{5y}=29.4\ kNm$, $s_{4y}=s_{6y}=147.7\ kNm$. Η υποτεθείσα πολυγραμμική και η αντίστοιχη μη-γραμμική συμπεριφορά φαίνονται στο Σχ. 19. Πιο συγκεκριμένα, για την πολυγραμμική συμπεριφορά των υποστυλωμάτων ισχύει $h_1=12041.4\ kNm\ z_1=0.005\ \lambda_1=1.1$, $h_2=6020.7\ kNm\ z_2=0.015\ \lambda_2=1.2$, $h_3=-6020.7\ kNm\ z_3=0.05\ \lambda_3=0.85$, $h_4=10^{-6}\ kNm\ z_4=0.06\ \lambda_4=0.85$, ενώ για τις διατομές δοκών

h_1=1476.7 kNm z_1=0.005 λ_1=1.05, h_2=738.4 kNm z_2=0.015 λ_2=1.1, h_3=-1230.58 kNm z_3=0.05 λ_3=0.85, h_4=10^{-6} kNm z_4=0.06 λ_4=0.85. Η μη-γραμμική συμπεριφορά περιγράφεται από ένα πολυώνυμο 4^{ου} βαθμού βασιζόμενο στα δεδομένα του Πίνακα 4. Οι τιμές του z_4 αποτελούν άνω όριο για τις διατομές υποστυλωμάτων και δοκών, ενώ για όλες τις μετατοπίσεις έχει θεωρηθεί κάτω όριο $u_l = -10$ και άνω όριο $u_u = 10$.

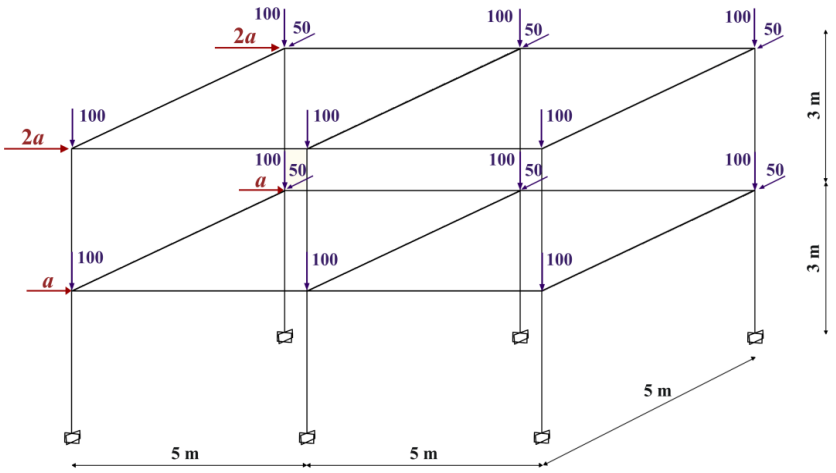

Σχ. 18: Τρισδιάστατο πλαίσιο με σταθερά και μεταβλητά φορτία.

Πίνακας 4: Εξισώσεις πολυωνυμικών γραμμών της μη-γραμμικής συμπεριφοράς.

x	0.00	0.001	0.002	0.005	0.007	0.01	0.015	0.020	0.025	0.028	0.030	0.035	0.038	0.040	0.045	0.060
f(x)	1.00	1.05	1.10	1.15	1.18	1.20	1.18	1.15	1.12	1.10	1.05	1.02	1.00	0.95	0.90	0.85
Polynomial line for column cross sections								$f(x)=p_1\cdot x^4+p_2\cdot x^3+p_3\cdot x^2+p_4\cdot x+p_5$ $p_1=-1.83\cdot10^5, p_2=3.14\cdot10^4, p_3=-1817, p_4=32.54, p_5=1.02$								
x	0.00	0.0010	0.002	0.005	0.007	0.010	0.015	0.020	0.025	0.028	0.030	0.035	0.038	0.040	0.045	0.050
f(x)	1.00	1.00	1.008	1.05	1.08	1.10	1.08	1.05	1.03	1.008	0.96	0.94	0.92	0.87	0.825	0.80
Polynomial line for beam cross sections								$f(x)=p_1\cdot x^4+p_2\cdot x^3+p_3\cdot x^2+p_4\cdot x+p_5$ $p_1=-1.39\cdot10^4, p_2=1.02\cdot10^4, p_3=-901.3, p_4=17.84, p_5=0.99$								

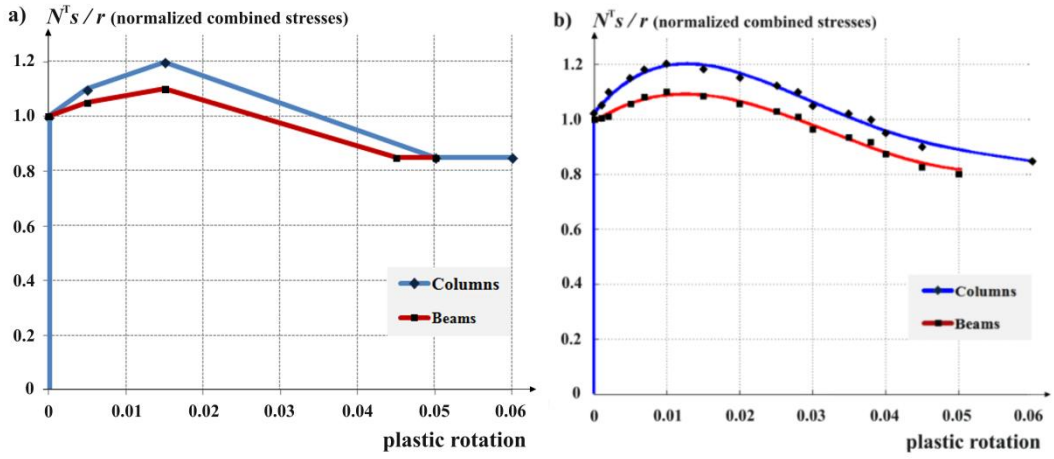

Σχ. 19: a) Πολυγραμμική και b) μη γραμμική συμπεριφορά κράτυνσης/χαλάρωσης.

Πίνακας 5: Αποτελέσματα αναλύσεων για όλες τις περιπτώσεις.

Cases	NMyMz rigid-p.plastic (a)	NMyMz PWL (b)	NMyMz NL-PWL (c)	NMyMz NL (d)
number of variables n_{var}	157	281		
number of equality constraints n_{eq}	72	228		
number of inequality constraints n_{inq}	1664	52		
maximum load factor a (kN)	188.50	204.13	211.98	215.07
number of plastic hinges	22	22	22	22
total computational time (s)	10.97	189.97	2953.38	2192.69
number of iterations	—	28	359	280
complementarity condition $w^T z$	—	4.74E-05	4.50E-12	3.04E-07
initial values of ρ	—	10^9	10^4	100

Τα αποτελέσματα των αναλύσεων φαίνονται στον Πίνακα 5. Η πρώτη περίπτωση της τελείως πλαστικής συμπεριφοράς διατυπώνεται ως ένα πρόβλημα γραμμικού προγραμματισμού με λιγότερες μεταβλητές και λιγότερους ισοτικούς περιορισμούς, σε σχέση με τις υπόλοιπες περιπτώσεις. Ωστόσο, οι ανισοτικοί περιορισμοί είναι περισσότεροι, καθώς στη μόρφωση της συνθήκης διαρροής μετέχουν όλα τα δυνατά επίπεδα. Η τιμή του φορτικού συντελεστή είναι η μικρότερη για αυτήν την περίπτωση και ο απαιτούμενος χρόνος σύγκλισης είναι σαφώς μικρότερος, αφού αντιστοιχεί σε πρόβλημα γραμμικού προγραμματισμού. Οι περιπτώσεις (b), (c) και (d) περιλαμβάνουν τον ίδιο αριθμό μεταβλητών και περιορισμών ανεξαρτήτως της γραμμικότητας (ή μη) της συμπεριφοράς της κατασκευής και του τρόπου γραμμικοποίησης της επιφάνειας διαρροής. Συγκρίνοντας τις περιπτώσεις (b) και (c) που αντιστοιχούν σε πολυγραμμική συμπεριφορά κράτυνσης/χαλάρωσης (hardening/softening), παρατηρείται ότι η μέθοδος τοπικής γραμμικοποίησης της επιφάνειας διαρροής δίνει ακριβέστερες λύσεις επιτυγχάνοντας μεγαλύτερες τιμές φορτικού συντελεστή. Συγκρίνοντας τις περιπτώσεις (c) και (d) που αντιστοιχούν στην τοπική γραμμικοποίηση της επιφάνειας διαρροής, διαπιστώνεται ότι ο μεγαλύτερος φορτικός συντελεστής εμφανίζεται για την περίπτωση της μη-γραμμικής συμπεριφοράς κράτυνσης/χαλάρωσης.

Η οριακή κατάσταση για όλες τις περιπτώσεις φαίνεται στο Σχ. 20, η οποία αντιστοιχεί στο σχηματισμό 22 πλαστικών αρθρώσεων. Ενδεικτικά παρουσιάζεται το διάγραμμα αλληλεπίδρασης για την τελευταία περίπτωση στο Σχ. 21. Οι διατομές των δοκών εντείνονται κυρίως λόγω της αλληλεπίδρασης αξονικής δύναμης-ροπής περί τον τοπικό z άξονα (η επιρροή της ροπής m_y είναι αμελητέα), ενώ οι διατομές των υποστυλωμάτων δέχονται την επίδραση αξονικής δύναμης-διαξονικής κάμψης.

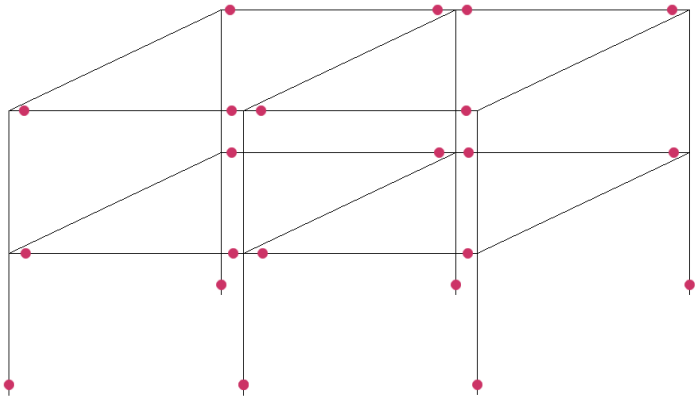

Σχ. 20: Οριακή κατάσταση για όλες τις περιπτώσεις.

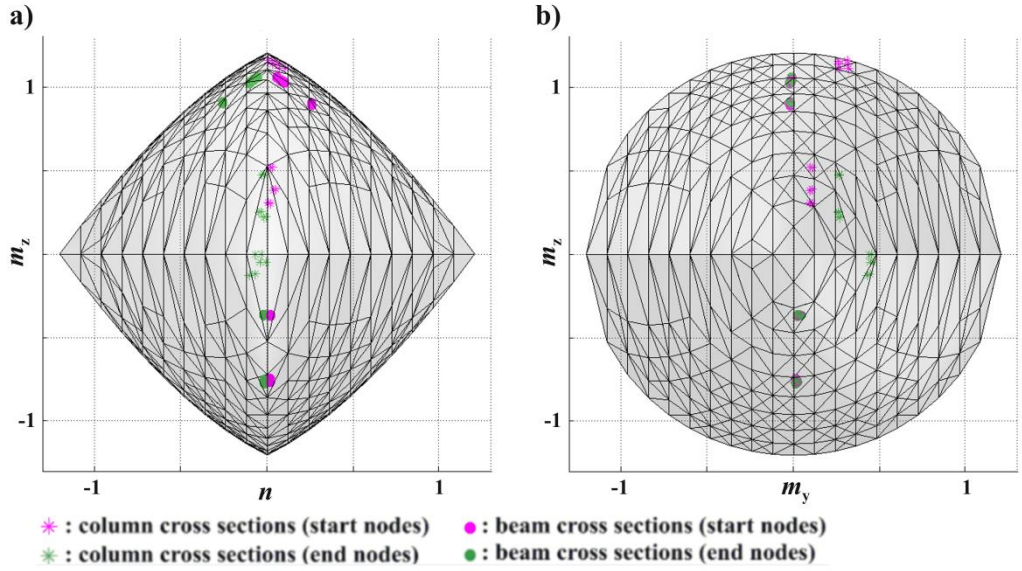

Σχ. 21: Διάγραμμα αλληλεπίδρασης για την περίπτωση (d).

Η υπολογιστική επίδοση του αλγορίθμου για όλες τις περιπτώσεις φαίνεται στα Σχήματα 22, 23 και 24. Για την περίπτωση (b) ο αλγόριθμος συγκλίνει μετά από 28 επαναλήψεις και σε 189.97s. Σημειώνεται ότι η τιμή της αντικειμενικής συνάρτησης ανέρχεται στις –47145.83, ενώ η τιμή του φορτικού συντελεστή είναι μόλις

204.13kN. Η διαφορά αυτή οφείλεται στις μεγάλες τιμές της παραμέτρου ποινής ρ, η οποία μεγεθύνει τις αποκλίσεις του όρου της συμπληρωματικότητας. Η εξέλιξη της διαδικασίας βελτιστοποίησης για την περίπτωση (c) παρουσιάζεται στο Σχ. 23. Η σύγκλιση επιτυγχάνεται μετά από 359 επαναλήψεις σε 2953.38s. Η ομαλή πορεία του αλγορίθμου διακόπτεται από κάποιες αιχμές της αντικειμενικής συνάρτησης, που οφείλονται στον όρο της συνθήκης συμπληρωματικότητας. Η αλγοριθμική πορεία για την περίπτωση (d) παρουσιάζεται στο Σχ. 24. Η πορεία της διαδικασίας βελτιστοποίησης είναι σχετικά ομαλή (συγκρινόμενη με τις υπόλοιπες περιπτώσεις), ενώ απαιτούνται 280 επαναλήψεις και 2192.69s μέχρι τη σύγκλιση.

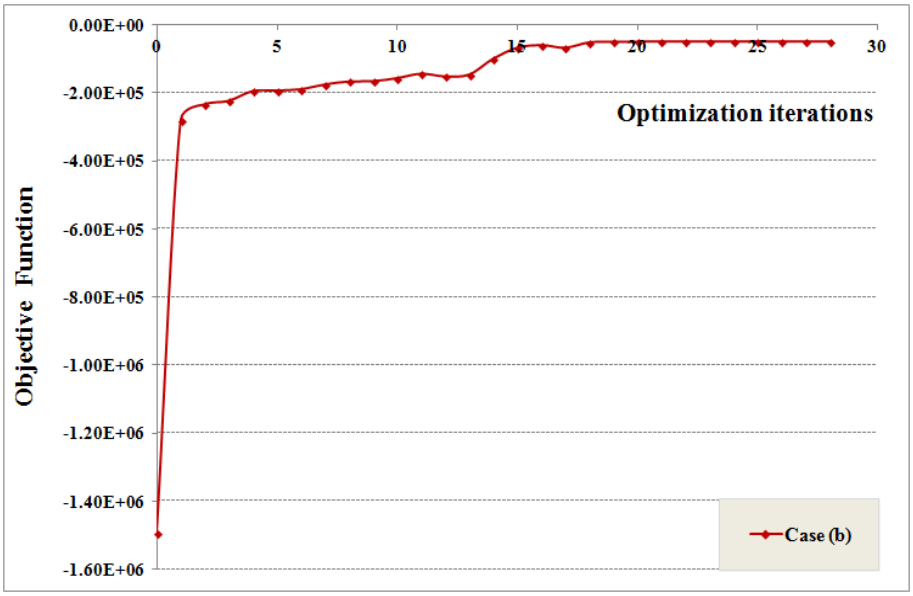

Σχ. 22: Εξέλιξη της διαδικασίας βελτιστοποίησης για την περίπτωση (b).

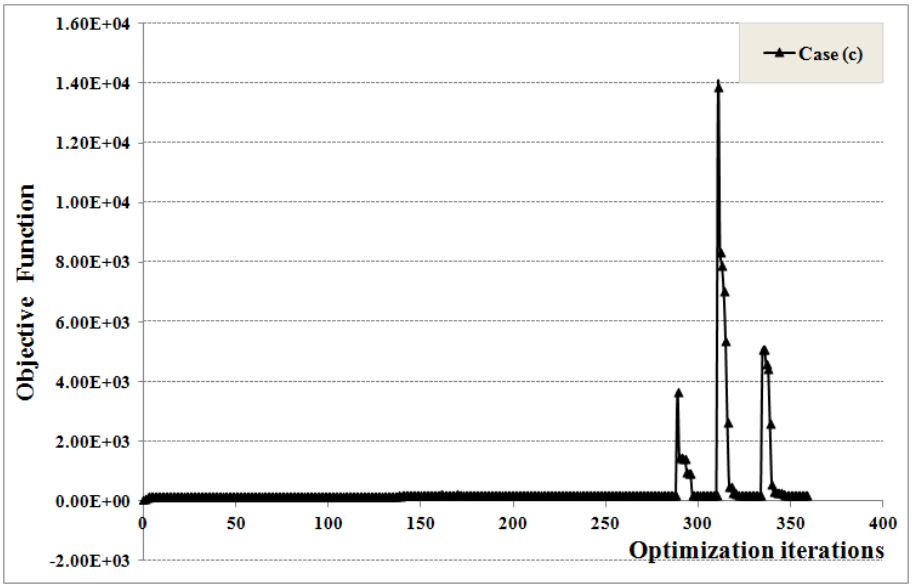

Σχ. 23: Εξέλιξη της διαδικασίας βελτιστοποίησης για την περίπτωση (c).

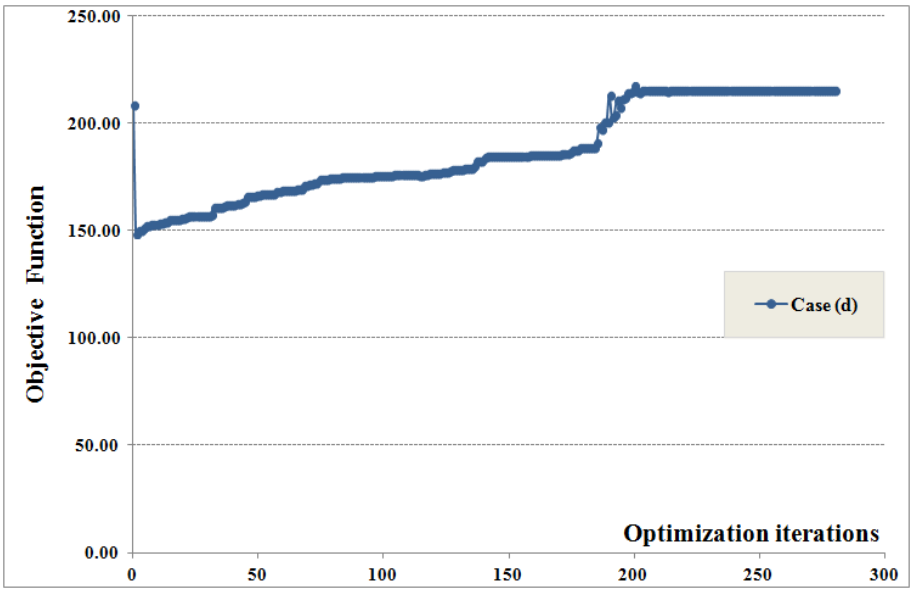

Σχ. 24: Εξέλιξη της διαδικασίας βελτιστοποίησης για την περίπτωση (d).

V. Συμπεράσματα-Προτάσεις για μελλοντική έρευνα

Η παρούσα διατριβή πραγματεύτηκε την οριακή και παραμορφωσιακή ανάλυση στο πλαίσιο του μαθηματικού προγραμματισμού. Στόχος ήταν η ανάδειξη της εσωτερικής δομής του προβλήματος και των μειονεκτημάτων της, καθώς επίσης και η πρόταση νέων θεωρήσεων, οι οποίες διευρύνουν την εφαρμοσιμότητα της οριακής και παραμορφωσιακής ανάλυσης με χρήση μεθόδων μαθηματικού προγραμματισμού. Στη διατριβή αυτή πραγματοποιήθηκε μια αναδόμηση του προβλήματος, αποφεύγοντας τις περιττές περιπλοκές για λόγους μαθηματικού φορμαλισμού και διατηρώντας μόνο τις πληροφορίες που έχουν φυσικό νόημα. Στο πλαίσιο αυτό, χρησιμοποιήθηκαν φυσικές θεωρήσεις για την έκφραση της συνθήκης διαρροής και την ενσωμάτωση πολυγραμμικών ή μη-γραμμικών νόμων κράτυνσης/χαλάρωσης, οι οποίες αποσυμπλέκουν το μέγεθος του προβλήματος (αριθμός μεταβλητών και περιορισμών) από οποιαδήποτε διακριτοποίηση.

Σε αυτήν την κατεύθυνση, η συνθήκη διαρροής εκφράστηκε με τρεις διαφορετικούς τρόπους: i) με θεώρηση κυρτού πολύεδρου (convex hull), ii) με εντοπισμό του κρίσιμου κώνου (cone identification) και iii) εφαρμόζοντας τοπική γραμμικοποίηση. Για την πρώτη περίπτωση, το πολύεδρο διαρροής εκφράζεται ως γραμμικός συνδυασμός των διανυσμάτων, που αντιστοιχούν στις κορυφές του και οδηγεί στην τελική έκφραση του κριτηρίου διαρροής με ισοτικούς περιορισμούς. Σε αυτήν την περίπτωση, ο αριθμός των περιορισμών είναι ανεξάρτητος από τη διακριτοποίηση της επιφάνειας διαρροής, αλλά ο αριθμός των μεταβλητών αυξάνεται

εξαιτίας της εισαγωγής ενός σετ μη-αρνητικών παραμέτρων. Η προτεινόμενη θεώρηση συγκρίθηκε με την υπάρχουσα, η οποία εκφράζει τη συνθήκη διαρροής ως τομή ημιχώρων. Οι δύο διατυπώσεις διαφέρουν ως προς τον αριθμό των μεταβλητών και των περιορισμών και διερευνήθηκε η αποτελεσματικότητά τους για αλληλεπίδραση αξονικής δύναμης-καμπτικής ροπής και αξονικής-τέμνουσας δύναμης-καμπτικής ροπής. Τα αποτελέσματα της ανάλυσης επίπεδων, μεταλλικών πλαισίων, αποδεικνύουν τα υπολογιστικά πλεονεκτήματα της διατύπωσης του κριτηρίου διαρροής με χρήση κυρτού πολυέδρου για το στατικό θεώρημα και για τις δυο περιπτώσεις αλληλεπίδρασης. Η ιδέα του εντοπισμού του κρίσιμου κώνου (cone identification) βασίζεται στο γεγονός ότι σε κάθε επανάληψη του αλγόριθμου βελτιστοποίησης, η εντατική κατάσταση κάθε διατομής ανήκει σε έναν συγκεκριμένο κώνο στοχεύοντας ή ενεργοποιώντας ένα μόνον επίπεδο διαρροής. Για αυτόν τον λόγο, αναπτύχθηκε αλγόριθμος, ο οποίος εντοπίζει τον κρίσιμο κώνο του γραμμικοποιημένου διαγράμματος αλληλεπίδρασης, στον οποίο ανήκει κάθε διατομή. Κατόπιν, ο περιορισμός διαρροής μορφώνεται για κάθε διατομή μόνο για το ευθύγραμμο τμήμα που αντιστοιχεί στον κώνο, σε αντίθεση με την υφιστάμενη μέθοδο, η οποία για κάθε διατομή διατυπώνει ισάριθμους περιορισμούς διαρροής με το πλήθος των ευθυγράμμων τμημάτων του κριτηρίου διαρροής. Κατά αυτόν τον τρόπο, το πλήθος των περιορισμών μειώνεται σημαντικά και το πρόβλημα γίνεται ανεξάρτητο από τη γραμμικοποίηση της επιφάνειας διαρροής. Προτάθηκαν δύο απλές μέθοδοι για τον εντοπισμό του κρίσιμου κώνου για δισδιάστατα και τρισδιάστατα κριτήρια διαρροής. Επεκτείνοντας την ιδέα εντοπισμού του κρίσιμου κώνου, εφαρμόστηκε μια τεχνική τοπικής γραμμικοποίησης του κριτηρίου διαρροής για κάθε διατομή, σε κάθε επανάληψη του αλγορίθμου βελτιστοποίησης. Σύμφωνα με την προτεινόμενη διαδικασία, τα επίπεδα διαρροής δεν είναι εκ των προτέρων καθορισμένα, αλλά προσδιορίζονται για κάθε διατομή, σε κάθε επανάληψη. Αυτή η διαδικασία παρέχει ακριβέστερες λύσεις, ενώ παράλληλα αποφεύγεται η εκ των προτέρων γραμμικοποίηση του κριτηρίου διαρροής.

Επιπλέον, και για αυτήν τη θεώρηση, ενσωματώθηκαν νόμοι πολυγραμμικής ή μη-γραμμικής κράτυνσης/χαλάρωσης (hardening/softening), χωρίς να επηρεάζεται το μέγεθος του προβλήματος. Στην περίπτωση της πολυγραμμικής κράτυνσης, εντοπίζεται το ευθύγραμμο τμήμα κράτυνσης, το οποίο αντιστοιχεί σε κάθε διατομή, μορφώνονται τα μητρώα κράτυνσης μόνο για το τμήμα αυτό (και όχι για όλα τα δυνατά). Στην περίπτωση της μη-γραμμικής κράτυνσης, ο υπολογισμός του

μεγεθυμένου/συρρικνωμένου ορίου διαρροής είναι άμεσος και προκύπτει από την τιμή του πλαστικού πολλαπλασιαστή.

Η υιοθέτηση των παραπάνω παρεμβάσεων επηρεάζουν και τη μόρφωση της συνθήκης συμπληρωματικότητας, μειώνοντας στο ελάχιστο το πλήθος τους. Κατ'αυτόν τον τρόπο, διευκολύνεται η σύγκλιση του αλγορίθμου βελτιστοποίησης, καθώς η συγκεκριμένη συνθήκη αποτελεί την πηγή της αριθμητικής αστάθειας του προβλήματος.

Τα αριθμητικά αποτελέσματα των αναλύσεων που πραγματοποιήθηκαν επιβεβαιώνουν την εφαρμοσιμότητα και την υπολογιστική αποτελεσματικότητα των προτεινόμενων θεωρήσεων σε επίπεδα και τρισδιάστατα πλαίσια. Τέλος, συμπεραίνεται ότι η αλληλεπίδραση των εντατικών μεγεθών επηρεάζει την και σε ορισμένες περιπτώσεις και τον μηχανισμό κατάρρευσης των κατασκευών και για αυτόν τον λόγο πρέπει να λαμβάνονται υπόψιν, στοχεύοντας σε έναν ασφαλέστερο σχεδιασμό των κατασκευών.

Τα αποτελέσματα της παρούσας εργασίας μπορούν να αποτελέσουν εφαλτήριο για μελλοντική έρευνα στις ακόλουθες κατευθύνσεις:

- Ενσωμάτωση της γεωμετρικής μη-γραμμικότητας στις προτεινόμενες θεωρήσεις.
- Η μη-ολονομική θεώρηση μπορεί να αντιμετωπιστεί σαν μια σταδιακή (stepwise) ολονομική, υιοθετώντας γραμμικοποιημένα ή μη-γραμμικά κριτήρια διαρροής και καταστατικούς νόμους.
- Η ανάπτυξη μαθηματικών διαδικασιών που χειρίζονται πιο αποτελεσματικά τη συνθήκη συμπληρωματικότητας.
- Εφαρμογή των προτεινόμενων προσεγγίσεων σε προβλήματα επίπεδης τάσης και επίπεδης παραμόρφωσης, σε προβλήματα μηχανικής ρωγμών (fracture mechanics) και σε γεωτεχνικά προβλήματα (slope stability analysis, lateral earth pressures on rigid retaining structures etc.).

Ο συνδυασμός της οριακής ανάλυσης με το μαθηματικό προγραμματισμό δημιουργεί ένα πολλά υποσχόμενο πεδίο, το οποί αντιμετωπίζει την ανάλυση των κατασκευών ακολουθώντας ένα μαθηματικό μονοπάτι με φυσικούς περιορισμούς. Η ανάγκη για την ανάπτυξη μιας θεωρίας, που θα παρέχει ένα θεωρητικό υπόβαθρο, αλλά και μια γόνιμη μεθοδολογία για αριθμητική επίλυση, παραμένει επιτακτική, για την πλήρη εκμετάλλευση του δυναμικού αυτών των μεθόδων.

Table of Contents

Chapter 4:
Limit Load and Deformation Analysis for Plane Frames: A Cone Identification Approach

Chapter 7:
Concluding Remarks and Future Research

Chapter 1

Introduction

1.1. Background and motivation

Structural analysis retains a central role in civil engineering field laying a solid base for safe and economic structural design. It deals with the determination of structural response (elastic and inelastic) when excited by specific loads. More specifically, structural analysis results in the evaluation of internal forces, stress resultants, displacements and deformations that are developed throughout the structure. A variety of methods have been developed to evaluate inelastic response of structural systems, most of which follow the evolution of the inelastic deformations within a structure until collapse. However, the ultimate state, which is of primal interest in engineering design, can be obtained almost instantaneously via limit analysis methods.

Limit analysis, which is based on the assumption of rigid-perfectly plastic constitutive behavior, aims at determining directly the ultimate load that a structure can sustain and has constituted a robust tool for structural design. The same notion of the direct determination of an ultimate -in mathematical terms- state is also enforced by mathematical programming that determines directly the values of a set of variables corresponding to the best (minimum or maximum) value of an objective function. The merging of limit analysis methods with mathematical programming offered the means for determining the ultimate structural state following a different mathematical path. A great variety of mathematical programming techniques appropriate to treat structural analysis problems has been enforced, depending on the structural behavior (path-dependent (nonholonomic) or path-independent (holonomic)), the constitutive laws (presence or absence of softening), the presence of ductility limitations, the approximation of the yield surface and the objective function.

Limit analysis for linearized yield criteria and rigid-perfectly plastic behavior can be cast as a Linear Programming (LP) problem enforcing the static (lower bound) and kinematic (upper bound) theorems. This formulation prompted and supported by the bloom of LP (Kantorovich 1940, Dantzig 1947) set the ground for the establishment of mathematical programming techniques in structural analysis. Since 1951 when Charnes and Greenberg implemented LP for the analysis of trusses for the first time, a remarkable progress has been exhibited in this field. Maier et al. (1967,1977, 2002,2003) extended the formulation addressing both perfectly plastic and hardening/softening structural behavior on the basis of holonomic (path-independent)

or nonholonomic (path-dependent) considerations. The central point of this formulation relies on the piecewise linearization of the yield criteria and constitutive relations that enable their expression as linear constraints. Incorporation of deformation constraints and/or softening behavior enforces the complementarity condition that excludes the activation of plastic deformation with nonzero strength reserves. It is of disjunctive nature and constitutes the main source of numerical instabilities of the problem. Thus, a variety of alternative mathematical programming procedures for structural analysis has been generated, such as iterative Linear Programming, Quadratic and Parametric Quadratic Programming, Restricted Basis Linear Programming, Linear and Parametric Linear Complementarity approaches, Mathematical Programming with Equilibrium Constraints (MPEC) (Luo, Pang and Ralph 1996, Maier et al. 1977,1979, Tangaramvong and Tin-Loi 2007). It is worth mentioning that these formulations for structural analysis have been supported and promoted by the developments in mathematical programming concerning the treatment of complementarity condition (Fukushima and Lin 2004). More recently, second-order cone programming (SOCP) has been employed for structural analysis that can be further generalized in the framework of semidefinite programming (SDP) (Martin and Makrodimopoulos 2008, Skordeli and Bisbos 2010).

The majority of the aforementioned mathematical programming approaches is based on an a priori piecewise linearization of the yield surface and constitutive laws, combining the size of the problem with the discretization. Yield condition is formulated calculating the strength reserves for every critical section and for all possible hyperplanes of the piecewise linearized yield surface. This defines a vector of reserves for every critical section with multiplicity equal to the number of hyperplanes of the yield hypersurface. The same number of plastic multipliers is also engaged for all possible plastic deformations, which together with the corresponding strength reserves compete within the discrete in nature complementarity condition. This perplexing procedure generates unnecessary information that increases prohibitively the size of the problem especially for a finer discretization of the yield surface.

1.2. Research objectives

This work aims at addressing limit analysis problems with hardening/softening behavior and ductility constraints in the framework of mathematical programming.

The combination of structural analysis with mathematical programming has mainly been based on the piecewise linearization of yield surface and constitutive laws. Although this approach proved versatile paving the way for the efficient use of a great variety of mathematical programming techniques, it may become prohibitive for large-scale problems or/and fine discretization. Thus, the aim of this work is to enhance the existing formulation by addressing limit structural analysis in the framework of mathematical programming in a unifying and more efficient way for large-scale problems.

The specific research objectives concerning the formulation and the treatment of the problem are:

- To highlight the inner structure and drawbacks of the existing methods.
- To enhance the existing formulation aiming at uncoupling the size of the problem from the discretization of the yield surface.
- To incorporate efficiently multi-linear or nonlinear constitutive laws.
- To apply the proposed formulations in plane and 3D frames and examine their computational efficiency compared to the existing formulation for multi-component interaction.

The problems that are addressed in this work concern holonomic (path-independent) structural behavior, while the considerations of constitutive behavior and yield surface are shown in Table 1.1.

Table 1.1: Considerations of constitutive behavior and yield surface.

Constitutive Behavior	Rigid-perfectly plastic behavior or hardening with unlimited ductility	
	Softening behavior or hardening with limited ductility	Piecewise Linear
		Nonlinear
Yield Surface	Piecewise Linear	Hyperplane Equations
		Convex Hull
	Nonlinear	

Based on these, the following problems are formulated and treated in this dissertation for limit analysis of structures in the context of mathematical programming:

1. Rigid-perfectly plastic behavior with piecewise linear (PWL) yield surface (hyperplane equations and convex hull formulation).
2. PWL hardening/softening behavior and PWL yield surface.
3. PWL hardening/softening behavior and nonlinear yield surface.
4. Nonlinear hardening/softening behavior and nonlinear yield surface.

The aforementioned problems enforce different mathematical programming techniques. The first category is formulated as a Linear Programming problem, while the other three are formulated as a Mathematical Programming with Equilibrium Constraints (MPEC) problem. The equilibrium constraints are in this case the complementarity conditions which are required due to the presence of softening or/and displacement limitations.

1.3. Outline of the dissertation

The content of this dissertation is outlined as follows:

In Chapter 2, a literature survey is presented reviewing the merging of limit analysis and mathematical programming and how this enriched structural analysis.

Chapter 3 deals with limit analysis of plane frames in the context of Linear Programming introducing a convex hull formulation for expressing the yield condition in static and kinematic theorem. The proposed formulation differs in the number of variables and yield constraints compared to the standard one, which expresses yield condition as the intersection of halfspaces. The two formulations are compared in terms of computational efficiency. Numerical results of plane steel frames prove the computational advantages of convex hull formulation especially for 3D stress resultant interaction and demonstrate the effect of combined stresses on the load carrying capacity.

In Chapter 4, limit load and deformation structural analysis under holonomic assumption is addressed in the context of mathematical programming, aiming at determining the ultimate load capacity of frame structures at incipient collapse. Equilibrium and compatibility requirements together with strength and complementarity constraints are used to formulate an optimization problem aiming at maximizing the loading factor. For every stress point and optimization iteration, a cone identification approach is proposed enabling the formulation of yield and complementarity conditions only for the specific targeted or activated yield

hyperplane. Moreover, multi-segmental isotropic hardening/softening behavior of critical sections is incorporated in a direct and efficient manner in the yield condition. The entire formulation is not affected by the linearization of either the yield surface or the constitutive relations and succeeds in reducing the size of yield and complementarity conditions to a minimum. The cases of axial force-bending moment and axial-shear force-bending moment interaction are included. Numerical results are presented verifying the validity and efficiency of the proposed method and underline the role of combined stresses in specific cases.

Chapter 5 deals with limit load and deformation analysis of plane structures considering nonlinear interaction and nonlinear structural behavior in the context of mathematical programming. A new approach is proposed that retains the nonlinearity of the yield surface applying a local linearization technique for every stress point and optimization iteration. Moreover, isotropic nonlinear hardening/softening cross-sectional behavior is efficiently incorporated. The final formulation of yield and complementarity condition is of a minimum size, while the linearity of the finally formed yield constraints is retained. The computational efficiency of the proposed method is compared to that of cone identification approach for several plane frames considering axial force-bending moment and axial-shear force-bending moment interaction.

In Chapter 6 limit load and deformation analysis with mathematical programming is extended to 3D frame analysis. The ultimate load is evaluated through a nonlinear programming problem with equilibrium, compatibility, yield and complementarity constraints. The nonlinear inelastic structural behavior is either approximated with linear segments (cone identification approach) or embedded retaining its nonlinearity (local linearization technique). Furthermore, a holonomic (path-independent) structural behavior is assumed and hardening/softening behavior is considered isotropic. Numerical results are presented to demonstrate the validity of the proposed method for 3D frame analysis, accounting for axial force-biaxial bending moment interaction.

In Chapter 7 the main conclusions of this work are presented, while future research directions are highlighted.

Moreover, five appendices are included. Appendix A concerns the standard form of Linear Programming problems and the primal-dual relations of Linear Programming. In Appendix B, Karush-Kuhn-Tucker conditions are included and the

barrier function interior-point method is presented. Appendix C contains the equations of yield lines for axial force-bending moment interaction, while Appendix D describes the equations of yield planes for axial-shear force-bending moment interaction. Appendix E describes the relations of first-optimality measure required for the optimization procedure.

Chapter 2

Limit Analysis and Mathematical Programming-Literature Review

2.1. Limit analysis

Limit analysis of structures based on rigid-perfectly plastic constitutive behavior has offered the means to assess directly the ultimate capacity of frame, plate and other structures. The incremental analysis physically traces the entire evolution of structural response to a monotonically increasing external loading identifying the sequence of plastic hinge formation until collapse. The main interest though from an engineering point is primarily on the final stage of plastic response-plastic collapse. In this respect, limit analysis has been proved very efficient in the determination of the ultimate structural state, affecting also the context of design of structures, components and connections.

In essence, limit load analysis monitors only the developed stresses disregarding the existing deformations, which do not participate in the problem. This one sided formulation is also carried out successfully by the driving power of optimization. The fundamental theorems of plasticity that serve as the solid base of limit analysis are the static, kinematic and uniqueness theorems (Neal 1977, Jiràsek and Bažant 2002). Attempts to formulate these theorems go back to the 18^{th} century, but it was Kazinczy (1914) that introduced plastic limit analysis by evaluating and verifying experimentally the failure load of a clamped beam. Kist (1917,1920) and Grüning (1926) utilized similar notions following rather an engineering intuition than a strict mathematical formulation. A proof was established by Gvozdev (1938) and later by Horne (1949) and by Greenberg and Prager (1951). According to the static (lower bound) theorem, the collapse load of a structure that corresponds to a statically admissible state (satisfying equilibrium and yield conditions) is either less than or equal to the true collapse load, while the kinematic (upper bound) theorem states that the collapse load or load factor obtained for a structure that corresponds to a kinematically admissible solution is either greater than or equal to the true collapse load. On the basis of the weak and strong duality theorems (Luenberger and Ye 2008), theoretically there is no duality gap, i.e. both theorems approach the true value from below and above respectively (uniqueness theorem).

2.2. Mathematical programming

Mathematical programming or mathematical optimization is the process followed for the selection of the best element (with regard to some criteria) from some set of available alternatives. The aim is to find the values of certain decision variables that give the minimum or maximum value of a real objective function, i.e. unconstrained optimization, which when subjected to equality or/and inequality constraints lead to constrained optimization problems. The generalization of optimization theory and techniques has allowed an amplified application in a large variety of fields, such as economics, mechanics, engineering, operation research, control engineering etc. Due to the great diversity of optimization problems, a corresponding large number of optimization methods and algorithms have been developed for their solution. The different types of optimization problems are classified as presented in Table 2.1 (Rao 2009). Linear and Nonlinear Programming constitute the two main optimization techniques used in structural analysis and therefore are shortly discussed in the following sections.

Table 2.1. Classification of optimization problems.

Classification based on…	Existence of Constraints	Constrained optimization problem
		Unconstrained optimization problem
	Nature of Design Variables	Parameter or static optimization problem
		Trajectory or dynamic optimization problem
	Physical Structure of the Problem	Optimal control problem
		Nonoptimal control problem
	Nature of Equations involved	Nonlinear programing problem
		Geometric programming problem
		Quadratic programming problem
		Linear programming problem
	Permissible Values of Design Variables	Integer programming problem
		Real-valued programming problem
	Deterministic Nature of the Variables	Deterministic programming problem
		Stohastic programming problem
	Separability of the Functions	Separable programming problem
		Nonseparable programming problem
	Number of the Objective Functions	Single-objective programming problem
		Multi-objective programming problem

2.2.1. Linear programming

Linear programming (LP) is the optimization process applicable for the solution of problems in which the objective function and the constraints (equality and inequality) appear as linear functions of the decision variables. Even though the problem of solving a system of linear inequalities dates back at least as far as Fourier, the Linear Programming method was first initiated by Kantorovich in 1939, aiming at maximizing the production in a plywood industry. The simplex method was devised and published after the war by Dantzig in 1947 amplifying the use of Linear Programming, while John von Neumann developed the theory of duality as a linear optimization solution and applied it in various fields and in game theory. Since then, Linear Programming meets a wide range of applications in many fields, for example operations research, economics, management and engineering.

The general Linear Programming problem can be established in the following standard forms (Luenberger and Ye 2008):

$$\left.\begin{array}{l} \text{Minimize} \quad f(x_1, x_2, ..., x_n) = c_1 x_1 + c_2 x_2 + \cdots + c_n x_n \\ \text{subject to:} \\ \qquad a_{11}x_1 + a_{12}x_2 + \cdots + a_{1n}x_n = b_1 \\ \qquad a_{21}x_1 + a_{22}x_2 + \cdots + a_{2n}x_n = b_2 \\ \qquad \vdots \\ \qquad a_{m1}x_1 + a_{m2}x_2 + \cdots + a_{mn}x_n = b_m \\ \qquad x_1 \geq 0 \\ \qquad x_2 \geq 0 \\ \qquad \vdots \\ \qquad x_n \geq 0 \end{array}\right\} \textit{scalar form} \tag{2.1}$$

where c_j, b_j and a_{ij} (i=1,2…,m; j=1,2,…,n) are known constants and x_j are the decision variables.

$$\left.\begin{array}{l} \text{Minimize} \quad f(\boldsymbol{X}) = \boldsymbol{c}^T \boldsymbol{X} \\ \text{subject to:} \\ \qquad \mathbf{aX} = \mathbf{b} \\ \qquad \mathbf{X} \geq \mathbf{0} \end{array}\right\} \textit{matrix form} \tag{2.2}$$

where

$$\boldsymbol{X} = \begin{Bmatrix} x_1 \\ x_2 \\ \vdots \\ x_n \end{Bmatrix}, \quad \mathbf{b} = \begin{Bmatrix} b_1 \\ b_2 \\ \vdots \\ b_n \end{Bmatrix}, \quad \mathbf{c} = \begin{Bmatrix} c_1 \\ c_2 \\ \vdots \\ c_n \end{Bmatrix},$$

$$\mathbf{a} = \begin{bmatrix} a_{11} & a_{12} & \cdots & a_{1n} \\ a_{21} & a_{22} & \cdots & a_{2n} \\ \vdots & & & \\ a_{m1} & a_{m2} & \cdots & a_{mn} \end{bmatrix}$$

The above relations refer to the standard form of the LP problem since the objective function is of minimization type, all constraints are of equality type and all decision variables are nonnegative (Appendix A). It is shown that any LP problem can be expressed in standard form by using appropriate transformations. The possible results of an LP problem are (1) a unique and finite optimum solution, (2) an infinite number of optimal solutions, (3) an unbounded solution, (4) no solution or (5) a unique feasible point. The geometrical representation of the solution includes a convex polytope dictated by the constraints, since they are expressed as the intersection of a finite number of halfspaces and hyperplanes. The objective function attains its smallest (or largest) value at an extreme point or vertex of the polyhedron (if such point exists).

As mentioned before, simplex method constitutes the first and most popular one for LP problems. It is based on a pivotal operation that generates all basic solutions and selects the one that is feasible and corresponds to the optimal value of the objective function (Spillers and MacBain 2009). However, for large scale problems simplex method is computationally cumbersome in terms of storage and time (the worst-case complexity of simplex method is exponential in the problem dimension). Khachiyan's ellipsoid method devised in 1979 is the first polynomial-time LP algorithm. In 1984 Karmarkar developed a more efficient algorithm known as interior-point method. Simplex method searches along the boundary of the feasible space by moving from one feasible vertex to a promising adjacent one until the optimum point is found. Karmarkar's method approaches the optimal solution following directions in the interior of the feasible space, attracted by the field of the objective function and repelled by the constraints.

LP problems are characterized by their duality (Appendix A). Every LP problem, considered as primal, is associated with another LP problem, the so-called dual. Given the optimal solution of the one, the optimal solution of the other can be obtained. In fact, it is immaterial which problem is designated the primal since the dual of a dual is the primal. Because of these properties, the solution of a linear programming problem can be obtained by solving either the primal or the dual, whichever is easier. The primal–dual relationships of a general LP problem aiming at minimizing or maximizing a linear objective function subject to a set of equality and inequality constraints with nonnegative variables or variables unrestricted in sign are given by the following relations (Rao 2009):

Primal	***Dual***
Minimize $\boldsymbol{c}^T\boldsymbol{X}$	Maximize $\boldsymbol{Y}^T\boldsymbol{b}$
variable $x_i \geq 0$	i^{th} *constraint* $\boldsymbol{Y}^T A_i \leq c_i$
variable x_i *unrestricted in sign*	i^{th} *constraint* $\boldsymbol{Y}^T A_i = c_i$
j^{th} *constraint* $A_j\boldsymbol{X} = b_j$	j^{th} *variable* y_j *unrestricted in sign*
j^{th} *constraint* $A_j\boldsymbol{X} \geq b_j$	j^{th} *variable* $y_j \geq 0$
Coefficient matrix $\boldsymbol{A} = [\boldsymbol{A}_1 \quad \dots \quad \boldsymbol{A}_m]$	*Coefficient matrix* $\boldsymbol{A}^T = [\boldsymbol{A}_1 \quad \dots \quad \boldsymbol{A}_m]^T$
Right - hand - side vector $\boldsymbol{b}$	*Right - hand - side vector* $\boldsymbol{c}$
Cost coefficients $\boldsymbol{c}$	*Cost coefficients* $\boldsymbol{b}$

(2.3)

If there is a difference between the optimal value of the primal and the optimal value of the dual problem, then weak duality holds and the difference of the primal values is called duality gap. Strong duality holds if and only if the duality gap is zero.

2.2.2. Nonlinear programming

Nonlinear programming (NLP) is the optimization process applicable for the solution of problems in which the objective function or/and the constraints (equality or/and inequality) appear as nonlinear functions of the decision variables. The general formulation of a constrained nonlinear optimization problem is as follows:

$$\begin{aligned} &\text{minimize} \quad f(\boldsymbol{X}) \\ &\text{subject to} \quad g_i(\boldsymbol{X}) \leq 0, \; i = 1, 2, \dots m \\ &\qquad\qquad\; h_j(\boldsymbol{X}) = 0, \; j = 1, 2, \dots l \end{aligned} \tag{2.4}$$

In nonlinear programming, Karush-Kuhn-Tucker (KKT) conditions (Karush 1939) are first-order necessary conditions for a solution to be optimal (Appendix B), provided that some regularity conditions are also satisfied. The most used regularity conditions are (Bertsekas 1995) the: Linearity Constraint Qualification (if g_i and h_j are affine functions, then no other condition is needed), Linear Independence Constraint Qualification (the gradients of the active inequality and the gradients of the equality constraints are linearly independent at the solution point) and Mangasarian–Fromovitz Constraint Qualification (the gradients of the active inequality constraints and the gradients of the equality constraints are positive-linearly independent at the solution point). The necessary conditions are sufficient, if the problem is convex, namely the objective function is concave (maximization problem) or convex (minimization problem) and the constraint set is also convex. In general, though, the necessary conditions are not sufficient for optimality and additional information is required, such as the Second Order Sufficient Conditions (SOSC). As far as the methods that treat NLP problems are concerned, convex optimization problems can be solved by the following contemporary methods: bundle methods, subgradient projection methods, interior-point methods, cutting-plane methods, ellipsoid method etc. (Hiriart-Urruty and Lemaréchal 1993, Boyd and Vandenberghe 2009). For nonconvex optimization problems several approaches are available, such as extended bundle methods, branch and bound methods, evolutionary approaches etc. (Bertsekas 2003, Boyd and Vandenberghe 2009).

2.3. Limit load and deformation analysis with mathematical programming

The structural response in the general case involves a linear elastic and a plastic part. The evolution of plastic behavior can be described following either a path-independent or a path-dependent mathematical formulation. The first one includes constraints of holonomic form, i.e. $f(q_1, q_2 ... q_n, t) = 0$ depending only on the coordinates q_j of the system and time t, while the path-dependent behavior includes non-holonomic constraints of the form $f(q_1, q_2 ... q_n, \dot{q}_1, \dot{q}_2, ... \dot{q}_n, t) = 0$ that are also velocity-dependent (Greenwood 2003). The path-independent plastic behavior, denoted also as holonomic, assumes that any local unloading occurs along the load-

displacement path (Fig. 2.1a) and the flow rule in that case is expressed in total quantities (deformation theory). The nonholonomic behavior is depicted in Fig. 2.1b and the flow rule includes rate quantities (flow rule theory) (Lubliner 2006).

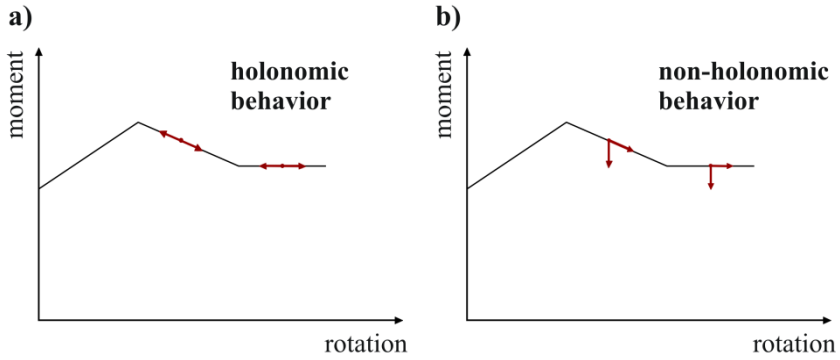

Fig. 2.1: a) Holonomic and b) nonholonomic consideration.

The treatment of structural analysis in the framework of mathematical programming depends on the structural behavior (path-dependent (nonholonomic) or independent (holonomic)), the constitutive laws (presence or absence of softening), the presence of ductility limitations (limited displacements or/and deformations), the approximation of the yield surface and the choice of the objective function.

For linearized yield criteria and rigid-perfectly plastic behavior, as well as hardening behavior with unbounded plastic deformations, limit analysis can be cast as a Linear Programming (LP) problem that is computationally advantageous. The use of LP and its duality offer the supportive mathematical structure for the two theorems of limit analysis, i.e. the static (lower bound) theorem and the kinematic (upper bound) theorem. The first approaches the true load factor from below for statically admissible trials that satisfy equilibrium and yield conditions, while the second determines an upper bound of the load factor among kinematically admissible solutions that are stressed within the yield limits (Jiràsek and Bažant 2002, Wong 2009).

Incorporation of Linear Programming (LP) into limit analysis was introduced by Fourier as stated by Prager and pointed out by Maier (1984). Charnes and GreenBerg (1951) implemented LP for the ultimate state analysis of trusses. A finite element approach to optimal design of plastic structures in plane stress was proposed by Maier et al. (1972) formulating and mechanically interpreting both primal and dual problems. Limit analysis for two- and three-dimensional structures using finite

element procedures and linear programming techniques was also described and discussed by Anderheggen and Knöpfel (1972). Plane stress problems were addressed by Zavelani (1973,1974) in the context of linear programming expressing the stress vectors as linear nonnegative combinations of the vertices of the yield polyhedron. This expression, denoted as vertex or corners formulation, resulted in a reduced formulation of the yield condition and it was used for the optimal distribution of thickness following static and kinematic approaches. The same yield expression was used for the shakedown analysis of two- and three- dimensional structures with LP initiating the primal and dual formulations of the problem (Corradi and Zavelani 1974). A variety of alternative mathematical programming procedures for limit analysis of discrete structures described by piecewise linear (PWL) elastic-perfectly plastic constitutive laws were formulated and compared with respect to their computational merit by Maier et al. (1977). Franchi and Cohn (1980) presented also a finite element formulation for elastic-plastic problems with mathematical programming using a general software appropriate for structural plasticity by mathematical programming (Franchi 1977). The effect of combined stresses on the ultimate state of structures was addressed by Polizzotto (1975) and generalized by Grierson and Aly (1980).

For the case of softening or hardening with limited ductility, the need of complementarity condition emerges. This condition expresses mutually exclusive situations in the form of an inner product of two nonnegative vectors that should be zero. Its physical interpretation relies on the fact that simultaneous activation of plastic deformation with strength reserves is meaningless. The consideration of deformations for the complementarity condition generates the need for compatibility relations. Thus, structural analysis is formed as an optimization problem with constraints imposed by equilibrium, compatibility relations, yield and complementarity conditions.

This extended formulation of structural analysis in the context of mathematical programming was initiated by Maier and coworkers accounting for isotropic and kinematic hardening/softening behavior and addressing both holonomic and non-holonomic problems. Piecewise linearization of yield surface and constitutive laws results in the linear expression of all relations. However, the complementarity condition, triggered by the presence of softening, is of disjunctive nature and its special treatment has raised the development of specific mathematical programming

algorithms. A quadratic programming approach was used for structural analysis based on piecewise linearized yield surfaces and multi-linear constitutive relations (Maier 1968, 1970, Capurso and Maier 1970). De Donato and Maier (1972) treated the inelastic analysis of reinforced concrete frames with limited rotation capacity as a Linear Complementarity Problem (LCP). This was further extended to a Parametric Linear Complementarity Problem (PLCP) for the elastoplastic analysis of frames (De Donato and Maier 1976). Alternatively, Maier et al. (1979) presented a Restricted Basis Linear Programming (RBLP) formulation for the analysis of discrete structures which is based on a LP procedure enriched with an additional rule for the enforcement of complementarity relation at each pivotal step. Later, Kaneko and Maier (1981) proposed a branch-and-bound technique and an iterative procedure for the optimal design of truss structures under displacement and deformation constraints. Wakefield and Tin-Loi (1990) adopted Kaneko's formulation (1979) for the nonholonomic elastoplastic analysis detecting non-uniqueness of deformation history. Incorporation of nonlinear hardening laws in elastoplastic analysis led to the formulation of a Nonlinear Complementarity Problem (NCP) that was solved at each loading instance in the context of a stepwise holonomic approach (Tin-Loi and Pang 1993). Ferris and Tin-Loi (1999) formulated the minimum weight design problem as a Mathematical Programming with Equilibrium Constraints (MPEC) problem and via GAMS modeling language proposed two algorithms for its solution, i.e. a penalty formulation and a relaxation approach that treat appropriately the complementarity condition. The latter was also used for limit analysis of frictional block assemblies (Ferris and Tin-Loi 2001). The MPEC formulation -appropriately converted into a NLP problem- was also adopted for i) the elastoplastic analysis of semirigid frames under quasistatic loads and geometric nonlinearity consideration (Tangaramvong and Tin-Loi 2011), ii) the ultimate load determination of structures with frictional contact supports under the effect of stress interaction for nonholonomic and holonomic considerations (Tangaramvong and Tin-Loi 2011, 2012) and iii) the post-collapse response of rigid-perfectly plastic structures (Tangaramvong et al. 2011).

Limit load and deformation analysis including softening behavior was examined by Maier et al. (1967, 1973). Tin-Loi and Xia (2001) formulated holonomic structural analysis with nonlinear and piecewise linear softening behavior as a complementarity problem and implemented it in PATH solver (Dirkse and Ferris 1995). Cocchetti and Maier (2003) discussed softening behavior for elastic-plastic and combined limit load

and deformation analysis in the framework of mathematical programming. Tangaramvong and Tin-Loi (2007) used a Mixed Complementarity Problem (MCP) formulation for both holonomic and nonholomic structural considerations and compared their results for isotropic softening under the effect of combined stresses (axial force-bending moment interaction). It was concluded that holonomic analysis is sufficiently accurate for the case of monotonically increasing loading. Holonomic analysis for softening behavior under combined stresses was also formulated as a MPEC problem proposing various nonlinear programming based algorithms for its solution (Tangaramvong and Tin-Loi 2008). A combined limit load and deformation analysis method based on mathematical programming was proposed by Ardito et al. (2008) appropriate to address also nonassociated flow rules and softening structural behavior. Moreover, a "sifting" procedure was developed that reduces the size of yield condition. A constrained non-linear system approach for structural analysis as a MPEC problem was presented by Tangaramvong and Tin-Loi (2010), while the same authors in a separate work incorporated geometric nonlinearity effects in nonholonomic analysis with softening structural behavior (2010). More recently, the analysis of softening frames was dealt as a RBLP problem by Mahini et al. (2014), using a dissipated energy maximization approach (Mahini et al. 2013).

It is worth noting that the aforementioned enhancement of structural analysis was driven and supported by the developments in mathematical programming that treated properly complementarity problems. Lemke's algorithm was one of them, appropriate for LCP and Mixed LCP (Lemke 1965). Furthermore, the exploration of the complementarity problem by Cottle (1972) directed the formulation of elastoplastic analysis in the form of a LCP or PLCP, while Kaneko later proposed a reformulation of this problem (1979). Tin-Loi and Tseng (2003) proposed a computationally efficient method suitable for capturing the multiplicity of solutions of the LCP in quasibrittle fracture analysis. From a mathematical standpoint, solution for LCP remains an open issue (Hadjidimos et. al 2012). Dirkse and Ferris (1995) developed the PATH solver, a software appropriate for Mixed Complementarity problems. Furthermore, the development of algorithms appropriate for Mathematical Programming with Equilibrium Constraints (MPEC) problems (Luo et al. 1996) extended the potential of the proposed methods for structural analysis for both holonomic and nonholonomic assumptions. The equilibrium constraints -that for structural analysis problems are actually the complementarity constraints- fail to

satisfy the Linear Independence Constraint Qualification (LICQ) or the Mangasarian–Fromovitz Constraint Qualification (MFCQ), making the feasible region of the problem nonconvex and not connected. Thus, the MPEC problem requires special treatment and can be solved as a sequence of nonlinear programming problems adopting approaches (Fukushima and Lin 2004), such as relaxation methods (Lin and Fukushima 2005), smoothing formulations (Facchinei et al. 1999, Fukushima and Pang 1999, Lin and Fukushima 2003, Yu and Pu 2011), the penalty function approach (Huang et al. 2006, Lin and Fukushima 2003), the active-set identification method (Fukushima and Tseng 2002), sequential quadratic programming (SQP) (Fletcher et al. 2001, Jiang and Ralph 2000), the filter-SQP (Fletcher and Leyffer 2002) and interior point methods (Liu and Sun 2002). It is worth noting that the aforementioned methods provide local optimal solutions and therefore a variety of branch and bound techniques has been proposed for global optimal solutions (Liu and Zhang 2002).

The approximation of the nonlinear yield surface is interlinked with the enforcement of the mathematical programming technique appropriate for the structural analysis and therefore deserves a special reference. The piecewise linearization of the nonlinear yield surface enables the expression of yield condition as a set of linear constraints. This kind of approximation offers computational advantages either under the assumption of unlimited ductility allowing for the use of LP or combined with any other mathematical programming approach. Hodge (1977) initiated a method for automatic piecewise linearization of an arbitrary yield surface, while Cannarozzi (1980) used a sequence of circumscribing polyhedra for the approximation of the yield surface. Other methods were proposed by Wong and Tin-Loi (1986), Tin-Loi (1990) and Ardito et al. (2008). More recently, methods for approximating the yield surface with ellipsoids were proposed forming second-order cone programming (SOCP) problems (Skordeli and Bisbos 2010, Bleyer and Buhan 2013) and semidefinite programming (SDP) problems (Martin and Makrodimopoulos 2008).

It is worth noting that the majority of the aforementioned formulations depends on the piecewise linearization of yield surface and constitutive laws that allow for their expression as linear constraints. Despite the computational advantages of this linearization technique, the size of the problem is combined with the discretization, restricting the applicability of these methods, especially for the case of large-scale problems and/or fine discretization of the yield surface.

Chapter 3

Limit Analysis for Plane Frames:
A Convex Hull Formulation

3.1. Basic assumptions

The ultimate state of a structure under the assumption of rigid-perfectly plastic behavior can be determined by using the lower and upper bound theorems of limit analysis. The static limit theorem provides a lower bound of load factor that satisfies equilibrium and yield condition. The kinematic static theorem determines an upper bound of the load factor among all kinematically admissible solutions.

Plane frames are considered herein consisting of prismatic elements subjected only to nodal loading for simplicity reasons. Moreover, small displacements are assumed to establish equilibrium equations at the initial undeformed configuration. In addition, plastic behavior, if present, is considered only at preselected critical sections, i.e. the end sections of the elements, whereas the remaining parts behave elastically. Yield conditions are appropriately linearized and the behavior of all critical sections is considered rigid-perfectly plastic.

Matrix notation is adopted throughout. Matrices are represented by capital bold-face letters, while vectors by lowercase bold characters.

3.2. Equilibrium of plane frames

Each plane beam element develops six stress resultants at its ends, as shown in Fig. 3.1. Herein, the axial force (s_1^i), bending moment at the start node j (s_2^i) and bending moment at the end node k (s_3^i), are considered as independent primary actions for member i. Thus, the six end actions of the element can be expressed at the global axes system in terms of the local basic actions by using the corresponding equilibrium matrix as follows:

$$\begin{Bmatrix} F_x^j \\ F_y^j \\ M^j \\ F_x^k \\ F_y^k \\ M^k \end{Bmatrix} = \begin{bmatrix} \cos\omega^i & -\sin\omega^i/L^i & -\sin\omega^i/L^i \\ \sin\omega^i & \cos\omega^i/L^i & \cos\omega^i/L^i \\ 0 & 1 & 0 \\ -\cos\omega^i & \sin\omega^i/L^i & \sin\omega^i/L^i \\ -\sin\omega^i & -\cos\omega^i/L^i & -\cos\omega^i/L^i \\ 0 & 0 & 1 \end{bmatrix} \cdot \begin{Bmatrix} s_1^i \\ s_2^i \\ s_3^i \end{Bmatrix} = \boldsymbol{B}^i \cdot \boldsymbol{s}^i \qquad (3.1)$$

where F_x^j, F_y^j, M^j are the global X and global Y forces and bending moment at the start node and F_x^k, F_y^k, M^k are the actions at the end node of the element i at the global system, ω^i is the angle formed rotating the global X-axis counterclockwise to meet the local x-axis and L^i is the element length, $\boldsymbol{B}^i$ is the (6×3) equilibrium matrix of the element and $\boldsymbol{s}^i$ is the (3×1) stress vector of the element.

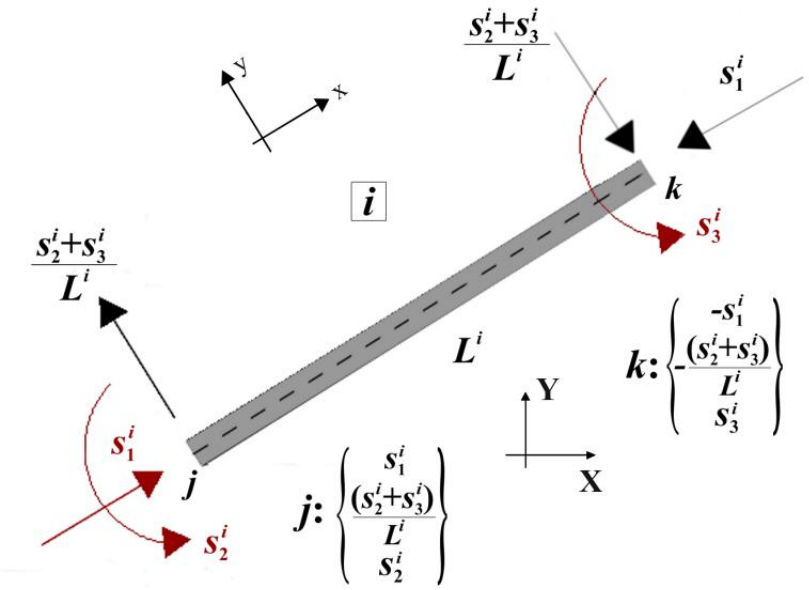

Fig.3.1: Frame element i with equilibrated stress resultants-end actions.

The equilibrium for the whole structure is then established in terms of the unknown vector of stresses of all members as:

$$\boldsymbol{B}\cdot\boldsymbol{s} = a\cdot\boldsymbol{f} + \boldsymbol{f}_d \tag{3.2}$$

where $\boldsymbol{B}$ is the $(n_f\times3n_{el})$ structural equilibrium matrix, assembled by the corresponding element equilibrium matrices arranged in a block diagonal manner, $\boldsymbol{s}$ is a $(3n_{el}\times1)$ vector of all stresses in local systems, a is a scalar load factor, $\boldsymbol{f}$ the $(n_f\times1)$ vector of nodal loading in the global system, $\boldsymbol{f}_d$ is the $(n_f\times1)$ fixed nodal load vector, n_{el} denotes the number of elements and n_f the number of degrees of freedom.

3.3. Deformation decomposition and compatibility relation

The deformations of a frame element i consists (Fig. 3.2) of the axial deformation q_1^i and the two end chord rotations q_2^i, q_3^i of the member. These in general consist of an elastic and plastic part. Since structural behavior is herein considered rigid-perfectly plastic, elastic deformations are not defined and the plastic ones are considered developed along the normal to the yield surface (associative plasticity) at the touching point moving on the surface for further plastic deformation (consistency condition). Thus deformation decomposition for the entire structure is expressed by:

$$\boldsymbol{q} = \boldsymbol{e} + \boldsymbol{p} = \boldsymbol{N} \cdot \mathbf{z} \tag{3.3}$$

where $\boldsymbol{q}$ is the ($3n_{el} \times 1$) deformation vector, $\boldsymbol{e}$ and $\boldsymbol{p}$ are the ($3n_{el} \times 1$) vectors of elastic and plastic deformations respectively, $\boldsymbol{N}$ is the matrix which contains all normal-to yield planes-vectors and is defined in detail in section 3.4.

Compatibility conditions relate the member deformations $\boldsymbol{q}^i$ (Fig. 3.2) to the nodal displacements $\boldsymbol{u}^i$. The compatibility condition for the whole structure is given as:

$$\boldsymbol{q} = \boldsymbol{B}^T \cdot \boldsymbol{u} \Leftrightarrow \boldsymbol{N} \cdot \mathbf{z} = \boldsymbol{B}^T \cdot \boldsymbol{u} \tag{3.4}$$

where and $\boldsymbol{u}$ is the ($n_f \times 1$) nodal displacement vector.

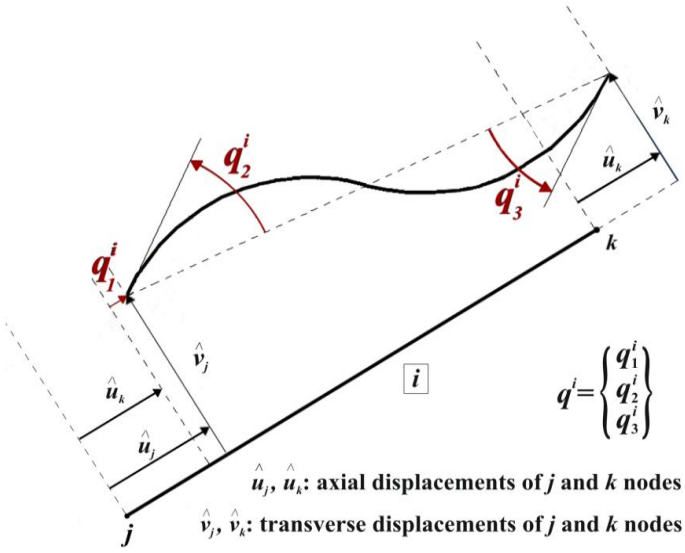

Fig. 3.2: Displacements and deformations of element i.

3.4. Yield condition for multi-component interaction

3.4.1. Hyperplane equations - standard formulation

The nonlinear yield criterion is a priori linearized forming a polyhedron that facilitates the expression of the yield condition as a set of linear constraints. The elastic domain is denoted by the common space of all halfspaces in the form (Boyd and Vandenberghe 2009):

$$\left\{ \boldsymbol{s_d} \mid \mathbf{a}^T \cdot \boldsymbol{s_d} \leq \boldsymbol{r_d} \right\} \tag{3.5}$$

where $\mathbf{a}$ is the unit normal vector of the hyperplane, $\boldsymbol{s}_d$ is the vector of normalized stresses and $\boldsymbol{r}_d$ determines the offset of the hyperplane from the origin**.** The geometrical interpretation of yield condition is presented in Fig. 3.3, where the dimensionless quantity $\boldsymbol{w}_d$ denotes the normalized reserve of the particular cross section.

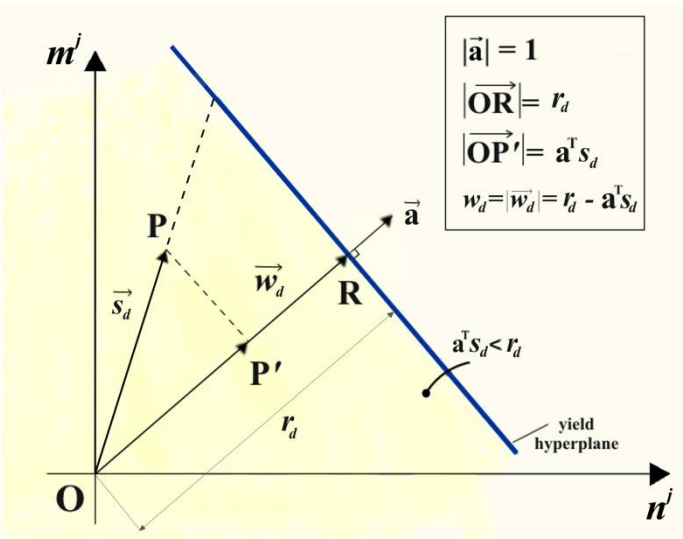

Fig. 3.3: Geometrical interpretation of yielding.

In this section, yield condition is defined as a set of a finite number of linear inequalities, which geometrically represent the intersection of a finite number of halfspaces and hyperplanes. In general, considering the interaction of d number of stress resultants (d -component interaction) and the yield surface of dimension d is

approximated with h hyperplanes, the yield condition for all critical sections of the whole frame is formed in terms of stresses $\boldsymbol{s}$ as:

$$\boldsymbol{N}^T \cdot \boldsymbol{s} \le \boldsymbol{r} \tag{3.6}$$

where $\boldsymbol{N}$ is the $(3n_{el} \times 2hn_{el})$ matrix of all scaled -with respect to yield capacities of stresses- normal vectors and $\boldsymbol{r}$ is the $(2hn_{el} \times 1)$ vector that includes the yield limits of all yield hyperplanes (Maier 1970). Relation (3.6) is analyzed in detail for 2D (axial force-bending moment) and 3D (axial-shear force-bending moment) interaction in sections 3.6.2 and 3.6.3 respectively.

3.4.2. Convex hull formulation

3.4.2.1. Mathematical description

The convex hull of a set of points or vertices is the domain within and on the envelope formed by the outer vertices. Mathematically a set *C* is convex if the line segment between any two points in *C* lies in *C*, i.e., if for any x_1, $x_2 \in C$ and any θ with $0 \le \theta \le 1$, $\theta \cdot x_1 + (1 - \theta) \cdot x_2 \in C$. Furthermore, a point of the form $\theta_1 \cdot x_1 + \ldots + \theta_n \cdot x_n$, where $\theta_1 + \ldots + \theta_n = 1$ and $\theta_i \ge 0$, $i = 1 \ldots n$, is a convex combination of the points-vertices $x_1, \ldots, x_n$ (Boyd and Vandenberghe 2009).

The convex hull of a set of points *C* (Fig.3.4a), denoted by ***conv*** *C*, is the set of all convex combinations of points in *C*:

$$\textbf{\textit{conv}}\, C = \left\{ \theta_1 x_1 + \ldots + \theta_n x_n \mid x_i \in C, \quad \theta_i \ge 0,\ i = 1 \ldots n, \quad \theta_1 + \ldots + \theta_n = 1 \right\} \tag{3.7}$$

where θ_i are nonnegative coefficients and $x_1, \ldots, x_n$ are the points-vertices. The convex hull or convex envelope of set *C* is the smallest convex set that contains *C* (Boyd and Vandenberghe 2009).

A convex polyhedron can be described either as a bounded intersection of a finite number of closed half spaces, or as the convex hull of a finite number of points (Luenberger and Ye 2008). In this work, the concept of convex hull is used to express the linearized yield surface. For the case of 2D interaction, convex hull is outlined by n_v fixed vertices of known coordinates on the yield surface that form the

corresponding vectors x_i. Every stress vector $\boldsymbol{s}_d$ is expressed as a linear combination of the vectors that correspond to the specific vertices, provided that the sum of nonnegative coefficients $\theta_i,\ i=1...n_v$ equals to one $\left(\sum_{i=1}^{n_v}\theta_i=1\right)$. This means that for every critical section there are as many nonnegative coefficients θ_i as the vertices of the yield polyhedron (Fig. 3.4b). If the stress point reaches the yield limit, the corresponding stress vector is expressed as a linear combination of the cone vectors of the activated yield hyperplane (Fig. 3.4c). For the special case of only one coefficient θ_i obtaining the value of unity, with all the remaining equal to zero, the stress point coincides with the corresponding vertex of the linearized yield surface (Fig. 3.4d).

The concept of convex hull can be extended in *d* dimensional spaces engaging points –vertices with *d* number of coordinates.

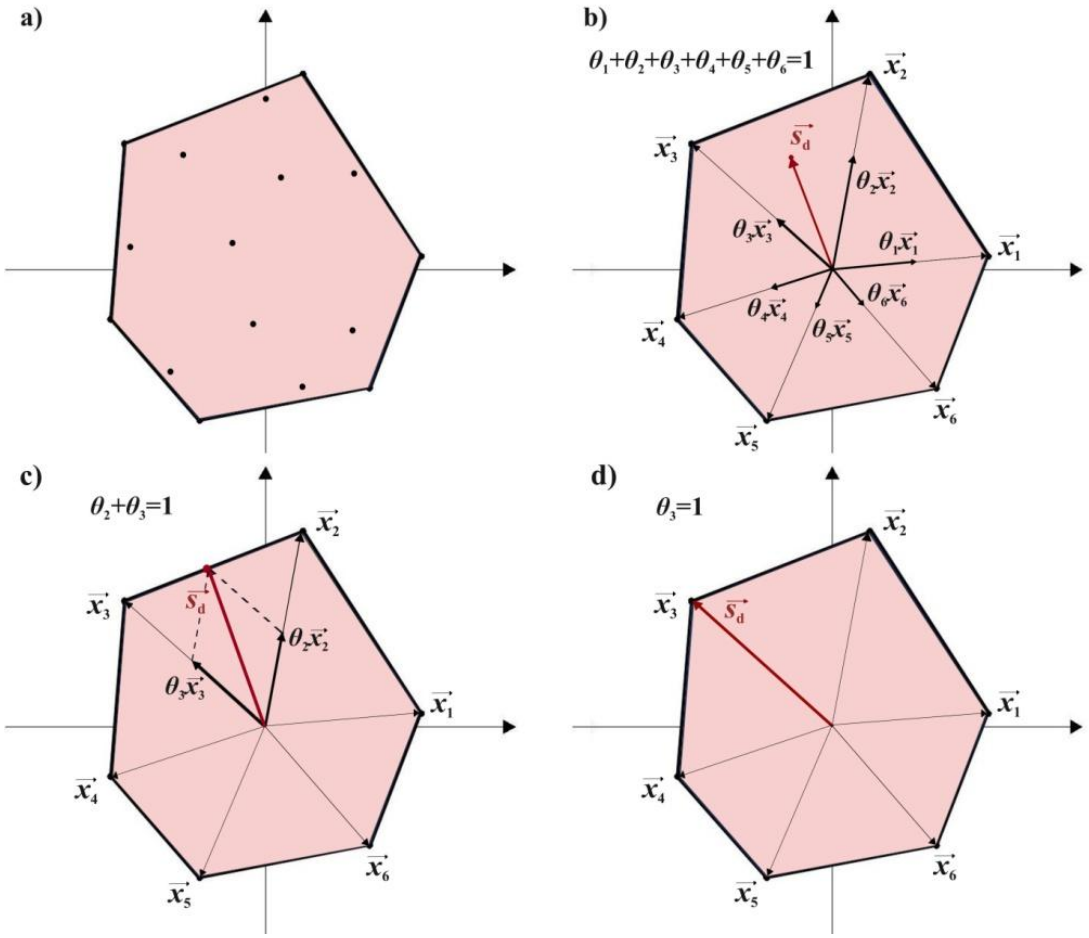

Fig. 3.4: Stress vector expressed in terms of convex hull.

3.4.2.2. Yield condition formulation

The a priori linearized yield surface constitutes a polytope that can be expressed as the convex hull of its n_v fixed vertices (Boyd and Vandenberghe 2009, Manola and Koumousis 2015). Yield condition states that every normalized stress point should reside in or on this yield polytope. Therefore, for *j* element end the following relation holds $\boldsymbol{s}_d^j = \theta_1 \cdot \boldsymbol{x}_1 + ... + \theta_{n_v} \cdot \boldsymbol{x}_{n_v}$ with $\sum_1^{n_v} \theta_i = 1$ and $\theta_i \geq 0$ and a similar one for *k* element end. Thus, yield condition for the whole structure can be established in matrix form as:

$$\boldsymbol{s}_d - \boldsymbol{C} \cdot \boldsymbol{\theta} = \boldsymbol{0}, \;\; \boldsymbol{I}_{eq} \cdot \boldsymbol{\theta} = 1 \;, \;\; \boldsymbol{\theta} \geq \boldsymbol{0} \tag{3.8}$$

where $\boldsymbol{s}_d$ is the *(2dn$_{el}$×1)* vector of the normalized stresses for all elements, $\boldsymbol{C}$ is the (2*dn$_{el}$*×*2n$_v$n$_{el}$*) matrix containing the coordinates of the vertices of all yield hyperplanes for all elements, $\boldsymbol{\theta}$ is the (2*n$_v$n$_{el}$*×*1*) vector including the coefficients θ_i for all vectors of the vertices n_v for all the elements and $\boldsymbol{I}_{eq}$ is the (*2n$_{el}$*×*2n$_v$n$_{el}$*) matrix that sums the corresponding θ_i at every element end. Expression (3.8) is particularized for 2D (axial force-bending moment) and 3D (axial-shear force-bending moment) interaction in sections 3.6.2 and 3.6.3 respectively.

It is noted that yield conditions following a convex hull formulation (equation 3.6) are expressed with strict equality constraints and their number (i.e. the number of rows of the matrix relation) corresponds to the number of all critical sections multiplied by the dimensionality of the interaction, i.e. 2*d*×*n$_{el}$*, and is independent of the number of hyperplanes that approximate the nonlinear yield surface. It depends though on the introduced (*2n$_v$n$_{el}$*×*1*) vector $\boldsymbol{\theta}$ which increases accordingly the number of decision variables of the problem.

3.5. Limit analysis with Linear Programming

3.5.1. General primal-dual formulation

The primal–dual relationships of a general Linear Programming problem aiming at maximizing or minimizing a linear objective function subject to a set of equality and

inequality constraints with nonnegative variables or variables unrestricted in sign are given by the following relations (Rao 2009):

Primal	***Dual***
Maximize $f=\sum_{i=1}^{n} c_i \cdot x_i$, s.t.	Minimize $\upsilon=\sum_{i=1}^{m} y_i \cdot b_i$, s.t.
$\sum_{j=1}^{n} a_{ij} \cdot x_j = b_i \ , i=1,2,\ldots,m^*$	$\sum_{i=1}^{m} y_i \cdot a_{ij} = c_j \ , \ j=n^*+1, n^*+2,\ldots,n$
$\sum_{j=1}^{n} a_{ij} \cdot x_j \le b_i \ , i=m^*+1, m^*+2,\ldots,m$	$\sum_{i=1}^{m} y_i \cdot a_{ij} \ge c_j \ , \ j=1,2,\ldots,n^*$
where	where
$x_i \ge 0, \ i=1,2,\ldots,n^*$	$y_i \ge 0, \ i=m^*+1, m^*+2,\ldots,m$
and	and
x_i unrestricted in sign,	y_i unrestricted in sign,
$i=n^*+1, n^*+2,\ldots,n$	$i=1,2,\ldots,m^*$

(3.9)

Note that the primal problem is bounded from above by the dual, utilizing as many variables as the number of constraints of the primal and establishing as many constraints as the number of variables of the primal that bound the primal cost coefficients. The solution of a LP problem can be obtained by solving either the primal or the dual and since the dual of the dual is the primal, it is immaterial which problem (minimization or maximization) is designated as primal.

3.5.2. Hyperplane equations (standard) formulation

The static theorem of limit analysis can be stated in the form of a LP problem as:

$$\begin{aligned} &\textit{maximize} && \alpha && \\ &\textit{subject to} && -\boldsymbol{B}\cdot\boldsymbol{s}+a\cdot\boldsymbol{f}=-\boldsymbol{f}_d && n_f \textit{ constraints} \\ & && \boldsymbol{N}^T\cdot\boldsymbol{s}\le\boldsymbol{r} && 2h\, n_{el} \textit{ constraints} \\ & && \boldsymbol{s}:\textit{unrestricted}, a\ge 0 && \end{aligned} \tag{3.10}$$

where the decision variables are the stresses $\boldsymbol{s}$ and the load factor a.

Based on the above, the dual problem, which represents the kinematic theorem, can be readily obtained as:

$$\begin{aligned} &\textit{minimize} && -\boldsymbol{f}_d^T \cdot \boldsymbol{u} + \boldsymbol{r}^T \cdot \mathbf{z} && \\ &\textit{subject to} && -\boldsymbol{B}^T \cdot \boldsymbol{u} + \boldsymbol{N} \cdot \mathbf{z} = \mathbf{0} && 3n_{el} \ \textit{constraints} \\ & && \boldsymbol{f}^T \boldsymbol{u} \geq 1 && 1 \quad \textit{constraint} \\ & && \boldsymbol{u}: \textit{unrestricted}, \mathbf{z} \geq \mathbf{0} && \end{aligned} \tag{3.11}$$

where the decision variables are now the nodal displacements $\boldsymbol{u}$ and the plastic multipliers $\mathbf{z}$. The objective function expresses the dissipated plastic energy $(\boldsymbol{r}^T\mathbf{z})$ minus the work of permanent loading $(\boldsymbol{f}_d^T\boldsymbol{u})$. This emerges from the work equation $a\boldsymbol{f}^T\boldsymbol{u} + \boldsymbol{f}_d^T\boldsymbol{u} = \boldsymbol{r}^T\mathbf{z}$ (external work rate is equal to the internal dissipation). The first constraint set represents compatibility and the inequality constraints a normalized external work term, which can be considered as a strict equality avoiding a floating normalization. In this case the objective function expresses the loading factor *a*.

It is noted that the number of constraints of the dual problem is smaller compared to that of the primal. It is known that an additional constraint requires more computational effort than an additional variable in a linear programming problem (Rao 2009). Thus, it becomes evident that, although the primal static or safe theorem is from an engineering perspective preferable, computationally is more efficient to solve the dual problem (kinematic theorem) following the standard formulation.

3.5.3. Convex hull formulation

Formulation of the static theorem of limit analysis using a convex hull description for the yield surface is given as:

$$\begin{aligned} &\textit{maximize} && \alpha && \\ &\textit{subject to} && -\boldsymbol{B} \cdot \boldsymbol{s} + a \cdot \boldsymbol{f} = -\boldsymbol{f}_d && n_f \ \textit{constraints} \\ & && \boldsymbol{T} \cdot \boldsymbol{s} - \boldsymbol{C} \cdot \boldsymbol{\theta} = \mathbf{0} && 2dn_{el} \ \textit{constraints} \\ & && \boldsymbol{I}_{eq} \cdot \boldsymbol{\theta} = 1 && 2n_{el} \ \textit{constraints} \\ & && \boldsymbol{s}: \textit{unrestricted}, \boldsymbol{\theta} \geq \mathbf{0} \ , a \geq 0 && \end{aligned} \tag{3.12}$$

where the decision variables of the problem are the stresses $\boldsymbol{s}$, parameters $\boldsymbol{\theta}$ and the load factor *a*.

The dual problem (kinematic theorem) can be cast as:

$$
\begin{aligned}
&\textit{minimize} && -\boldsymbol{f}_d^T \cdot \boldsymbol{u} + \boldsymbol{I}^T \cdot \boldsymbol{\varphi} && \\
&\textit{subject to} && -\boldsymbol{B}^T \cdot \boldsymbol{u} + \boldsymbol{T}^T \cdot \boldsymbol{\omega} = \boldsymbol{0} && 3n_{el}\ \textit{constraints} \\
& && -\boldsymbol{C}^T \cdot \boldsymbol{\omega} + \boldsymbol{I}_{eq}^T \cdot \boldsymbol{\varphi} \geq \boldsymbol{0} && 2n_v n_{el}\ \textit{constraints} \\
& && \boldsymbol{f}^T \cdot \boldsymbol{u} \geq 1 && 1\ \textit{constraint} \\
& && \boldsymbol{u}, \boldsymbol{\omega}, \boldsymbol{\varphi}\ \ \textit{unrestricted} &&
\end{aligned}
\tag{3.13}
$$

where the unknown variables are now the nodal displacements $\boldsymbol{u}$, together with $\boldsymbol{\omega}$ and $\boldsymbol{\varphi}$ which express plastic work. The objective function concerns the internal dissipation energy $\left(\boldsymbol{I}^T \cdot \boldsymbol{\varphi} = \sum \boldsymbol{\varphi}\right)$ minus the work of permanent loading $\left(\boldsymbol{f}_d^T \boldsymbol{u}\right)$. This emerges from the work equation $a\boldsymbol{f}^T \boldsymbol{u} + \boldsymbol{f}_d^T \boldsymbol{u} = \boldsymbol{I}^T \boldsymbol{\varphi}$ (external work rate is equal to the internal dissipation). The first constraint set represents compatibility conditions with $\boldsymbol{T}^T \cdot \boldsymbol{\omega}$ determining plastic deformation; the second set of the inequality constraints is the dual expression of convex hull for plastic deformations and the last concerns a normalized external work term, which again can be interpreted as a strict equality.

It is noted that the number of constraints for the dual problem is significantly greater compared to that of the primal. Thus, it is evident that the static theorem, which is of primal interest in engineering, turns out as computationally more efficient following the convex hull formulation.

3.5.4. Comparison of the two formulations

Convex hull formulation determines yield condition as a set of equality constraints, the number of which is independent of the discretization of the yield surface. The number of variables though is increased as compared to the standard formulation since parameters θ_i are introduced. For the general case of piecewise linearization of a yield hyper-surface with h hyperplanes and n_v number of vertices, the comparison between standard and convex hull formulation is summarized in the following table (Table 3.1). Since for multi-component interaction ($d > 2$) the number of vertices n_v is noticeably smaller than the number of hyperplanes h, convex hull formulation becomes considerably advantageous in terms of computational efficiency in expressing the yield condition.

Table 3.1: Comparison between standard and convex hull formulation.

	Standard Formulation	**Convex Hull Formulation**
Number of variables $\boldsymbol{n_{var}}$	$3n_{el}+1$	$3n_{el}+2n_v n_{el}+1$
Number of equality constraints $\boldsymbol{n_{eq}}$	n_f	$n_f + 2\cdot(d+1)n_{el}$
Number of inequality constraints $\boldsymbol{n_{inq}}$	$2hn_{el}$	—
Number of side constraints **(upper and lower bounds)**	$2\cdot(3n_{el}+1)$	$2\cdot(3n_{el}+2n_v n_{el}+1)$

3.6. Yield condition for 2D and 3D interaction

3.6.1. Yield criterion

Various yield criteria have been proposed for different materials and/or cross-sectional shapes that incorporate the interaction of all stresses. Herein, two alternatives are examined, i.e. axial force-bending moment (NM) interaction and axial-shear force-bending moment (NQM) interaction.

For the case of axial force-bending moment (NM) interaction the stress state at each element section is depicted in Fig. 3.5a. Since interaction diagrams are expressed in normalized form, the yield condition for each critical section is also expressed in terms of nondimensional stresses, normalized with respect to the corresponding plastic capacities. Thus, at every element *i*, plastic behavior is described at start node *j* by the normalized stress vector $\left\{n^j \quad m^j\right\}^T = \left\{s_1^i/s_{1y}^i \quad s_2^i/s_{2y}^i\right\}^T$ and at end node *k* by $\left\{n^k \quad m^k\right\}^T = \left\{-s_1^i/s_{1y}^i \quad s_3^i/s_{3y}^i\right\}^T$, where n^j, m^j and n^k, m^k are the normalized axial forces and bending moments of j and k element ends, whereas s_{1y}^i is the axial plastic capacity for both ends, s_{2y}^i, s_{3y}^i are the bending moment plastic capacities of j and k element ends respectively. The stress state under the combined effect of axial-shear force-bending moment interaction (NQM interaction) at each element section is depicted in Fig. 3.5b. In terms of normalized stresses, plastic hinges at start nodes *j* are formed under the combined effect of

$\left\{n^j \;\; v^j \;\; m^j\right\}^T = \left\{s_1^i / s_{1y}^i \quad \left(s_2^i + s_3^i\right) / L^i v_y^i \quad s_2^i / s_{2y}^i\right\}^T$ and at end node k due to $\left\{n^k \; v^k \; m^k\right\}^T = \left\{-s_1^i / s_{1y}^i \quad -\left(s_2^i + s_3^i\right) / L^i v_y^i \quad s_3^i / s_{3y}^i\right\}^T$, where v^j, v^k are the normalized shear force at element ends j and k respectively, v_y^i is the shear force yield limit of the element, and L^i is the element length.

Notice that different capacities can be considered for the two element ends to account also for concrete elements with constant cross section, but different bar reinforcement at the two ends. Thus, yielding at the two critical end sections of the element will be expressed with respect to the three primary element actions; with the minus sign at end k expressing the pre-established equilibrium within the element along the local x and y direction.

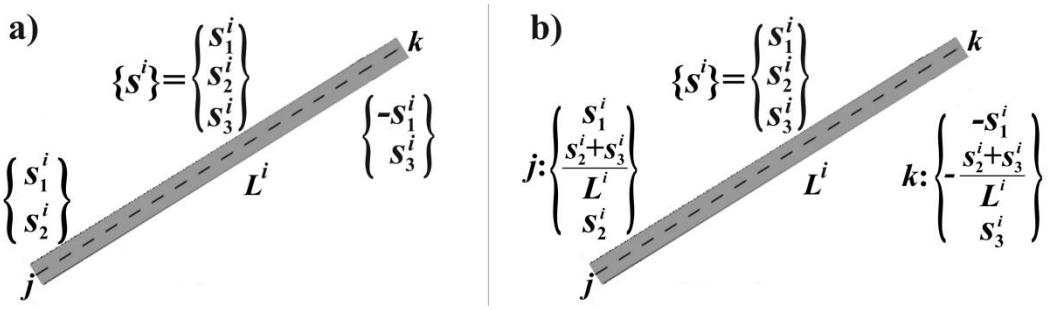

Fig.3.5: Stress state at element critical sections for a) NM and b) NQM interaction.

In this work, the Gendy-Saleeb yield criterion including the combined effect of axial force and bending moment is employed (Gendy and Saleeb 1992):

$$\Phi = n^2 + \frac{1}{\lambda_m} m^2 - 1 \tag{3.14}$$

The above yield relation is valid for both rectangular and I-cross sections. The introduced shape dependent parameter λ_m is evaluated for rectangular cross sections and I-sections respectively using the following relations:

$$\lambda_m = 1 - n^2, \quad \lambda_m = 1 - 1.1|n| \tag{3.15}$$

The interaction curve of equation is approximated in the sequel with eight linear segments that denote the corresponding yield limits, as shown in Fig. 3.6.

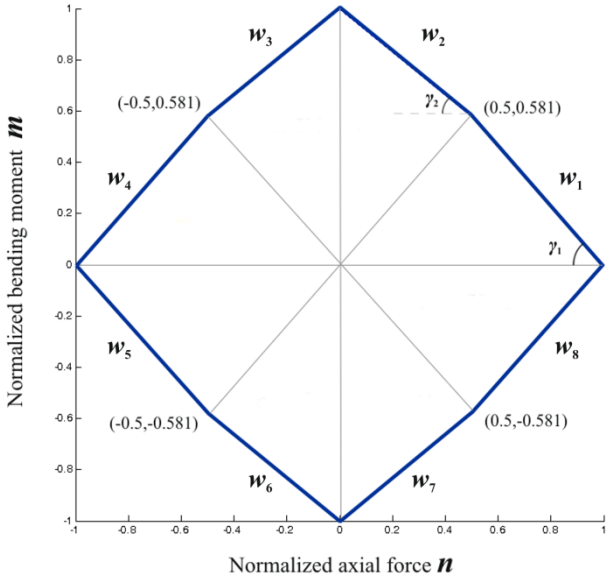

Fig.3.6: Linearized Gendy-Saleeb yield criterion for NM interaction.

Including the effect of shear force, the adopted yield criterion is of the form (Gendy and Saleeb 1992):

$$\Phi = n^2 + v^2 + \frac{1}{\lambda_m} m^2 - 1 \tag{3.16}$$

The aforementioned relation is represented by a 3D nonlinear surface which is herein approximated using 32 plane triangles, as shown in Fig. 3.7.

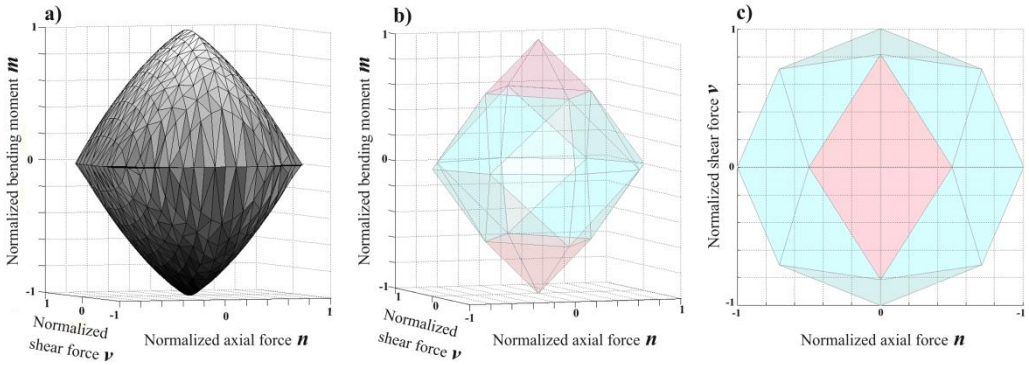

Fig.3.7: a) Nonlinear Gendy-Saleeb yield criterion, b) Linearized yield criterion and c) Plan view of linearized criterion.

3.6.2. Axial force-bending moment (NM) interaction

The equations of the linear segments ($h=8$ in Fig. 3.5) approximating the yield surface for both element ends are of the form:

$$\begin{aligned} \tilde{A}^j \cdot n^j + \tilde{B}^j \cdot m^j &= \tilde{C}^j \\ \tilde{A}^k \cdot n^k + \tilde{B}^k \cdot m^k &= \tilde{C}^k \end{aligned} \tag{3.17}$$

where the coefficients $\tilde{A}^j, \tilde{B}^j, \tilde{A}^k, \tilde{B}^k$ are the components of the unit normal vector of each yield line for j and k element ends and coefficients $\tilde{C}^j, \tilde{C}^k$ form the yield limits. For an element i the yield condition is expressed in matrix form as:

$$\begin{bmatrix} \tilde{A}_1^j & \tilde{B}_1^j & 0 \\ \vdots & \vdots & \vdots \\ \tilde{A}_8^j & \tilde{B}_8^j & 0 \\ \tilde{A}_1^k & 0 & \tilde{B}_1^k \\ \vdots & \vdots & \vdots \\ \tilde{A}_8^k & 0 & \tilde{B}_8^k \end{bmatrix} \cdot \begin{bmatrix} 1/s_{1y}^i & 0 & 0 \\ 0 & 1/s_{2y}^i & 0 \\ 0 & 0 & 1/s_{3y}^i \end{bmatrix} \cdot \begin{Bmatrix} s_1^i \\ s_2^i \\ s_3^i \end{Bmatrix} \le \begin{Bmatrix} \tilde{C}_1^j \\ \vdots \\ \tilde{C}_8^j \\ \tilde{C}_1^k \\ \vdots \\ \tilde{C}_8^k \end{Bmatrix} \Leftrightarrow$$

$$\tilde{\boldsymbol{N}}^{iT} \cdot \boldsymbol{R}^i \cdot \boldsymbol{s}^i \le \boldsymbol{r}^i \Leftrightarrow \boldsymbol{N}^{iT} \cdot \boldsymbol{s}^i \le \boldsymbol{r}^i \tag{3.18}$$

where $\tilde{\boldsymbol{N}}^i$ is the (*3×16*) matrix that contains the horizontal and vertical components, i.e. the direction cosines, of the unit normal of all yield lines for both element ends, $\boldsymbol{R}^i$ is the (*3×3*) matrix that contains the yield capacities of all stresses of the element, $\boldsymbol{N}^i$ is the (*3×16*) matrix of the scaled coefficients of all yield lines of the element and $\boldsymbol{r}^i$ is the (*16×1*) vector that contains all $\tilde{C}^j, \tilde{C}^k$ coefficients (Appendix A). Thus, in equation (3.6) $\boldsymbol{N}$ is the *($3n_{el}$×$16n_{el}$)* assembled block diagonal matrix of all $\boldsymbol{N}^i$ matrices and $\boldsymbol{r} = \left\{ \boldsymbol{r}^1 \ldots \boldsymbol{r}^{n_{el}} \right\}^T$ is the (*$16n_{el}$×1)* vector that includes the yield limits of all yield lines.

For convex hull formulation and NM interaction, the number of vertices coincides with that of the linear segments ($n_v = h = 8$ in Fig. 3.6). Yield condition in terms of convex hull is expressed for *j* element end by the following relations:

$$\begin{Bmatrix} n^j \\ m^j \end{Bmatrix} = \theta_1^j \begin{Bmatrix} x_1 \\ y_1 \end{Bmatrix} + \theta_2^j \begin{Bmatrix} x_2 \\ y_2 \end{Bmatrix} + \ldots + \theta_8^j \begin{Bmatrix} x_8 \\ y_8 \end{Bmatrix} \Leftrightarrow$$

$$\begin{Bmatrix} n^j \\ m^j \end{Bmatrix} - \begin{bmatrix} x_1 & x_2 & \ldots & x_8 \\ y_1 & y_2 & \ldots & y_8 \end{bmatrix} \cdot \begin{Bmatrix} \theta_1^j \\ \theta_2^j \\ \vdots \\ \theta_8^j \end{Bmatrix} = \begin{Bmatrix} 0 \\ 0 \end{Bmatrix}, \qquad (3.19)$$

$$with \;\; \mathbf{1}^T \boldsymbol{\theta}^j = \mathbf{1}, \;\; where \; \boldsymbol{\theta}^{jT} = \begin{Bmatrix} \theta_1^j & \theta_2^j & \ldots & \theta_8^j \end{Bmatrix} \geq \mathbf{0}$$

where $(x_i\,,\, y_i)$, $i = 1...8$ are the coordinates of the vertices of the linearized yield surface common for all critical sections and $\boldsymbol{\theta}^j$ is the (8×1) vector of coefficients θ_i for j element end. Similarly, yield condition is expressed for *k* element end.

Thus, expressing the normalized stresses as $\boldsymbol{s}_d = \boldsymbol{T} \cdot \boldsymbol{s}$, matrices and vectors in equation (3.8) are of the following form:

$$\boldsymbol{s}_d = \begin{Bmatrix} \boldsymbol{s}_d^1 \ldots \boldsymbol{s}_d^{n_{el}} \end{Bmatrix}^T = (4n_{el} \times 1), \qquad \boldsymbol{s}_d^i = \begin{Bmatrix} s_1^i / s_{1y}^i & s_2^i / s_{2y}^i & -s_1^i / s_{1y}^i & s_3^i / s_{3y}^i \end{Bmatrix}^T,$$

$$\boldsymbol{T} = diag\left[\boldsymbol{T}^1 \ldots \boldsymbol{T}^{n_{el}}\right] = (4n_{el} \times 3n_{el}), \qquad \boldsymbol{T}^i = \begin{bmatrix} 1/s_{1y}^i & 0 & 0 \\ 0 & 1/s_{2y}^i & 0 \\ -1/s_{1y}^i & 0 & 0 \\ 0 & 0 & 1/s_{3y}^i \end{bmatrix},$$

$$\boldsymbol{C} = diag\left[\boldsymbol{C}^1 \ldots \boldsymbol{C}^{n_{el}}\right] = (4n_{el} \times 16n_{el})$$

$$\boldsymbol{C}^i = \begin{bmatrix} x_1 & \ldots & x_8 & 0 & \ldots & 0 \\ y_1 & \ldots & y_8 & 0 & \ldots & 0 \\ 0 & \ldots & 0 & x_1 & \ldots & x_8 \\ 0 & \ldots & 0 & y_1 & \ldots & y_8 \end{bmatrix},$$

$$\boldsymbol{\theta} = \begin{Bmatrix} \boldsymbol{\theta}_1 \ldots \boldsymbol{\theta}_{n_{el}} \end{Bmatrix}^T = (16n_{el} \times 1), \;\; \boldsymbol{\theta}_i = \begin{Bmatrix} \boldsymbol{\theta}_i^j & \boldsymbol{\theta}_i^k \end{Bmatrix}^T,$$

$$\boldsymbol{I}_{eq} = diag[\boldsymbol{I}_{eq}^1 \ldots \boldsymbol{I}_{eq}^{n_{el}}] = (2n_{el} \times 16n_{el}), \qquad (3.20)$$

$$\boldsymbol{I}_{eq}^i = \begin{bmatrix} 1 & \ldots & 1 & 0 & \ldots & 0 \\ 0 & \ldots & 0 & 1 & \ldots & 1 \end{bmatrix}$$

3.6.3. Axial-shear force-bending moment (NQM) interaction

The 3D nonlinear yield surface is approximated with $h=32$ plane triangles (Fig.3.7) corresponding to the same number equations for the corresponding planes in $n-v-m$ space, which are of the following form for the two element ends:

$$\begin{aligned}\tilde{A}^j n^j + \tilde{B}^j v^j + \tilde{C}^j m^j + \tilde{D}^j = 0\\ \tilde{A}^k n^k + \tilde{B}^k v^k + \tilde{C}^k m^k + \tilde{D}^k = 0\end{aligned} \tag{3.21}$$

where $\tilde{A},\tilde{B},\tilde{C}$ are the components of the unit normal vector of the plane and $-\tilde{D}$ is the distance of the plane from the origin. For an element i the yield condition is expressed in matrix form as:

$$\begin{bmatrix} \tilde{A}_1^j & \tilde{B}_1^j & \tilde{C}_1^j & 0 & 0 & 0 \\ \vdots & \vdots & \vdots & \vdots & \vdots & \vdots \\ \tilde{A}_\ell^j & \tilde{B}_\ell^j & \tilde{C}_\ell^j & 0 & 0 & 0 \\ 0 & 0 & 0 & \tilde{A}_1^k & \tilde{B}_1^k & \tilde{C}_1^k \\ \vdots & \vdots & \vdots & \vdots & \vdots & \vdots \\ 0 & 0 & 0 & \tilde{A}_\ell^k & \tilde{B}_\ell^k & \tilde{C}_\ell^k \end{bmatrix} \cdot \begin{bmatrix} 1/s_{1y}^i & 0 & 0 \\ 0 & 1/L^i v_y^i & 1/L^i v_y^i \\ 0 & 1/s_{2y}^i & 0 \\ -1/s_{1y}^i & 0 & 0 \\ 0 & -1/L^i v_y^i & -1/L^i v_y^i \\ 0 & 0 & 1/s_{3y}^i \end{bmatrix} \cdot \begin{Bmatrix} s_1^i \\ s_2^i \\ s_3^i \end{Bmatrix} \le \begin{Bmatrix} -\tilde{D}_1^j \\ \vdots \\ -\tilde{D}_\ell^j \\ -\tilde{D}_1^k \\ \vdots \\ -\tilde{D}_\ell^k \end{Bmatrix} \Leftrightarrow$$

$$\tilde{\boldsymbol{N}}^{iT} \cdot \boldsymbol{R}^i \cdot \boldsymbol{s}^i \le \boldsymbol{r}^i \Leftrightarrow \boldsymbol{N}^{iT} \cdot \boldsymbol{s}^i \le \boldsymbol{r}^i \tag{3.22}$$

where $\tilde{\boldsymbol{N}}^i$ is the (*6×64*) matrix that contains the coefficients of all yield planes for both element ends, $\boldsymbol{R}^i$ is the (*6×3*) matrix that contains the yield capacities of all stresses of the element, $\boldsymbol{N}^i$ is the (*3×64*) matrix of the scaled coefficients of all yield planes of the element and $\boldsymbol{r}^i$ is the (*64×1*) vector that contains all $-\tilde{D}^j, -\tilde{D}^k$ coefficients (Appendix B). Thus, in equation (3.6) $\boldsymbol{N}$ is the *($3n_{el}$×$64n_{el}$)* assembled block diagonal matrix of all $\boldsymbol{N}^i$ matrices and $\boldsymbol{r} = \left\{ \boldsymbol{r}^1 \ldots \boldsymbol{r}^{n_{el}} \right\}^T$ is the (*$64n_{el}$×1)* vector that includes the yield limits of all yield planes.

For convex hull formulation and NQM interaction, the number of vertices is $n_v = 18$ (Fig. 3.7), while the number of planes is $h = 32$. The number of vertices is significantly smaller than that of the planes ($n_v < h$). Yield condition in terms of convex hull is expressed for *j* element end by the relations:

$$\begin{Bmatrix} n^j \\ v^j \\ m^j \end{Bmatrix} = \theta_1^j \begin{Bmatrix} x_1 \\ y_1 \\ z_1 \end{Bmatrix} + \theta_2^j \begin{Bmatrix} x_2 \\ y_2 \\ z_2 \end{Bmatrix} + \ldots + \theta_{18}^j \begin{Bmatrix} x_{18} \\ y_{18} \\ z_{18} \end{Bmatrix} \Leftrightarrow$$

$$\begin{Bmatrix} n^j \\ v^j \\ m^j \end{Bmatrix} - \begin{bmatrix} x_1 & x_2 & \cdots & x_{18} \\ y_1 & y_2 & \cdots & y_{18} \\ z_1 & z_2 & \cdots & z_{18} \end{bmatrix} \cdot \begin{Bmatrix} \theta_1^j \\ \theta_2^j \\ \vdots \\ \theta_{18}^j \end{Bmatrix} = \begin{Bmatrix} 0 \\ 0 \\ 0 \end{Bmatrix}, \qquad (3.23)$$

$$with \quad \mathbf{1}^T \boldsymbol{\theta}^j = \mathbf{1}, \quad where \; \boldsymbol{\theta}^{jT} = \begin{Bmatrix} \theta_1^j & \theta_2^j & \ldots & \theta_{18}^j \end{Bmatrix} \geq \mathbf{0}$$

where (x_i, y_i, z_i), $i = 1 \ldots n_v$ are the coordinates of the vertices of the linearized yield surface, common for all critical sections of all elements, and $\boldsymbol{\theta}^j$ is the $(n_v \times 1)$ vector of coefficients θ_i for j element end. Similarly, the yield condition is expressed for *k* element end.

Thus, matrices and vectors in equation (3.8), given that the normalized stresses are expressed as $\boldsymbol{s}_d = \boldsymbol{T} \cdot \boldsymbol{s}$, are of the following form:

$$\boldsymbol{s}_d = \left\{ s_d^1 \ldots s_d^{n_{el}} \right\}^T = (6n_{el} \times 1),$$

$$\boldsymbol{s}_d^i = \left\{ s_1^i / s_{1y}^i \quad (s_2^i + s_3^i)/L^i v_y^i \quad s_2^i / s_{2y}^i \quad -s_1^i / s_{1y}^i \quad -(s_2^i + s_3^i)/L^i v_y^i \quad s_3^i / s_{3y}^i \right\}^T,$$

$$\boldsymbol{T} = diag\left[\boldsymbol{T}^1 \ldots \boldsymbol{T}^{n_{el}} \right] = (6n_{el} \times 3n_{el}),$$

$$\boldsymbol{T}^{Ti} = \begin{bmatrix} 1/s_{1y}^i & 0 & 0 & -1/s_{1y}^i & 0 & 0 \\ 0 & 1/L^i v_y^i & 1/s_{2y}^i & 0 & -1/L^i v_y^i & 0 \\ 0 & 1/L^i v_y^i & 0 & 0 & -1/L^i v_y^i & 1/s_{3y}^i \end{bmatrix},$$

$$\boldsymbol{C} = diag\left[\boldsymbol{C}^1 \ldots \boldsymbol{C}^{n_{el}} \right] = (6n_{el} \times 36n_{el}),$$

$$\boldsymbol{C}^i = \begin{bmatrix} x_1 & \ldots & x_{18} & 0 & \ldots & 0 \\ y_1 & \ldots & y_{18} & 0 & \ldots & 0 \\ z_1 & \ldots & z_{18} & 0 & \ldots & 0 \\ 0 & \ldots & 0 & x_1 & \ldots & x_{18} \\ 0 & \ldots & 0 & y_1 & \ldots & y_{18} \\ 0 & \ldots & 0 & z_1 & \ldots & z_{18} \end{bmatrix},$$

$$\boldsymbol{\theta} = \left\{ \boldsymbol{\theta}_1 \ldots \boldsymbol{\theta}_{n_{el}} \right\}^T = (36n_{el} \times 1), \ \boldsymbol{\theta}_i = \left\{ \boldsymbol{\theta}_i^j \ \boldsymbol{\theta}_i^k \right\}^T,$$

$$\boldsymbol{I}_{eq} = diag[\boldsymbol{I}_{eq}^1 \ldots \boldsymbol{I}_{eq}^{n_{el}}] = (2n_{el} \times 36n_{el}),$$

$$\boldsymbol{I}_{eq}^i = \begin{bmatrix} 1 & \ldots & 1 & 0 & \ldots & 0 \\ 0 & \ldots & 0 & 1 & \ldots & 1 \end{bmatrix} \tag{3.24}$$

It is noted that the introduced vector $\boldsymbol{\theta}$ depends on the number of vertices n_v of the yield polyhedron, which for 3D interaction is considerably smaller than the number of yield planes h. This makes convex hull formulation more advantageous compared to the standard one for the expression of yield condition including the interaction of three or more stresses, since the constraint reduction is greater than the introduced number of variables.

3.7. Numerical examples

The optimization problems described above are implemented in Matlab code for the analysis of frame steel structures with rigid-perfectly plastic behavior. The data are processed by *linprog* solver that is appropriate for linear programming problems.

The aim is to compare the two formulations for the yield condition and investigate the influence of combined stresses on the ultimate load. For this purpose, four steel plane frames are examined for the following cases:

- Case (a): Bending.
- Case (b): Axial force-bending moment interaction (NM interaction) with 1) standard formulation and 2) convex hull formulation.
- Case (c): Axial-shear force-bending moment interaction (NQM interaction) with 1) standard formulation and 2) convex hull formulation.

For case (a) the formulation of the problem is simplified since yield constraints consist of upper and lower bounds (side constraints) for the values of bending moments and matrix $\boldsymbol{N}$ is not required.

All analyses are conducted on a PC with a Core Duo Quad CPU and 4GB of RAM and the results of all cases are presented below. Notice that the analysis method follows the sign convention of matrix structural analysis, whereas final results are presented on the basis of engineering sign convention.

3.7.1. Example #1

The first example concerns a three-storey, two-bay steel frame shown in Fig. 3.8a. The frame is discretized into 15 elements, 12 nodes and 27 degrees of freedom. The steel grade is S235 with $E=2\times10^8$kN/m^2. The material properties are as follows: sections with $A=112.5\times10^{-4}$ m^2, $I=18260\times10^{-8}$ m^4, $s_{1y}=2643.75$ kN, $v_y=505.4$ kN, $s_{2y}=325$ kNm, $s_{3y}=325$ kNm are employed for all columns, sections with $A=28.48\times10^{-4}$ m^2, $I=1943\times10^{-8}$ m^4, $s_{1y}=669.28$ kN, $v_y=189.89$ kN, $s_{2y}=51.84$ kNm, $s_{3y}=51.84$ kNm for all beams. Analysis results of all cases are presented in Table 3.2.

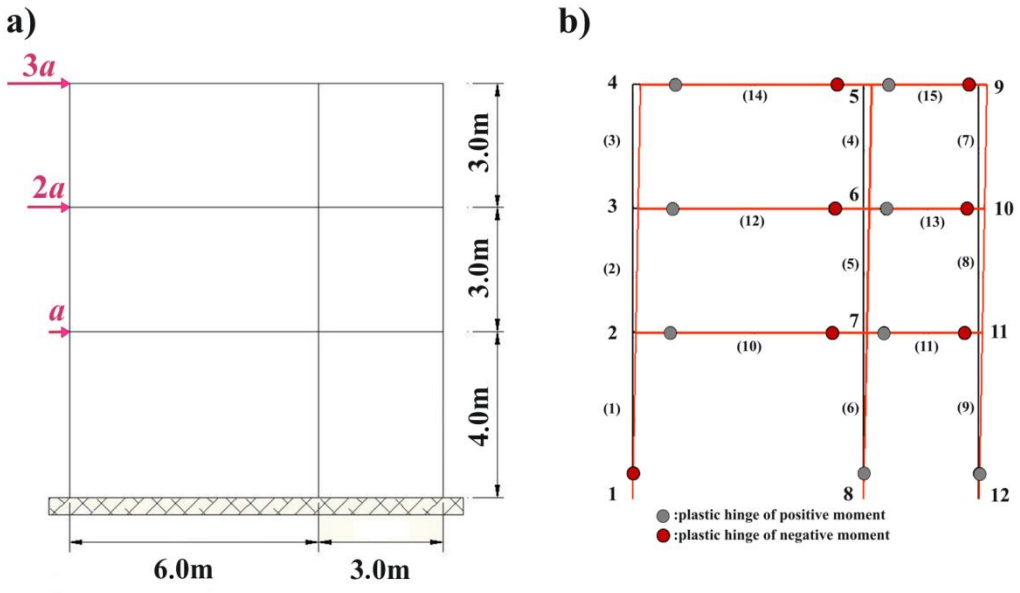

Fig. 3.8: a) Three-storey, two-bay steel frame and b) its deformed shape for all analysis cases.

Table 3.2: Analysis results of all cases for example #1.

Cases	Bending (a)	NM interaction (b_1)	NM interaction Convex Hull (b_2)	NQM interaction (c_1)	NQM interaction Convex Hull (c_2)
number of variables n_{var}	**46**	**46**	**286**	**46**	**586**
number of equality constraints n_{eq}	**27**	**27**	**117**	**27**	**147**
number of inequality constraints n_{inq}	—	**240**	—	**960**	—
maximum load factor a (kN)	**33.27**	**32.42**	**32.42**	**30.40**	**30.40**
number of plastic hinges	**15**	**15**	**15**	**15**	**15**
total computational time (s)	**0.40**	**0.59**	**0.56**	**8.88**	**0.59**
computational time for the optimization process (s)	**0.38**	**0.56**	**0.48**	**0.87**	**0.51**

The effect of combined stresses leads to a reduction of the maximum load factor compared to pure bending consideration. For cases of combined stresses ((b) and (c)) expressed either with equations of lines/planes or with convex hulls, analysis results

are identical. However, the convex hull formulation converges slightly faster (1.05 times) for case (b) and 15.05 times faster for case (c). This concerns the total computational time including both matrix formulation and optimization procedure. The required time for the mere optimization procedure is shown at the last line of Table 3.2. According to this, the optimization problem with convex hull formulation is solved 1.17 times faster for case (b) and 1.71 times faster for case (c). This is due to fewer constraints, while the greater number of variables seems to have slight influence on the computational efficiency. The benefits of convex hull formulation are mainly evident for case (c), because the number of constraints is independent of the number of planes of the 3D linearized yield surface, whereas the number of the initiated variables is related to the number of vertices of yield polyhedron ($n_v<h$).

The plastic hinge pattern (i.e. number and location) is the same for all analysis cases, although they correspond to similar stresses, as shown in Fig. 3.8b. The corresponding interaction diagrams are presented in Fig. 3.9 and Fig. 3.10. The frame is mainly stressed due to bending moment (the dispersion of stress points is wider along the bending moment axis).

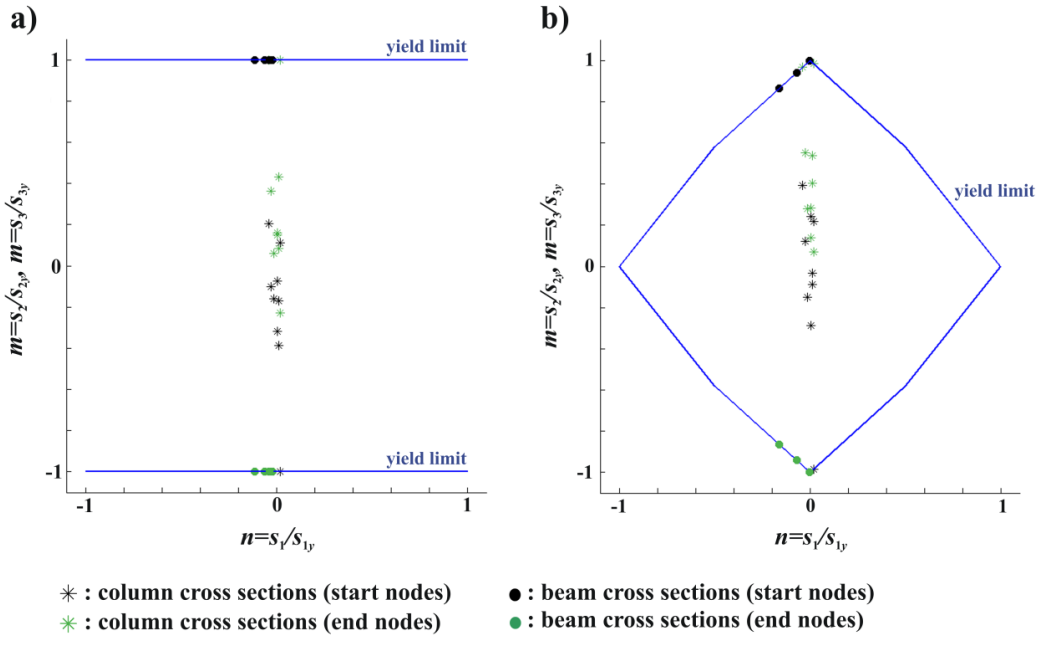

Fig. 3.9: Interaction diagrams for a) pure bending and b) NM interaction.

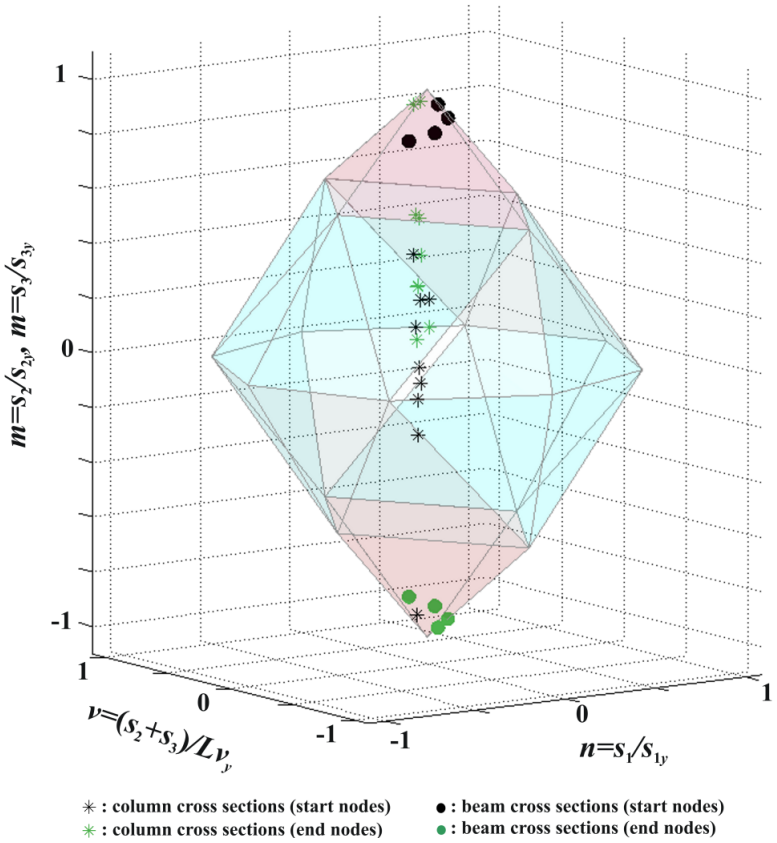

Fig. 3.10: Interaction diagrams for NQM interaction.

3.7.2. Example #2

The second example concerns the three-storey, four-bay plane frame, shown in Fig. 3.11, which is subjected to increasing lateral and fixed vertical loading. The frame is discretized into 39 elements, 32 nodes and 81 degrees of freedom. The steel grade is S235 with $E=2\times10^8$kN/m^2. Sections with $A=112.5\times10^{-4}$ m^2, $I=18260\times10^{-8}$ m^4, $s_{1y}=2643.75$ kN, $v_y=505.4$ kN, $s_{2y}=325$ kNm, $s_{3y}=325$ kNm and sections with $A=62.61\times10^{-4}$ m^2, $I=11770\times10^{-8}$ m^4, $s_{1y}=1471.34$ kN, $v_y=418.06$ kN, $s_{2y}=189.01$ kNm, $s_{3y}=189.01$ kNm are employed for all columns and beams respectively. Analysis results of all cases are presented in Table 3.3.

The maximum load factor attains its greatest value for pure bending consideration and the smallest for NQM interaction. Results of convex hull formulation (cases (b_2) and (c_2)) are the same (values of variables and collapse mechanism) with those of cases (b_1) and (c_1) correspondingly. However, convex hull formulation converges in 1.14 times less time for case (b) and 14.92 times faster for case (c), taking into account the required time for both matrix formulation and the optimization procedure.

In terms of time of mere optimization process, convex hull formulation converges 1.20 times faster for case (b) and 2.45 times faster for case (c), due to the presence of significantly fewer constraints.

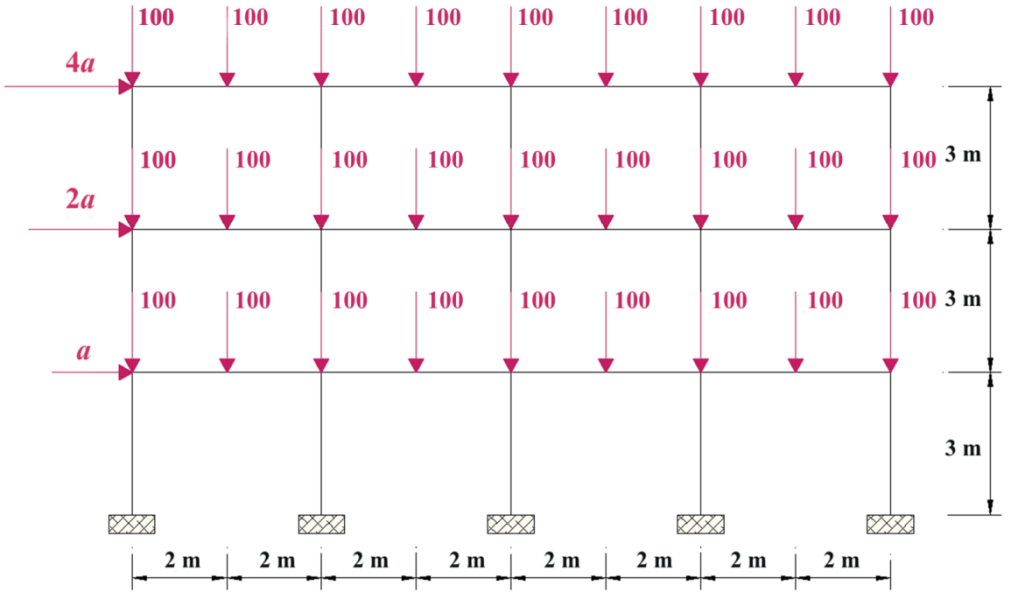

Fig. 3.11: Three-storey, four-bay steel frame.

Table 3.3: Analysis results of all cases for example #2.

Cases	Bending (a)	NM interaction (b_1)	NM interaction Convex Hull (b_2)	NQM interaction (c_1)	NQM interaction Convex Hull (c_2)
number of variables n_{var}	**118**	**118**	**742**	**118**	**1522**
number of equality constraints n_{eq}	**81**	**81**	**315**	**81**	**393**
number of inequality constraints n_{inq}	—	**624**	—	**2496**	—
maximum load factor α (kN)	**117.69**	**108.33**	**108.33**	**95.29**	**95.29**
number of plastic hinges	**26**	**33**	**33**	**34**	**34**
total computational time (s)	**0.40**	**0.66**	**0.58**	**11.49**	**0.77**
computational time for the optimization process (s)	**0.38**	**0.61**	**0.51**	**1.59**	**0.65**

Collapse mechanisms (number and position of plastic hinges) is also affected by the assumed interaction of stresses. For case (a) fewer plastic hinges are formed that reach their yield limit due to bending moment, as shown in Fig. 3.12. Plastic hinge patterns for cases (b) and (c) are shown in Fig. 3.13a and Fig. 3.14a . The role of bending moment is dominant for all cases. However, the effect of axial force is evident at column cross sections that yield under the effect of combined stresses (Fig. 3.13b), while they reside in the elastic region for pure bending consideration (Fig. 3.12b). Moreover, the effect of shear force for some beam and column cross sections is more intense than that of axial force, as shown in Fig. 3.14d.

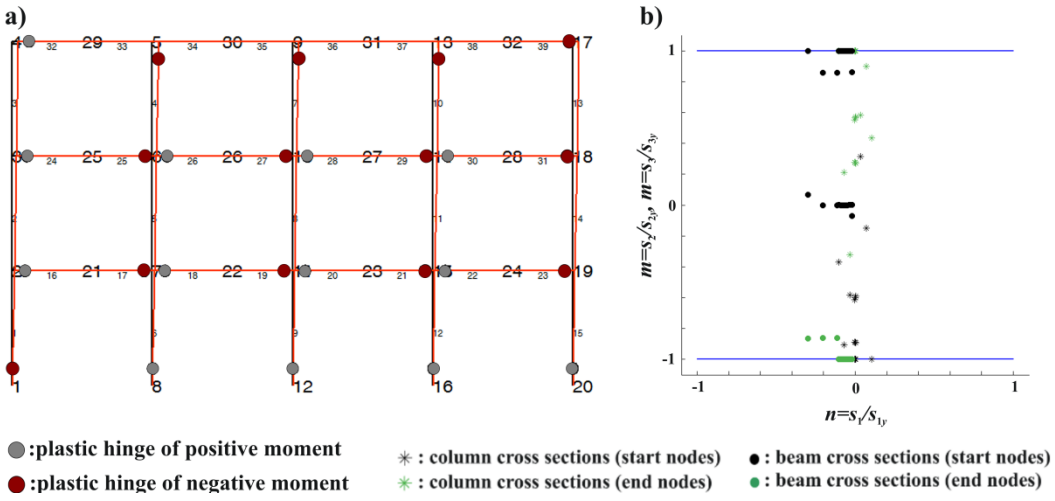

Fig. 3.12: a) Plastic hinge pattern and b) interaction diagram for pure bending.

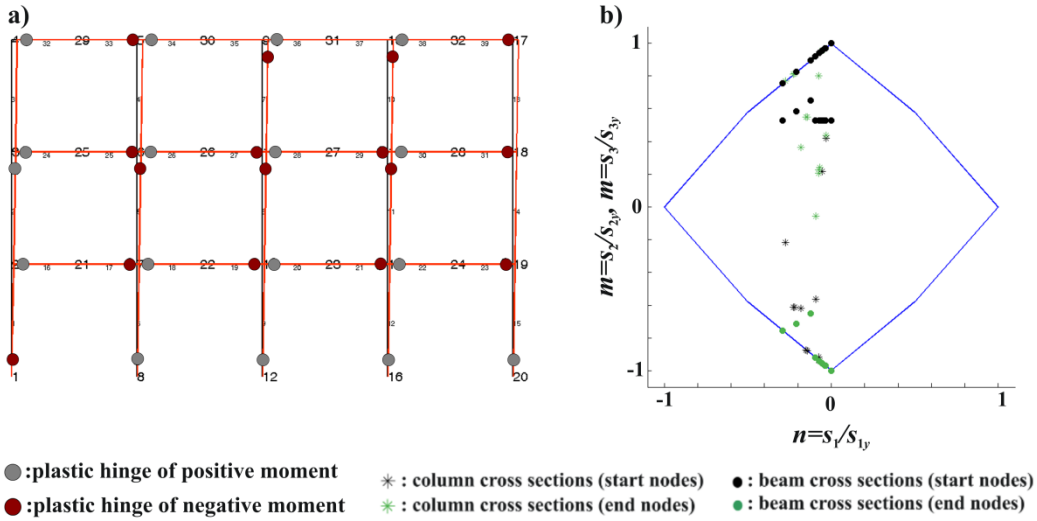

Fig. 3.13: a) Plastic hinge pattern and b) interaction diagram for NM interaction.

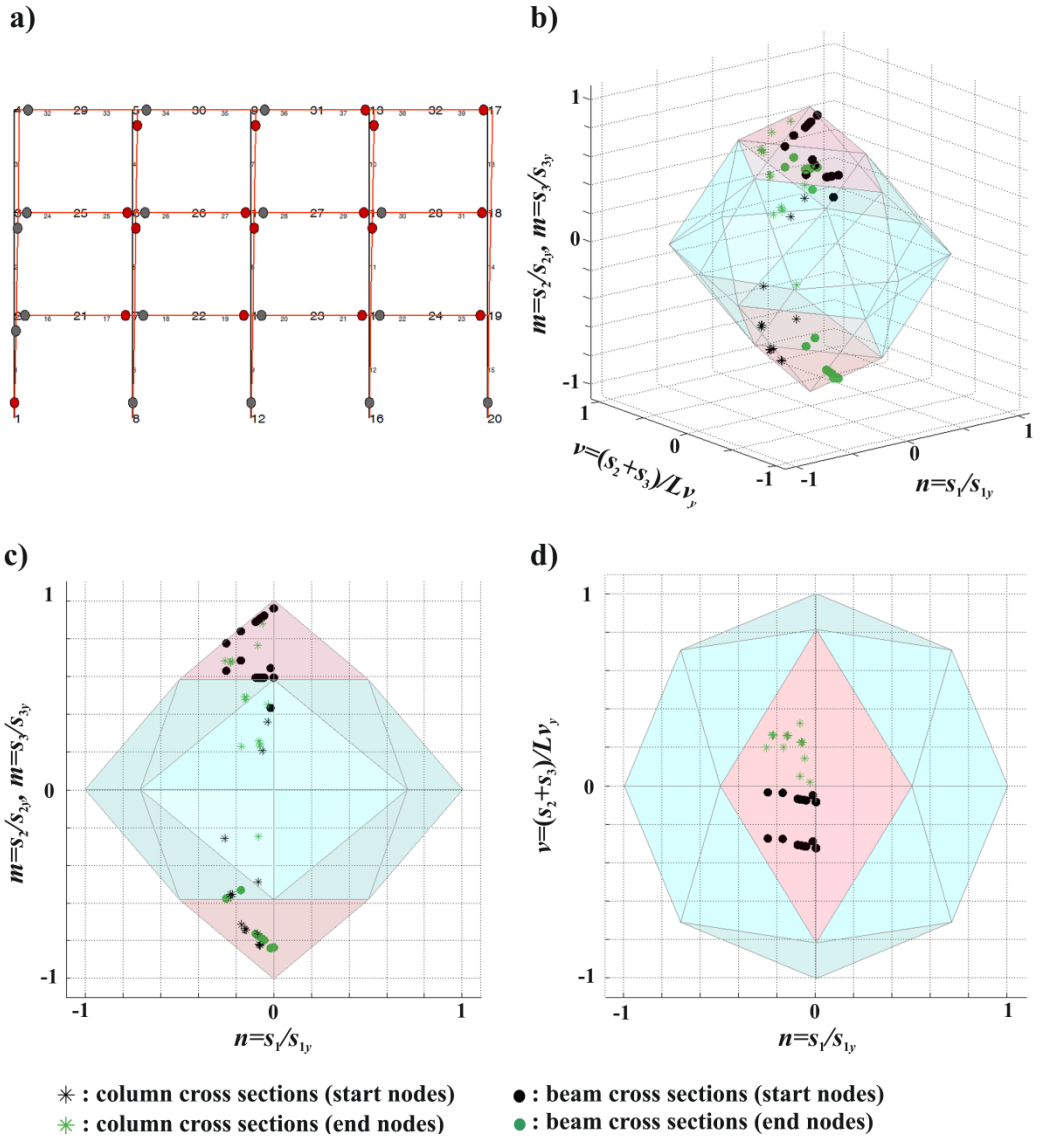

Fig. 3.14: a) Plastic hinge pattern and b), c) and d) views of the interaction diagram for NQM interaction.

3.7.3. Example #3

The third example concerns the six-storey, four-bay plane frame, shown in Fig. 3.15, that is subjected to increasing lateral and fixed vertical loading. The frame is discretized into 78 elements, 59 nodes and 162 degrees of freedom. The steel grade is S235 with $E=2\times10^8$kN/m^2. Sections with $A=197.5\times10^{-4}$ m^2, $I=86970\times10^{-8}$ m^4, $s_{1y}=4641.3$ kN, $v_y=1013.24$ kN, $s_{2y}=928.02$ kNm, $s_{3y}=928.02$ kNm and sections with $A=84.46\times10^{-4}$ m^2, $I=23130\times10^{-8}$ m^4, $s_{1y}=1984$ kN, $v_y=579.22$ kN, $s_{2y}=307.15$ kNm, $s_{3y}=307.15$ kNm are employed for all columns and beams respectively. Analysis results of all cases are presented in Table 3.4.

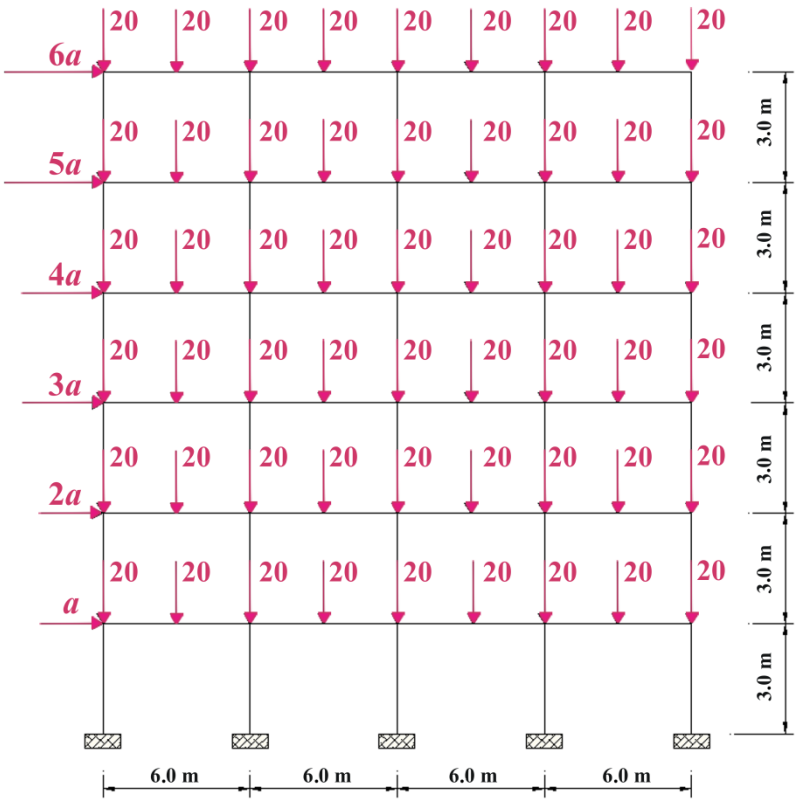

Fig. 3.15: Six-storey, four-bay plane steel frame.

Table 3.4: Analysis results of all cases for example #3.

Cases	Bending (a)	NM interaction (b_1)	NM interaction Convex Hull (b_2)	NQM interaction (c_1)	NQM interaction Convex Hull (c_2)
number of variables n_{var}	**235**	**235**	**1483**	**235**	**3043**
number of equality constraints n_{eq}	**162**	**162**	**630**	**162**	**786**
number of inequality constraints n_{inq}	—	**1248**	—	**4992**	—
maximum load factor a (kN)	**71.00**	**67.26**	**67.26**	**59.25**	**59.25**
number of plastic hinges	**53**	**58**	**58**	**58**	**58**
total computational time (s)	**0.42**	**0.89**	**0.76**	**18.92**	**1.10**
computational time for the optimization process (s)	**0.40**	**0.79**	**0.67**	**2.39**	**0.90**

The axial-shear force-bending moment interaction corresponds to the lowest value of the maximum load factor and pure bending consideration to the greatest, as expected. Analysis results of standard and convex hull formulation are identical for both NM and NQM interaction. The computational efficiency of convex hull formulation is evident, since the solution is obtained 1.17 times and 17.2 times faster for cases (b) and (c) respectively. This concerns the total computational time (formulation of the required matrices and optimization process), while the mere optimization procedure of convex hull formulation is 1.18 times faster for case (b) and 2.66 times for case (c).

The plastic hinge pattern (number and location) differs for pure bending and combined stresses, as shown in Fig. 3.16. Fewer plastic hinges are formed for case (a) that reach their yield limit due to bending moment. The effect of combined stresses is evident at the yielded column cross sections (Fig. 3.16b) that under pure bending consideration remain elastic. The corresponding interaction diagrams are presented in Fig. 3.17. The frame is mainly stressed due to bending moment (the dispersion of stress points is wider along the bending moment axis) for all cases.

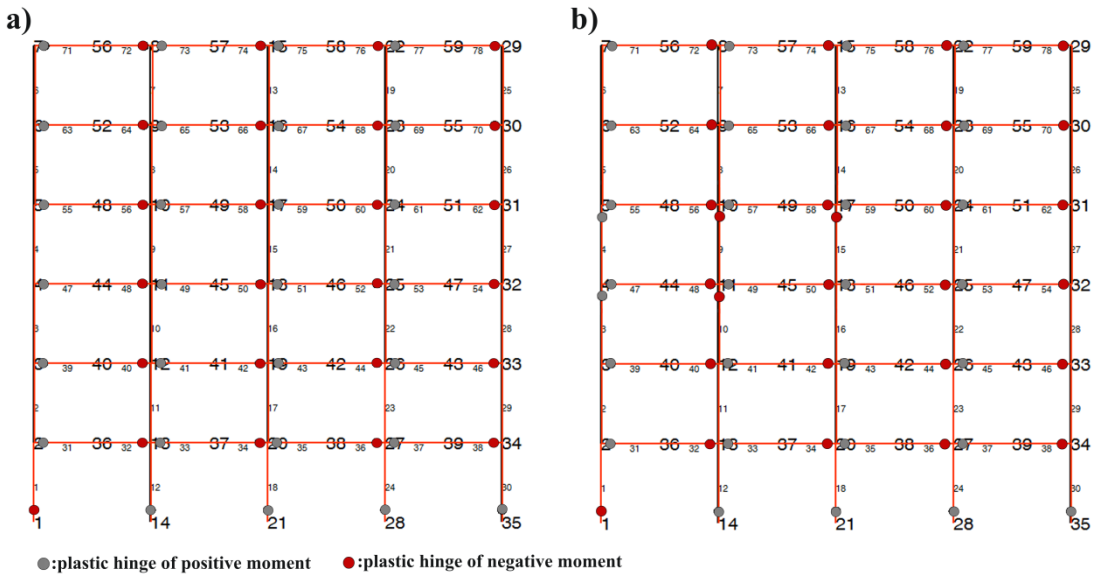

Fig. 3.16: Plastic hinge patterns for a) pure bending and b) NM and NQM interaction.

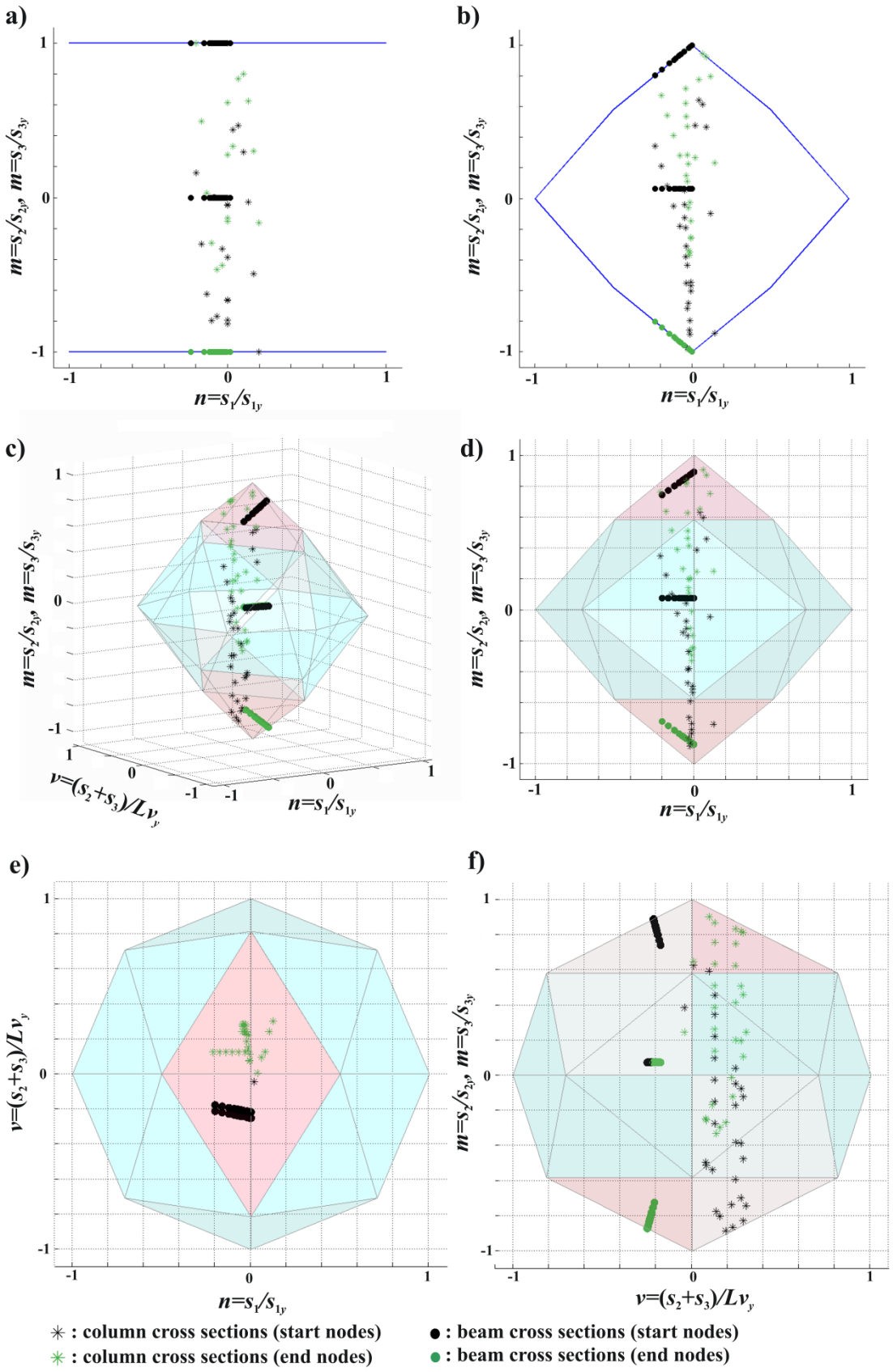

Fig. 3.17: Interaction diagrams for all analysis cases.

3.7.4. Example #4

The fourth example concerns the six-storey, four-bay plane frame, shown in Fig. 3.18, that is subjected to increasing lateral and fixed vertical loading. The frame is discretized into 73 elements, 56 nodes and 153 degrees of freedom. The steel grade is S235 with $E=2\times10^8$kN/m^2. Sections with $A=197.5\times10^{-4}$ m^2, $I=86970\times10^{-8}$ m^4, $s_{1y}=4641.3$ kN, $v_y=1013.24$ kN, $s_{2y}=928.02$ kNm, $s_{3y}=928.02$ kNm and sections with $A=84.46\times10^{-4}$ m^2, $I=23130\times10^{-8}$ m^4, $s_{1y}=1984$ kN, $v_y=579.22$ kN, $s_{2y}=307.15$ kNm, $s_{3y}=307.15$ kNm are employed for all columns and beams respectively. Analysis results of all cases are presented in Table 3.5.

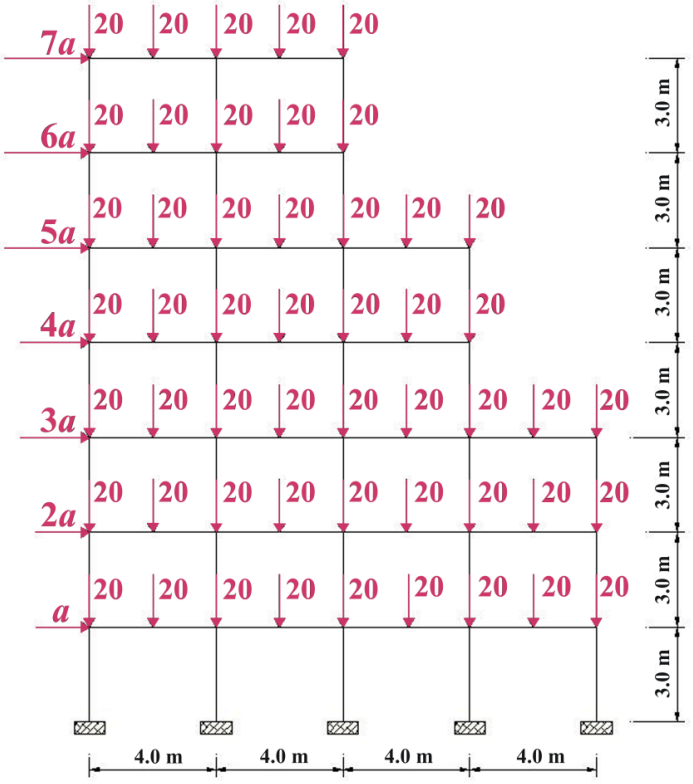

Fig. 3.18: Plane steel frame, example#4.

It is evident that multi-component interaction yields reduced load factors compared to pure bending consideration. Results of convex hull formulation (cases (b_2) and (c_2)) are the same (values of variables and collapse mechanism) with those of cases (b_1) and (c_1) correspondingly. However, the standard compared to convex hull formulation requires more computational time, i.e. 1.03 times for case (b) and 12.67 times for case

(c). In terms of time of mere optimization process, the corresponding values are 1.05 and 2.26 times.

Table 3.5: Analysis results of all cases for example #4.

Cases	Bending (a)	NM interaction (b_1)	NM interaction Convex Hull (b_2)	NQM interaction (c_1)	NQM interaction Convex Hull (c_2)
number of variables n_{var}	**220**	**220**	**1388**	**220**	**2848**
number of equality constraints n_{eq}	**153**	**153**	**591**	**153**	**737**
number of inequality constraints n_{inq}	—	**1168**	—	**4672**	—
maximum load factor a (kN)	**43.26**	**40.92**	**40.92**	**36.29**	**36.29**
number of plastic hinges	**49**	**51**	**51**	**52**	**52**
total computational time (s)	**0.41**	**0.94**	**0.91**	**15.59**	**1.23**
computational time for the optimization process (s)	**0.39**	**0.87**	**0.83**	**2.21**	**0.98**

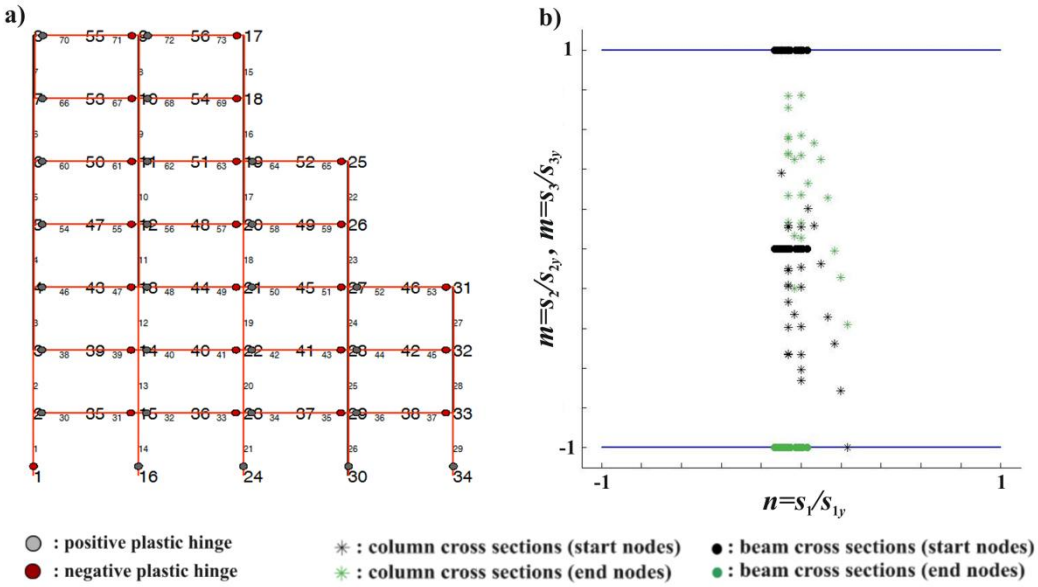

Fig. 3.19: a) *Plastic hinge pattern and b) interaction diagram for pure bending.*

The interaction of stresses affects also the collapse mechanisms (number and position of plastic hinges). For case (a) fewer plastic hinges are formed that reach their yield limit due to bending moment, as shown in Fig. 3.19. Plastic hinge patterns for cases (b) and (c) are shown in Fig. 3.20a and Fig. 3.21a . The role of bending moment is dominant for all cases. However, the effect of axial force is evident at column cross sections that yield under the effect of combined stresses (Fig. 3.20b, Fig. 3.22a), while they reside in the elastic region for pure bending consideration (Fig. 3.19b). Moreover, the effect of shear force for some beam and column cross sections is more intense than that of axial force, as shown in Fig. 3.22b.

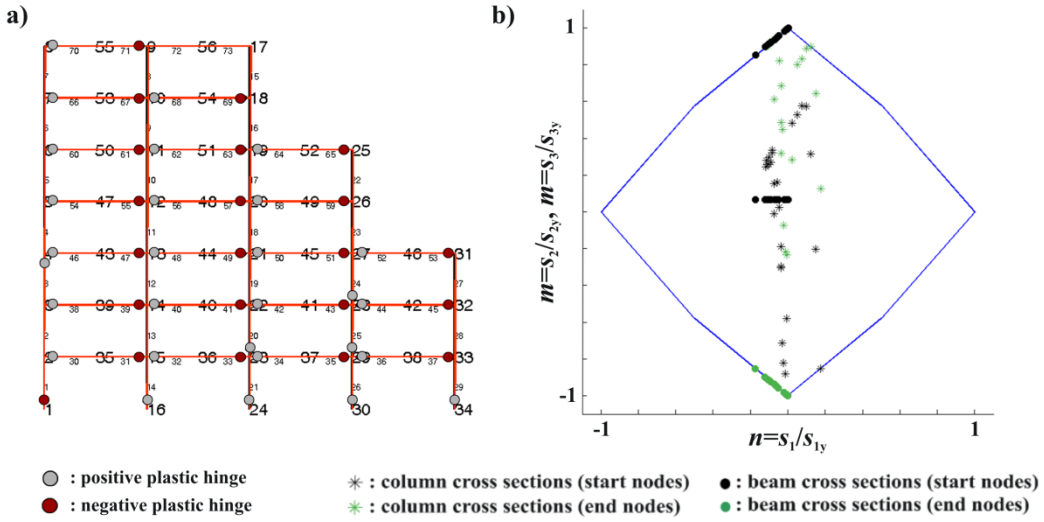

Fig. 3.20: a) *Plastic hinge pattern and b) interaction diagram for NM interaction.*

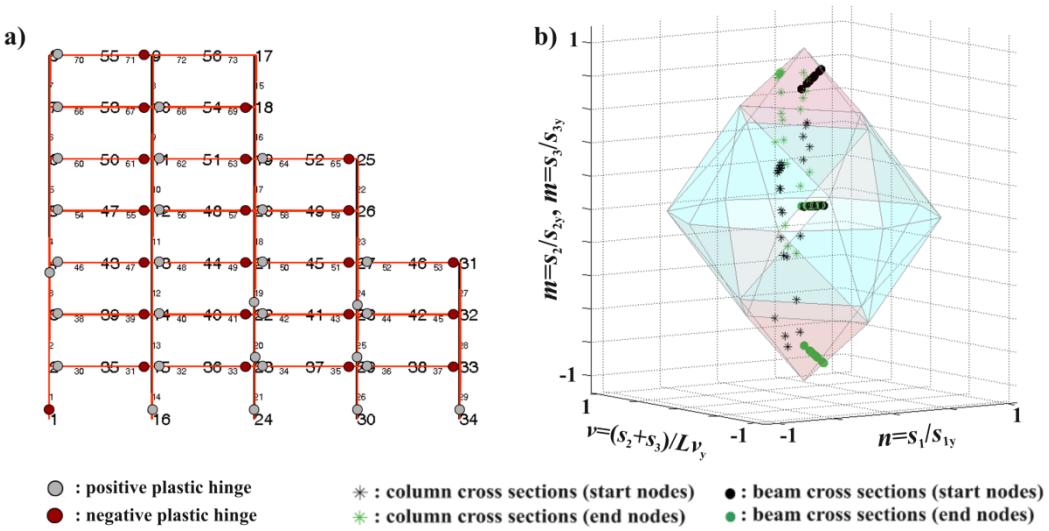

Fig. 3.21: a) *Plastic hinge pattern and b) interaction diagram for NQM interaction.*

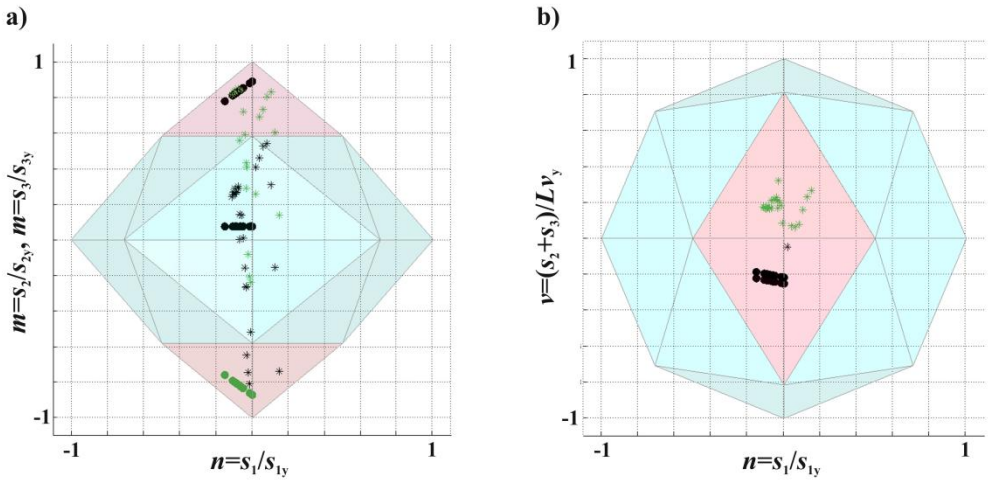

Fig. 3.22: Plan views of NQM interaction diagram.

3.8. Concluding remarks

In this chapter limit analysis is treated in the framework of mathematical programming introducing a convex hull formulation for the yield condition for both static and kinematic theorems.

The yield polyhedron is usually considered as the intersection of a finite number of halfspaces and hyperplanes, according to the standard formulation. This is expressed by a set of inequality constraints, the number of which depends on the number of hyperplanes. Alternatively, a convex hull formulation expresses the yield condition in the form of a linear combination of the vectors corresponding to all vertices that define the a priori linearized yield hypersurface. This leads to a set of equality constraints, the number of which depends on the dimensionality of interaction and thus independent of the number of the yield hyperplanes. However, the number of variables is increased compared to the standard formulation, since nonnegative coefficients θ are introduced. The two yield formulations generate the corresponding static (primal) LP problems that differ in the number of variables and yield constraints. These are compared in terms of their computational efficiency for axial force-bending moment (NM) and axial-shear force-bending moment interaction (NQM). Moreover, the dual kinematic theorem is stated following the two alternative formulations for the yield conditions and the features of the dual problem are compared and discussed.

The presented numerical examples prove that convex hull formulation requires significantly less computing time compared to the standard one for both cases of interaction. More specifically, for NQM interaction the computational efficiency of convex hull formulation corresponds to a more than 15 times reduction in computing time. This concerns the total computational time including both matrix formulation and optimization procedure. In terms of time of the mere optimization process, convex hull formulation converges almost 2.5 times faster compared to the hyperplane (standard) formulation. This is due to fewer constraints since the convex hull formulation is independent of the number of planes that approximate the nonlinear yield surface, contrary to the standard approach. Moreover, the increased number of variables for convex hull formulation is associated with the number of vertices, which is noticeably smaller compared to the number of planes for the case of 3D interaction. Thus, convex hull formulation favors the conservative static theorem expressing advantageously multi-component interaction, enabling also finer discretization of the nonlinear yield surface.

Convex hull formulation results more efficient in analyzing the effect of axial force-bending moment (NM) and axial-shear force-bending moment (NQM) interaction on the ultimate load and collapse mechanism of a structure. The combined stresses generally correspond to reduced maximum load factors and to collapse mechanisms with more plastic hinges, compared to bending consideration with no interaction, and thus their effect should be taken into account for safer structural design.

Chapter 4

Limit Load and Deformation Analysis for Plane Frames: A Cone Identification Approach

4.1. Basic assumptions

Limit analysis determines the ultimate load of a structure under equilibrium and yield constraints, whereas deformation analysis refers to restrictions imposed by compatibility relations. These constraints together with complementarity conditions form a mathematical programming problem that aims at the maximization of the load factor that a structure can sustain. The fundamental relations that describe the problem are discussed in detail in the following sections.

The entire formulation is based on the following assumptions. Plane frames consist of n_{el} straight prismatic elements, with n_f nodal degrees of freedom subjected only to nodal loading for reasons of simplicity. Frame displacements are assumed small enough so that the equilibrium equations refer to the initial undeformed configuration. Plastic hinges are considered formed only at critical sections, i.e. the end sections of the elements, whereas the remaining parts behave elastically. The nonlinear inelastic behavior at critical sections is described by a multi-linear model and yield conditions are beforehand appropriately linearized. The cases of axial force-bending moment (NM) interaction and axial-shear force-bending moment (NQM) interaction are examined. Euler-Bernoulli or Timoshenko beam theory accounting for shear deformation effects is considered offering accurate stresses for regular and deep sections respectively. In both cases comparatively large shear forces may be induced that should be taken into account in the strength interaction. Apparent softening behavior (caused by local buckling, lateral-torsional buckling or by the semi-rigid nature of some steel connection types) is incorporated. Furthermore, under the external loading, if local unloading occurs, is assumed happening along the load displacement path and not as elastic unloading, adopting a holonomic, i.e. path-independent structural behavior. Although this is a simplified assumption, especially for the case of softening behavior, it can be considered reasonable for monotonically increasing external actions (Donato and Maier 1976, Tangaramvong and Tin-Loi 2007, 2008). Moreover, isotropic hardening is adopted, which under holonomic assumption and monotonic loading yields satisfactory results. For cyclic loading though, kinematic hardening is more appropriate and definitively closer to real behavior of steel structures.

The formulation of the problem requires treatment at three different levels, i.e. the level of critical cross sections, the element level and the structural level. All final

equations are expressed in dimensional form at the structural level. The yield conditions, though, are first introduced in nondimensional form. Moreover, the method follows the sign convention of matrix structural analysis, whereas final results are presented on the basis of engineering sign convention.

4.2. Equilibrium of plane frames

It is reminded that the structural equilibrium relationship for the whole structure is established as:

$$\boldsymbol{B}\cdot\boldsymbol{s} = a\cdot\boldsymbol{f} + \boldsymbol{f_d} \tag{4.1}$$

which is analytically defined in Chapter 3, section 3.2.

4.3. Compatibility condition

For small displacements considered in this work, the relation between the member deformation $\boldsymbol{q}^i$ in the local system and the nodal displacements $\boldsymbol{u}^i$ at global axes system is given as:

$$\boldsymbol{q}^i = \boldsymbol{B}^{iT}\cdot\boldsymbol{u}^i \tag{4.2}$$

where $\boldsymbol{q}^i = \left\{ q_1^i \quad q_2^i \quad q_3^i \right\}^T$, q_1^i and q_2^i are the axial deformation and the rotation of the chord at the start node j and q_3^i is the rotation of the chord at the end node k of the member, $\boldsymbol{u}^i = \left\{ \mathrm{u}^j \quad \mathrm{v}^j \quad \theta^j \quad \mathrm{u}^k \quad \mathrm{v}^k \quad \theta^k \right\}^T$ is the vector of nodal displacements expressed at the global coordinate system containing the global X and global Y displacements and rotations of start node j and end node k respectively. The (3×1) vector $\boldsymbol{q}^i$ determines directly the deformation state of the element and dictates the selection of the primary end actions in the equilibrium relation (4.1).

The compatibility condition for the whole structure is then given by the following linear compatibility relation:

$$\boldsymbol{q} = \boldsymbol{B}^T \cdot \boldsymbol{u} \tag{4.3}$$

where $\boldsymbol{q}$ is the ($3n_{el} \times 1$) deformation vector of the structure and $\boldsymbol{u}$ is the ($n_f \times 1$) nodal displacement vector.

4.4. Constitutive relations

The constitutive relations that govern the behavior of an element in the elastic and inelastic regime are based on the decomposition of deformation into an elastic and plastic component. For each element this is expressed as:

$$\boldsymbol{q}^i = \boldsymbol{e}^i + \boldsymbol{p}^i \tag{4.4}$$

where $\boldsymbol{e}^i$ is the (3×1) element elastic deformation vector and $\boldsymbol{p}^i$ is the (3×1) element plastic deformation vector.

The elastic part is fully described by the relation:

$$\begin{Bmatrix} s_1^i \\ s_2^i \\ s_3^i \end{Bmatrix} = \begin{bmatrix} EA^i / L^i & 0 & 0 \\ 0 & 4EI^i/L^i & 2EI^i/L^i \\ 0 & 2EI^i/L^i & 4EI^i/L^i \end{bmatrix} \cdot \begin{Bmatrix} e_1^i \\ e_2^i \\ e_3^i \end{Bmatrix} \quad or \quad \boldsymbol{s}^i = \boldsymbol{S}^i \cdot \boldsymbol{e}^i \tag{4.5}$$

where E is the modulus of elasticity, A^i is the area of the element cross section , $\boldsymbol{I}^i$ is the moment of inertia of the element, e_1^i, e_2^i are the elastic axial deformation and rotation of the chord at the start node j , e_3^i is the elastic rotation of the chord at end node k and $\boldsymbol{S}^i$ is the (3×3) element stiffness matrix. Accounting also for shear deformations effects, within the Timoshenko beam theory, the element elastic stiffness matrix is modified as (Oñate 2013):

$$\boldsymbol{S}^i = \begin{bmatrix} EA^i / L^i & 0 & 0 \\ 0 & \dfrac{4+\beta^i}{1+\beta^i}\dfrac{EI^i}{L^i} & \dfrac{2-\beta^i}{1+\beta^i}\dfrac{EI^i}{L^i} \\ 0 & \dfrac{2-\beta^i}{1+\beta^i}\dfrac{EI^i}{L^i} & \dfrac{4+\beta^i}{1+\beta^i}\dfrac{EI^i}{L^i} \end{bmatrix} \tag{4.6}$$

where the term β^i expresses the relative importance of the bending deformations to the shear deformations as:

$$\beta^i = \frac{12E^iI^i}{GA^i_{vz}L^{i2}} \tag{4.7}$$

where G is the shear modulus and A^i_{vz} is the shear area of element cross section. It is noted that shear deformation effects are significant for relative deep beams, for which Timoshenko beam theory is more appropriate. For $\beta^i = 0$ shear deformation effects are neglected and the stiffness matrix of equation (4.6) is reduced to that of equation (4.5).

Following the notions of classical plasticity, element plastic deformations $\boldsymbol{p}^i$ are considered perpendicular to the yield surface, which for a piecewise linear approximation and in view of the holonomic assumption can be defined as follows:

$$\begin{Bmatrix} p^i_1 \\ p^i_2 \\ p^i_3 \end{Bmatrix} = \begin{bmatrix} \left(s^i_{2y}a^j_1\right)/\left(s^i_{1y}a^j_2\right) & -\left(s^i_{3y}a^k_1\right)/\left(s^i_{1y}a^k_2\right) \\ 1 & 0 \\ 0 & 1 \end{bmatrix} \begin{Bmatrix} \mathrm{z}^j \\ \mathrm{z}^k \end{Bmatrix} \quad or \quad \boldsymbol{p}^i = \boldsymbol{N}^i \cdot \mathbf{z}^i \tag{4.8}$$

where p^i_1, p^i_2 are the plastic axial deformation and rotation of the chord at the start node j, p^i_3 is the plastic rotation of the chord at end node k, z^j, z^k are the plastic multipliers for j and k element sections respectively, $\boldsymbol{N}^i$ is the matrix that contains the normal-to the yield surface-vectors (it is defined in detail in section 4.5) and $\mathbf{z}^i$ is the (2×1) vector of element plastic multipliers.

For the entire structure the deformation is decomposed into an elastic and plastic component as:

$$\boldsymbol{q} = \boldsymbol{e} + \boldsymbol{p} = \boldsymbol{S}^{-1} \cdot \boldsymbol{s} + \boldsymbol{N} \cdot \mathbf{z} \tag{4.9}$$

where $\boldsymbol{e}$ is the ($3n_{el} \times 1$) elastic and $\boldsymbol{p}$ the ($3n_{el} \times 1$) plastic component of deformation respectively, $\boldsymbol{S}$ is the ($3n_{el} \times 3n_{el}$) assembled block diagonal matrix of all element stiffness matrices and $\boldsymbol{N}$ is defined in the following section.

4.5. Yield condition

Yield condition is the one that denotes the limit between elastic and plastic region under the effect of combined stresses. Herein, two considerations are examined, i.e. axial force-bending moment (NM) interaction and axial-shear force-bending moment (NQM) interaction. For both considerations, the nonlinear yield criterion is beforehand appropriately linearized either with linear segments (case of 2D interaction) or plane triangles (case of 3D interaction).

4.5.1. Axial force-bending moment interaction (NM interaction)

At every element *i*, plastic behavior is described at start node *j* by the normalized stress vector $\left\{ n^j \quad m^j \right\}^T = \left\{ s_1^i / s_{1y}^i \quad s_2^i / s_{2y}^i \right\}^T$ and at end node *k* by $\left\{ n^k \quad m^k \right\}^T = \left\{ -s_1^i / s_{1y}^i \quad s_3^i / s_{3y}^i \right\}^T$, as defined in section 3.6. Notice that different capacities can be considered for the two element ends to account also for concrete elements with constant cross section, but different bar reinforcement at the two ends. Thus yielding at the two critical sections of the element will be expressed with respect to the three primary element actions; with the minus sign at end k expressing the pre-established equilibrium within the element along the local x direction.

The standard formulation (Maier 1970) involves all the lines describing the polygon of the PWL yield surface, which increases considerably the number of yield constraints per critical section, complicating the entire formulation also at later stages. It is feasible though, to identify the specific cone (sector of the interaction diagram) in which the stress vector resides and consider only one constraint associated to each critical section as potentially active or true active constraint. Moreover, this facilitates the incorporation of multi-linear hardening reducing the complexity of the whole problem, as described in section 4.5.3.

4.5.1.1. Cone identification for NM interaction

Joining the vertices of the linearized yield surface with the origin, a number of sectors-cones are formed that cover the entire domain (Fig. 4.1). Each stress vector corresponding to a critical section is associated to only one cone (Manola and Koumousis 2014).

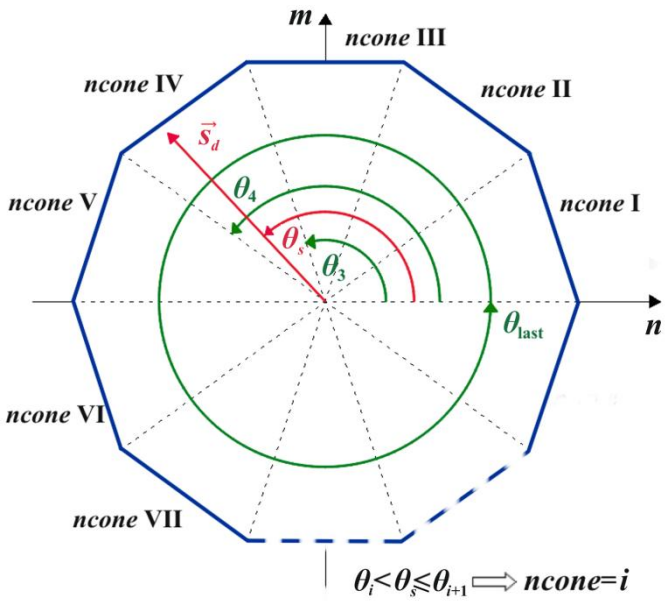

Fig. 4.1: Cone identification of stress vector.

For a given stress vector the identification of the associated cone is straight forward and results from a sorting process. First the vertices and the stress vector are transformed from Cartesian to polar coordinates. The counterclockwise angles θ_i that correspond to all vertices are sorted in increasing order. Then, the angle θ_s that refers to the normalized stress vector $\boldsymbol{s}_d$ of a particular critical section is identified at cone i for which the relation: $\theta_i < \theta_s \le \theta_{i+1}$, with $\theta_{last} = \theta_1 + 2\pi$. This simple procedure is invoked repeatedly, for every optimization iteration, offering the critical cones and the associated yield lines-hyperplanes for every cross section. Stress vectors that lie on a particular vertex may be treated differently, but herein are assigned to the cone with the smaller index.

Having this information, the yield constraint is formulated only for this specific yield line for every cross section and not for all linear segments of the PWL yield surface.

4.5.1.2. Final form of yield conditions for NM interaction

Yield conditions are generally expressed in terms of normalized quantities with respect to yield capacities. Thus, for each cross section at the start node *j* and the end node *k* the stress state is expressed as (Fig. 4.2):

$$\begin{aligned} &\mathrm{a}_1^j \cdot n^j + \mathrm{a}_2^j \cdot m^j + w_d^j = r_d^j \quad or \quad \mathrm{a}_1^j \cdot \frac{s_1^i}{s_{1y}^i} + \mathrm{a}_2^j \cdot \frac{s_2^i}{s_{2y}^i} + w_d^j = r_d^j \\ &\mathrm{a}_1^k \cdot n^k + \mathrm{a}_2^k \cdot m^k + w_d^k = r_d^k \quad or \quad -\mathrm{a}_1^k \cdot \frac{s_1^i}{s_{1y}^i} + \mathrm{a}_2^k \cdot \frac{s_3^i}{s_{3y}^i} + w_d^k = r_d^k \end{aligned} \tag{4.10}$$

where a_1^j, a_2^j and a_1^k, a_2^k are the direction cosines of the unit normal vectors a^j and a^k of the critical yield hyperplanes for sections j and k respectively, r_d^j, r_d^k are the distances of the critical hyperplanes from the origin for sections j and k respectively and w_d^j, w_d^k are the reserves in the normalized space for sections j and k respectively. It is noted that the main interest for the yield condition relies on the ratio of the strength reserve over the stress vector, which can be expressed along any direction (Fig. 4.3).

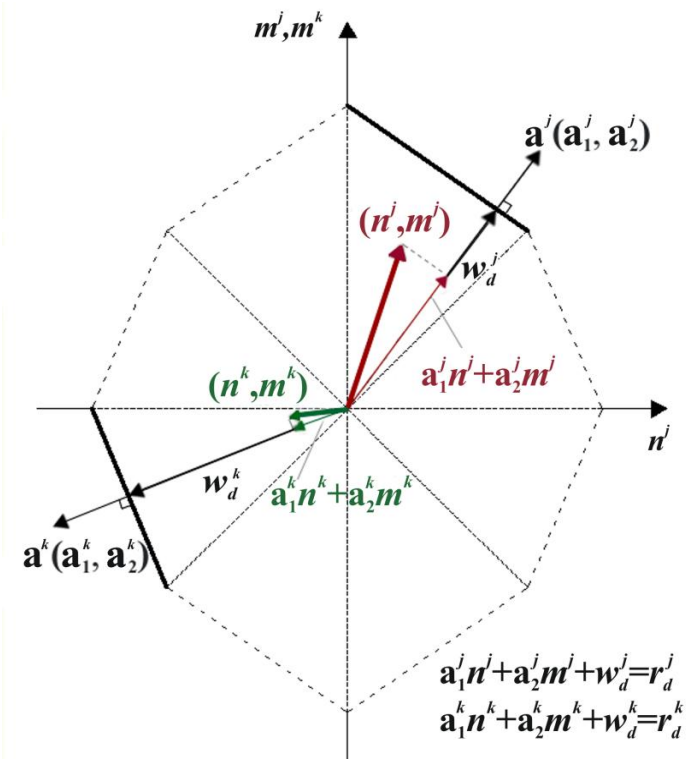

Fig. 4.2: Element stress state at both ends.

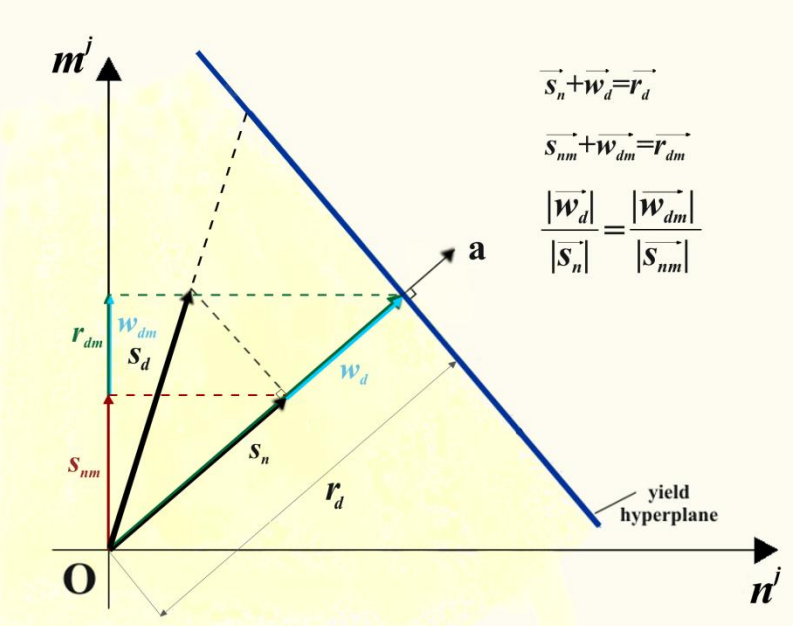

Fig. 4.3: Yield condition expressed along the direction of the normal vector and along m axis.

Herein the yield conditions are expressed in terms of dimensional stresses, which are part of the unknown vector of the present formulation, and more specifically in terms of bending moments. Thus, the above relations (4.10) are expressed as follows:

$$\begin{aligned} \frac{s_{2y}^i}{s_{1y}^i}\cdot\frac{\mathrm{a}_1^j}{\mathrm{a}_2^j}\cdot s_1^i + s_2^i + \frac{s_{2y}^i w_d^j}{\mathrm{a}_2^j} &= \tau^j \cdot s_{2y}^i \\ -\frac{s_{3y}^i}{s_{1y}^i}\cdot\frac{\mathrm{a}_1^k}{\mathrm{a}_2^k}\cdot s_1^i + s_3^i + \frac{s_{3y}^i w_d^k}{\mathrm{a}_2^k} &= \tau^k \cdot s_{3y}^i \end{aligned} \tag{4.11}$$

where $\tau^j = r_d^j / \mathrm{a}_2^j$, $\tau^k = r_d^k / \mathrm{a}_2^k$ are scaling factors for the yield moments of sections j and k respectively.

Thus the yield conditions at element level are expressed in terms of non-negative moment reserves at both element ends as:

$$\begin{Bmatrix} \mathrm{w}^j \\ \mathrm{w}^k \end{Bmatrix} = \begin{Bmatrix} \left(s_{2y}^i w_d^j\right)/\mathrm{a}_2^j \\ \left(s_{3y}^i w_d^k\right)/\mathrm{a}_2^k \end{Bmatrix} = -\begin{bmatrix} \left(s_{2y}^i \mathrm{a}_1^j\right)/\left(s_{1y}^i \mathrm{a}_2^j\right) & 1 & 0 \\ -\left(s_{3y}^i \mathrm{a}_1^k\right)/\left(s_{1y}^i \mathrm{a}_2^k\right) & 0 & 1 \end{bmatrix} \cdot \begin{Bmatrix} s_1^i \\ s_2^i \\ s_3^i \end{Bmatrix} + \begin{Bmatrix} \tau^j s_{2y}^i \\ \tau^k s_{3y}^i \end{Bmatrix} \geq 0 \ \ or \tag{4.12}$$

$$\boldsymbol{w}^i = -\boldsymbol{N}^{iT} \cdot \boldsymbol{s}^i + \boldsymbol{r}^i \geq \boldsymbol{0}$$

where $\boldsymbol{w}^j$, $\boldsymbol{w}^k$ are the moment reserves at element ends j and k respectively, $\boldsymbol{w}^i$ is the (2×1) vector that contains the moment reserves of both element ends, $\boldsymbol{N}^i$ is the (3×2) matrix that contains all scaled normal vectors of the identified yield hyperplanes and $\boldsymbol{r}^i$ is the (2×1) vector of the yield limits expressed in bending moment terms. It is noted

At structural level the yield condition is finally formed as:

$$\boldsymbol{w} = -\boldsymbol{N}^T \cdot \boldsymbol{s} + \boldsymbol{r} \geq \boldsymbol{0} \tag{4.13}$$

where $\boldsymbol{w} = \left\{\boldsymbol{w}^1 ... \boldsymbol{w}^n\right\}^T$ ($(2n_{el}\times1)$ vector), $\boldsymbol{N}$ ($(3n_{el}\times2n_{el})$ matrix) is the assembled block diagonal matrix of all $\boldsymbol{N}^i$ matrices and $\boldsymbol{r} = \left\{\boldsymbol{r}^1 ... \boldsymbol{r}^n\right\}^T$ is a $(2n_{el}\times1)$ vector.

According to the proposed formulation, incorporation of the cone identification procedure at this stage results into one yield constraint for every critical cross section. This corresponds to the hyperplane that is targeted or activated at this particular loading instance. Thus the number of the yield conditions is significantly reduced and the problem becomes independent of the number of linear segments used for the linearization of the yield surface. Cone identification is performed at every loading step generating only the necessary yield constraints with physical meaning for each particular cross section.

4.5.2. Axial-shear force-bending moment interaction (NQM interaction)

Plastic behavior is developed herein under the combined effect of axial-shear force-bending moment interaction (NQM interaction). Plastic hinges at start nodes j are formed under the combined normalized stresses $\left\{n^j \;\; v^j \;\; m^j\right\}^T = \left\{s_1^i / s_{1y}^i \quad \left(s_2^i + s_3^i\right) / L^i v_y^i \quad s_2^i / s_{2y}^i\right\}^T$ and at end node k due to $\left\{n^k \; v^k \; m^k\right\}^T = \left\{-s_1^i / s_{1y}^i \quad -\left(s_2^i + s_3^i\right) / L^i v_y^i \quad s_3^i / s_{3y}^i\right\}^T$, as defined in section 3.6. It is noted that yield limits of axial, shear force and bending moment are considered herein to be the same for both elements ends, but the formulation can incorporate also different yield limits appropriate for prismatic elements with different strengthening at the two end cross sections.

4.5.2.1. Cone Identification for NQM interaction

The 3D nonlinear yield surface is herein a priori linearized with appropriate tessellation of specific plane triangles. The vertices of each triangle (V_1, V_2, V_3) together with the origin (V_4) form one cone-tetrahedron (Fig. 4.4). Each stress point belongs only to one of these cones-tetrahedra and targets or resides on the corresponding plane triangle (Manola and Koumousis 2014). For the stress point $P = (n, v, m)$ and the tetrahedron having the vertices:

$$V_1 = (n_1, v_1, m_1),\ V_2 = (n_2, v_2, m_2),\ V_3 = (n_3, v_3, m_3),\ V_4 = (0, 0, 0) \tag{4.14}$$

the stress point P lies in the tetrahedron if the following five determinants have the same sign:

$$D_0 = \begin{vmatrix} n_1 & v_1 & m_1 & 1 \\ n_2 & v_2 & m_2 & 1 \\ n_3 & v_3 & m_3 & 1 \\ 0 & 0 & 0 & 1 \end{vmatrix},\ D_1 = \begin{vmatrix} n & v & m & 1 \\ n_2 & v_2 & m_2 & 1 \\ n_3 & v_3 & m_3 & 1 \\ 0 & 0 & 0 & 1 \end{vmatrix},\ D_2 = \begin{vmatrix} n_1 & v_1 & m_1 & 1 \\ n & v & m & 1 \\ n_3 & v_3 & m_3 & 1 \\ 0 & 0 & 0 & 1 \end{vmatrix},$$

$$D_3 = \begin{vmatrix} n_1 & v_1 & m_1 & 1 \\ n_2 & v_2 & m_2 & 1 \\ n & v & m & 1 \\ 0 & 0 & 0 & 1 \end{vmatrix},\ D_4 = \begin{vmatrix} n_1 & v_1 & m_1 & 1 \\ n_2 & v_2 & m_2 & 1 \\ n_3 & v_3 & m_3 & 1 \\ n & v & m & 1 \end{vmatrix} \tag{4.15}$$

Comparison of the signs of D_i and D_0 constitutes a check of whether P and V_i are on the same side of the plane i (namely the plane formed by the three points other than V_i). If P is inside all four boundary planes, then it is inside the tetrahedron. If the sign of any D_i differs from that of D_0 then P is outside boundary plane i, while if any of the determinants $D_i = 0$, then P lies on the boundary plane i.

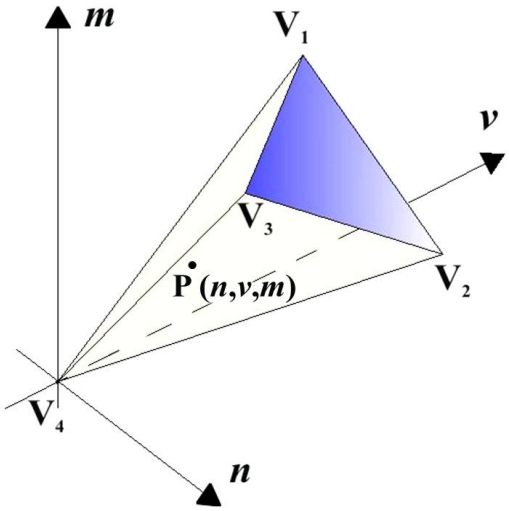

Fig. 4.4: Identification of the critical cone-tetrahedron for 3D interaction.

The aforementioned procedure is used as a basis for the identification of the critical yield plane that corresponds to each cross section at every optimization step. To avoid searching all cones for every stress point, a pruning technique is adopted that eliminates all vertices of the seven irrelevant subspaces out of the eight subspaces formed by the axes planes.

Based on coordinates (n,v,m) of each stress point, the corresponding subspace (one out of eight) is detected. Then, determinants of the tetrahedra belonging to that subspace are evaluated and compared and the critical tetrahedron corresponding to each cross section is identified. Following this procedure at every optimization step, the yield condition is formed only for the corresponding plane determined by the triangle (V_1,V_2,V_3), avoiding the formation of all unnecessary constraints of the standard formulation.

4.5.2.2. Final form of yield conditions for NQM interaction

The yield criterion for this case is represented by a 3D nonlinear surface that is approximated using plane triangles. This enables expressing the yield condition into a set of linear constraints, which is advantageous for the mathematical programming formulation of the problem. It is noted that the tessellation of the yield surface is such that the convexity of the yield criterion is retained. More specifically, the equations for the corresponding yield planes in $n-v-m$ space are of the following form:

$$\tilde{A}n+\tilde{B}v+\tilde{C}m+\tilde{D}=0 \tag{4.16}$$

where $\tilde{A},\tilde{B},\tilde{C}$ are the components of the unit normal vector of the plane and $-\tilde{D}$ is the distance of the plane from the origin. Performing appropriate algebraic manipulations, the following equations for the two element ends are obtained with respect to dimensional quantities s_1^i, s_2^i, s_3^i expressed in terms of bending moments. Thus, in these relations the coefficients of moments are deliberatively scaled to unity and the scaled yield limits are kept always positive:

$$\begin{aligned} A^j\cdot s_1^i+1\cdot s_2^i+C^j\cdot s_3^i&=D^j\cdot s_{2y}^i\\ A^k\cdot s_1^i+B^k\cdot s_2^i+1\cdot s_3^i&=D^k\cdot s_{3y}^i \end{aligned} \tag{4.17}$$

where i=1,...,n_{el} (number of elements). Relation (4.17) is written in matrix form as:

$$\begin{bmatrix} A^j & 1 & C^j\\ A^k & B^k & 1 \end{bmatrix}\cdot\begin{Bmatrix} s_1^i\\ s_2^i\\ s_3^i \end{Bmatrix}=\begin{Bmatrix} D^j\cdot s_{2y}^i\\ D^k\cdot s_{3y}^i \end{Bmatrix}\Leftrightarrow \boldsymbol{N}^{iT}\cdot\boldsymbol{s}^i=\boldsymbol{r}^i \tag{4.18}$$

where $\boldsymbol{N}^i$ is the (*3×2*) matrix of the scaled normal vectors for the element, $\boldsymbol{s}^i$ is the (*3×1*) stress vector of the element and $\boldsymbol{r}^i$ the *(2×1)* vector of the scaled yield limits of the element in terms of bending moment. The unit values in the $\boldsymbol{N}^i$ matrix facilitate the expression of plastic rotations equating them with the corresponding plastic multipliers, as presented in section 4.5.3.

Incorporating the concept of cone identification and adopting the aforementioned criterion, the yield condition for all critical sections of the frame is formed as:

$$\boldsymbol{w}=-\boldsymbol{N}^T\cdot\boldsymbol{s}+\boldsymbol{r}\geq\boldsymbol{0} \tag{4.19}$$

where $\boldsymbol{w}=\left\{\boldsymbol{w^1}...\boldsymbol{w^n}\right\}^T$ is the ($2n_{el}$ *×1)* vector containing the moment reserves of all stress points, $\boldsymbol{N}$ is the ($3n_{el}$ *×*$2n_{el}$) assembled block diagonal matrix of all $\boldsymbol{N}^i$

matrices and $\boldsymbol{r} = \left\{\boldsymbol{r^1}...\boldsymbol{r^n}\right\}^T$ is the $(2n_{el} \times 1)$ vector that includes the yield limits in terms of bending moment of the critical yield hyperplanes.

The standard formulation involves for each critical section as many yield constraints as the number of planes used for the linearization of the yield surface. Following the proposed cone identification approach only one yield constraint is required for each cross section, which reduces the total number of constraints drastically. This single constraint corresponds to the yield plane that is targeted or activated at this particular loading instance. Thus, cone identification is performed at every optimization step generating only the necessary yield constraints with physical meaning for each particular cross section. As a result, the number of yield conditions for the entire structure is not affected by the discretization of the yield surface, while the additional computational cost of the identification procedure turns out insignificant. From the optimization point of view this reduced set of yield constraints represents a mechanically dictated "active" set of constraints for the problem.

4.5.3. Incorporating hardening/softening behavior into yield condition

The combined stresses are expressed herein in terms of positive bending moment, for both cases of interaction. Thus the combination of multi-segmental constitutive relations needs also to be expressed in positive moment-rotation terms. The proportion of this combination is dictated by the particular yield hyperplane of the associated cone, depending upon the components of the normal vector of the hyperplane for a start end *j*. The initial constitutive relations of axial force-plastic axial deformation $\left(s_1 - p_1\right)$ and bending moment-plastic rotation of element end node k $\left(s_3 - p_3\right)$ are first expressed with respect to the absolute value of plastic rotation p_2. Then, they are combined with the bending moment-plastic rotation curve $\left(s_2 - p_2\right)$ to give the multi-segmental hardening/softening curve in $N^T \cdot s - p_2$ axes with reference to $s_1 - s_2 - s_3$ space (Fig. 4.5). It is noted that for end node k the constitutive relations are similarly combined and expressed with respect to plastic rotation p_3.

The above generated curves, corresponding to different cones, for symmetric constitutive relations and absolute value of plastic rotation determine a family of

curves that are parameterized in the y – axis by parameter $\tau = |D^j|$ *or* $\tau = |D^k|$ for the start and end sections j and k respectively.

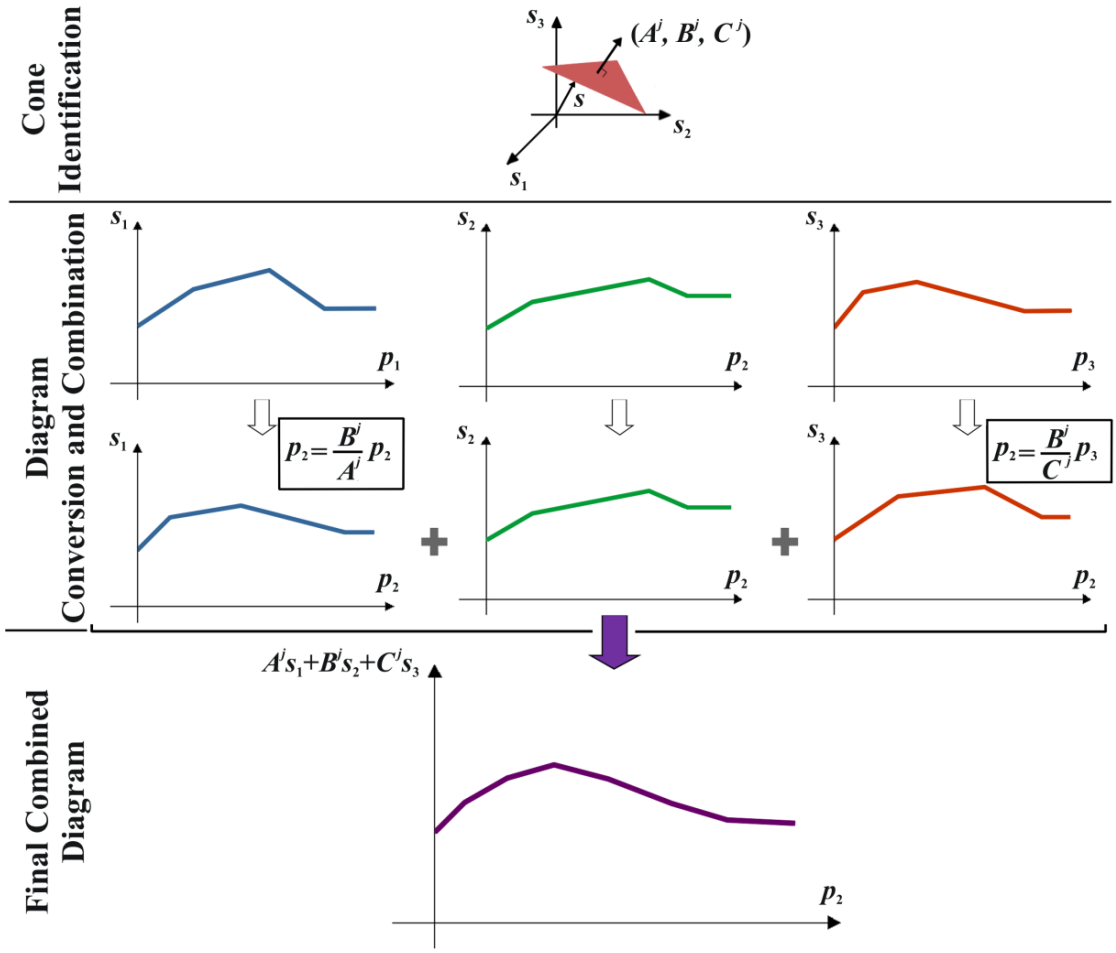

Fig. 4.5: Combined constitutive relation of a cross section j .

Moreover, the linearized yield surface is assumed to follow an isotropic multi-linear hardening law, which constitutes a simplistic consideration especially for softening behavior, but is frequently considered quite accurate for holonomic behavior and monotonically increasing loading (Tangaramvong and Tin-Loi 2008, Tin-Loi and Pang 1993). The parallel expansion/shrinkage of the identified yield plane is dictated by a multi-linear hardening/softening constitutive relation, as shown in Fig. 4.6. A plastic multiplier z_μ is assigned for each cross section μ, the non-zero value of which denotes that the specific cross section has entered the plastic region $(z_\mu \neq 0)$. Based on the particular non-zero value of the plastic multiplier, the

corresponding index n_s of the hardening segment for each cross section is identified to determine the associated stress level (Fig. 4.6c). Thus hardening matrices are built for each cross section and finally for the whole structure. The aim is to evaluate the plastic part of the combined stresses for all sections using a linear relation of the form $\boldsymbol{H}\cdot\mathbf{z}+\boldsymbol{c}$. In this, $\boldsymbol{H}$ is the hardening diagonal matrix with dimensions ($2n_{el}\times 2n_{el}$), $\mathbf{z}$ is the ($2n_{el}\times 1$) vector of all plastic multipliers and $\boldsymbol{c}$ is the ($2n_{el}\times 1$) vector, which in a recursive form accumulates all previous plastic behavior (Fig. 4.6c). For every cross section μ ($\mu=1,2...2n_{el}$) following a multi-linear hardening/softening law with total number of segments ℓ, the relations determining the non-zero entries of the hardening matrices are generated as:

$$H(\mu,\mu)=\tau\cdot h_{n_s} \qquad \mu=1...2n_{el},\ \ n_s=1...\ell \tag{4.20}$$

$$c(\mu,1)=\begin{cases} 0, & \text{for } n_s=1,\ \mu=1...2n_{el} \\ \tau\cdot\sum_{i=2}^{n_s}(h_{i-1}-h_i)\cdot \mathrm{z}_{i-1}, & \text{for } n_s\geq 2,\ i=2,3,...,n_s,\ \mu=1...2n_{el} \end{cases} \tag{4.21}$$

where λ_i is a scaling factor of the yield limit ($\lambda_0=1$) and z_i is the value of corresponding plastic multiplier at the end of segment i ($\mathrm{z}_0=0$) and $h_i=(\lambda_i-\lambda_{i-1})s_{2y}/(\mathrm{z}_i-\mathrm{z}_{i-1})$ is the dimensional inclination of the hardening/softening segments. Notice that for critical sections in the elastic region, the plastic multiplier and the hardening coefficients are zero. Moreover, for the first hardening segment $c(\mu,1)$ is zero in relation (4.21), since there is no previous plastic behavior. This means that $\boldsymbol{H}$ accounts for the current hardening/softening measure that corresponds to the identified segment, while $\boldsymbol{c}$ corresponds to the accumulated total constant previous hardening behavior.

The yield condition for the whole structure is then expressed as:

$$\boldsymbol{w}=\text{-}\boldsymbol{N}^T\cdot\boldsymbol{s}+\boldsymbol{r}'\geq\mathbf{0} \quad \text{and} \quad \boldsymbol{r}'=\boldsymbol{r}+\boldsymbol{H}\cdot\mathbf{z}+\boldsymbol{c} \tag{4.22}$$

where $\boldsymbol{r}'$ is the $(2n_{el} \times 1)$ vector including the extended limits expressed in terms of bending moment.

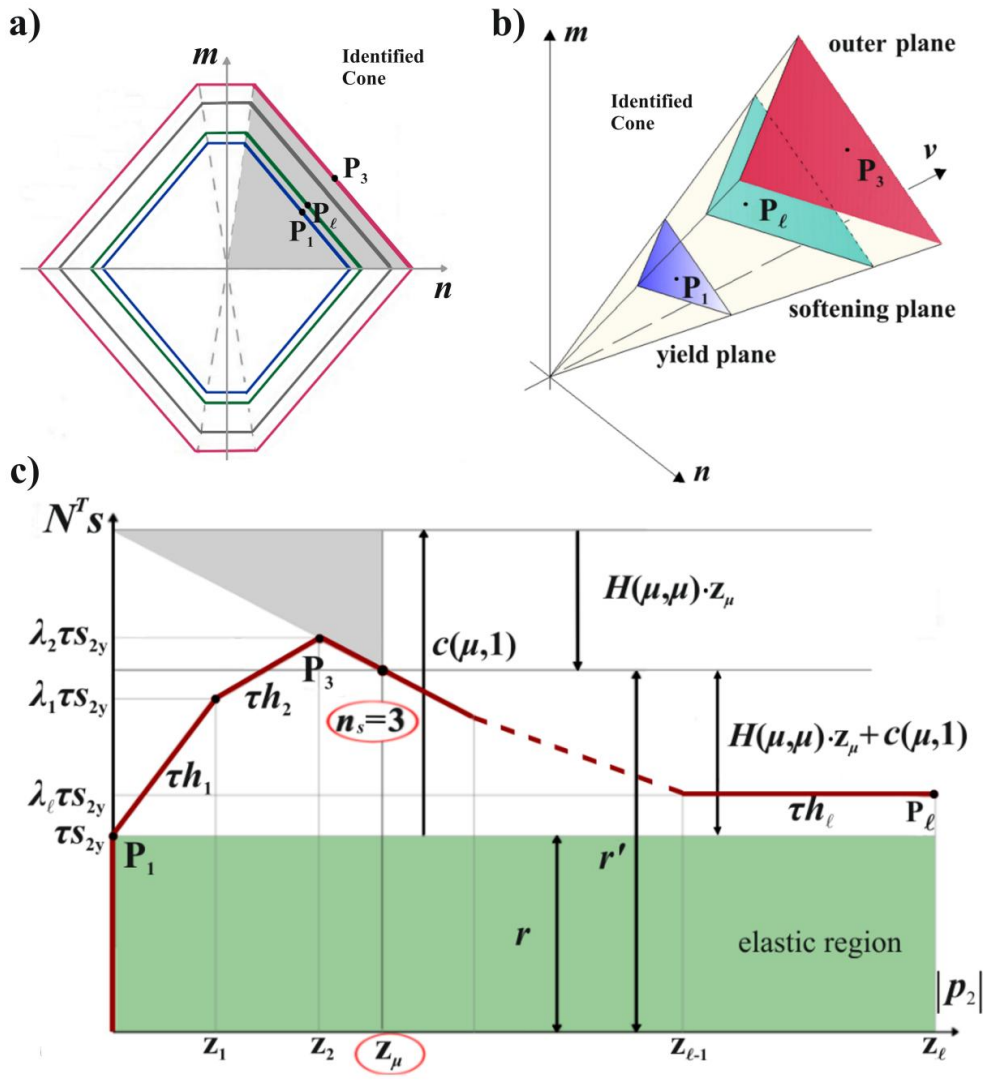

Fig. 4.6: Isotropic hardening/softening of yield plane for a) NM and b) NQM interaction and c) multi-linear hardening/softening behavior for a stress point.

This formulation avoids all unnecessary multi-segmental projections of the hardening/softening behavior along the normal vectors of all segments/planes of the yield surface for every critical section of the standard formulation. This part has been treated poorly in the literature, addressing only constitutive relations with only one softening branch and similar for all critical sections. The proposed scheme can be extended to any number of hardening/softening segments without affecting the dimensions of $\boldsymbol{H}$ and $\boldsymbol{c}$ matrices and thus the size of the yield condition. This notion is built on top of cone identification and incorporates effectively the multi-linear

hardening/softening behavior that addresses better real structural behavior. It insists though on staying on the multi-linear path, even in load reversals at certain cross sections due to redistribution of internal actions, which is inherent in the holonomic formulation and in most cases does not affect the solution noticeably.

4.6. Complementarity condition

Complementarity conditions express mutually exclusive situations in the form of an inner product of two nonnegative vectors that should be zero. They emerged as optimality conditions for continuous variable nonlinear programs involving inequality constraints, derived by Karush (1939). They indicate that simultaneous activation of plastic deformation and unloading is meaningless. More specifically, the complementarity condition implies that, when the identified yield hyperplane for a cross section μ is reached $(w_\mu = 0)$, the corresponding plastic multiplier z_μ should be greater than zero. Similarly, when the yield hyperplane is inactive $(w_\mu > 0)$, the corresponding plastic multiplier $z_\mu = 0$, indicating that no plastic deformation occurs.

In the case of elastoplastic analysis, complementarity conditions and systematic formulation of linear complementarity problems were introduced by Maier (1970). Herein, incorporating the concept of cone identification reduces significantly the number of the implemented complementarity constraints, since only one complementarity condition is considered for every cross-section. Thus for the entire structure the complementarity constraint is expressed as follows:

$$\boldsymbol{w}^T \cdot \mathbf{z} = \mathbf{0}, \quad \boldsymbol{w} \geq \mathbf{0}, \quad \mathbf{z} \geq \mathbf{0} \tag{4.23}$$

which, due to the non negativity of both vectors, holds also component wise.

4.7. Limit load and deformation analysis as an optimization problem

4.7.1. Formulation of the optimization problem

Equations (4.1), (4.3), (4.9), (4.22) and (4.23) formulate the holonomic elastoplastic problem that describes the whole structural behavior as:

$$\left.\begin{array}{ll} \boldsymbol{B}\cdot\boldsymbol{s}=a\cdot\boldsymbol{f}+\boldsymbol{f}_d & \textit{Equilibrium}\\ \boldsymbol{q}=\boldsymbol{B}^T\cdot\boldsymbol{u} & \textit{Compatibility}\\ \boldsymbol{q}=\boldsymbol{e}+\boldsymbol{p}=\boldsymbol{S}^{-1}\cdot\boldsymbol{s}+\boldsymbol{N}\cdot\mathbf{z} & \textit{Strain additivity}\\ \boldsymbol{w}=-\boldsymbol{N}^T\cdot\boldsymbol{s}+\boldsymbol{H}\cdot\mathbf{z}+\boldsymbol{c}+\boldsymbol{r}\geq\mathbf{0} & \textit{Yielding}\\ \boldsymbol{w}^T\cdot\mathbf{z}=0,\quad \mathbf{z}\geq 0 & \textit{Complementarity} \end{array}\right\} \tag{4.24}$$

The above system of equations can be simplified by retaining as decision variables the variables $a,\boldsymbol{s},\boldsymbol{u},\mathbf{z}$ to formulate a Mixed Complementarity Problem (MCP). This is equivalently converted into the following optimization problem, the solution of which provides simultaneously the load multiplier a, the corresponding stresses $\boldsymbol{s}$ and displacements $\boldsymbol{u}$ together with the plastic multipliers $\mathbf{z}$:

$$\left.\begin{array}{lc} \text{maximize} & a\\ \text{subject to} & \boldsymbol{B}\cdot\boldsymbol{s}-a\cdot\boldsymbol{f}=\boldsymbol{f}_d\\ & \boldsymbol{S}^{-1}\cdot\boldsymbol{s}-\boldsymbol{B}^T\cdot\boldsymbol{u}+\boldsymbol{N}\cdot\mathbf{z}=\mathbf{0}\\ & \boldsymbol{w}=-\boldsymbol{N}^T\cdot\boldsymbol{s}+\boldsymbol{H}\cdot\mathbf{z}+\boldsymbol{c}+\boldsymbol{r}\geq\mathbf{0}\\ & \boldsymbol{w}^T\cdot\mathbf{z}=\mathbf{0}\\ & \mathbf{0}\leq\mathbf{z}\leq\mathbf{z}_u\\ & \boldsymbol{u}_l\leq\boldsymbol{u}\leq\boldsymbol{u}_u \end{array}\right\} \tag{4.25}$$

The above optimization problem seeks for the maximum load factor a satisfying constraints imposed by equilibrium, compatibility, yielding, complementarity and lower and upper bounds for plastic deformations ($\mathbf{0},\mathbf{z}_u$) and displacements ($\boldsymbol{u}_l,\boldsymbol{u}_u$). Mathematically this is a nonconvex optimization problem that is known as a Mathematical Programming with Equilibrium Constraints (MPEC) problem (Luo et al. 1996), including the complementarity constraint that acts as a multi-switch and is of discrete rather than continuous nature, undermining the linearity of the formulation. This disjunctive constraint is difficult to handle numerically leading to numerical instabilities due to lack of convexity and smoothness. Despite all these inherent difficulties, the MPEC problem (4.25) can be solved by converting it into a standard, though still nonconvex, nonlinear programming (NLP) problem by suitably treating the complementarity condition. Several techniques have been proposed such as penalty function formulation, relaxation method, active set identification approach,

sequential quadratic programming (SQP) and interior point methods, among others (Fukushima and Lin 2004). Herein, the penalty function approach is followed (Tangaramvong and Tin-Loi 2007). According to this, the complementarity constraint is handled in the objective function by a parametric reformulation, in which an increased value of the parameter ρ exerts a pressure on the complementarity condition leading it to vanish. This formulation is as follows:

$$\left.\begin{array}{ll} \text{maximize} & a-\rho\cdot\boldsymbol{w}^T\cdot\mathbf{z} \\ \text{subject to} & \boldsymbol{B}\cdot\boldsymbol{s}-a\cdot\boldsymbol{f}=\boldsymbol{f}_d \\ & \boldsymbol{S}^{-1}\cdot\boldsymbol{s}-\boldsymbol{B}^T\cdot\boldsymbol{u}+\boldsymbol{N}\cdot\mathbf{z}=\mathbf{0} \\ & \boldsymbol{w}=-\boldsymbol{N}^T\cdot\boldsymbol{s}+\boldsymbol{H}\cdot\mathbf{z}+\boldsymbol{c}+\boldsymbol{r}\geq\mathbf{0} \\ & \mathbf{0}\leq\mathbf{z}\leq\mathbf{z}_u \\ & \boldsymbol{u}_l\leq\boldsymbol{u}\leq\boldsymbol{u}_u \end{array}\right\} \tag{4.26}$$

The above problem formulation incorporates the cone identification process at each iteration of the optimization problem. Thus all relations are independent of the number of lines/planes used in the linearization of the yield criterion and the number of linear hardening/softening segments as reflected in the compatibility and yielding conditions in relation (4.26). Matrices $\boldsymbol{N},\boldsymbol{H}$ and vectors $\boldsymbol{c},\boldsymbol{r}$ are updated for every iteration depending on the identified cone and the particular hardening segment of every critical section using the above relations. Moreover, it is worth noting that this NLP problem is sensitive to the initial values of ρ and its subsequent increase, as well as to the initial values of variables.

4.7.2. Remarks on the optimization formulation

Classical limit analysis of structures is based on rigid-perfectly plastic behavior and thus with no considerations on plastic deformations i.e. ductility. The formulation presented in relations (4.26) constitutes a combination of limit load and deformation analysis accounting for hardening/softening behavior and deformation constraints (Cocchetti and Maier 2003) and addresses more closely real situations and code based requirements related to performance based design. More specifically, the need of treating the apparent softening behavior engages the complementarity condition. This affects the mathematical structure of the problem converting it into a nonconvex one, while ductility requirements require the presence of the compatibility constraints. For

the case of rigid-perfectly plastic behavior or hardening behavior without ductility limitations, the problem can be solved as a standard Linear Programming (LP) problem subject only to equilibrium and yield constraints (Wong 2009).

The optimization process described in (4.26) follows a mathematical pace that attempts to maximize the load factor a for the holonomic formulation of the problem. This is performed in successive gradient-dictated trials for the entire vector of decision variables, namely the stresses $\boldsymbol{s}$, the displacements $\boldsymbol{u}$, the plastic multipliers $\mathbf{z}$ and the load factor a. What governs the optimization process is its tendency to successively increase the loading factor a satisfying the equality (i.e. equilibrium and compatibility) constraints and inequality (yield) constraints together with complementarity conditions. The cohesion of the problem that prohibits a random walk type of search, relies on internally computed gradient information depending on the specific optimization algorithm (herein interior point algorithm approaching through feasible solutions). Thus the path to the solution is determined by successive trials and generally differs from the actual path of a step-by-step method of finite element analysis, both though succeeding in finding the same solution.

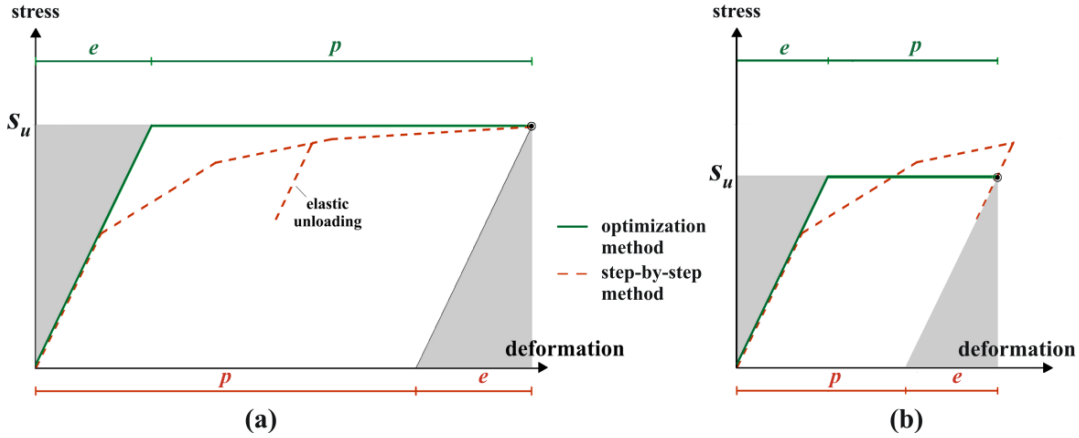

Fig. 4.7: Optimization versus step-by-step path for a) full and b) incomplete loading-unloading.

An explanation of the different paths followed by the optimization and the step-by-step method is presented for a particular cross section in Fig. 4.7. For a multi-linear hardening behavior, the step-by-step method provides the entire history of the response remaining on the track of the constitutive relation (dotted line). If full or incomplete reversals occur (Fig. 4.7a,b), these are considered elastic and therefore they do not consume energy. On the other hand, the optimization method targets the ultimate state following an artificial elastic-perfectly plastic path, as shown by the

solid line in Fig. 4.7a,b. The elastic deformation is determined on the basis of the initial stiffness matrix and the plastic deformation is developed under constant stress. Therefore, the optimization procedure inherently circumvents redistribution of forces targeting the non-affected ultimate state, since any unloading, if happens, does not consume energy.

Herein, a mechanically inspired subset-technique is embedded in the optimization problem (4.26) that reduces the number of unknowns and constraints to a minimum, acting as a physically filtered "active" set strategy. An outline of the proposed algorithm for every optimization iteration is as follows (Fig. 4.8):

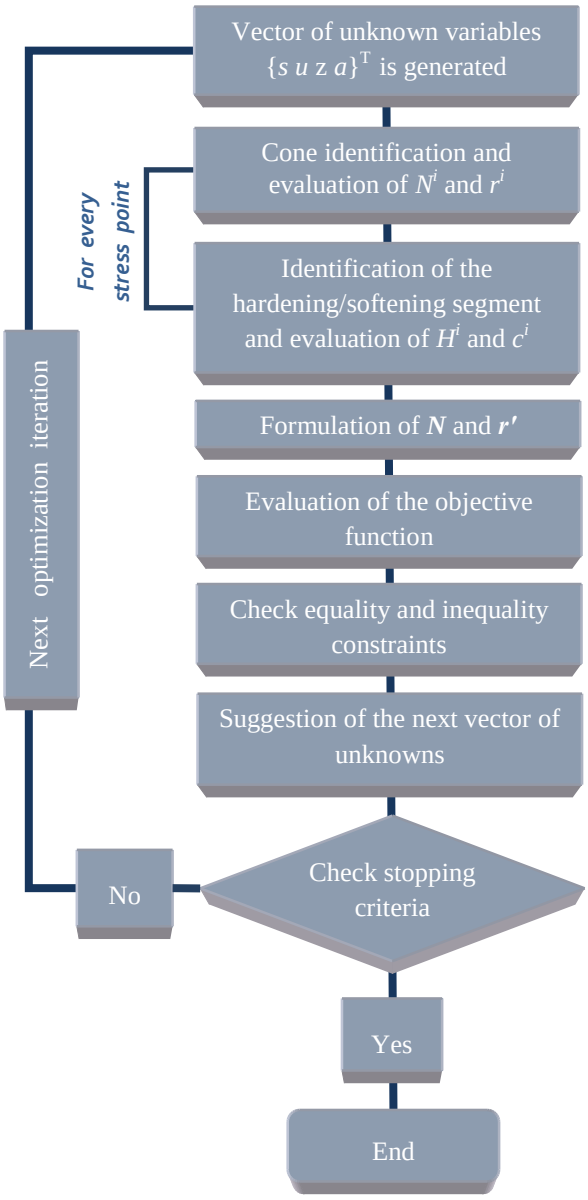

Fig. 4.8: Outline of the optimization procedure.

The identification of the critical cone and the specific hardening/softening segment at each iteration retains only the true or targeted active constraints for every cross section. Under this consideration, the size of the problem reduces to a minimum since all relations become independent from the number of planes of the yield surface and the number of linear hardening/softening segments.

From a mathematical standpoint the proposed algorithm does not belong to one of the well-studied problems of mathematical programming. This is due to cone identification that interferes in every step indicating the updated set of constraints at all critical sections. From a closer perspective, this can be seen as an active-set strategy on the standard formulation identifying always only the $2n_{el}$ physically needed constraints since all the remaining constraints are redundant.

4.8. Numerical examples

The optimization problem described in relation (4.26) is implemented in Matlab code for the analysis of plane frame steel structures. It is solved by *fmincon* solver (appropriate for the minimization of constrained nonlinear multivariable function), with the interior-point algorithm selected as optimization method.

4.8.1. Axial force-bending moment (NM) interaction

Herein the Massonet-Save yield criterion (1965) suitable for steel members is employed:

$$\Phi = (n^j)^2 + \left|m^j\right| - 1 \quad or \quad \Phi = (n^k)^2 + \left|m^k\right| - 1 \tag{4.27}$$

The axial force-bending moment Massonet-Save interaction curve is approximated in the sequel with six lines that denote the corresponding yield hyperplanes as shown in Fig. 4.9 (Tangaramvong and Tin-Loi 2008).

The aim is to verify the applicability of the proposed method, validate its efficiency and compare the analysis results with existing ones for the following cases:

- Case (a): Rigid-perfectly plastic behavior with axial force-bending moment interaction (LP problem).
- Case (b): Multi-segment isotropic hardening behavior in pure bending.

- Case (c): Multi-segment isotropic hardening behavior with axial force-bending moment interaction.

For this purpose, three steel frames are examined for the aforementioned cases and the corresponding results are presented below. It is noted that all analysis results of this method are presented following the engineering sign convention of structural analysis. The conversion from matrix to engineering convention is simply performed by changing the sign of axial and bending moment at start node and the sign of shearing force at end node.

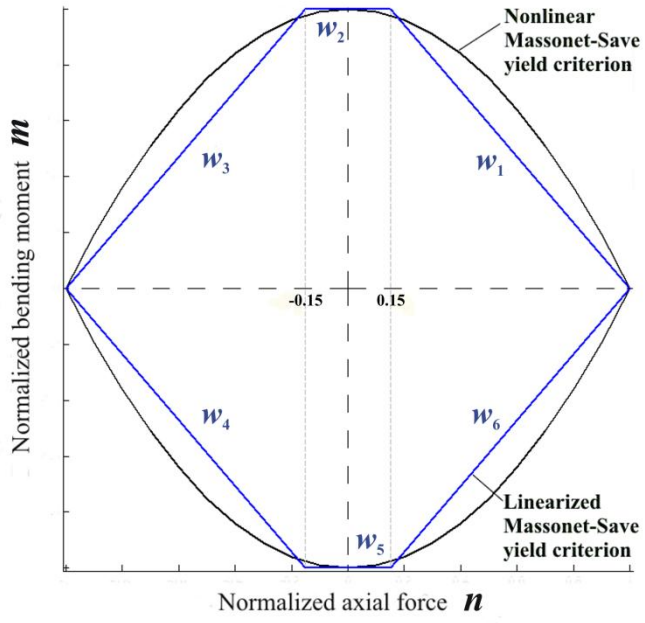

Fig. 4.9: Linearized Massonet-Save yield criterion.

4.8.1.1. Example #1

The first example concerns the three-storey, single bay, eccentrically braced frame shown in Fig.4.10a that is subjected to vertical loads a and lateral load $2a$ (Tangaramvong and Tin-Loi 2008, Karakostas and Mistakidis 2000). The frame is discretized into 21 elements, 14 nodes and 36 degrees of freedom. The material properties are as follows: Sections 310UC118 with $A=150\times10^{-4}\ m^2$, $I=27700\times10^{-8}\ m^4$, $s_{1y}=4200\ kN$, $s_{2y}=s_{3y}=548.8\ kNm$ are employed for all columns, 200UB18.2 with $A=23.2\times10^{-4}\ m^2$, $I=1580\times10^{-8}\ m^4$, $s_{1y}=742.40\ kN$, $s_{2y}=s_{3y}=57.60kNm$ for all beams and SHS125/125/9 with $A=41.76\times10^{-4}\ m^2$, $I=900\times10^{-8}\ m^4$, $s_{1y}=1365\ kN$, $s_{2y}=s_{3y}=57.75\ kNm$ for all braces. For all columns $h=-202.79\,kNm$, $\lambda=0.7$ is

considered, while for all beams $h=-41.04\,kNm$, $\lambda=0.7$. Bracings are considered to follow a rigid-perfectly plastic behavior. The upper bound vector of all plastic multipliers is $z_u=1$, while the upper bound vector of all displacements is $u_u=1$ and the lower bound vector $u_l=-1$. The initial values of $\rho=100$ for case (b) and (c) with an updating rule of $\rho=10\rho$ are used, until convergence with a tolerance of $w^T z \le 10^{-6}$ is reached.

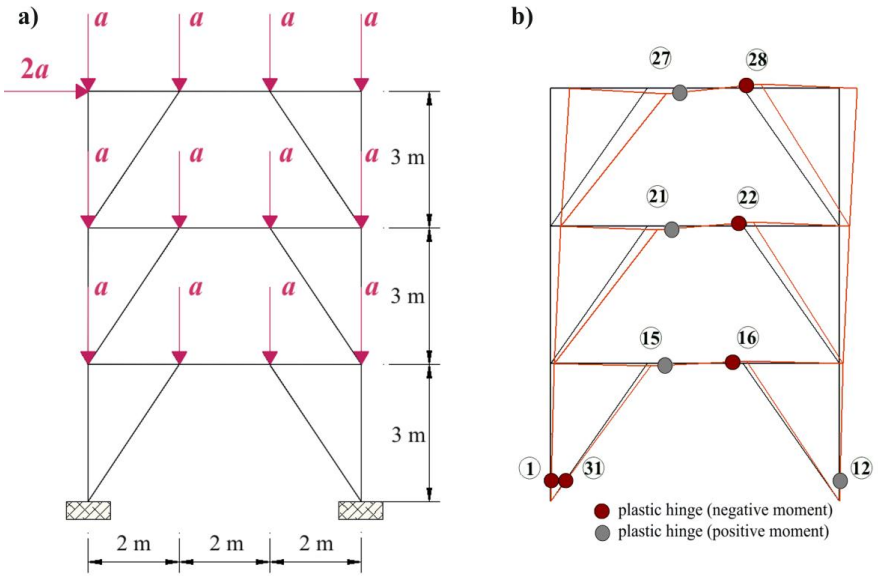

Fig. 4.10: a) Single-bay eccentrically braced frame and b) its deformed shape for cases (b),(c).

Table 4.1: Analysis results of frame 1.

	Case (a)	**Case (b)**	**Case (c)**
a (kN)	**124.148**	**120.01**	**117.862**
top-storey *u* (m)	**0.443**	**0.375**	**0.363**
computational time (s)	**0.49**	**14.74**	**24.73**

The results of all analysis cases for frame 1 are presented in Table 4.1. The maximum load a, as well as the top-storey displacement u, attain their maximum values for the case of rigid-perfectly plastic behavior. Moreover, for softening behavior, the case of pure bending attains a greater value of maximum load as compared to axial force-bending moment interaction. It is noted that these results, as

well as the corresponding failure mechanisms, coincide with those obtained by Tangaramvong and Tin-Loi (2008). The plastic hinge formation and deformed shape for cases (b) and (c) are depicted in Fig.4.10b, with numbers in circle denoting the particular cross-section. The corresponding interaction diagrams are presented in Fig.4.11. It is noted that for cases (b) and (c) plastic hinges of beam cross-sections have yielded and are at their softening branch.

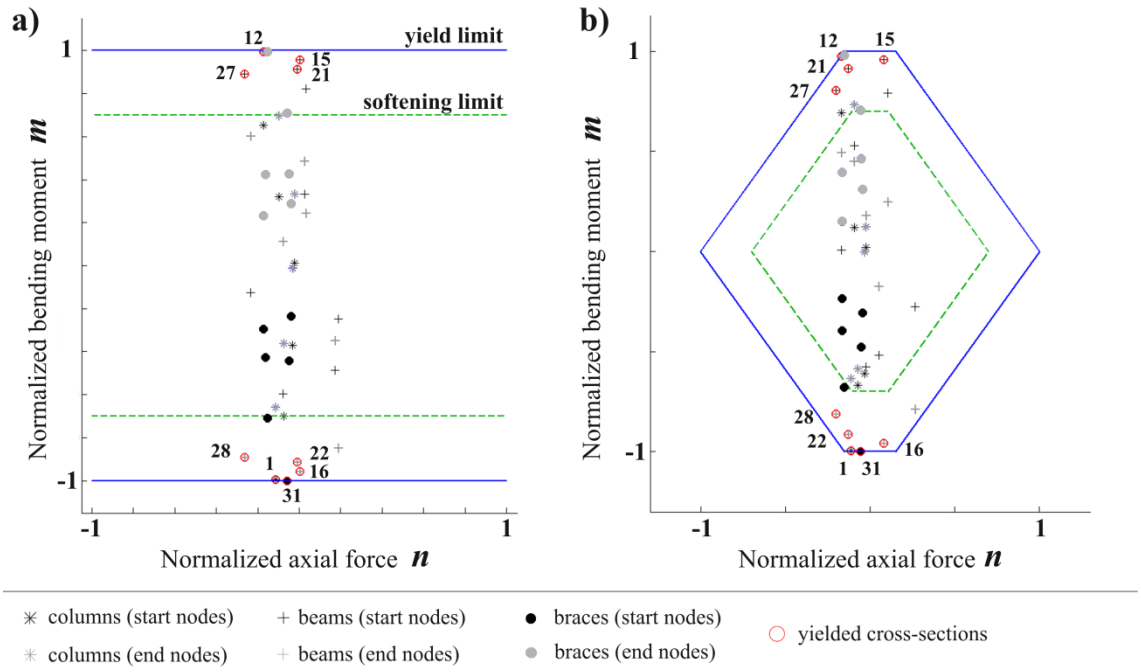

Fig. 4.11: Interaction diagrams for a) case (b) and b) case (c).

4.8.1.2. Example #2

The second example concerns the three-storey, four-bay plane frame shown in Fig.4.12a, subjected to increasing lateral and vertical loading. The frame is discretized into 39 elements, 32 nodes and 81 degrees of freedom. The steel grade is S235 with $E=2\times10^8$kN/m^2. Sections with $A=112.5\times10^{-4}\ m^2$, $I=18260\times10^{-8}\ m^4$, $s_{1y}=2643.75\ kN$, $s_{2y}=s_{3y}=325\ kNm$ and sections with $A=62.61\times10^{-4}\ m^2$, $I=11770\times10^{-8}\ m^4$, $s_{1y}=1471.34\ kN$, $s_{2y}=s_{3y}=189.01\ kNm$ are employed for all columns and beams respectively. The assumed multi-segment hardening/softening behavior is shown in Fig. 4.11b. More specifically, for columns $h_1=2600\ kNm$ $z_1=0.005$ $\lambda_1=1.04$, $h_2=1625\ kNm$ $z_2=0.015$ $\lambda_2=1.10$, $h_3=-1392\ kNm$ $z_3=0.05$ $\lambda_3=0.935$, while for beam cross sections $h_1=1260.1kNm$ $z_1=0.003$ $\lambda_1=1.02$, $h_2=810.04kNm$ $z_2=0.01$ $\lambda_2=1.05$, $h_3=-992.3kNm$ $z_3=0.03$ $\lambda_3=0.945$. The values of z_3 constitute the upper bounds for column and beam

cross sections respectively. The upper bound vector of all displacements is $u_u = 1$ and the lower bound vector $u_l = -1$. The initial values of $\rho = 100$ for case (b) and $\rho = 1000$ for case (c) with an updating rule of $\rho = 10\rho$ are used until convergence with a tolerance of $w^T z \leq 10^{-6}$ is reached.

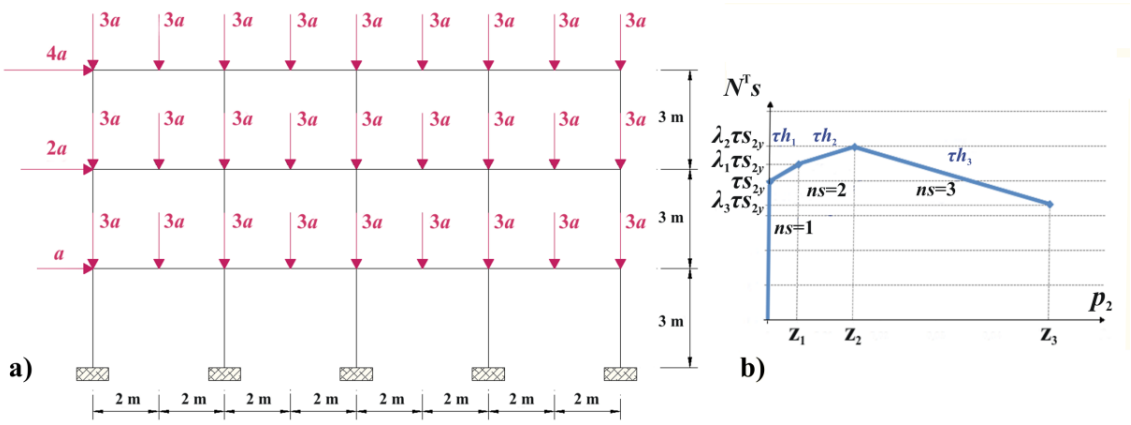

Fig. 4.12: a) Three-storey, four-bay plane frame and b) multi-segment hardening/softening diagram.

Table 4.2: Analysis results of frame 2.

	Case (a)	**Case (b)**	**Case (c)**
a (kN)	**80.97**	**88.21**	**81.67**
top-storey *u* (m)	**0.060**	**0.140**	**0.140**
computational time (s)	**0.55**	**86.26**	**151.56**

In Table 4.2 the results of all analysis cases are presented. It is evident that the smallest value of ultimate load corresponds to the case of perfectly plastic behavior. For the case of multi-segment hardening/softening behavior, the pure bending consideration results into greater value for the maximum load as compared to the case of axial force-bending moment interaction. As far as the computational time is concerned, it is apparent that for case (a) the computational time is very small as it refers to a Linear Programming problem. The greatest values of computational time correspond to case (c), due to the larger number of yield constraints. However, it is noted that the proposed formulation based on cone identification is computationally more efficient than the standard formulation. Indicatively, it is mentioned that the

present formulation converges in 64.45s for frame 2 as compared to the standard formulation which requires 141.67s, following only one segment of hardening behavior. Both analyses were conducted on a PC with a Core Duo Quad CPU and 4GB of RAM.

The sequence of plastic hinge formation for step-by-step analysis using SAP2000 version 14 and the ultimate state of frame 2 using mathematical programming are shown in Fig. 4.13a and 4.13b respectively. The ultimate carrying load capacities in terms of base shear force are practically the same for both types of analysis, i.e. 571.60kN for step-by-step analysis and 81.67×7=571.69kN for limit load and deformation analysis with mathematical programming, both resulting in the same ultimate pattern of hinge formation. In Fig. 4.13b for every plastic hinge the corresponding segment number at the hardening/softening diagram is indicated. It is evident that the right ends of all beams are more stressed as compared to the corresponding left ends, as shown in Fig. 4.14. The combined effect of vertical (Fig. 4.14a) and lateral loading (Fig. 4.14b) is depicted in Fig.4.14c following the engineering sign convention.

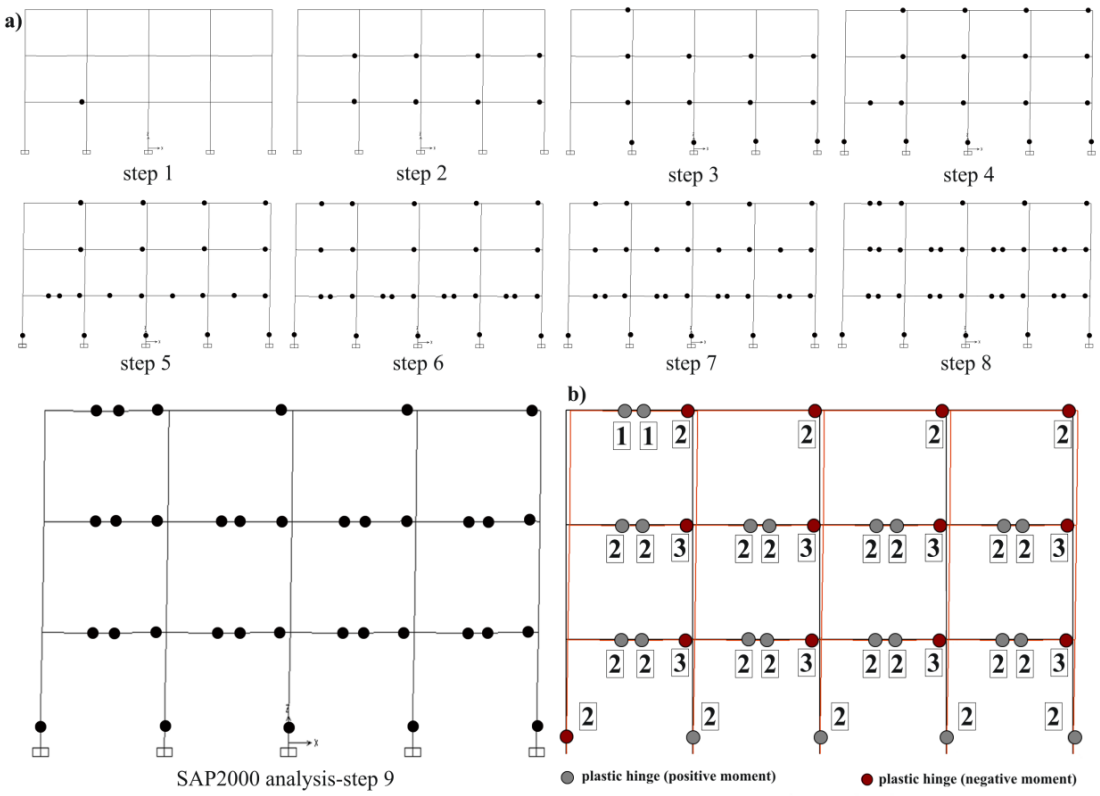

Fig. 4.13: Plastic hinge disposition and deformed shape of frame 2 for a) step-by-step inelastic analysis, b) proposed formulation.

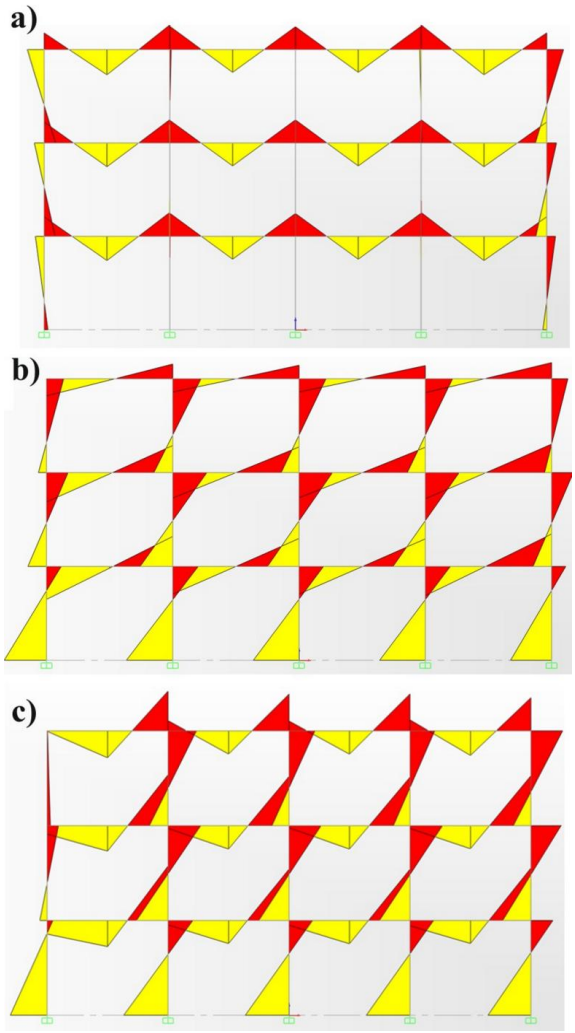

Fig. 4.14: Moment diagrams with engineering sign convention for a) vertical, b) lateral load and c) their combination.

4.8.1.3. Example #3

The third example concerns the six-storey plane frame shown in Fig.4.15a. The frame consists of 66 elements, 51 nodes and 138 degrees of freedom. The material properties are as follows: The steel grade is S235 with $E=2\times10^{8}$kN/m^2. For all columns sections with $A=197.5\times10^{-4}m^2$, $I=86970\times10^{-8}m^4$, $s_{1y}=4641.3kN$, $s_{2y}=s_{3y}=928.02$ *kNm* are employed and for all beams sections with $A=84.46\times10^{-4}\ m^2$, $I=23130\times10^{-8}\ m^4$, $s_{1y}=1984kN$, $s_{2y}=s_{3y}=307.15kNm$ are used. The assumed multi-segment hardening/softening behavior is shown in Fig. 4.15b. More specifically, for column cross-sections $h_1=18560.4kNm$ $z_1=0.005$ $\lambda_1=1.10$, $h_2=9280.2$ *kNm* $z_2=0.015$ $\lambda_2=1.20$, $h_3=-14848.3kNm$ $z_3=0.03$ $\lambda_3=0.96$ and $h_4=10^{-6}$ *kNm* $z_4=0.05$ $\lambda_4=0.96$, while for beam cross-sections $h_1=5119.2kNm$ $z_1=0.003$ $\lambda_1=1.05$, $h_2=2193.93$ *kNm* $z_2=0.01$ $\lambda_2=1.10$, $h_3=-6757.3$ *kNm* $z_3=0.02$ $\lambda_3=0.88$ and

$h_4=10^{-6}\,kNm$ $z_4=0.04$ $\lambda_4=0.88$. The upper bound vector for column and beam cross sections is $z_u=0.05$. The upper bound vector of all displacements is $u_u=10$ and the lower bound vector $u_l=-10$. The initial value of $\rho=100$ with an update rule of $\rho=10\rho$ is used until an appropriate convergence tolerance is reached $(w^T z \le 10^{-6})$.

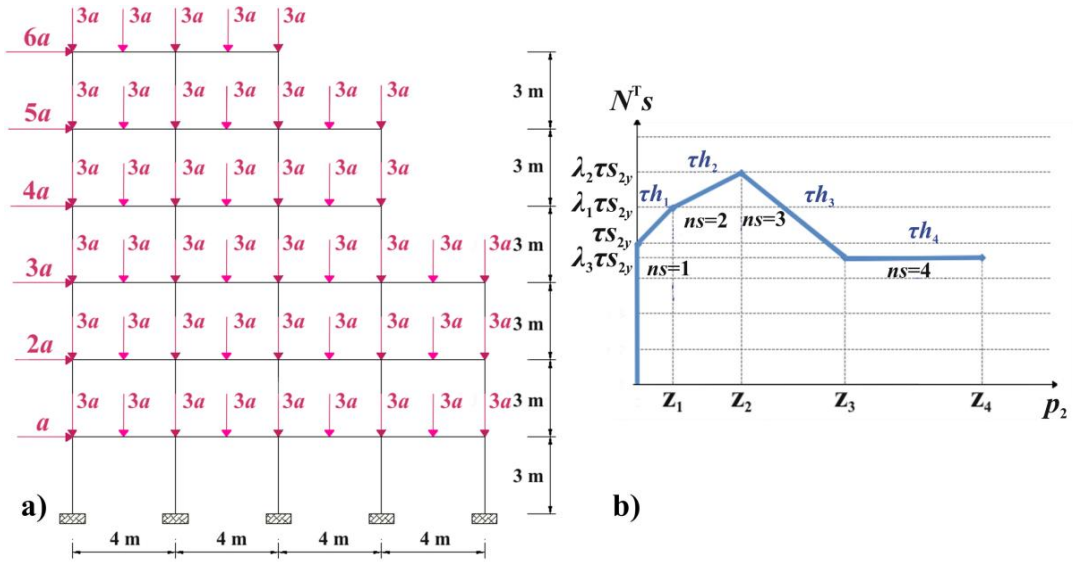

Fig. 4.15: a) Six-storey plane frame and b) multi-segment hardening/softening diagram.

Results for all analysis cases are shown in Table 4.3. Cases (b) and (c) of hardening/softening behavior attain greater values of maximum load as compared to rigid-perfectly plastic behavior. In Fig. 4.16 ultimate states for cases (b) and (c) are presented. The effect of axial force is evident mainly in Fig. 4.16b where the first-storey columns are more heavily stressed. More specifically, the three middle columns have reached the second segment of hardening, while the two outer columns have yielded.

Table 4.3: Analysis results of example #3.

	Case (a)	**Case (b)**	**Case (c)**
a (kN)	**58.05**	**63.89**	**60.90**
top-storey *u* (m)	**0.060**	**0.258**	**0.248**
computational time (s)	**0.59**	**558.28**	**674.07**

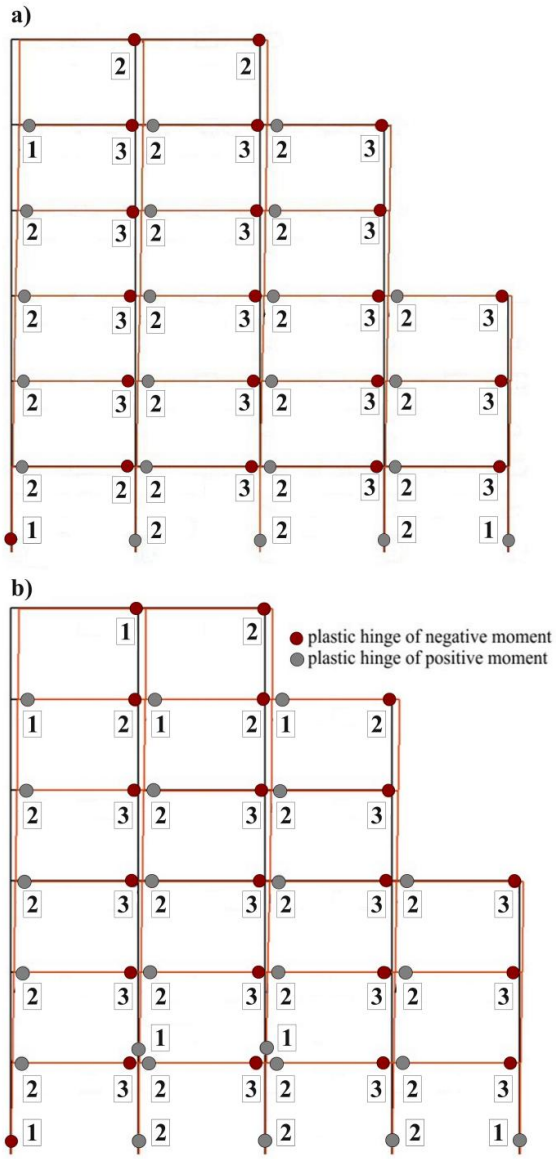

Fig. 4.16: Plastic hinge formation for a) pure bending and b) NM interaction.

4.8.2. Computational performance for NM interaction

The evolution of the proposed algorithm during the optimization steps is presented in more detail for all the above examples. The efficiency of the computational procedure is examined through variation of the objective function and first-order optimality measure (Appendix C) for the entire history of optimization.

The first example is analyzed using both the proposed formulation and the standard one. The performance of the algorithm for both formulations is depicted in Fig. 4.17. It is observed that, for the same initial values and upper and lower bounds of the variables, the proposed algorithm converged after 104 iterations, while the standard

formulation after 596 iterations. It is highlighted that the standard formulation requires 352 unknown variables and 252 yield constraints versus 142 variables and 42 yield constraints of the cone identification procedure. Due to the reduced size of the problem, the proposed algorithm finds the path to the optimum easier, while the standard formulation needs more iterations in trying to find the final path. This is also reflected on the computational time, where convergence for the standard formulation is achieved in 131.93s, while for the cone identification procedure in 24.73s.

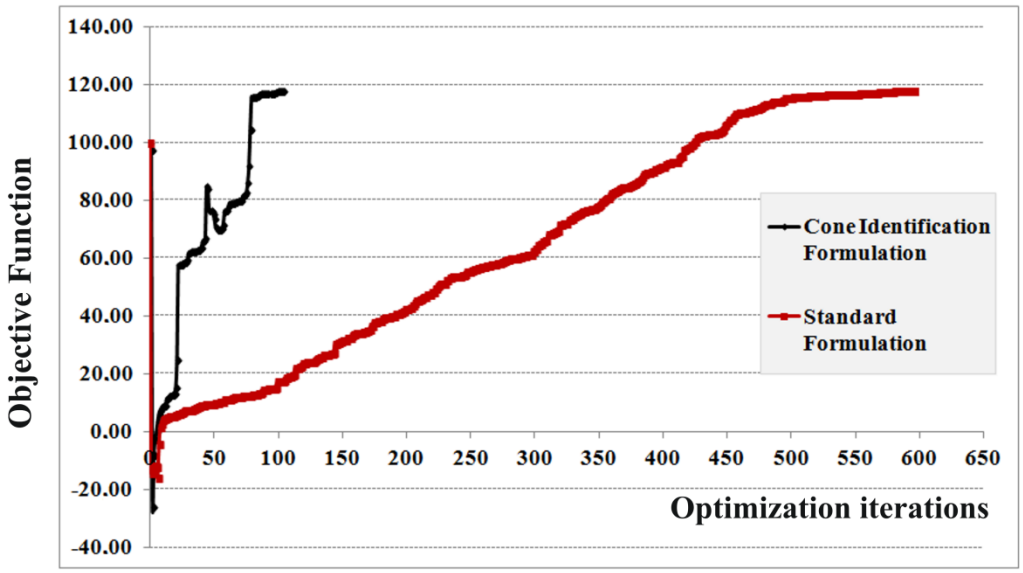

Fig. 4.17: Comparison of computational procedure for the proposed and the standard formulation for example #1.

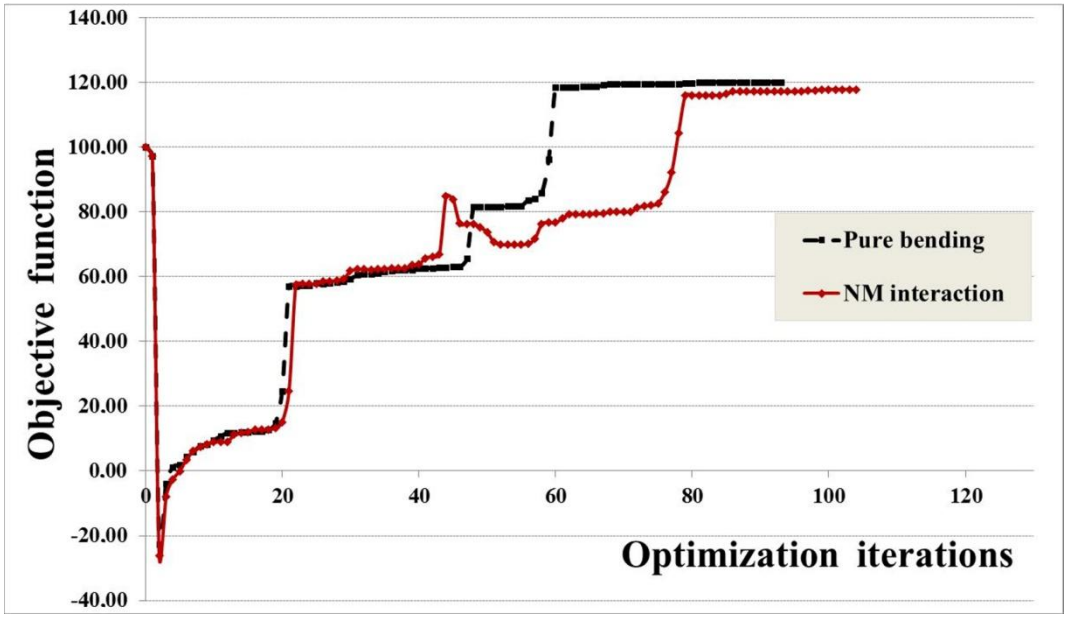

Fig. 4.18: Evolution of the objective function for example #1.

The computational performance of the cone identification method is also examined considering pure bending and NM interaction for example #1. For the same initial values of all variables, the nonlinear optimization algorithm converges faster and smoother for pure bending, as shown in Fig. 4.18, needing 93 iterations versus 104 required for NM interaction.

The evolution of the objective function and the first-order optimality measure for example #2 are shown in Figs. 4.19 and 4.20. The starting point is the same for both cases, but extreme values corresponding to initial iterations are omitted for scaling reasons. The performance of the algorithm is proved to be smoother and the convergence faster for the case of pure bending, needing 237 iterations compared to 287 for NM interaction.

The computational performance of the nonlinear algorithm for example #3 is depicted in Figs. 4.21 and 4.22. Extreme values of initial iterations are omitted for scaling reasons. However, it is noted that the starting point is different for cases (b) and (c) converging for different number of iterations (443 for pure bending versus 429 for NM interaction). Although the number of iterations is smaller for NM interaction, the corresponding computational time is greater compared to that of pure bending. This is due to the larger number of potential yield lines for case (c) associated also with the corresponding plastic multipliers, which increases the required computational time until convergence.

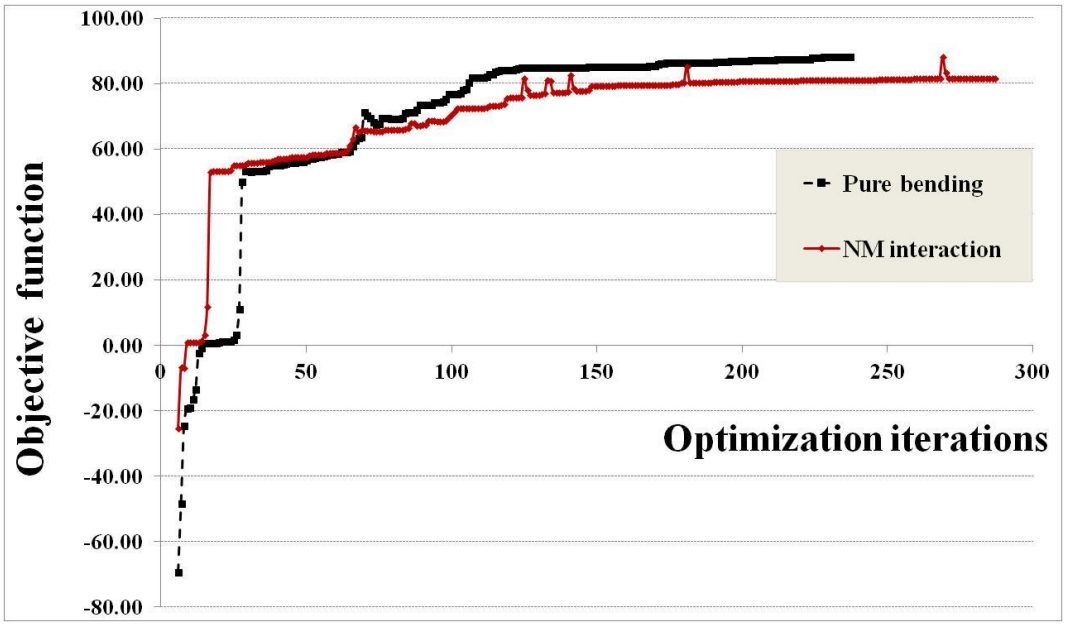

Fig. 4.19: Evolution of the objective function for example #2.

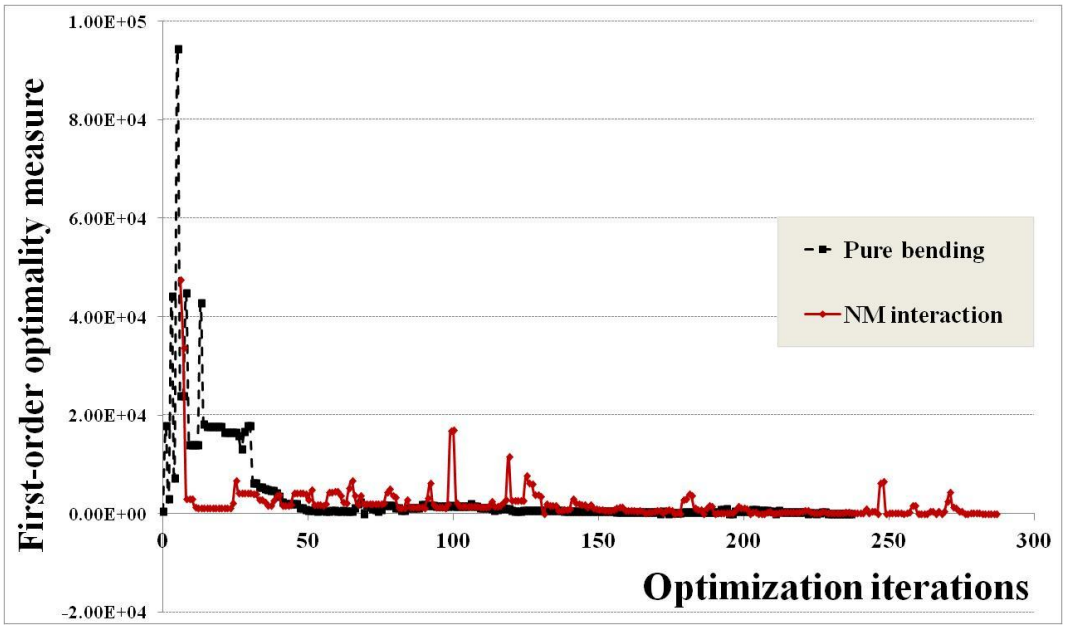

Fig. 4.20: Evolution of first-order optimality measure for example #2.

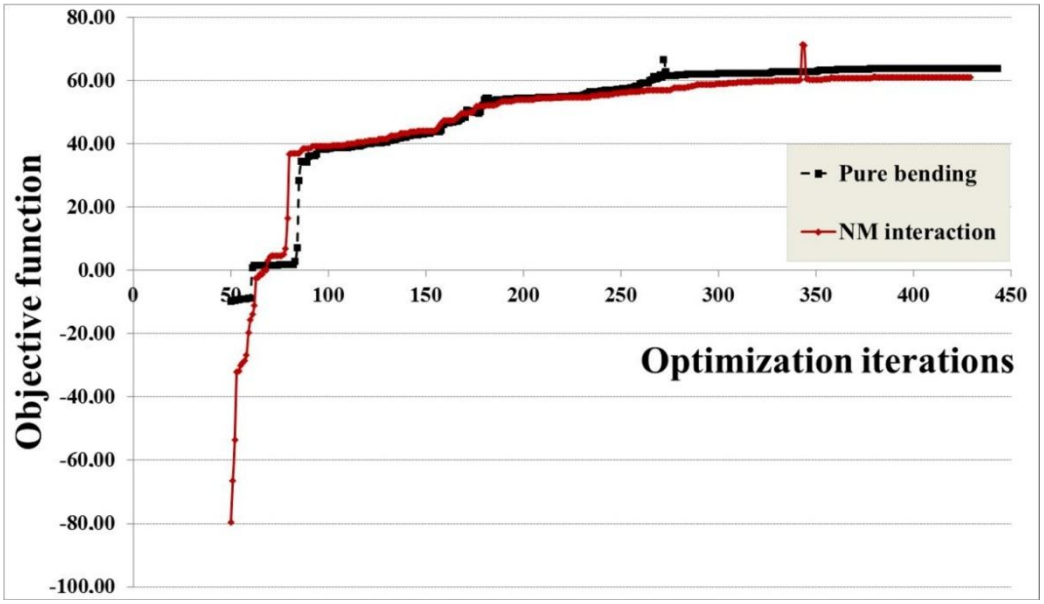

Fig. 4.21: Evolution of the objective function for example #3.

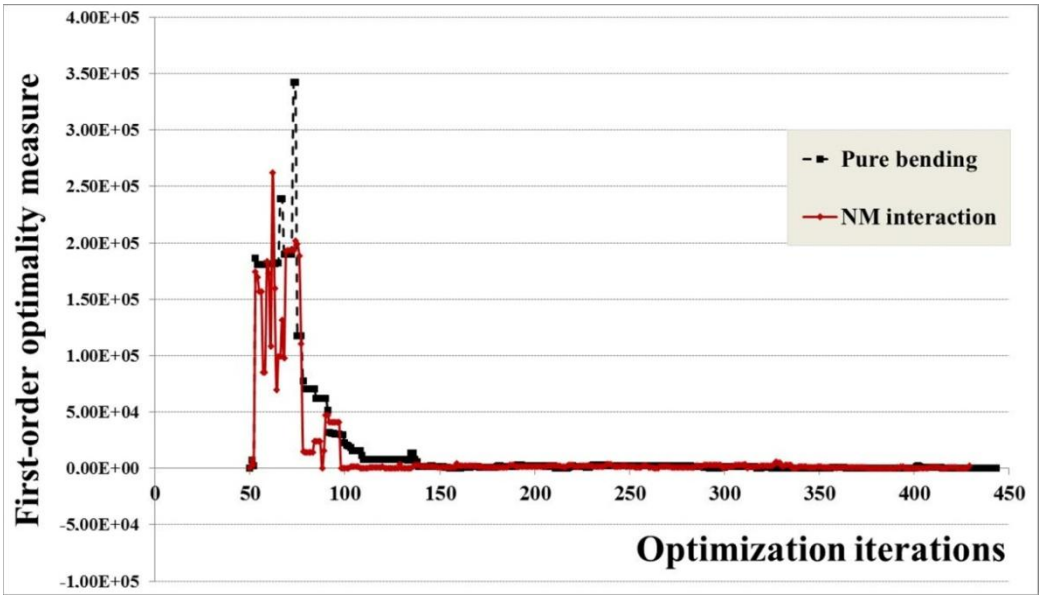

Fig. 4.22: Evolution of first-order optimality measure for example #3.

4.8.3. Axial-shear force-bending moment (NQM) interaction

The generalized Gendy-Saleeb yield criterion (1992) is adopted, represented by a 3D nonlinear surface that is approximated using 32 plane triangles (section 3.6.1). It is noted that the tessellation of the yield surface is such that the convexity of the yield criterion is retained.

The aim is to investigate the role of combined axial-shear force-bending moment interaction and its influence on structural behavior. For this purpose, three steel plane frames are examined for the following cases:

- Case (a): Multi-segment isotropic hardening behavior with axial force-bending moment interaction (NM interaction).
- Case (b): Multi-segment isotropic hardening behavior with axial-shear force-bending moment interaction (NQM interaction).

For case (a) the Gendy-Saleeb criterion without the effect of the shear force is used. This is appropriately linearized with eight linear segments, as shown in section 3.6.1. The analysis results of all cases are presented below. Notice that the analysis method follows the sign convention of matrix structural analysis, whereas final results are presented on the basis of engineering sign convention.

4.8.3.1. Example #1

The first example is a three-storey, single-bay steel frame shown in Fig. 4.23. The frame is discretized into 9 elements, 8 nodes and 18 degrees of freedom. The steel grade is S235 with $E=2\times10^8$kN/m^2. The material properties are as follows: sections

with $A=112.5\times10^{-4}\ m^2$, $I=18260\times10^{-8}\ m^4$, $s_{1u}=3172.5\ kN$, $v_u=933.73\ kN$, $s_{2u}=390\ kNm$, $s_{3u}=390\ kNm$ are employed for all columns, sections with $A=28.48\times10^{-4}\ m^2$, $I=1943\times10^{-8}\ m^4$, $s_{1u}=736.21\ kN$, $v_u=208.88\ kN$, $s_{2u}=57.02\ kNm$, $s_{3u}=57.02\ kNm$ for all beams. Softening behavior is considered determined by one branch that for columns is described by $h_1=-2600\ kNm$ $z_1=0.05$ and for beams by $h_1=-311.04\ kNm$ $z_1=0.05$. The values of z_1 constitute the upper bounds for column and beam cross sections respectively. The upper bound vector of all displacements is $u_u=1$ and the lower bound vector $u_l=-1$. The initial value of $\rho=10$ for case (b).

The aim is to compare the cone identification formulation to the standard one that forms all yield constraints. It is mentioned that for the proposed formulation the number of variables is 64 and the number of yield constraints 18, as compared to 622 and 576 respectively for the standard formulation. For both formulations, analysis results are identical and more specifically, the maximum load factor is $a=24.49\,kN$ and the deformed shape together with the plastic hinge pattern are shown in Fig. 4.24. The algorithm converged after 59 optimization iterations in 39.20s for the proposed formulation, while for the standard after 103 iterations in 311.22s, both starting from the same initial point.

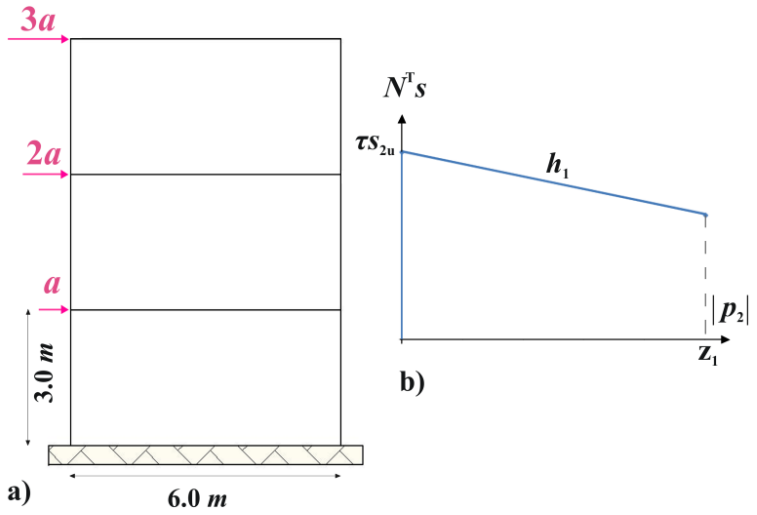

Fig. 4.23: a) Frame 1 and b) its softening segment.

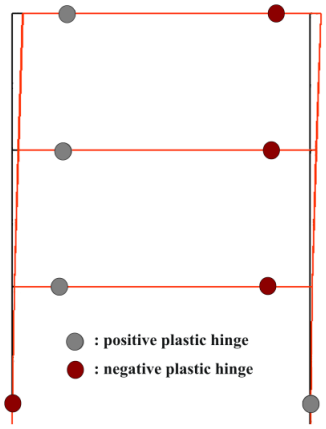

Fig. 4.24: Deformed shape and plastic hinge formation for both formulations.

4.8.3.2. Example #2

The second example concerns two variations of a three-storey, two-bay steel frame shown in Fig. 4.25a. The frame is discretized into 15 elements, 12 nodes and 27 degrees of freedom. The steel grade is S235 with E=2×10^{8}kN/m^2. The material properties are as follows: sections with $A=112.5\times10^{-4}m^2$, $I=18260\times10^{-8}m^4$, $s_{1y}=2643.75kN$, $v_y=778.11kN$, $s_{2y}=s_{3y}=325kNm$ are employed for all columns, sections with $A=28.48\times10^{-4}m^2$, $I=1943\times10^{-8}\ m^4$, $s_{1y}=669.28kN$, $v_y=189.89kN$, $s_{2y}=s_{3y}=51.84\ kNm$ for all beams. The corresponding multi-segment hardening behavior is shown in Fig. 4.24b and depends on the parameters of every section. More specifically, for columns $h_1=6500kNm\ \ z_1=0.005\ \lambda_1=1.1$, $h_2=3250kNm\ \ z_2=0.015\ \lambda_2=1.20$, $h_3=-5200kNm\ \ z_3=0.04\ \lambda_3=0.8$, $h_4=0.000001kNm\ \ z_4=0.04\ \lambda_4=0.8$, while for beam cross sections $h_1=2592kNm\ \ z_1=0.001\ \ \lambda_1=1.05$, $h_2=1296kNm\ \ z_2=0.003\ \lambda_2=1.10$, $h_3=-576kNm\ \ z_3=0.03\ \lambda_3=0.80$, $h_4=0.000001kNm\ \ z_4=0.04\ \lambda_4=0.80$. The values of z_4 constitute the upper bounds for column and beam cross sections respectively. The upper bound vector of all displacements is $u_u=1$ and the lower bound vector $u_l=-1$. For frame 2a the initial value of $\rho=10$ for case (a) and $\rho=10$ for case (b), while for frame 2b the initial value of $\rho=10$ for case (a) and $\rho=100$ for case (b) with an updating rule of $\rho=10\rho$ after each NLP solution until an appropriate convergence tolerance is reached $(w^Tz \le 10^{-5})$. The algorithm for both cases has stopped because change in the vector of unknown variables and maximum constraint violation were less than the preselected tolerances (10^{-10}).

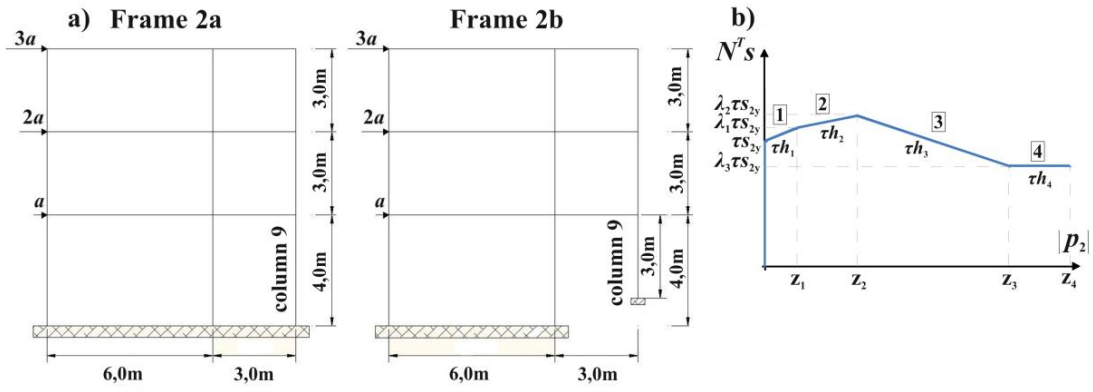

Fig. 4.25: a) Variations of frame 2 and b) multi-linear hardening behavior for both frames.

Table 4.4: Analysis results of example #2.

	Cases	α (kN)	top-storey u (m)	$w^T z$
Frame 2α	(a)	33.43	0.379	2.63E-11
	(b)	31.25	0.281	1.34E-06
Frame 2b	(a)	34.80	0.317	3.24E-11
	(b)	32.98	0.280	9.13E-10

All analysis results are presented in Table 4.4. The effect of shear force is observed in the reduction of the load carrying capacity of both frames. However, frame 2b presents greater values of load factor and top-storey displacement for both cases due to its greater stiffness (shorter column 9).

In Fig.4.26 the ultimate states of frames 2a and 2b for both cases are presented. Each plastic hinge is accompanied by a number that designates the corresponding hardening/softening segment, as defined in Fig. 4.25b. Top-storey displacements and plastic rotations are smaller for both frames for NQM interaction (case (b)). The corresponding interaction diagrams are shown in Fig. 4.27. It is observed that the role of bending moment is dominant for both frames, while at column cross sections shear force effect is more intense than that of axial force due to the presence of lateral loading. Focusing on the base cross section of column 9, it is noted that for frame 2a *n=-0.0289*, *v=0.0754*, *m=1.0370*, while for frame 2b *n=-0.0282*, *v=0.1146*, *m=1.0916*. The difference in shear force is significant.

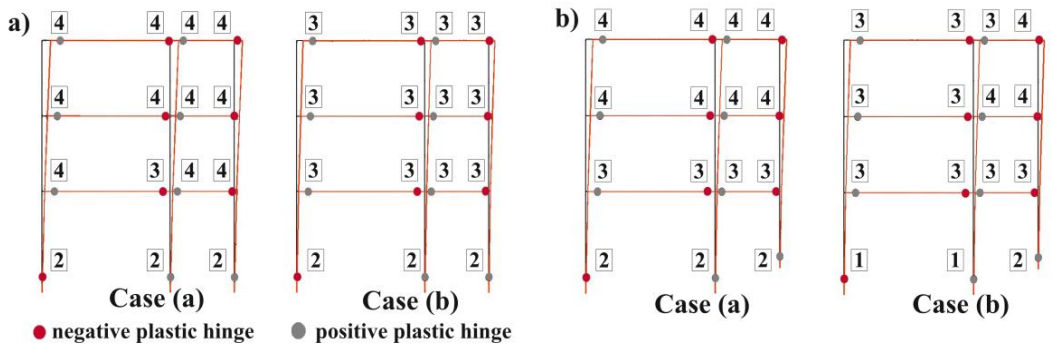

Fig. 4.26: Deformed shape and plastic hinge formation for frame a) 2a and b) 2b.

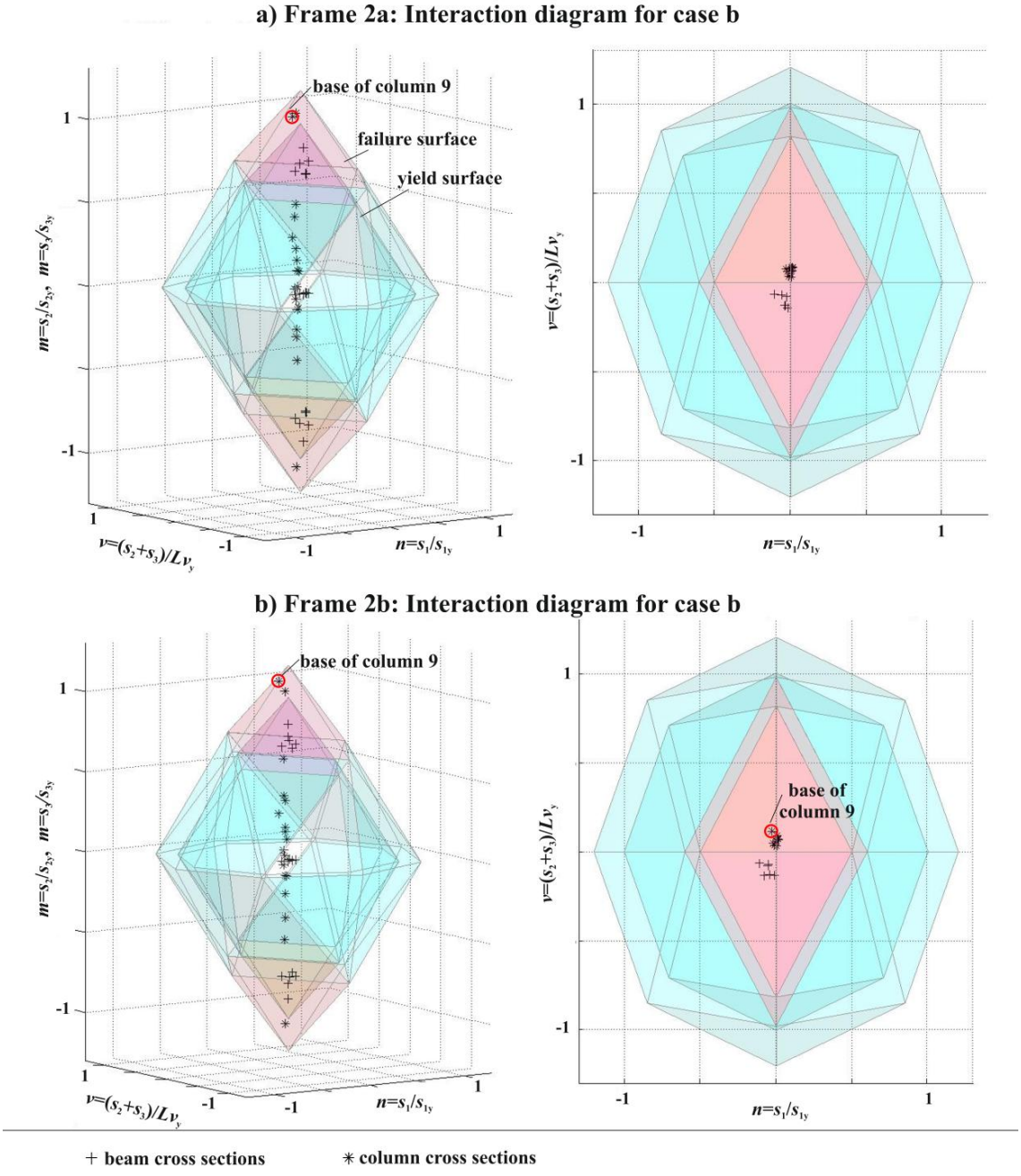

Fig. 4.27: Interaction diagrams for case (b) for a) frame 2a and b) frame 2b.

4.8.3.3. Example #3

The third example concerns the three-storey, four-bay plane frame, shown in Fig. 4.28, that is subjected to increasing lateral and fixed vertical loading. The frame is discretized into 39 elements, 32 nodes and 81 degrees of freedom. The steel grade is S235 with $E=2\times10^8$kN/m^2. Sections with $A=112.5\times10^{-4}\ m^2$, $I=18260\times10^{-8}\ m^4$, $s_{1y}=2643.75$ kN, $v_y=505.4$ kN, $s_{2y}=325$ kNm, $s_{3y}=325$ kNm and sections with $A=62.61\times10^{-4}\ m^2$, $I=11770\times10^{-8}\ m^4$, $s_{1y}=1471.34$ kN, $v_y=418.06$ kN, $s_{2y}=189.01$ kNm, $s_{3y}=189.01$ kNm are employed for all columns and beams respectively. The multi-segment hardening behavior is shown in Fig. 4.28b and depends on the parameters of every section. More specifically, for columns $h_1=6500$kNm $z_1=0.005$ $\lambda_1=1.10$, $h_2=3250$kNm $z_2=0.015$ $\lambda_2=1.20$, $h_3=-5200$kNm $z_3=0.04$ $\lambda_3=0.80$, $h_4=10^{-6}$kNm $z_4=0.05$ $\lambda_4=0.80$, while for beam cross sections $h_1=3780.2$kNm $z_1=0.001$ $\lambda_1=1.02$, $h_2=2835.15$kNm $z_2=0.003$ $\lambda_2=1.05$, $h_3=-1750.1$kNm $z_3=0.03$ $\lambda_3=0.8$, $h_4=10^{-6}$kNm $z_4=0.05$ $\lambda_4=0.8$. The values of z_4 constitute the upper bounds for column and beam cross sections respectively. The upper bound vector of all displacements is $u_u=1$ and the lower bound vector $u_l=-1$. The initial value of $\rho=100$ for case (a) and $\rho=1000$ for case (b) with an updating rule of $\rho=10\rho$ after each NLP solution until an appropriate convergence tolerance is reached ($w^T z \le 10^{-5}$). The algorithm for all cases has stopped because change in the vector of unknown variables and maximum constraint violation were less than the preselected tolerances (10^{-10}).

Results analysis are shown in Table 4.5. It is noted that for both interaction cases the frame has been analysed including the shear deformation effect (Timoshenko beam element stiffness matrix-section 4.6) that influences slightly the analysis results, i.e. collapse mechanisms are invariable, load factor and sway-displacement are slightly increased,while plastic deformations are slightly decreased. In Fig. 4.29 the ultimate states for both cases (*i*) are presented. Positive and negative plastic hinges are classified according to bending moment sign. The corresponding interaction diagrams for cases (a)-*i* and (b)-*i* are depicted in Fig. 4.30. The dominant role of bending moment is evident, while, as no diaphragmatic action is considered, the role of axial force is more intense in beam cross sections, especially for the right ends of first and second storeys that reside at their third hardening branch. In Fig. 4.31 the interaction diagram for case (b)–*i* is presented focusing on the dispersion of stress points. Although the stress state in $n-m$ plan-view is almost the same with that of NM

interaction (Fig. 4.31a), it is evident that the shear force effect is stronger than that of axial force, as shown in plan views $n-v$ (Fig. 4.31b).

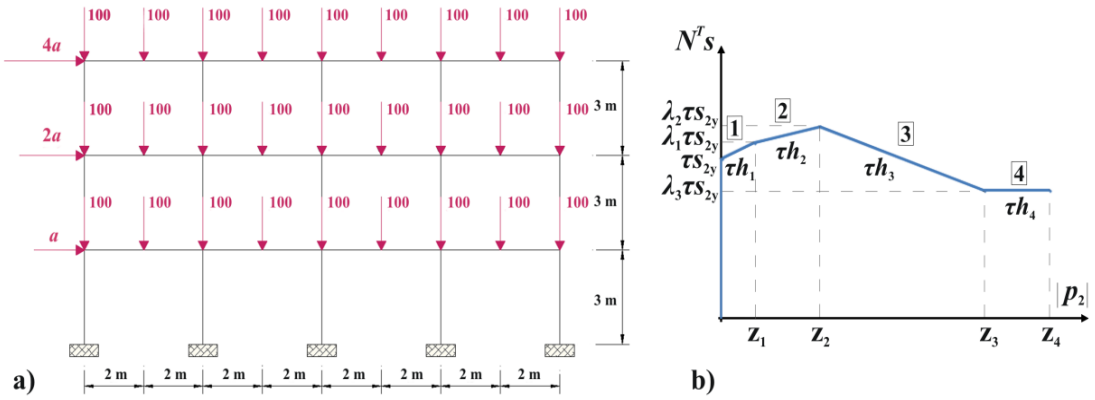

Fig. 4.28: a) Three-storey, four-bay plane frame and b) multi-segment hardening behavior.

Table 4.5: Analysis results of example #3.

Cases		a (kN)	top-storey u (m)	$w^T z$
(a)	i : no shear deformations	**109.87**	**0.147**	**2.79E-08**
	ii : shear deformation effect	**110.11**	**0.159**	**2.72E-08**
(b)	i : no shear deformations	**97.55**	**0.153**	**4.99E-09**
	ii : shear deformation effect	**97.56**	**0.158**	**3.10E-07**

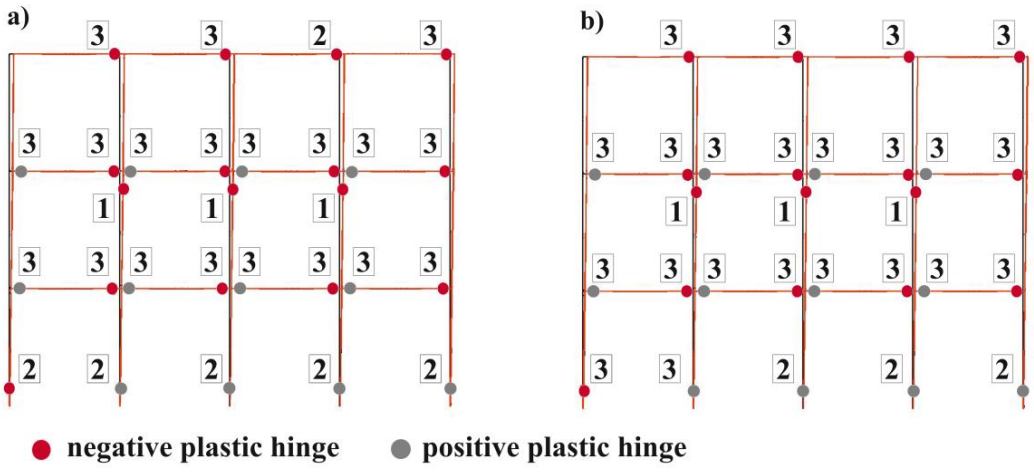

Fig. 4.29: Plastic hinge formation of frame 3 for cases (a)-i and (b)-i.

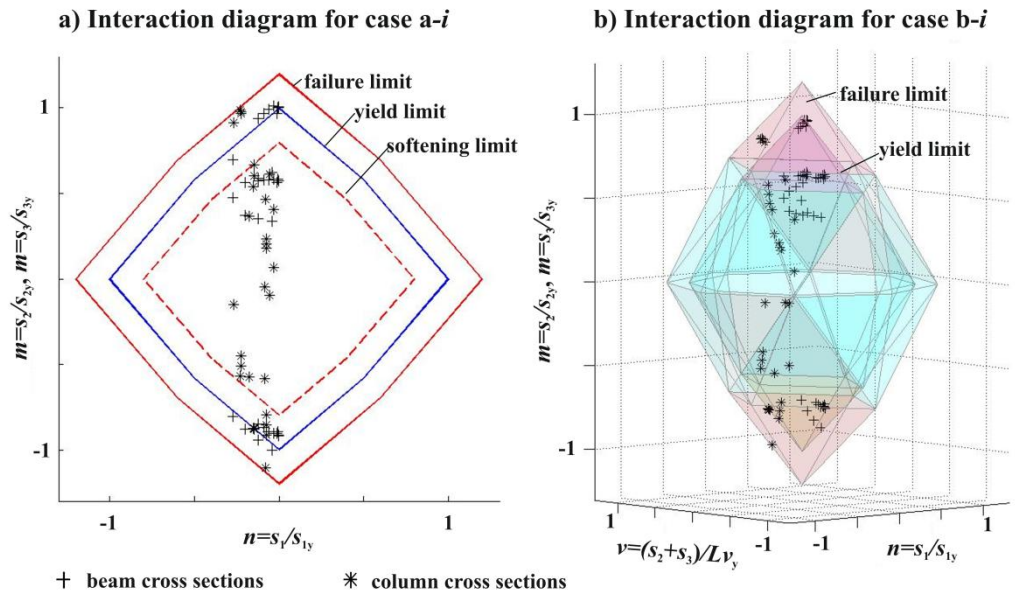

Fig. 4.30: Interaction diagrams of frame 3 for cases (a)-i and (b)-i.

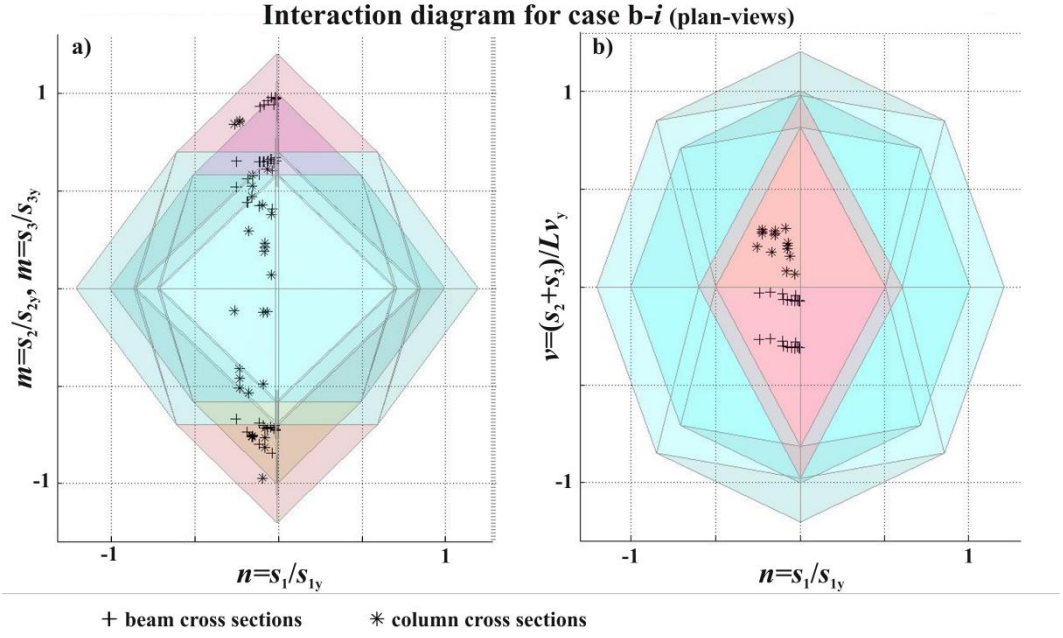

Fig. 4.31: Interaction diagrams of frame 3 for case (b)-i (plan-views).

4.8.4. Computational performance for NQM interaction

The evolution of the proposed algorithm during the optimization steps is presented in more detail for all the above examples. The efficiency of the computational procedure is examined through variation of the objective function and first-order optimality measure (Appendix C) for the entire history of optimization.

The performance of the algorithm for example #1 is depicted in Fig. 4.32. It is observed that, for the same initial values and upper and lower bounds of the variables, the proposed algorithm converged after 59 iterations, while the standard formulation after 103 iterations. It is highlighted that the standard formulation after the 41st iteration seems to follow almost the same path to the solution as the cone identification procedure. Due to the reduced size of the problem, the proposed algorithm finds the path to the optimum easier, while the standard formulation needs more iterations in trying to find the final path. Moreover, it is noted that the standard formulation that incorporates all yield constraints is more sensitive to initial values than the proposed algorithm.

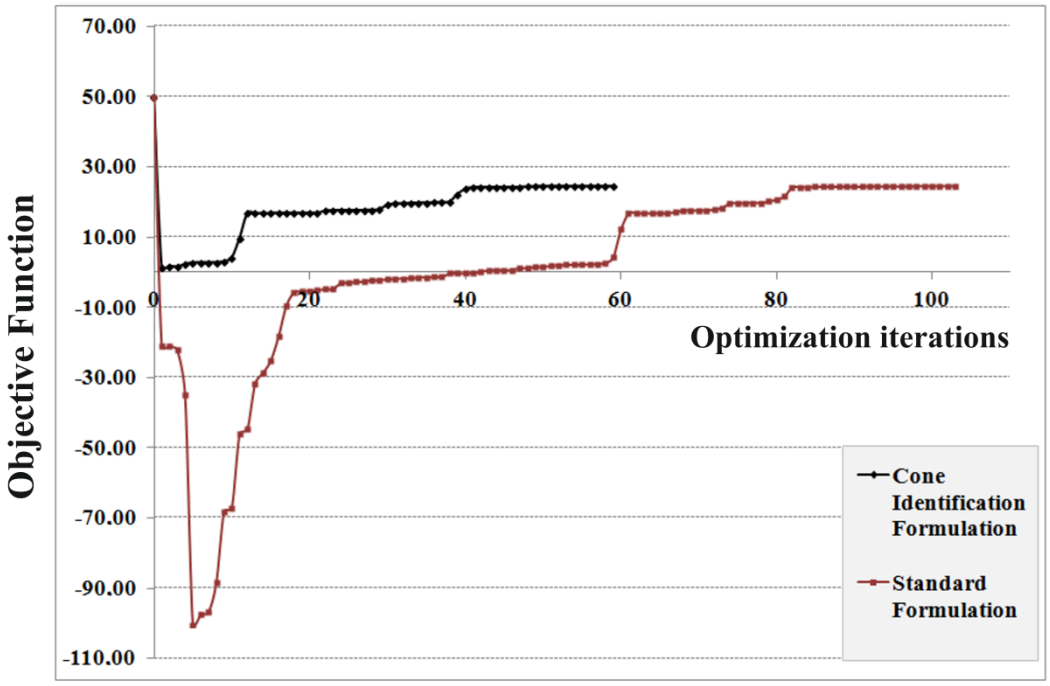

Fig. 4.32: *Comparison of computational procedure for the proposed and the standard formulation.*

The observed behavior of the computational procedure for frames 2a and 3 are presented in terms of objective function evolution and first-order optimality measure variation in Figs. 4.33-4.36, omitting the initial iterations for scaling reasons. For NM interaction the convergence of the algorithm is smoother as compared to NQM interaction since yield conditions for the latter case are more complex. The evolution of the optimality measure turns out smoother for cases (b). This though cannot be considered systematic but only indicative. The smooth tendency of the algorithm to

attain larger values of the loading factor a is distracted by the penalty term, which aims at establishing the disjunctive nature of the complementarity condition. This is manifested in Fig. 4.37 where the evolution of a is separated from the complementarity term in (4.26) for frame 2a. It turns out that in most cases the peaks correspond to negative values for the reserves due to overshooting of stresses. For the iterations corresponding to the sharp peaks, the generated vector of variables $\boldsymbol{s}$ and $\mathbf{z}$ determine a dot product $\boldsymbol{w}^T\mathbf{z}$ that deviates slightly from zero. This is magnified by the increasing parameter ρ affecting noticeably the value of the objective function (Fig. 4.37).

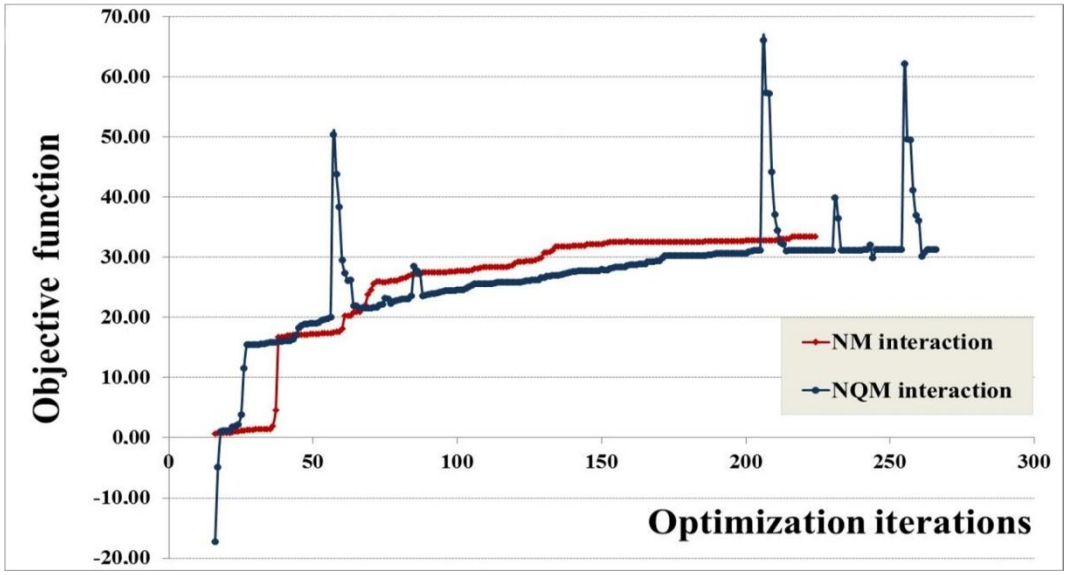

Fig. 4.33: *Evolution of the objective function for frame 2a.*

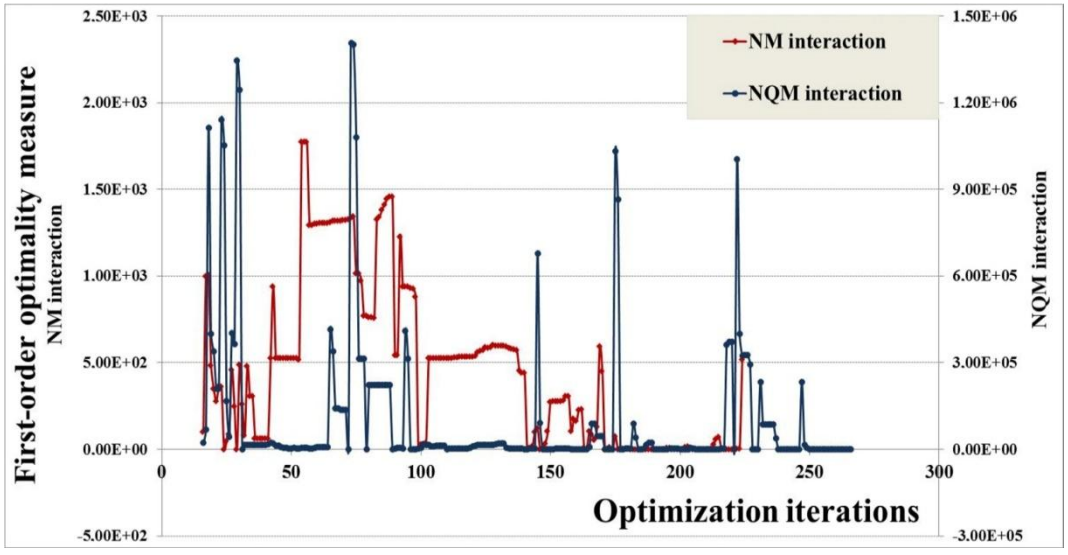

Fig. 4.34: *Evolution of the first-order optimality measure for frame 2a.*

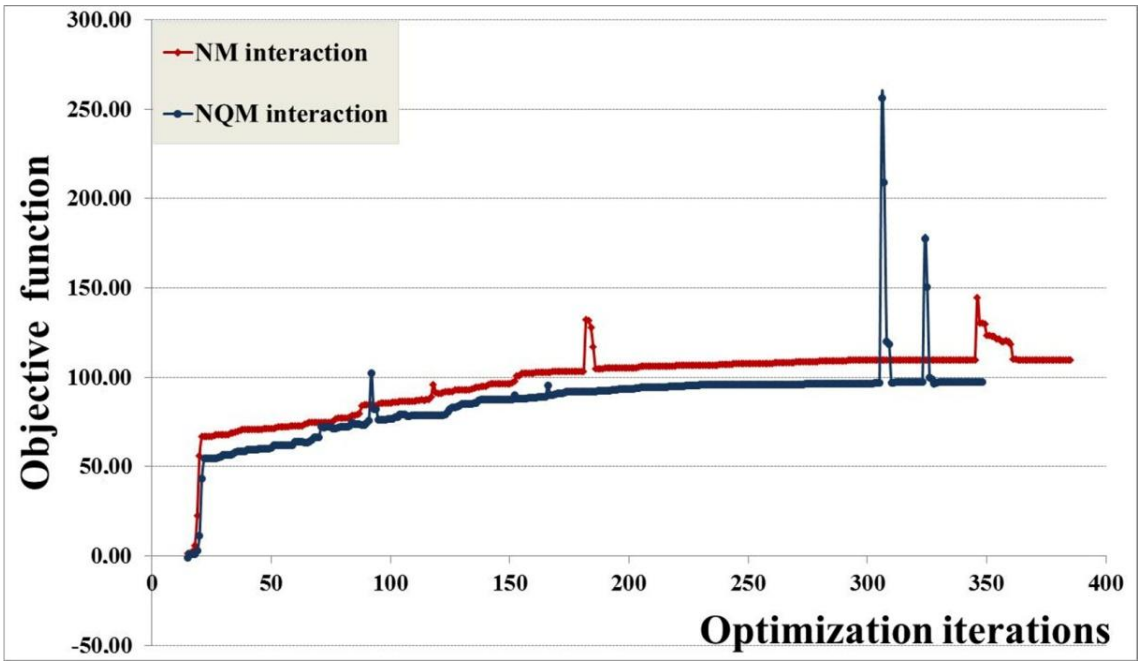

Fig. 4.35: *Evolution of the objective function for frame 3.*

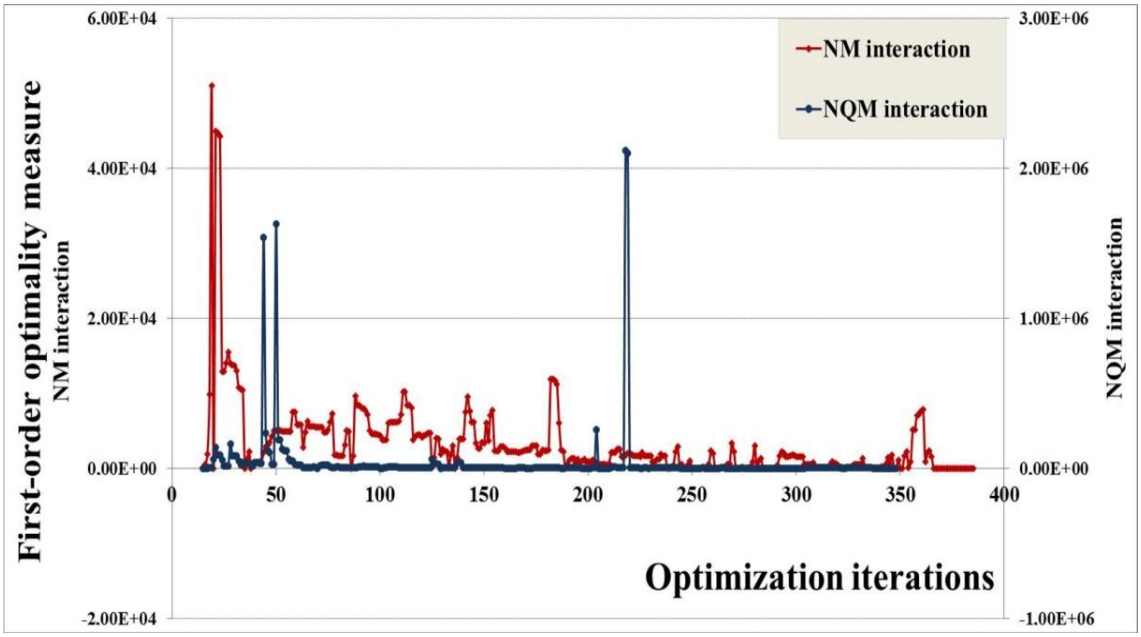

Fig. 4.36: *Evolution of the first-order optimality measure for frame 3.*

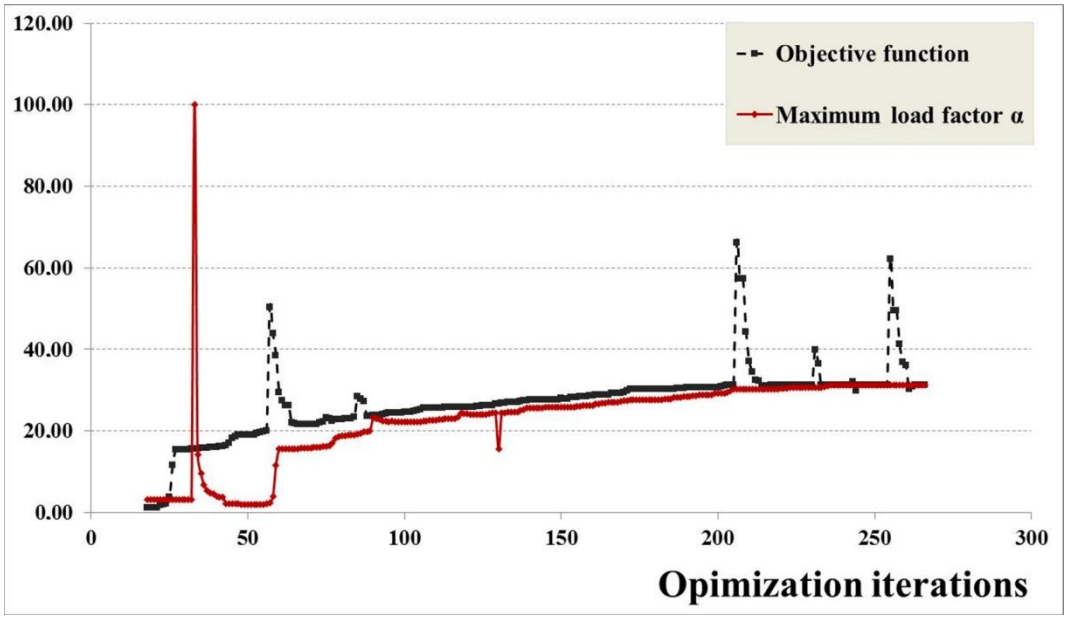

Fig. 4.37: *Evolution of the objective function and maximum load factor for NQM interaction.*

4.9. Concluding remarks

Limit load and deformation analysis is treated herein in the framework of mathematical programming. The ultimate state of a structure and its maximum load carrying capacity is determined by solving an optimization problem that aims at maximizing the load factor *a* subjected to constraints that enforce equilibrium, compatibility, yielding and complementarity conditions. Due to the disjunctive nature of the latter, the problem lacks in convexity and smoothness. Using a penalty function method, it is reformulated into a NLP problem depending on initial values and lower and upper bounds of variables. The optimization process follows a gradient-based mathematical pace that tends to increase the load factor *a* satisfying the imposed constraints at each optimization iteration. Successive trials determine the path to the solution that generally differs from the actual path of a step-by-step method of finite element analysis, both though succeeding in finding the same solution.

In this work, a reduced in size and independent-from the order of piecewise linearization of the yield surface and constitutive law- method is proposed for holonomic elastoplastic analysis with mathematical programming accounting for axial-bending moment (NM) and axial-shear force-bending moment (NQM) interaction and piecewise linear hardening/softening behavior. The concept is based on the identification of one specific yield line/plane and hardening branch for every cross section. At each optimization iteration, the vector of the decision variables (i.e. stresses ***s***, displacements ***u***, plastic multipliers **z** and the load factor *a* is generated. Every critical section belongs to a specific cone of the interaction diagram targeting

only one yield hyperplane. Given the stresses, the specific cone of the interaction diagram is detected. Having the critical yield hyperplane identified, only one plastic multiplier is required for each cross section. The linear hardening/softening segment that corresponds to this plastic multiplier is then identified and as a consequence, hardening matrices are formed for each cross section only for the specific segment. Thus the yield condition for each cross section is formed only for the identified yield plane and the identified hardening/softening branch and not for all unnecessary ones. This reduces considerably the number of yield and complementarity constraints decreasing significantly the complexity of the formulation, as the size of the problem becomes independent of the type of linearization.

The generalized Gendy-Saleeb yield criterion was adopted that accounts for the axial force-bending moment and axial-shear force-bending moment interaction. Numerical results demonstrate the validity of the proposed method and the need to account for shear force effects that lead to reduction of the load carrying capacity, as compared to axial force-bending moment interaction, and thus to safer designs, especially for structures characterized by intense shearing forces.

From the presented examples, it becomes evident that the computational performance of the proposed formulation is considerably more efficient than the standard one, enabling an ample use of multi-segment hardening/softening behavior and thus addressing more accurately real structural response.

Chapter 5

Limit Load and Deformation Analysis for Plane Frames with Nonlinear Interaction and Constitutive Laws

5.1. Introduction

This chapter deals with limit load and deformation analysis of structures considering nonlinear interaction and structural behavior. The existing formulation, as well as the proposed enhanced formulations of previous chapters (3 and 4), are based on the a priori linearization of the yield surface and constitutive laws. Herein, a new approach is proposed that retains the nonlinearity of the yield surface applying a local linearization technique. Moreover, isotropic nonlinear hardening/softening cross-sectional behavior is efficiently incorporated. The ultimate state of the structure is determined as an optimization problem with linear equilibrium, compatibility and yield constraints together with a nonlinear complementarity constraint. The disjunctive nature of the latter enforces the formulation of a non-linear programming problem using a penalty function method.

5.2. Problem formulation

The formulation of the optimization problem includes constraints imposed by equilibrium, compatibility, yield condition, lower and upper bounds for plastic deformations and displacements, while the complementarity condition appropriately penalizes the objective function as:

$$\left.\begin{array}{lcl} \text{maximize} & a-\rho\cdot\boldsymbol{w}^T\cdot\mathbf{z} & (i)\\ \text{subject to} & \boldsymbol{B}\cdot\boldsymbol{s}-a\cdot\boldsymbol{f}=\boldsymbol{f}_d & (ii)\\ & \boldsymbol{S}^{-1}\cdot\boldsymbol{s}-\boldsymbol{B}^T\cdot\boldsymbol{u}+\boldsymbol{N}\cdot\mathbf{z}=\mathbf{0} & (iii)\\ & \boldsymbol{w}=-\boldsymbol{N}^T\cdot\boldsymbol{s}+\boldsymbol{r}'\geq\mathbf{0} & (iv)\\ & \mathbf{0}\leq\mathbf{z}\leq\mathbf{z}_u & \\ & \boldsymbol{u}_l\leq\boldsymbol{u}\leq\boldsymbol{u}_u & \end{array}\right\} \tag{5.1}$$

The solution of this NLP problem provides simultaneously the load multiplier a, the corresponding stresses $\boldsymbol{s}$ and displacements $\boldsymbol{u}$ together with the plastic multipliers $\mathbf{z}$. In this section, a new procedure is proposed for the formulation of the yield condition that abandons the existing notion of the a priori piecewise linearization of both yield surface and constitutive laws. The nonlinear yield criterion is locally linearized within the algorithm for every stress point, while the nonlinearity of constitutive laws is retained.

5.2.1. Local linearization of yield criterion

Yield criteria expressing mathematically the multi-component interaction of stresses are general nonlinear. Their linear expression, though, offers computational advantages for the constraint formulation of the problem. The herein proposed method applies the linearization of the yield surface locally for every stress point. The proposed process constitutes an extension of the cone identification approach and is based on the concept that for every stress vector only one yield hyperplane is targeted or activated. This hyperplane is not a priori defined, but is determined at each optimization iteration for every stress point. First, the intersection point of every stress vector with the nonlinear yield surface is defined. Then, the corresponding tangent hyperplane and its normal vector are determined (Fig. 5.1). The normalized ratio of the reserves as compared to the stress vector is of interest, normalized appropriately. Thus, for every cross section only one yield condition is formed and the dimensions of matrix $\boldsymbol{N}$ and vectors $\boldsymbol{w}$ and $\boldsymbol{r'}$ in equation (5.1*iv*) are exactly the same as in section 4.3. It is noted that the implementation of the method is depicted for a 2D yield criterion in Fig. 5.1. The proposed formulation is nevertheless general and can be efficiently applied for *d*-component interaction.

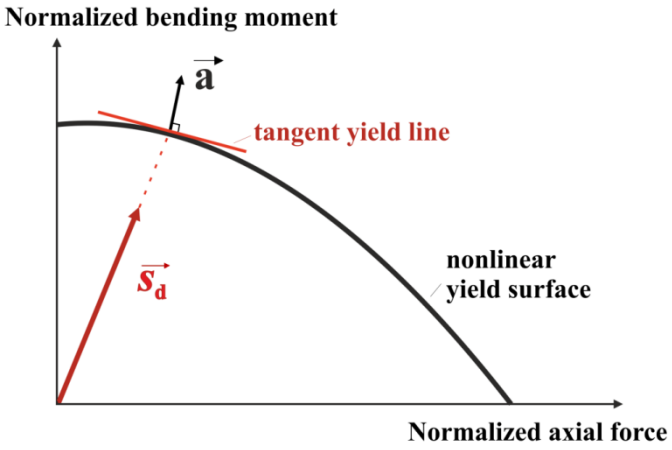

Fig. 5.1: Local linearization of the yield surface for a stress point.

5.2.2. Nonlinear structural behavior

The structural behavior is assumed to follow an isotropic nonlinear hardening/softening law. Having experimental data, given as a set of points for axial force-plastic axial deformation and bending moment-plastic rotation, the corresponding nonlinear curves are formed using a curve fitting tool. Then, they are

combined by a proportion dictated by the components of the normal vector of the determined yield hyperplane resulting in a curve that relates finally the combined stresses versus plastic rotation. A plastic multiplier z_μ is assigned to every cross section μ at each optimization iteration, the non-zero value of which denotes that the specific cross section has entered the plastic region. Based on the particular non-zero value of the plastic multiplier and having the analytical expression of the nonlinear hardening/softening behavior, the extended/shrunk yield limit of the stress point is directly evaluated (Fig. 5.2). It is actually the ordinate of the identified curve point that represents the corresponding extended/shrunk yield limit r'_μ required for the formulation of the yield condition (equation 5.1 *iv*).

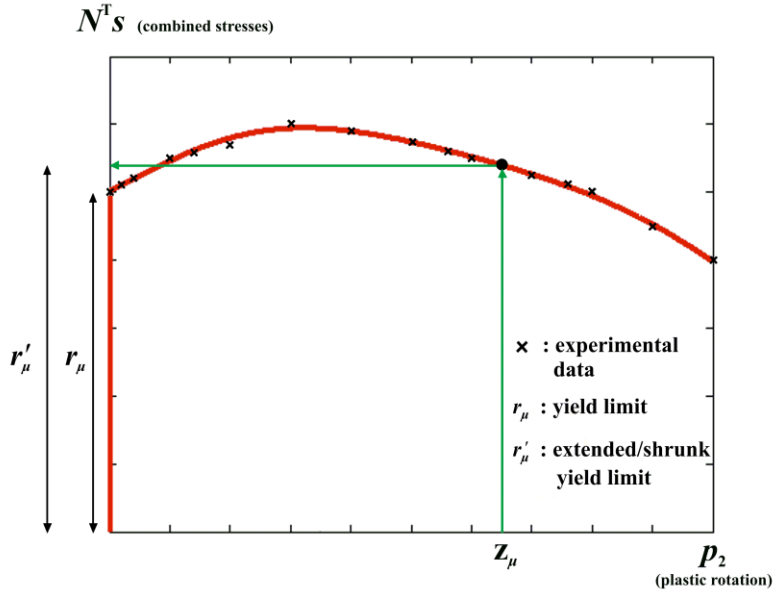

Fig. 5.2: Nonlinear hardening/softening behavior using curve fitting tool.

5.2.3. Optimization procedure

The optimization process is based on successive generations of the entire vector of decision variables dictated by gradient information that force the load factor to higher values satisfying all constraints at the same time. The herein proposed method acts as a filter formulating only the active or potentially active constraints for every stress point at each optimization iteration. The linearization technique of the yield surface is implemented internally at the optimization process, while the nonlinearity of constitutive law is maintained. An outline of the proposed algorithm for every optimization iteration is shown in Fig. 5.3.

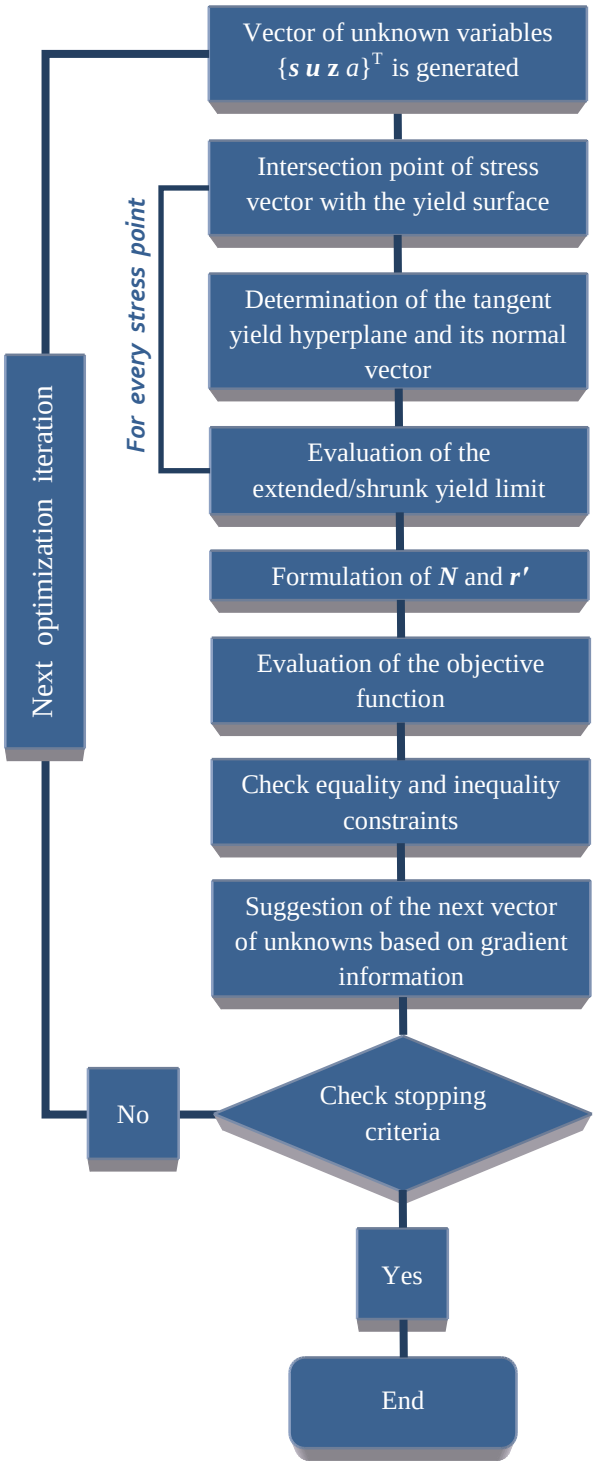

Fig. 5.3: Outline of the optimization procedure.

5.3. Numerical examples

The optimization problem incorporating the proposed method is implemented in Matlab code using *fmincon* solver (appropriate for the minimization of constrained

nonlinear multivariable function), with the interior-point algorithm selected as optimization method. The aim is to verify the applicability of the introduced approach, validate its efficiency and compare the analysis results with existing ones for the following cases:

- Case (a): **NM** interaction with :
    1. PWL yield condition and constitutive laws.
    2. Nonlinear yield condition and PWL constitutive laws.
    3. Nonlinear yield condition and constitutive laws.
- Case (b): **NQM** interaction with:
    1. PWL yield condition and constitutive laws.
    2. Nonlinear yield condition and PWL constitutive laws.
    3. Nonlinear yield condition and constitutive laws.

For this purpose, three steel frames are examined for the aforementioned cases and the corresponding results are presented below. It is noted that all analysis results of this method are presented following the engineering sign convention of structural analysis.

5.3.1. Example #1

The first example concerns one plane frame shown in Fig. 5.4a and serves demonstration purposes. It is subjected to increasing lateral and vertical loading and it is discretized into 4 elements, 5 nodes and 9 degrees of freedom. The steel grade is S235 with $E=2\times10^8$kN/m^2. Sections with $A=28.48\times10^{-4}m^2$, $I=1943\times10^{-8}m^4$, $s_{1y}=669.28kN$, $s_{2y}=s_{3y}=51.84kNm$ and sections with $A=16.43\times10^{-4}\ m^2$, $I=5412\times10^{-8}\ m^4$, $s_{1y}=386.1kN$, $s_{2y}=s_{3y}=20.76kNm$ are employed for all columns and beams respectively. The assumed multi-linear and the corresponding nonlinear hardening/softening behavior is shown in Fig. 5.5. More specifically, for columns $h_1=1036.8kNm$ $z_1=0.005$ $\lambda_1=1.1$, $h_2=518.4kNm$ $z_2=0.015$ $\lambda_2=1.2$, $h_3=-592.46kNm$ $z_3=0.05$ $\lambda_3=0.8$, $h_4=10^{-6}kNm$ $z_4=0.06$ $\lambda_4=0.8$, while for beam cross sections $h_1=415.2kNm$ $z_1=0.005$ $\lambda_1=1.1$, $h_2=207.6kNm$ $z_2=0.015$ $\lambda_2=1.2$, $h_3=-237.26kNm$ $z_3=0.05$ $\lambda_3=0.8$, $h_4=10^{-6}kNm$ $z_4=0.06$ $\lambda_4=0.80$, concerning the multi-linear behavior (Fig. 5.5a). The nonlinear structural behavior is described by a 4th degree polynomial line (Fig. 5.5b) based on data presented in Table 5.1. The values of z_4 constitute the upper bounds for column and beam cross sections respectively. The upper bound

vector of all displacements is $u_u = 1$ and the lower bound vector $u_l = -1$. An updating rule of $\rho=10\rho$ is used until convergence with a tolerance of $w^T z \leq 10^{-5}$ is reached.

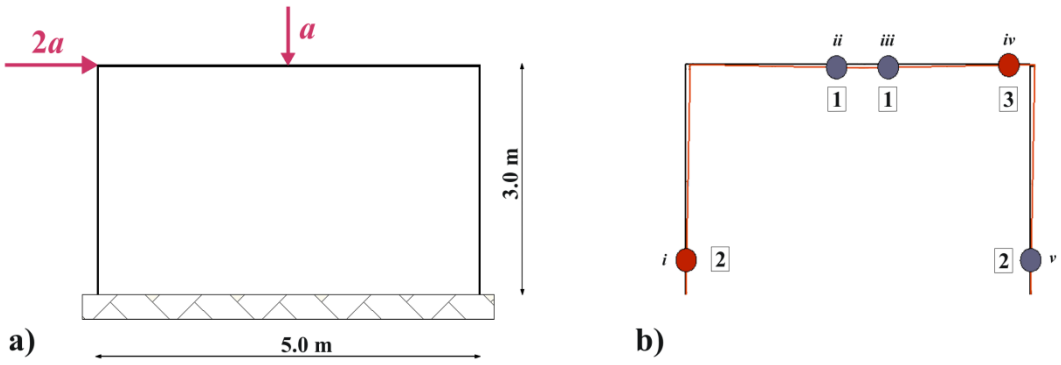

Fig. 5.4: a) Example #1 and b) plastic hinge formation for all analysis cases.

Table 5.1: Polynomial line of structural behavior.

x	0.00	0.0005	0.001	0.002	0.005	0.01	0.012	0.030	0.04	0.06
f(x)	1.00	1.02	1.04	1.05	1.10	1.12	1.15	1.15	1.00	0.80
Polynomial Line	$f(x) = p_1x^4 + p_2x^3 + p_3x^2 + p_4x + p_5$ $p_1 = 2.256 \cdot 10^5,\ p_2 = -1.997 \cdot 10^4,\ p_3 = 116.9,\ p_4 = 12.52,\ p_5 = 1.017$									

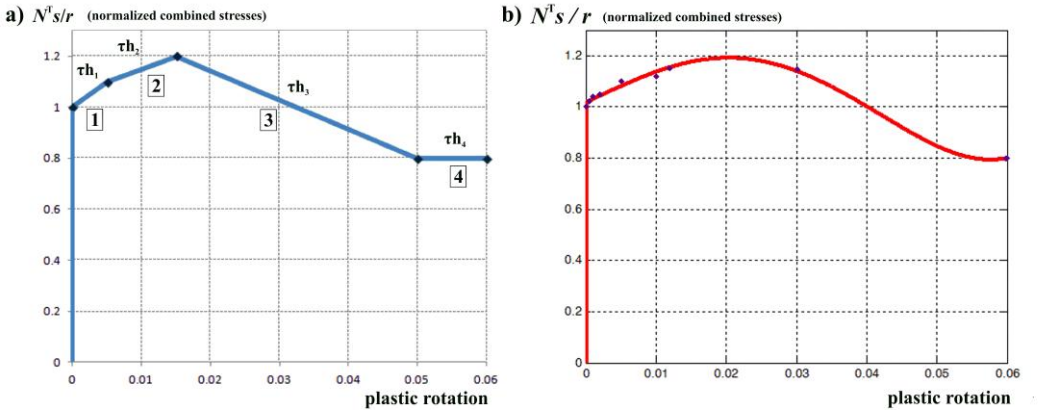

Fig. 5.5: a) Multi-linear and b) nonlinear hardening/softening structural behavior.

Table 5.2. Analysis results for all cases for example #1.

Cases	Case (a_1)	Case (a_2)	Case (a_3)	Case (b_1)	Case (b_2)	Case (b_3)
number of variables n_{var}	30					
number of equality constraints n_{eq}	21					
number of inequality constraints n_{inq}	8					
maximum load factor a (kN)	**23.14**	**23.35**	**23.95**	**21.87**	**23.18**	**23.78**
number of plastic hinges	**5**	**5**	**5**	**5**	**5**	**5**
total computational time (s)	**3.27**	**10.08**	**6.49**	**9.20**	**15.57**	**9.71**
number of iterations	**92**	**66**	**41**	**64**	**98**	**63**
complementarity condition $w^T z$	**6.39E-10**	**7.89E-09**	**2.40E-07**	**8.97E-11**	**3.31E-09**	**4.49E-12**
initial values of ρ	**1000**	**100**	**10**	**10**	**1000**	**10**

All analysis results are presented in Table 5.2. The method of local linearization of the yield condition (cases 2 and 3) corresponds to greater values of maximum load factor for both cases of interaction. This is due to the fact that nonlinearity of yield condition is retained offering more accurate solutions, having, nevertheless, the corresponding computational cost (total computational time includes both matrix formulation and optimization procedure). The difference in maximum load factors is more evident for the case of NQM interaction and it is related to the coarse PWL approximation of the yield surface for case (b_1). In Fig. 5.4b the ultimate state of the frame for all analysis cases is depicted. Each plastic hinge is associated with a roman number, while the corresponding hardening/softening segment for cases of PWL (a_1, a_2 and b_1, b_2) is denoted by an arabic number (Fig. 5.4b). The interaction diagrams are shown in Figs. 5.6 and 5.7. The effect of bending moment is dominant; while the effect of shear force is presented to be more intense than that of axial force (dispersion of stress points is ampler for shear force Fig. 5.7). Yielded stress points are assigned with the corresponding roman number. It is noted that stress point *iv* lies on its softening branch for all cases.

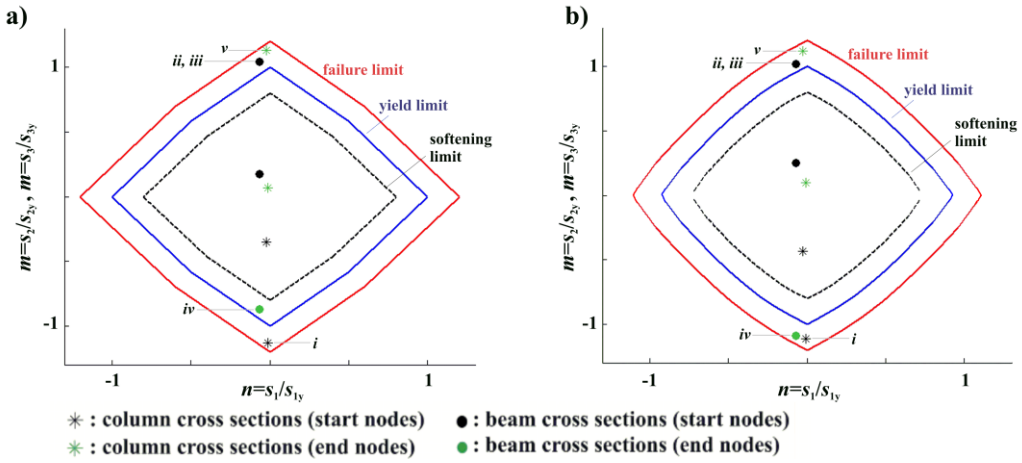

Fig. 5.6: NM interaction diagrams of example #1 for a) case (a_1) and b) case (a_3).

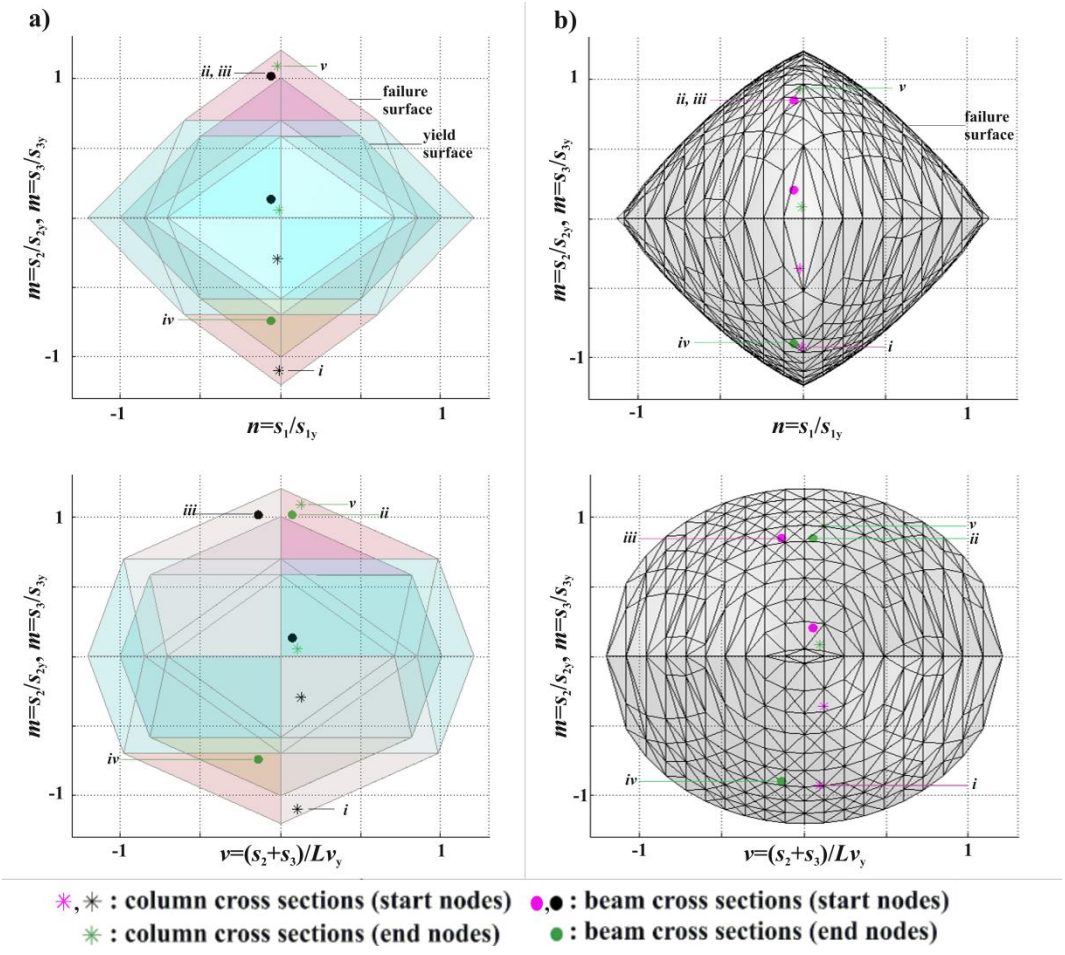

Fig. 5.7: NQM interaction diagrams of example #1 for a) case (b_1) and b) case (b_3).

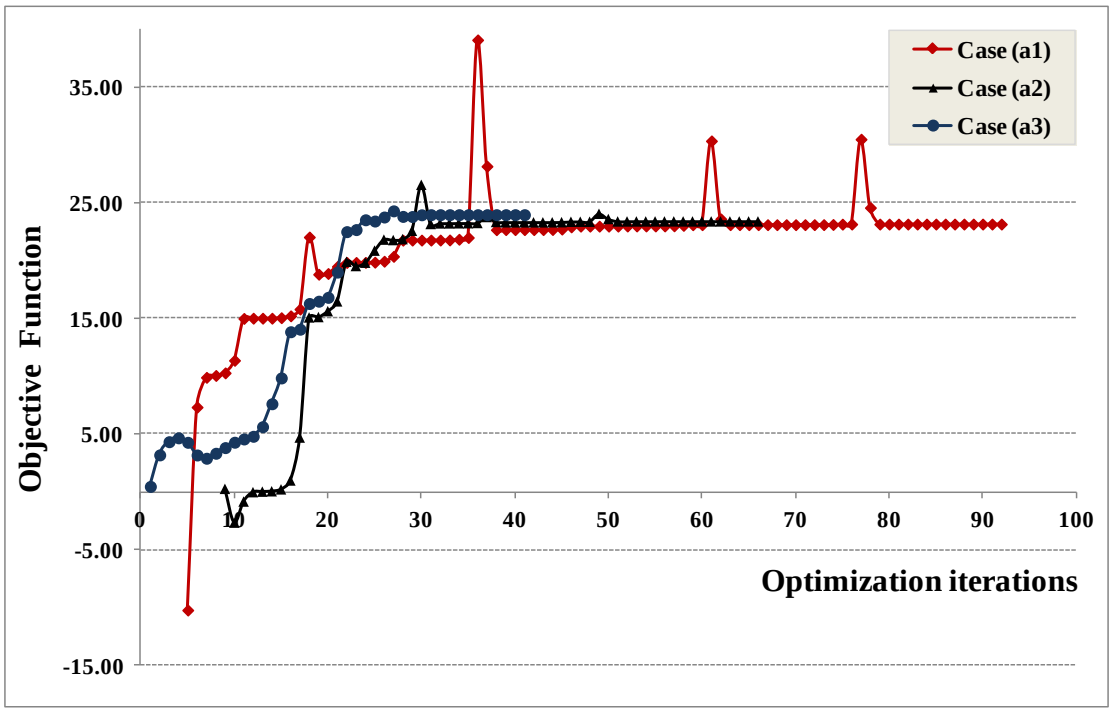

Fig. 5.8: Evolution of the optimization procedure of example #1 for NM interaction.

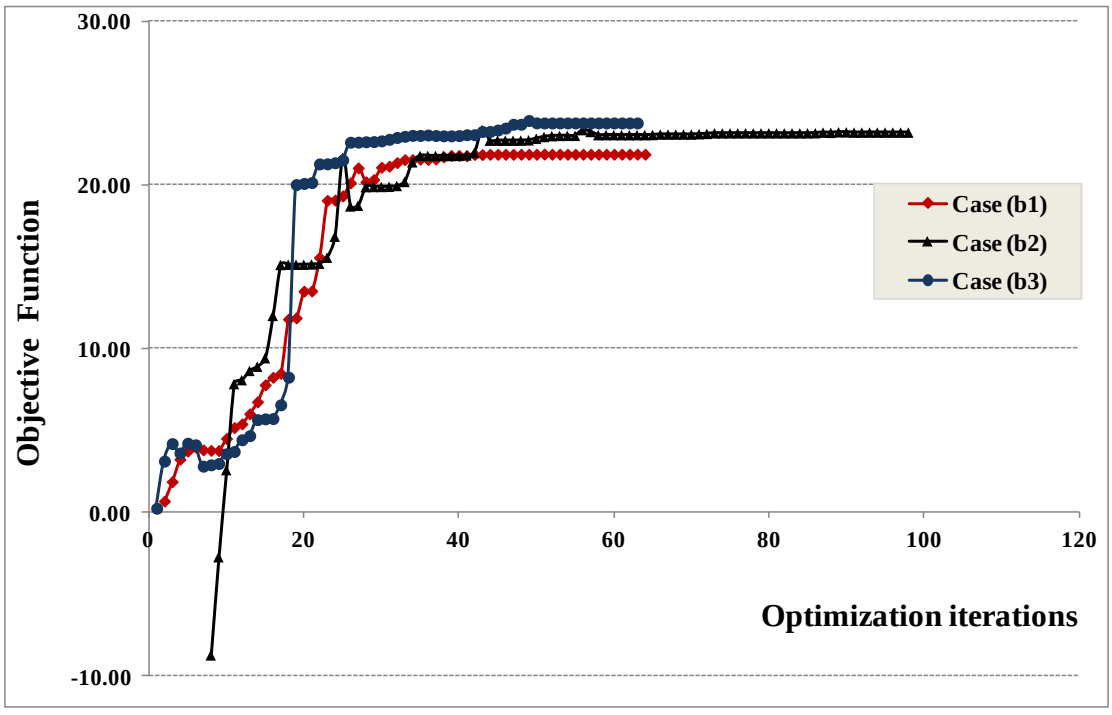

Fig. 5.9: Evolution of the optimization procedure of example #1 for NQM interaction.

The nonlinear formulation (either concerning only the yield condition or both the yield condition and constitutive laws) is generally more susceptible to initial values and lower and upper bounds of variables. The computational performance for NM interaction is presented in Fig. 5.8, omitting initial iterations for scaling reasons. It is

noted that for all cases (a_1, a_2 and a_3) the initial values of the unknown vector are the same, while the corresponding initial values of the objective function are not identical. This lies on the fact that the objective function includes the values of $\boldsymbol{w}$ that differ for PWL and nonlinear approach. Moreover, it is observed that cases (a_2) and (a_3) require fewer iterations until convergence compared to case (a_1), consuming more computational time, though. This is due to the fact that cone identification for 2D interaction is a straightforward and faster procedure compared to local linearization method. The evolution of the optimization process for NQM interaction is depicted in Fig. 5.9, omitting initial iterations for demonstration purposes. The number of required iterations is almost the same for both cases (b_1 and b_3), while the corresponding computational time is slightly higher for the nonlinear consideration.

5.3.2. Example #2

The second example concerns a three-storey, two-bay steel frame shown in Fig. 5.10. The frame is discretized into 30 elements, 21 nodes and 54 degrees of freedom. The steel grade is S235 with $E=2\times10^8$kN/m^2. The material properties are as follows: sections with $A=112.5\times10^{-4}\ m^2$, $I=18260\times10^{-8}\ m^4$, $s_{1y}=2643.75kN$, $v_y=505.41kN$, $s_{2y}=s_{3y}=325kNm$ are employed for all columns, sections with $A=28.48\times10^{-4}\ m^2$, $I=1943\times10^{-8}\ m^4$, $s_{1y}=669.28kN$, $v_y=189.89kN$, $s_{2y}=s_{3y}=51.84kNm$ for all beams. The corresponding multi-segment hardening behavior is shown in Fig. 5.11a and depends on the parameters of every section. More specifically, for columns $h_1=6500kNm$ $z_1=0.005$ $\lambda_1=1.1$, $h_2=3250kNm$ $z_2=0.015$ $\lambda_2=1.20$, $h_3=-5200kNm$ $z_3=0.04$ $\lambda_3=0.8$, $h_4=10^{-6}kNm$ $z_4=0.05$ $\lambda_4=0.8$, while for beam cross sections $h_1=518.4kNm$ $z_1=0.005$ $\lambda_1=1.05$, $h_2=259.2kNm$ $z_2=0.015$ $\lambda_2=1.10$, $h_3=-777.6kNm$ $z_3=0.035$ $\lambda_3=0.80$, $h_4=10^{-6}kNm$ $z_4=0.04$ $\lambda_4=0.80$. The nonlinear structural behavior for column and beam cross sections is depicted in Fig. 5.11b using 4th degree polynomial lines, based on data presented in Table 5.3. The values of z_4 constitute the upper bounds for column and beam cross sections respectively. The upper bound vector of all displacements is $u_u=1$ and the lower bound vector $u_l=-1$ (for case b_1 the corresponding bounds are set as 2 and -2). An updating rule of $\rho=10\rho$ after each NLP solution until an appropriate convergence tolerance is reached $(w^T z \le 10^{-5})$.

All analysis results are presented in Table 5.3. Load factors of nonlinear approach for both interaction considerations are slightly greater than that of PWL approach, as

expected. Moreover, the effect of shear force is evident in the reduction of the load carrying capacity. The plastic hinge pattern is identical for all analysis cases (Fig. 5.10b), but different stress states correspond to plastic hinges for each case. The corresponding interaction diagrams are shown in Figs. 5.12 and 5.13. Cross sections are stressed mainly due to bending moment, with some beam sections lying on their softening branch. The effect of axial force is observed mainly in beam cross sections (Fig. 5.12 and *n-m* diagrams of Fig. 5.13), while the effect of shear force is obvious and more intense than that of axial force in both beam and column cross sections (*v-m* diagrams of Fig. 5.13).

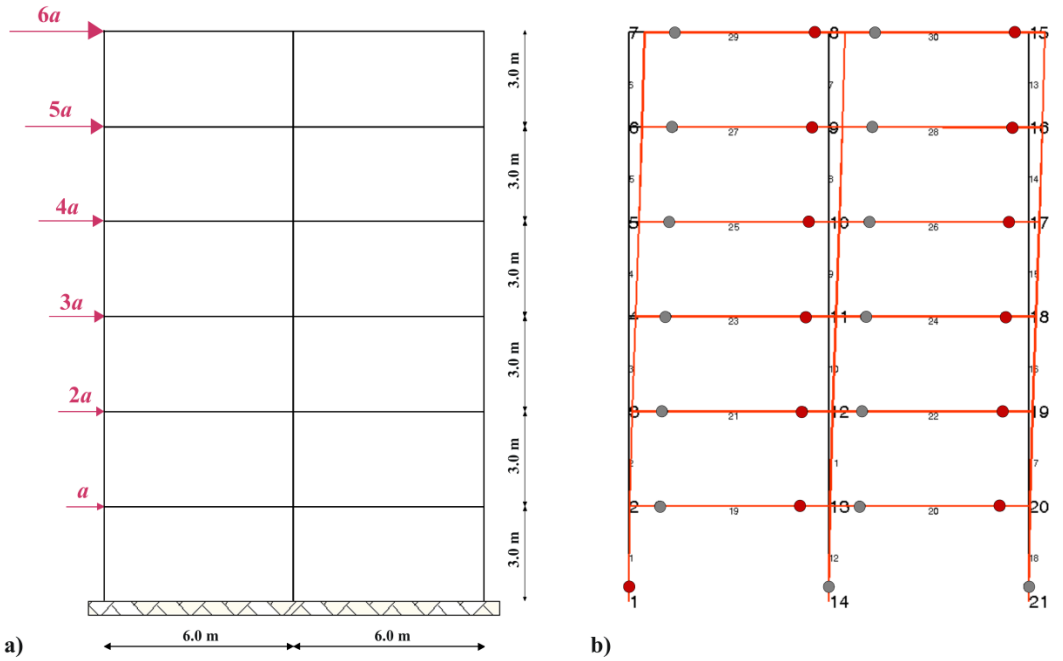

Fig. 5.10: a) Example #2 and b) plastic hinge formation for all analysis cases.

Table 5.3: Polynomial lines of structural behavior.

x	0.00	0.001	0.002	0.005	0.007	0.01	0.015	0.020	0.025	0.028	0.030	0.035	0.038	0.040	0.045	0.050
f(x)	1.00	1.05	1.10	1.15	1.18	1.20	1.18	1.10	1.05	1.00	1.10	0.95	0.90	0.85	0.80	0.80
Polynomial line for column cross sections								$f(x)=p_1\cdot x^4+p_2\cdot x^3+p_3\cdot x^2+p_4\cdot x+p_5$ $p_1=-2.17\cdot10^5, p_2=4.19\cdot10^4, p_3=-2411, p_4=38.55, p_5=1.014$								
x	0.00	0.0005	0.001	0.005	0.008	0.015	0.017	0.019	0.020	0.021	0.023	0.025	0.028	0.030	0.035	0.050
f(x)	1.00	1.01	1.03	1.05	1.08	1.10	1.09	1.07	1.05	1.02	1.00	0.95	0.90	0.87	0.83	0.80
Polynomial line for beam cross sections								$f(x)=p_1\cdot x^4+p_2\cdot x^3+p_3\cdot x^2+p_4\cdot x+p_5$ $p_1=2.38\cdot10^5,\ p_2=-4310,\ p_3=-827,\ p_4=18.24,\ p_5=0.9998$								

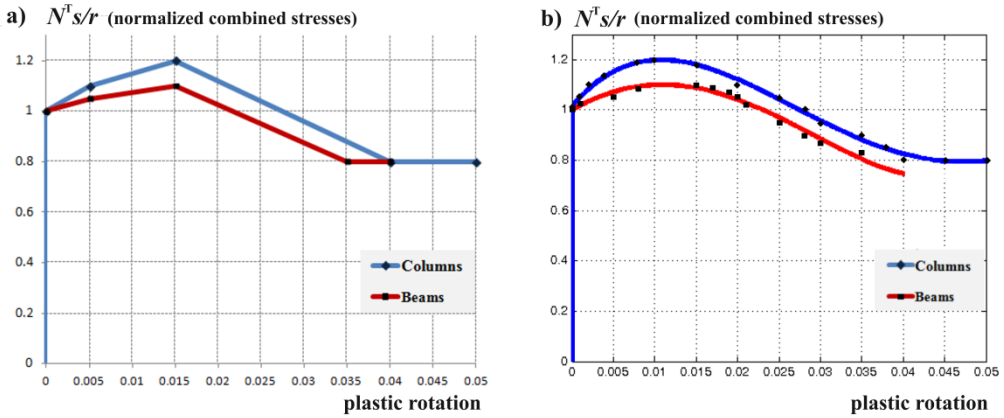

Fig. 5.11: a) Multi-linear and b) nonlinear hardening/softening structural behavior.

Table 5.4: Analysis results for all cases for example #2.

Cases	Case (a_1)	Case (a_2)	Case (a_3)	Case (b_1)	Case (b_2)	Case (b_3)
number of variables n_{var}	**205**					
number of equality constraints n_{eq}	**144**					
number of inequality constraints n_{inq}	**60**					
maximum load factor a (kN)	**8.24**	**8.28**	**8.35**	**7.90**	**8.25**	**8.31**
number of plastic hinges	**27**	**27**	**27**	**27**	**27**	**27**
total computational time (s)	**18.82**	**483.61**	**542.47**	**825.10**	**536.51**	**715.52**
number of iterations	**59**	**80**	**84**	**102**	**83**	**95**
complementarity condition $w^T z$	**7.35E-12**	**1.84E-10**	**4.56E-11**	**1.82E-10**	**9.40E-13**	**1.50E-12**
initial values of ρ	**10**	**10**	**10**	**10^5**	**100**	**10**

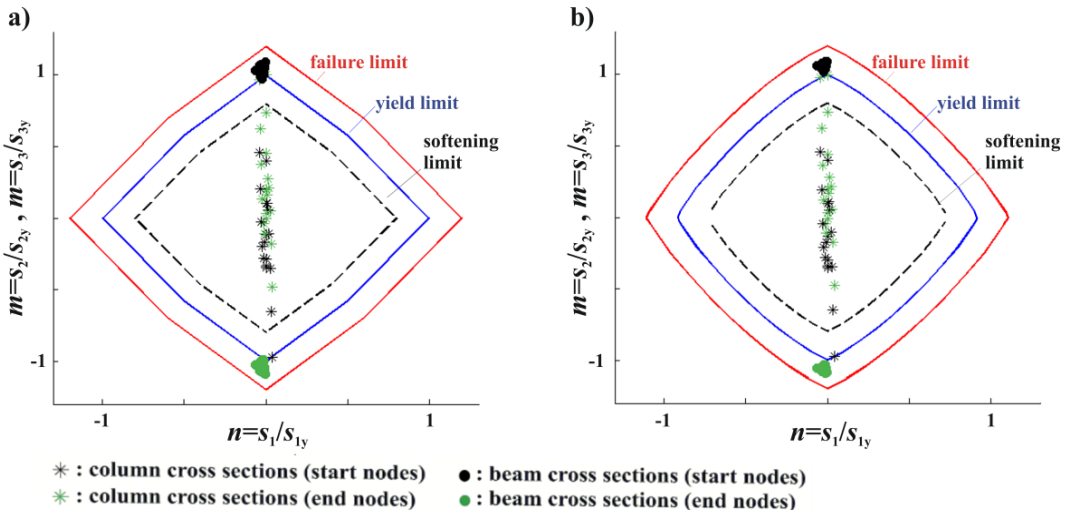

Fig. 5.12: NM interaction diagrams of example #2 for a) case (a_1) and b) case (a_3).

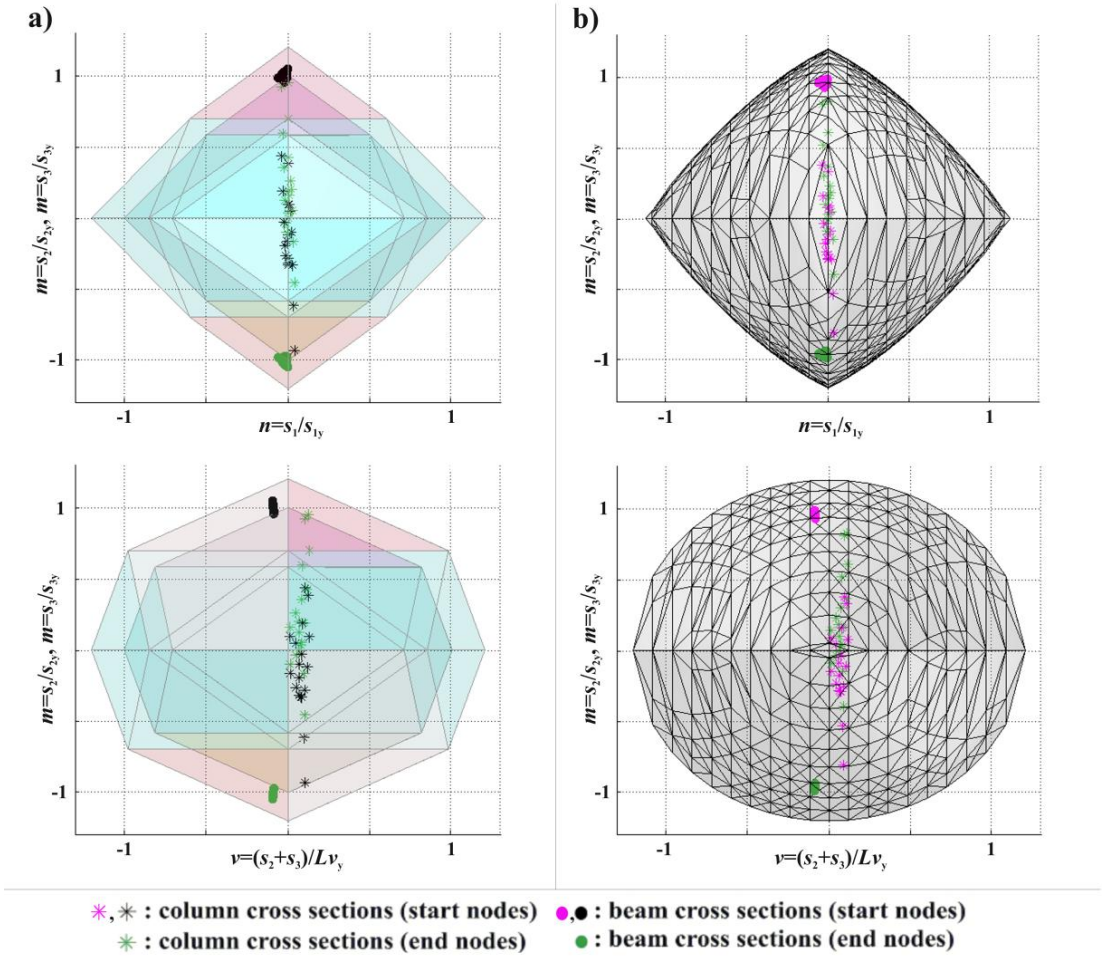

Fig. 5.13: NQM interaction diagrams of example #2 for a) case (b_1) and b) case (b_3).

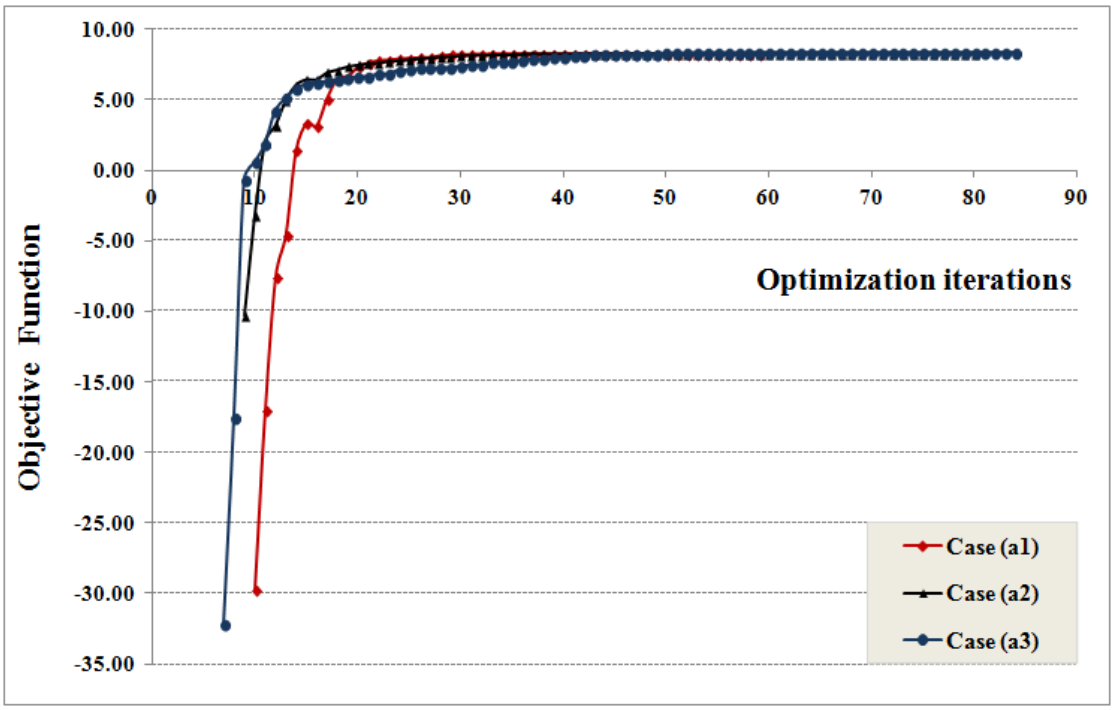

Fig. 5.14: Evolution of the optimization procedure of example #2 for NM interaction.

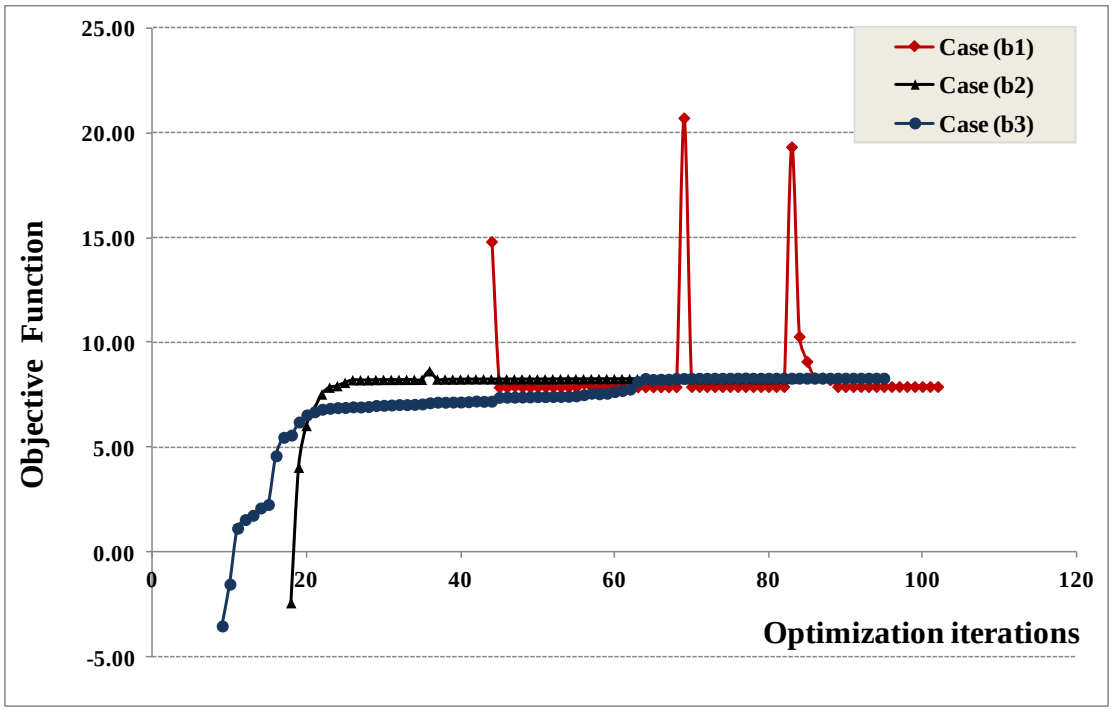

Fig. 5.15: Evolution of the optimization procedure of example #2 for NQM interaction.

The computational performance for NM and NQM interaction is presented in Fig. 5.14 and 5.15 respectively, omitting initial iterations for demonstration purposes. It is observed that for NM interaction the algorithm for all formulations seems to follow almost the same path. However, the nonlinear formulations (cases a_2 and a_3) need

more iterations and consequently significantly more computational time compared to the PWL approach (case a_1). For NQM interaction, the optimization procedure of the local linearization procedure (cases b_2 and b_3) requires fewer iterations compared to the PWL one (83 and 95 iterations versus 102) and less computational time (536.51s, 715.52s versus 825.10s). This is due to the fact that cone identification procedure for 3D interaction consumes more computational time compared to local linearization of the yield surface. The sharp peaks that are presented for case (b_1) are due to the penalized term of the complementarity condition in the objective function. The generated vector of variables $\boldsymbol{s}$ and $\mathbf{z}$ determine a dot product $\boldsymbol{w}^T\mathbf{z}$ that deviates slightly from zero, but this is magnified by the penalty parameter ρ affecting noticeably the value of the objective function.

5.3.3. Example #3

The third example concerns the six-storey, four-bay plane frame, shown in Fig. 5.16, that is subjected to increasing lateral and fixed vertical loading. The frame is discretized into 55 elements, 36 nodes and 90 degrees of freedom. The steel grade is S235 with E=2×10^{8}kN/m^2. Sections with $A=159\times10^{-4}\ m^2$, $I=45070\times10^{-8}\ m^4$, $s_{1y}=3736.5\ kN$, $v_y=505.41\ kN$, $s_{2y}=602.1\ kNm$, $s_{3y}=602.1\ kNm$ and sections with $A=53.81\times10^{-4}\ m^2$, $I=8356\times10^{-8}\ m^4$, $s_{1y}=1264.5\ kN$, $v_y=348.4\ kN$, $s_{2y}=147.7\ kNm$, $s_{3y}=147.7\ kNm$ are employed for all columns and beams respectively. The corresponding multi-segment hardening behavior is shown in Fig.5.17a and depends on the parameters of every section. More specifically, for columns $h_1=30103.5\ kNm$ $z_1=0.002$ $\lambda_1=1.1$, $h_2=7525.9\ kNm$ $z_2=0.01$ $\lambda_2=1.20$, $h_3=-6880.8\ kNm$ $z_3=0.045$ $\lambda_3=0.8$, $h_4=10^{-6}kNm$ $z_4=0.05$ $\lambda_4=0.8$, while for beam cross sections $h_1=7383.5\ kNm$ $z_1=0.001$ $\lambda_1=1.05$, $h_2=1845.9\ kNm$ $z_2=0.005$ $\lambda_2=1.10$, $h_3=-1265.7\ kNm$ $z_3=0.04$ $\lambda_3=0.80$, $h_4=10^{-6}kNm$ $z_4=0.05$ $\lambda_4=0.80$. The nonlinear structural behavior for column and beam cross sections is depicted in Fig. 5.17b using 4th degree polynomial lines, based on data presented in Table 5.5. The values of z_4 constitute the upper bounds for column and beam cross sections respectively. The upper bound vector of all displacements is $u_u=1$ and the lower bound vector $u_l=-1$. An updating rule of $\rho=10\rho$ after each NLP solution until an appropriate convergence tolerance is reached $(w^T z \le 10^{-5})$.

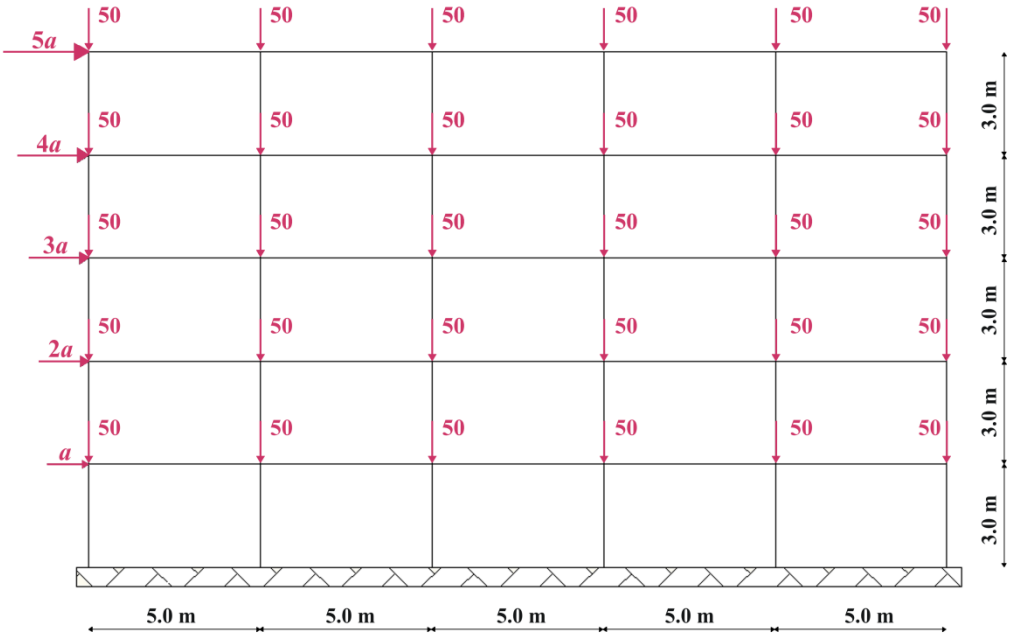

Fig. 5.16: Example #3.

Table 5.5. Polynomial lines of structural behavior.

x	0.00	0.001	0.002	0.005	0.007	0.01	0.015	0.020	0.025	0.028	0.030	0.035	0.038	0.040	0.045	0.060
f(x)	1.00	1.05	1.10	1.15	1.18	1.20	1.15	1.08	1.05	1.02	0.98	0.95	0.85	0.85	0.80	0.80
Polynomial line for column cross sections	$f(x) = p_1 \cdot x^4 + p_2 \cdot x^3 + p_3 \cdot x^2 + p_4 \cdot x + p_5$ $p_1 = -2.15 \cdot 10^5,\ p_2 = 3.78 \cdot 10^4,\ p_3 = -2122,\ p_4 = 33.88,\ p_5 = 1.022$															
x	0.00	0.0005	0.0008	0.001	0.003	0.005	0.010	0.015	0.020	0.022	0.025	0.025	0.028	0.030	0.035	0.050
f(x)	1.00	1.01	1.03	1.05	1.08	1.10	1.09	1.07	1.05	1.02	1.00	0.97	0.93	0.90	0.85	0.78
Polynomial line for beam cross sections	$f(x) = p_1 \cdot x^4 + p_2 \cdot x^3 + p_3 \cdot x^2 + p_2 \cdot x + p_1$ $p_1 = -7.84 \cdot 10^4,\ p_2 = 2.16 \cdot 10^4,\ p_3 = -1402,\ p_4 = 21.33,\ p_5 = 1.01$															

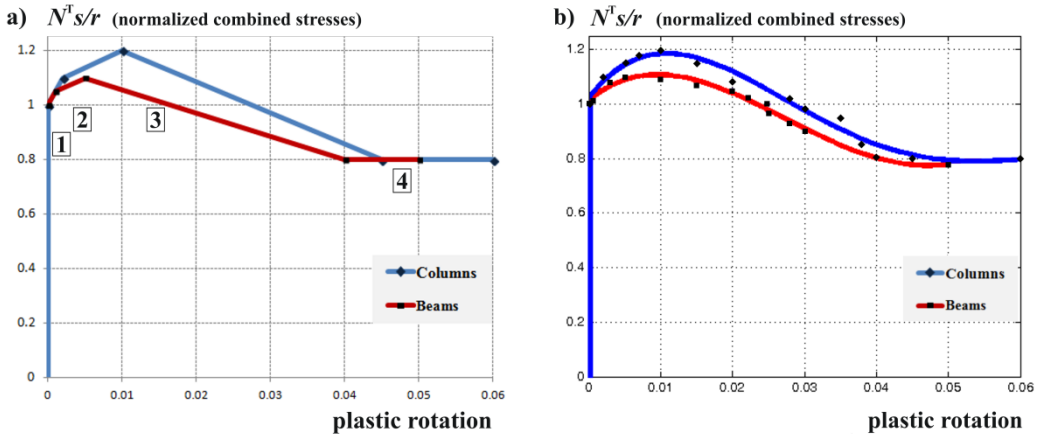

Fig 5.17: a) Multi-linear and b) nonlinear hardening/softening structural behavior.

Table 5.6. Analysis results for all cases for example #3.

Cases	Case (a_1)	Case (a_2)	Case (a_3)
number of variables n_{var}	**366**		
number of equality constraints n_{eq}	**255**		
number of inequality constraints n_{inq}	**110**		
maximum load factor a (kN)	**67.57**	**68.37**	**70.59**
number of plastic hinges	**56**	**56**	**56**
total computational time (s)	**60.49**	**1109.29**	**1010.86**
number of iterations	**54**	**57**	**47**
complementarity condition $w^T z$	**1.48E-09**	**2.55E-15**	**9.25E-12**
initial values of ρ	**1000**	**10^8**	**10^{12}**

All analysis results are presented in Table 5.6. The local linearization method results in more accurate (greater) values of maximum load factor compared to PWL approach, having the corresponding computational cost though. The required computational time is almost 18 times greater for the local linearization technique, while the number of iterations presents slight differences. The plastic hinge pattern is identical for all analysis cases (Fig. 5.18), but different stress states correspond to plastic hinges for each case. For case a_1 each plastic hinge is accompanied with a number that designates the corresponding hardening/softening on which it resides. All beam cross sections (except for those of the last storey) are on their softening branch, with those of the second and third storey more heavily stressed. Bases of columns lay on their second hardening segment, while the rest column sections remain in the elastic region. The corresponding interaction diagrams for cases a_1 and a_3 are shown in Figs. 5.19 and 5.20. The role of bending moment is more intense and the effect of axial force is evident mainly in beam cross sections.

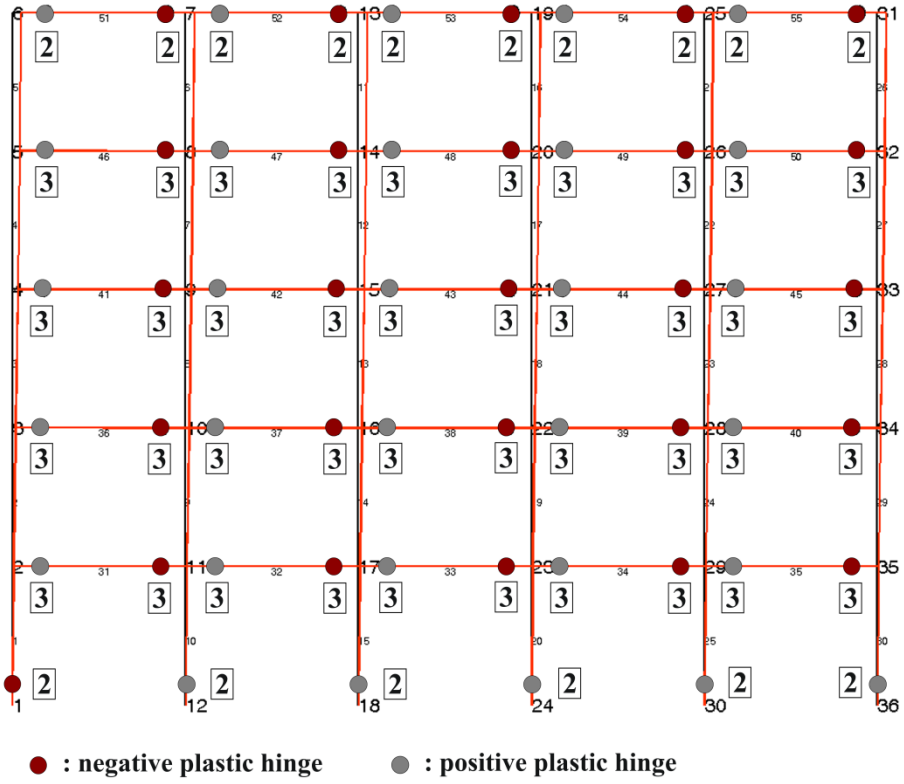

Fig 5.18: Deformed shape of example #3 for all cases of NM interaction.

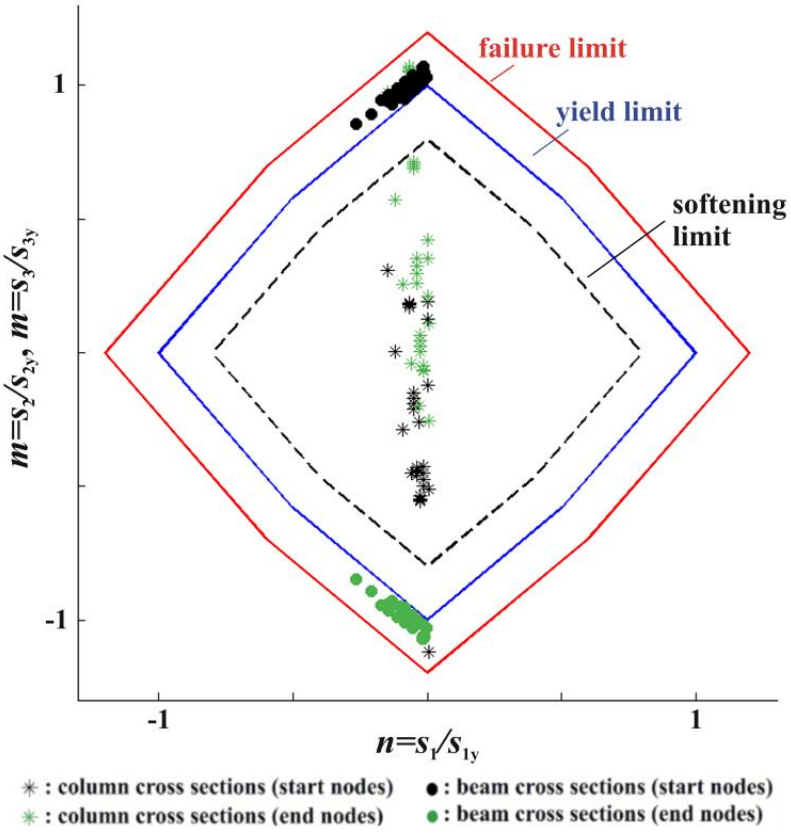

Fig 5.19: Interaction diagram of example #3 for case a_1.

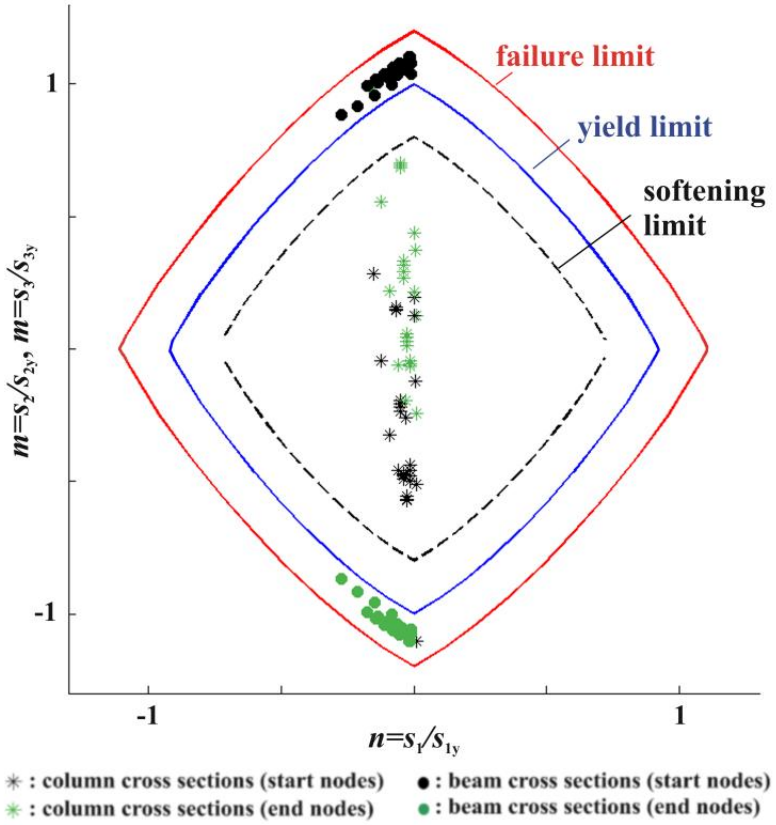

Fig 5.20: Interaction diagram of example #3 for case a_3.

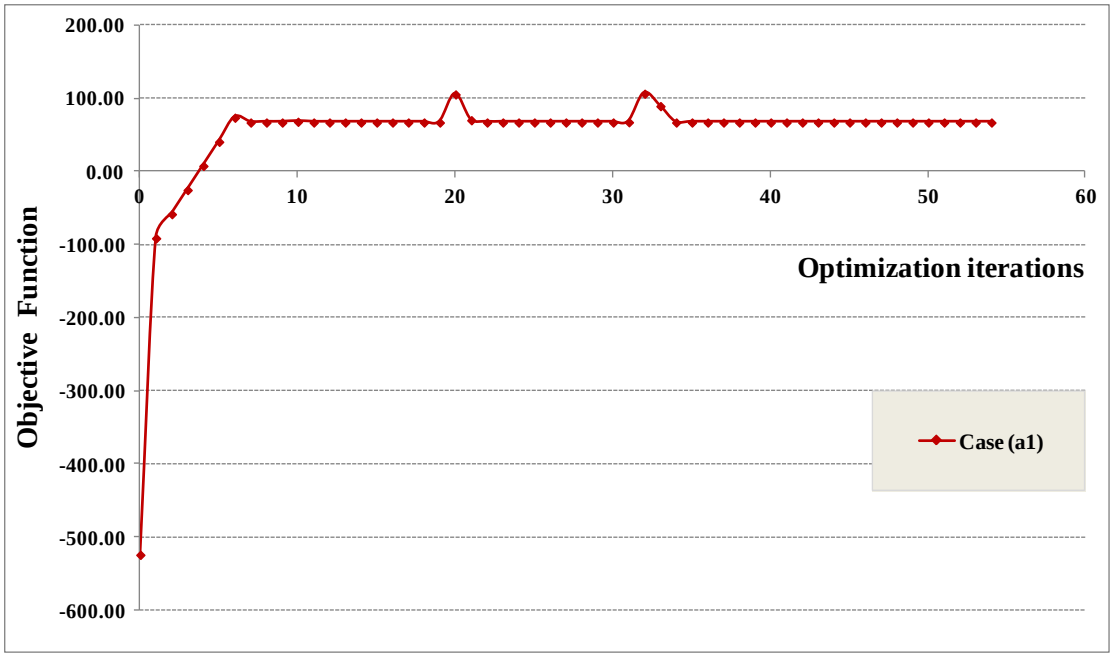

Fig. 5.21: Evolution of the optimization procedure of example #3 for case a_1.

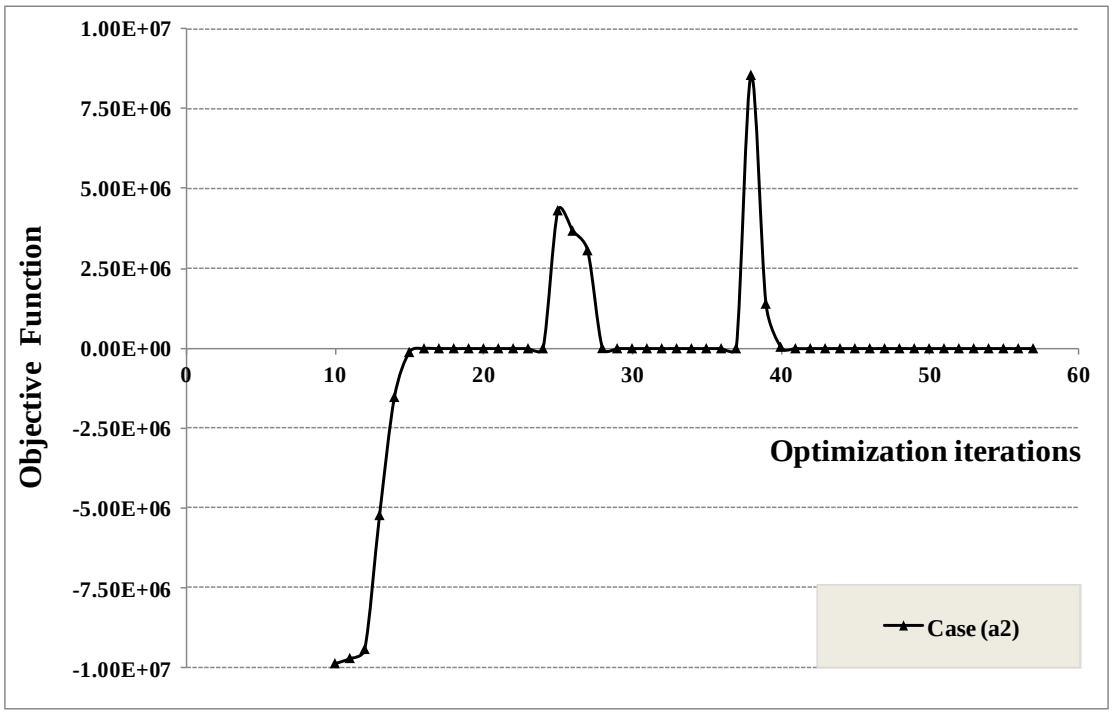

Fig. 5.22: Evolution of the optimization procedure of example #3 for case a_2.

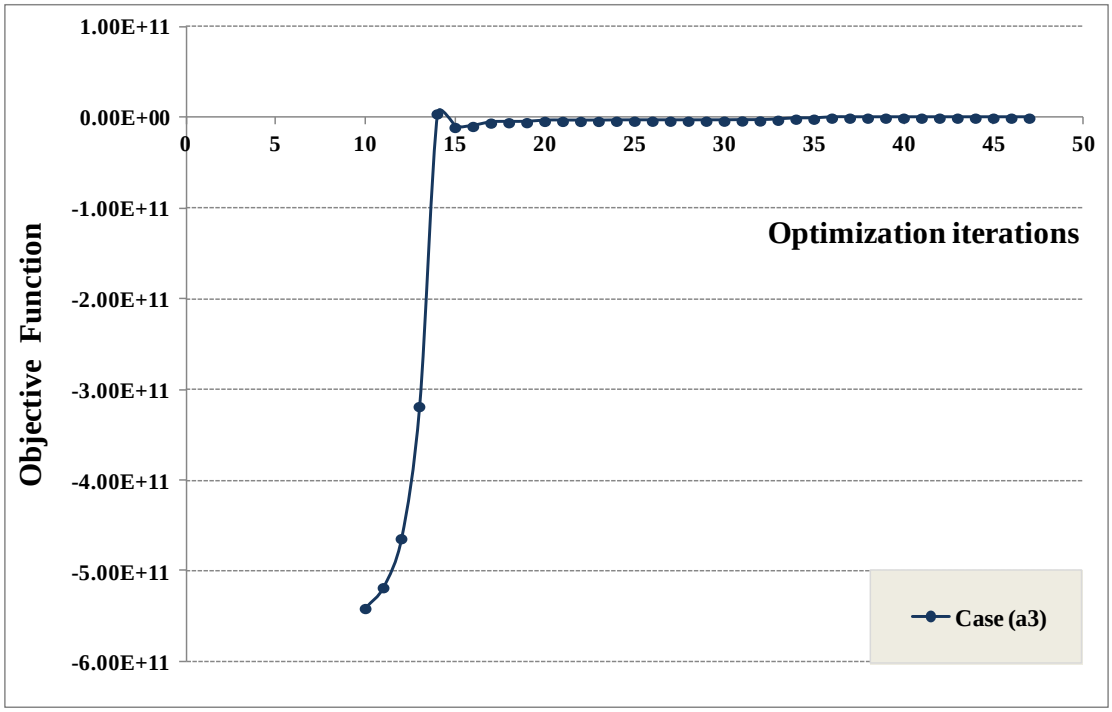

Fig. 5.23: Evolution of the optimization procedure of example #3 for case a_3.

The computational performance for cases (a_1), (a_2), (a_3) are presented in Fig. 5.21, 5.22 and 5.23 respectively, omitting initial iterations for demonstration purposes. For case (a_1) the convergence seems smoother, while for cases (a_2), (a_3) the objective

function attains values of higher order (due to the initial values of the parameter ρ) covering a great range until convergence. The sharp peaks that are presented are due to the penalized term of the complementarity condition in the objective function. The generated vector of variables $\boldsymbol{s}$ and $\mathbf{z}$ determine a dot product $\boldsymbol{w}^T\mathbf{z}$ that deviates slightly from zero, but this is magnified by the penalty parameter ρ affecting noticeably the value of the objective function.

5.4. Concluding remarks

Limit load and deformation analysis of plane frames under holonomic consideration is dealt as a nonlinear programming problem incorporating appropriately nonlinear interaction and constitutive laws. The proposed method constitutes an extension of cone identification procedure and is based on the local linearization of the yield surface, while constitutive laws are embedded retaining their nonlinearity. The whole formulation preserves the linear formulation of the yield condition and reduces its size to a minimum (compared to the standard formulation) of both yield and complementarity conditions. At each optimization iteration and for every cross section the targeted or activated yield hyperplane is determined by locally linearizing the yield surface. Nonlinear structural behavior is also incorporated without affecting the linearity or the size of yield condition. From the examples presented, the proposed formulation proved to be more time consuming and more sensitive to initial values and bounds of the unknown variables. Nevertheless, more accurate solutions compared to PWL method are provided avoiding the cumbersome procedure of the a priori linearization of the yield surface and constitutive laws.

Chapter 6

Limit Load and Deformation Analysis for 3D Frames

6.1. Introduction

In this chapter limit load and deformation analysis in the framework of mathematical programming is extended to 3D frame analysis. The ultimate load is evaluated through a nonlinear programming problem with equilibrium, compatibility, yield and complementarity constraints (section 4.7). Frames are considered to consist of n_{el} number of elements and n_f degrees of freedom. Equilibrium equations refer to the initial undeformed configuration and yield surface is either a priori or locally linearized. The nonlinear inelastic structural behavior is utilized either approximated with linear segments or in its nonlinear form. Furthermore, a holonomic (path-independent) structural behavior is assumed and hardening/softening behavior is considered isotropic (the yield surface expands/shrinks retaining its shape).

6.2. Equilibrium of 3D frames

For a double-symmetric 3D prismatic beam element, equilibrium is established with six equations that involves the twelve actions of the two element ends (Fig. 6.1).

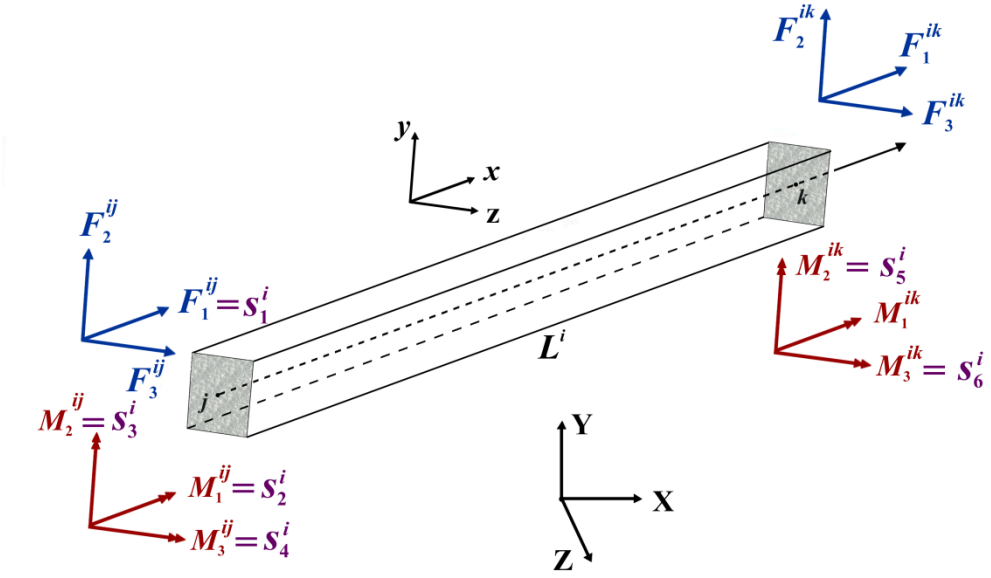

Fig. 6.1: Spatial beam element i with positive stress resultants-end actions.

Herein, the axial force $(F_1^{ij}=s_1^i)$, torsional moment at the start node j $(M_1^{ij}=s_2^i)$, bending moment along y-axis at the start node j $(M_2^{ij}=s_3^i)$, bending moment along z-axis at the start node j $(M_3^{ij}=s_4^i)$, bending moment along y-axis at the end node k

$(M_2^{ik} = s_5^i)$ and bending moment along z-axis at the end node k $(M_3^{ik} = s_6^i)$ are considered as independent stresses for member i. The twelve end actions of an element *i* are related to the six independent one at the local axis system as:

$$\begin{Bmatrix} F_1^{ij} \\ F_2^{ij} \\ F_3^{ij} \\ M_1^{ij} \\ M_2^{ij} \\ M_3^{ij} \\ F_1^{ik} \\ F_2^{ik} \\ F_3^{ik} \\ M_1^{ik} \\ M_2^{ik} \\ M_3^{ik} \end{Bmatrix} = \begin{bmatrix} 1 & 0 & 0 & 0 & 0 & 0 \\ 0 & 0 & 0 & 1/L^i & 0 & 1/L^i \\ 0 & 0 & -1/L^i & 0 & -1/L^i & 0 \\ 0 & 1 & 0 & 0 & 0 & 0 \\ 0 & 0 & 1 & 0 & 0 & 0 \\ 0 & 0 & 0 & 1 & 0 & 0 \\ -1 & 0 & 0 & 0 & 0 & 0 \\ 0 & 0 & 0 & -1/L^i & 0 & -1/L^i \\ 0 & 0 & 1/L^i & 0 & 1/L^i & 0 \\ 0 & -1 & 0 & 0 & 0 & 0 \\ 0 & 0 & 0 & 0 & 1 & 0 \\ 0 & 0 & 0 & 0 & 0 & 1 \end{bmatrix} \cdot \begin{Bmatrix} s_1^i \\ s_2^i \\ s_3^i \\ s_4^i \\ s_5^i \\ s_6^i \end{Bmatrix} = \boldsymbol{E}^i \cdot \boldsymbol{s}^i \qquad (6.1)$$

where $\boldsymbol{E}^i$ is the (*12×6*) local equilibrium matrix of the element and $\boldsymbol{s}^i$ is the (*6×1*) vector of the independent stresses. The local equilibrium matrix $\boldsymbol{E}^i$ is multiplied by the (*12×12*) transpose transformation matrix $\boldsymbol{R}^{iT}$ to express equilibrium at the global axis system. Thus the equilibrium matrix of the element is given as:

$$\boldsymbol{B}^i = \boldsymbol{R}^{iT} \cdot \boldsymbol{E}^i \qquad (6.2)$$

Thus the equilibrium for the whole structure can be expressed as:

$$\boldsymbol{B} \cdot \boldsymbol{s} - a \cdot \boldsymbol{f} = \boldsymbol{f}_d \qquad (6.3)$$

where $\boldsymbol{B}$ is the ($12n_{el} \times 6n_{el}$) equilibrium matrix of the structure, $\boldsymbol{s}$ is the ($6n_{el} \times 1$) vector of independent stresses of all elements, a is a scalar load factor, $\boldsymbol{f}$ is the ($n_f \times 1$) vector of nodal loading in the global system and $\boldsymbol{f}_d$ is the ($n_f \times 1$) vector of fixed nodal loading in the global system.

6.3. Compatibility condition

Compatibility of member deformations and nodal displacements are established with relation:

$$\boldsymbol{q} = \boldsymbol{B}^T \cdot \boldsymbol{u} \tag{6.4}$$

where $\boldsymbol{q}$ is the $(6n_{el}\times 1)$ vector of deformations of all members and $\boldsymbol{u}$ the $(6n_{el}\times 1)$ vector of the corresponding nodal displacements (Fig. 6.2). Notice that for the axial deformation the displacements of both ends are engaged, whereas for the rotation of the chord at each end the displacements of both ends and the rotations of the respective end are engaged.

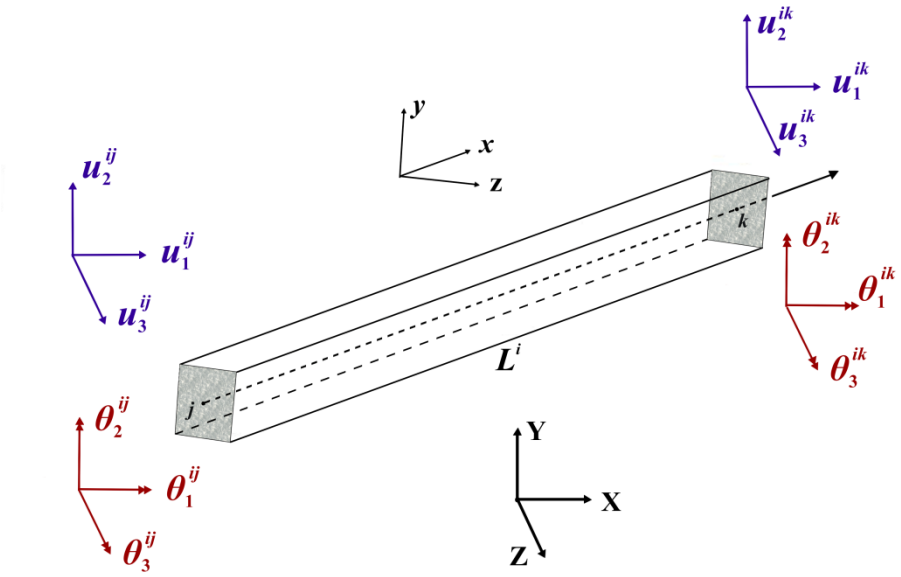

Fig. 6.2: Spatial beam element with nodal displacements and rotations.

6.4. Constitutive relations

Deformations are composed by elastic and plastic part as:

$$\boldsymbol{q} = \boldsymbol{e} + \boldsymbol{p} \tag{6.5}$$

where $\boldsymbol{e}$ and $\boldsymbol{p}$ are the $(6n_{el}\times 1)$ vectors of elastic and plastic deformations of all members respectively. The elastic part is described by the relation:

$$\boldsymbol{s} = \boldsymbol{S} \cdot \boldsymbol{e} \tag{6.6}$$

where $\boldsymbol{S}$ is the ($6n_{el} \times 6n_{el}$) assembled block diagonal matrix of all element stiffness matrices $\boldsymbol{S}^i$. For an element i the stiffness matrix is given as:

$$\boldsymbol{S}^i = \begin{bmatrix} EA^i / L^i & 0 & 0 & 0 & 0 & 0 \\ 0 & GI_t^i / L^i & 0 & 0 & 0 & 0 \\ 0 & 0 & 4EI_y^i / L^i & 0 & 2EI_y^i / L^i & 0 \\ 0 & 0 & 0 & 4EI_z^i / L^i & 0 & 2EI_z^i / L^i \\ 0 & 0 & 2EI_y^i / L^i & 0 & 4EI_y^i / L^i & 0 \\ 0 & 0 & 0 & 2EI_z^i / L^i & 0 & 4EI_z^i / L^i \end{bmatrix} \tag{6.7}$$

where E is the modulus of elasticity, A^i is the area of the element cross section , L^i is the element length, G is the shear modulus, I_t^i is the torsional moment of inertia of the element, I_y^i is the moment of inertia of the element with respect to local y-axis, I_z^i is the moment of inertia of the element with respect to local z-axis. Plastic deformations of the structure, that are considered perpendicular to the yield surface, are given as:

$$\boldsymbol{p} = \boldsymbol{N} \cdot \mathbf{z} \tag{6.8}$$

where $\boldsymbol{N}$ is the ($6n_{el} \times 2n_{el}$) matrix containing the scaled normal vectors of the identified yield hyperplanes and $\mathbf{z}$ is the ($2n_{el} \times 1$) vector of the plastic multipliers. The compatibility relation for the whole structure is formed as:

$$\boldsymbol{S}^{-1} \cdot \boldsymbol{s} + \boldsymbol{N} \cdot \mathbf{z} - \boldsymbol{B}^T \cdot \boldsymbol{u} = \mathbf{0} \tag{6.9}$$

where the terms result from the combination of equations (6.4), (6.5), (6.6) and (6.8).

6.5. Yield condition

6.5.1. Formulation of yield condition

Yield surfaces involving the interaction of stresses are generally nonlinear. However, they are approximated with linear segments or -for the general case- with hyperplanes enforcing their linear expression, which is computational advantageous. In general, considering the interaction of d number of stress resultants (d-component interaction) and the yield surface of dimension d is approximated with h hyperplanes, yield condition for 3D frames may be formulated following four different schemes:

1. *Hyperplane equations formulation*

   According to this formulation, yield condition for every cross section is expressed mathematically as the subtraction of the length of two vectors, i.e. the vector of the stress state and the vector of the yield limit. This presupposes that the vectors are expressed along the same direction, which is that of the appropriately scaled normal vector of every yield hyperplane. For the whole structure, yield condition is formed in terms of stresses $\boldsymbol{s}$ as:

$$\boldsymbol{w} = -\boldsymbol{N}^T \cdot \boldsymbol{s} + \boldsymbol{r} \geq \boldsymbol{0} \tag{6.10}$$

   where $\boldsymbol{w}$ is the $(2hn_{el} \times 1)$ vector of all strength reserves, $\boldsymbol{N}$ is the $(6n_{el} \times 2hn_{el})$ matrix of all scaled -with respect to yield capacities of stresses- normal vectors and $\boldsymbol{r}$ is the $(2hn_{el} \times 1)$ vector that includes the yield limits of all yield hyperplanes. Notice that this formulation involves all the yield hyperplanes that approximate the yield surface increasing considerably the number of yield constraints per critical section.

2. *Convex hull formulation*

   The yield polytope can be expressed as the convex hull of its n_v fixed vertices (section 3.3.2.2). Under this concept, yield condition is formulated as a set of equality constraints, the number of which depends on the dimensionality of interaction and thus independent of the number of the yield hyperplanes. For this consideration, yield condition for a 3D structure is expressed as:

$$\boldsymbol{s}_d - \boldsymbol{C} \cdot \boldsymbol{\theta} = \boldsymbol{0}, \;\; \boldsymbol{I}_{eq} \cdot \boldsymbol{\theta} = \boldsymbol{1} \;, \;\; \boldsymbol{\theta} \geq \boldsymbol{0} \tag{6.11}$$

where $\boldsymbol{s}_d$ is the $(2dn_{el} \times 1)$ vector of the normalized stresses for all elements, $\boldsymbol{C}$ is the $(2dn_{el} \times 2n_v n_{el})$ matrix containing the coordinates of the vertices of all yield hyperplanes for all elements, $\boldsymbol{\theta}$ is the $(2n_v n_{el} \times 1)$ vector including the coefficients θ_i for all vectors of the vertices n_v for all the elements and $\boldsymbol{I}_{eq}$ is the $(2n_{el} \times 2n_v n_{el})$ matrix that sums the corresponding θ_i at every element end.

3. *Cone identification approach*

   Cone identification approach (section 4.3) depends on the notion that only one yield hyperplane is targeted or activated for every cross section. Thus, it is unnecessary to compare the stress vector with all possible yield limits; it is sufficient to form the yield condition only for one critical hyperplane per cross section. This is achieved following an identification process that specifies the cone in which the stress vector resides and then yield condition is formed only for the identified hyperplane. The mathematical expression of yield condition for the whole structure is that of equation (6.4), including, though, matrices of smaller size, i.e. $\boldsymbol{w}$ is the $(2n_{el} \times 1)$ vector of all strength reserves, $\boldsymbol{N}$ is the $(6n_{el} \times 2n_{el})$ matrix of all scaled -with respect to yield capacities of stresses- normal vectors of the identified yield hyperplanes and $\boldsymbol{r}$ is the $(2n_{el} \times 1)$ vector that includes the yield limits of all identified yield hyperplanes.

4. *Local linearization technique*

   This approach is based on the local linearization of the yield surface for every cross section and constitutes an extension of cone identification approach (section 5.2.1). The yield surface is not a priori linearized and thus the yield hyperplane is not a priori defined, but is determined at each optimization iteration for every stress point. The mathematical expression of yield condition for this approach is the same with that of cone identification formulation, including matrices with the same dimensions.

It is noted that the last two formulations of yield condition may be adopted for the case of structural analysis formulated as a NLP problem.

6.5.2. Incorporation of hardening/softening behavior

The structural behavior is considered linearized or nonlinear and it is incorporated in the expression of yield condition by using extended or shrunk yield limits $\boldsymbol{r'}$ (instead of the initial $\boldsymbol{r}$). In the general case, any of the presented approaches of the yield condition can be combined with any considerations of hardening/softening behavior. However, the two last approaches of yield condition result in a formulation of a minimum size and thus can incorporate more efficiently any consideration of structural behavior. The specific considerations of hardening/ softening behavior are:

1. *Multi-linear hardening/softening behavior*

   For this case, the critical segment of the structural behavior is identified for every yielded cross section based on the value of its plastic rotation (section 4.3.3). The extended/shrunk yield limits for all cross sections are given as:

$$\boldsymbol{r'} = \boldsymbol{r} + \boldsymbol{H} \cdot \mathbf{z} + \boldsymbol{c} \tag{6.12}$$

   where $\boldsymbol{H}$ is the hardening diagonal matrix with dimensions ($2n_{el} \times 2n_{el}$), $\mathbf{z}$ is the ($2n_{el} \times 1$) vector of all plastic multipliers and $\boldsymbol{c}$ is the ($2n_{el} \times 1$) vector, which in a recursive form accumulates all previous plastic behavior. For the case that a cross section remains elastic, equation (6.6) degenerates to $\boldsymbol{r'}=\boldsymbol{r}$.

2. *Nonlinear hardening/softening behavior*

   Structural behavior may be also incorporated retaining its nonlinearity (section 5.2.2). The extended/shrunk yield limit for every yielded cross section is determined straightforward from the analytical expression of the nonlinear curve of the structural behavior, given the value of the abscissa.

6.6. Complementarity condition

Complementarity condition that excludes the simultaneous activation of yield condition with zero plastic deformation are necessary, when softening or/and ductility limitations are considered. The relation that expresses the complementarity condition for the whole structure is given as:

$$\boldsymbol{w}^T \cdot \mathbf{z} = \mathbf{0}, \quad \boldsymbol{w} \geq \mathbf{0}, \quad \mathbf{z} \geq \mathbf{0} \tag{6.13}$$

The size of the components of the above relation is reduced to a minimum by adopting either the cone identification or the local linearization technique for the expression of the yield condition.

6.7. Formulation of the optimization problem

The analysis of 3D frames in the context of mathematical programming is formulated as a LP or a NLP problem depending on the assumed structural behavior. For the case of rigid-perfectly plastic behavior or hardening behavior, the ultimate structural state is determined using the following formulations:

Hyperplane equations formulation	***Convex hull formulation***
$max. \quad \alpha$	$max. \quad \alpha$
$s.t. \quad \boldsymbol{B} \cdot \boldsymbol{s} - a \cdot \boldsymbol{f} = \boldsymbol{f}_d$	$s.t. \quad \boldsymbol{B} \cdot \boldsymbol{s} - a \cdot \boldsymbol{f} = \boldsymbol{f}_d$
$\boldsymbol{N}^T \cdot \boldsymbol{s} \leq \boldsymbol{r}$	$\boldsymbol{T} \cdot \boldsymbol{s} - \boldsymbol{C} \cdot \boldsymbol{\theta} = \mathbf{0}$
$\boldsymbol{s}: unrestricted, a \geq 0$	$\boldsymbol{I}_{eq} \cdot \boldsymbol{\theta} = 1$
	$\boldsymbol{s}: unrestricted, \boldsymbol{\theta} \geq \mathbf{0}, a \geq 0$

(6.14)

where the unknown variables for the first formulation are the stresses $\boldsymbol{s}$ and the load factor a, while for convex hull formulation the nonnegative parameters $\boldsymbol{\theta}$ are added. For the case of softening behavior or/and limited ductility, the formulation of the problem is as follows:

$$\left.\begin{array}{ll} max. & a \\ s.t. & \boldsymbol{B} \cdot \boldsymbol{s} - a \cdot \boldsymbol{f} = \boldsymbol{f}_d \\ & \boldsymbol{S}^{-1} \cdot \boldsymbol{s} - \boldsymbol{B}^T \cdot \boldsymbol{u} + \boldsymbol{N} \cdot \mathbf{z} = \mathbf{0} \\ & \boldsymbol{w} = -\boldsymbol{N}^T \cdot \boldsymbol{s} + \boldsymbol{r}' \geq \mathbf{0} \\ & \boldsymbol{w}^T \cdot \mathbf{z} = \mathbf{0} \\ & \mathbf{0} \leq \mathbf{z} \leq \mathbf{z}_u \\ & \boldsymbol{u}_l \leq \boldsymbol{u} \leq \boldsymbol{u}_u \end{array}\right\} \Rightarrow \begin{array}{ll} max. & a - \rho \cdot \boldsymbol{w}^T \cdot \mathbf{z} \\ s.t. & \boldsymbol{B} \cdot \boldsymbol{s} - a \cdot \boldsymbol{f} = \boldsymbol{f}_d \\ & \boldsymbol{S}^{-1} \cdot \boldsymbol{s} - \boldsymbol{B}^T \cdot \boldsymbol{u} + \boldsymbol{N} \cdot \mathbf{z} = \mathbf{0} \\ & \boldsymbol{w} = -\boldsymbol{N}^T \cdot \boldsymbol{s} + \boldsymbol{r}' \geq \mathbf{0} \\ & \mathbf{0} \leq \mathbf{z} \leq \mathbf{z}_u \\ & \boldsymbol{u}_l \leq \boldsymbol{u} \leq \boldsymbol{u}_u \end{array} \tag{6.15}$$

The vector of the unknown variables for the above NLP problem contains the stresses $\boldsymbol{s}$, the displacements $\boldsymbol{u}$, the plastic multipliers $\mathbf{z}$ and the load factor a. The formulation

of the problem may incorporate the cone identification approach or the local linearization of the yield surface and multi-linear or nonlinear structural behavior. It is noted that the optimization problem is parameter dependent and the proper choice of the initial values of variable, as well as the lower and upper bounds may be decisive in achieving the desired convergence.

6.8. Numerical examples

Limit load and deformation analysis is implemented as a NL programming problem in Matlab code using *fmincon* solver (appropriate for the minimization of constrained nonlinear multivariable function), with the interior-point algorithm selected as optimization method.

The aim is to verify the applicability of the introduced approaches in 3D frames and validate their efficiency for axial force-biaxial bending moment (NM_yM_z) interaction for the following cases:

- Case (a): PWL yield condition and rigid-perfectly plastic behavior.
- Case (b): PWL yield condition and constitutive laws - Cone identification procedure.
- Case (c): Nonlinear yield condition and multi-linear constitutive laws.
- Case (d): Nonlinear yield condition and constitutive laws.

For this purpose, two 3D steel frames are examined for the aforementioned cases and the corresponding results are presented below. The generalized Gendy-Saleeb yield criterion is adopted for axial force-biaxial bending moment interaction (NM_yM_z):

$$\Phi = n^2 + \frac{1}{\lambda_y} \cdot m_y^2 + \frac{1}{\lambda_z} \cdot m_z^2 - 1 \tag{6.16}$$

where parameters λ_y and λ_z are shape dependent. For rectangular cross sections they assume the following form:

$$\lambda_y = \lambda_z = 1 - n^2 \tag{6.17}$$

while for I-beams the corresponding expressions are:

$$\lambda_y = 1 - |n|, \ \lambda_z = 1 - 1.1|n| \tag{6.18}$$

The aforementioned yield criterion of equation (6.16) is represented by a 3D nonlinear surface that is approximated using 32 plane triangles, as shown in Fig. 6.3.

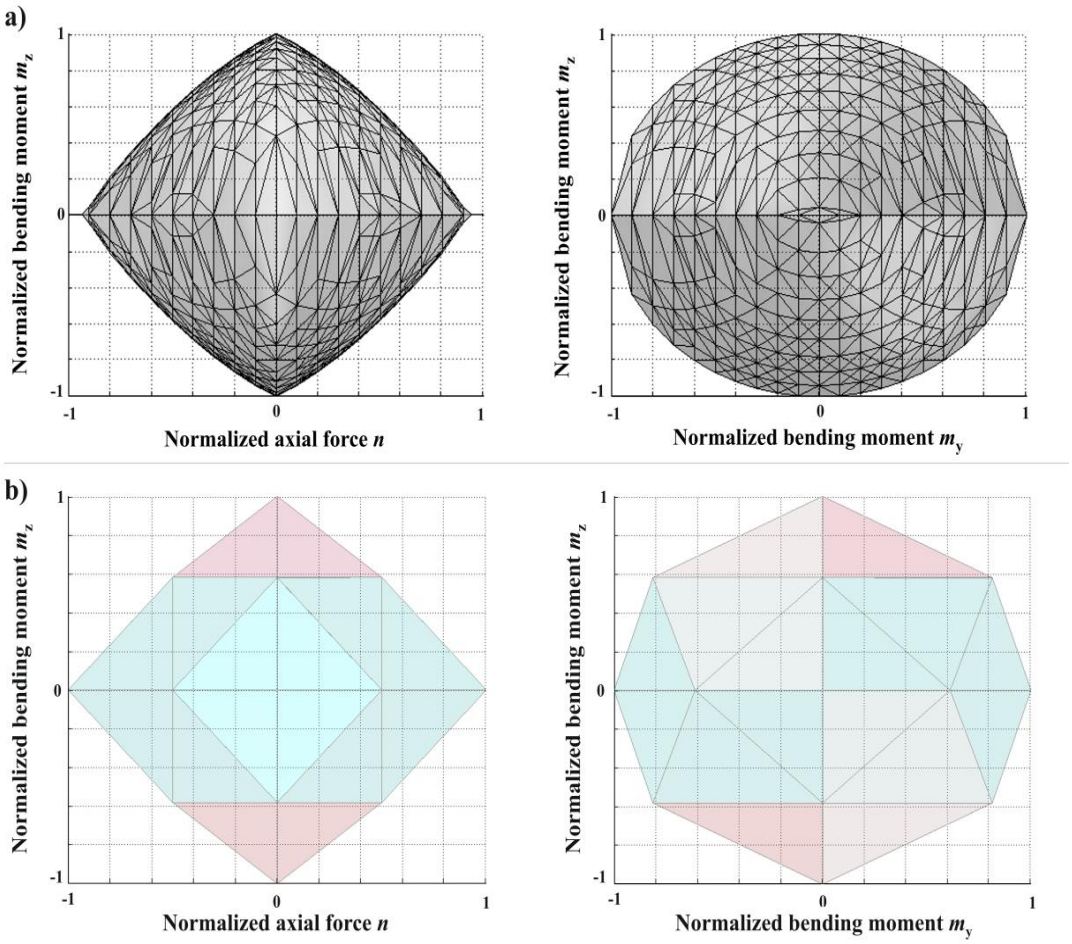

Fig. 6.3: a) Nonlinear and b) PWL yield surface.

6.8.1. Example #1

The first example concerns one simple 3D frame shown in Fig. 6.4 and serves demonstration purposes. It is subjected to increasing lateral and vertical loading and it is discretized into 8 elements, 8 nodes and 24 degrees of freedom. The steel grade is S235 with $E=2\times10^8$kN/m^2. Sections with $A=53.81\times10^{-4}m^2$, $I=8356\times10^{-8}m^4$ (strong axis), $I=603.8\times10^{-8}m^4$ (weak axis), $I=20.12\times10^{-8}m^4$ (torsional), $s_{1y}=1264.54$ *kN*, $s_{2y}=65.33$ *kNm*, $s_{3y}=s_{5y}=29.42$ *kNm*, $s_{4y}=s_{6y}=147.67$ *kNm* and sections with

$A=16.43\times10^{-4}\ m^2$, $I=5412\times10^{-8}\ m^4$ (strong axis), $I=44.92\times10^{-8}\ m^4$ (weak axis), $I=2.45\times10^{-8}m^4$ (torsional), $s_{1y}=386.1\ kN$, $s_{2y}=9.57\ kNm$, $s_{3y}=s_{5y}=4.52\ kNm$, $s_{4y}=s_{6y}=20.76\ kNm$ are employed for all columns and beams respectively. The assumed multi-linear and the corresponding nonlinear hardening/softening behavior is shown in Fig. 5.5. More specifically, for columns $h_1=2953.4\ kNm\ z_1=0.005\ \lambda_1=1.1$, $h_2=1476.7\ kNm\ z_2=0.015\ \lambda_2=1.2$, $h_3=-1687.7\ kNm\ z_3=0.05\ \lambda_3=0.8$, $h_4=10^{-6}\ kNm\ z_4=0.06\ \lambda_4=0.8$, while for beam cross sections $h_1=415.2\ kNm\ z_1=0.005\ \lambda_1=1.1$, $h_2=207.6\ kNm\ z_2=0.015\ \lambda_2=1.2$, $h_3=-237.26\ kNm\ z_3=0.05\ \lambda_3=0.8$, $h_4=10^{-6}\ kNm\ z_4=0.06\ \lambda_4=0.80$, concerning the multi-linear behavior (Fig. 6.5a). The nonlinear structural behavior is described by a 4th degree polynomial line (Fig. 6.5b) based on data presented in Table 6.1. The values of z_4 constitute the upper bounds for column and beam cross sections respectively. The upper bound vector of all displacements is $u_u=1$ and the lower bound vector $u_l=-1$. An updating rule of $\rho=10\rho$ is used until convergence with a tolerance of $w^T z\le10^{-4}$ is reached.

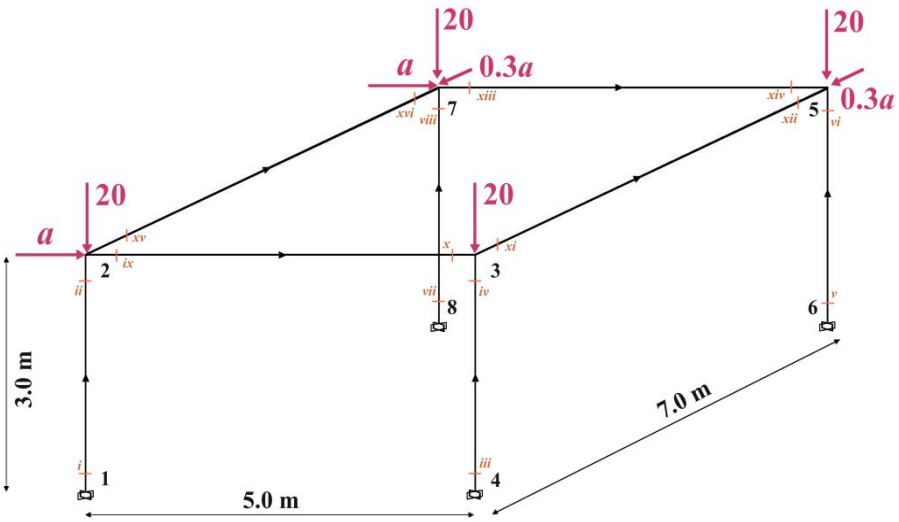

Fig. 6.4: Example #1.

Table 6.1: Polynomial line of structural behavior.

x	0.00	0.0005	0.001	0.002	0.005	0.01	0.012	0.030	0.04	0.06
f(x)	1.00	1.02	1.04	1.05	1.10	1.12	1.15	1.15	1.00	0.80
Polynomial Line	$f(x)=p_1x^4+p_2x^3+p_3x^2+p_4x+p_5$ $p_1=2.256\cdot10^5,\ p_2=-1.997\cdot10^4,\ p_3=116.9,\ p_4=12.52,\ p_5=1.017$									

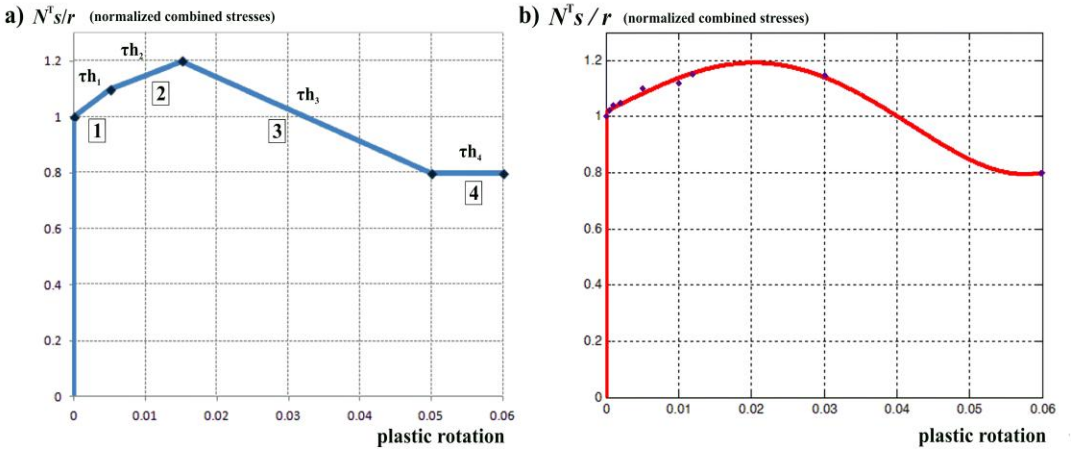

Fig. 6.5: a) Multi-linear and b) nonlinear hardening/softening structural behavior.

Table 6.2. Analysis results for all cases for example #1.

Cases	NMyMz rigid-p.plastic (a)	NMyMz PWL (b)	NMyMz NL-PWL (c)	NMyMz NL (d)
number of variables n_{var}	**49**	**89**		
number of equality constraints n_{eq}	**24**	**72**		
number of inequality constraints n_{inq}	**512**	**16**		
maximum load factor a (kN)	**78.52**	**90.14**	**101.75**	**102.28**
number of plastic hinges	**12**	**12**	**12**	**12**
total computational time (s)	**8.69**	**73.18**	**186.06**	**37.3**
number of iterations	**—**	**90**	**189**	**45**
complementarity condition $w^T z$	**—**	**5.00E-06**	**2.56E-11**	**6.03E-04**
initial values of ρ	**—**	**100**	**10^4**	**10^6**

All analysis results are shown in Table 6.2. Rigid-perfectly plastic behavior (case a) corresponds to a LP problem including only equilibrium and yield conditions. And yields the smallest maximum load factor a in the shortest computational time. For

hardening/softening behavior it is observed that the number of variables and constraints is the same regardless of the linearity or nonlinearity of the structural behavior and of the a priori or local linearization of the yield surface. Comparing cases (b) and (c) that correspond to the same multi-linear structural behavior, it is observed that the local linearization approach yields greater value of maximum load factor since the nonlinearity of the yield surface is retained. Number of plastic hinges and collapse mechanisms are identical for both cases. Comparing cases (c) and (d) that correspond to local linearization of the nonlinear yield surface, the maximum load factor is slightly greater for the case of nonlinear structural behavior presenting the same ultimate state.

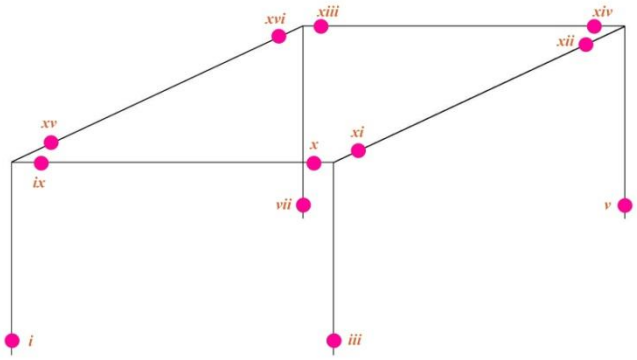

Fig. 6.6: Plastic hinge formation for case (a).

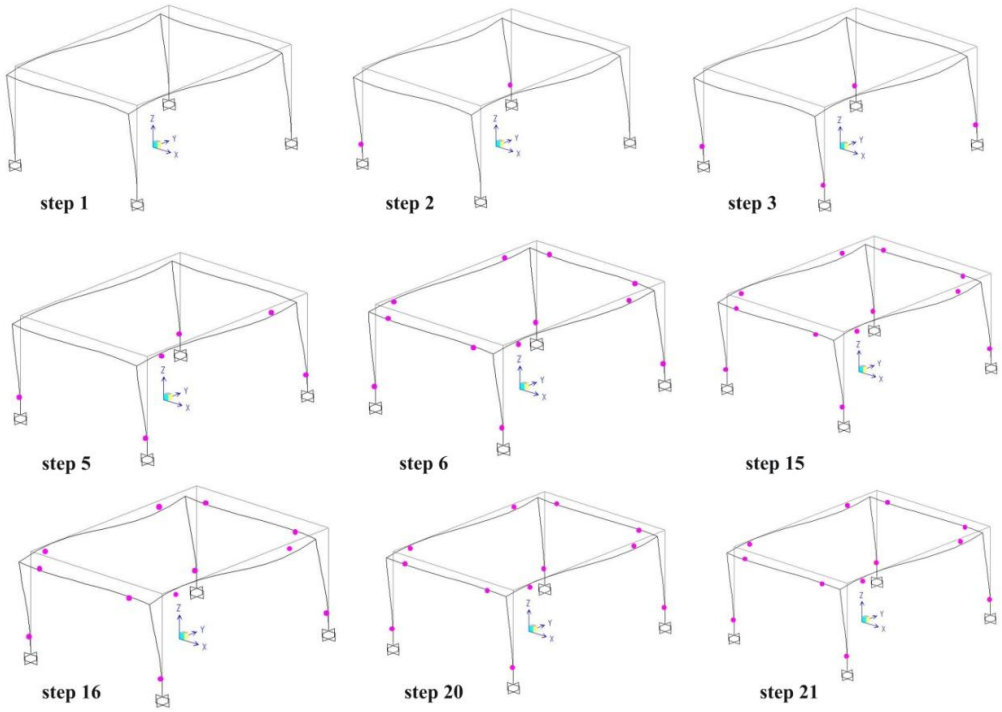

Fig. 6.7: Plastic hinge formation with step-by-step analysis for case (a).

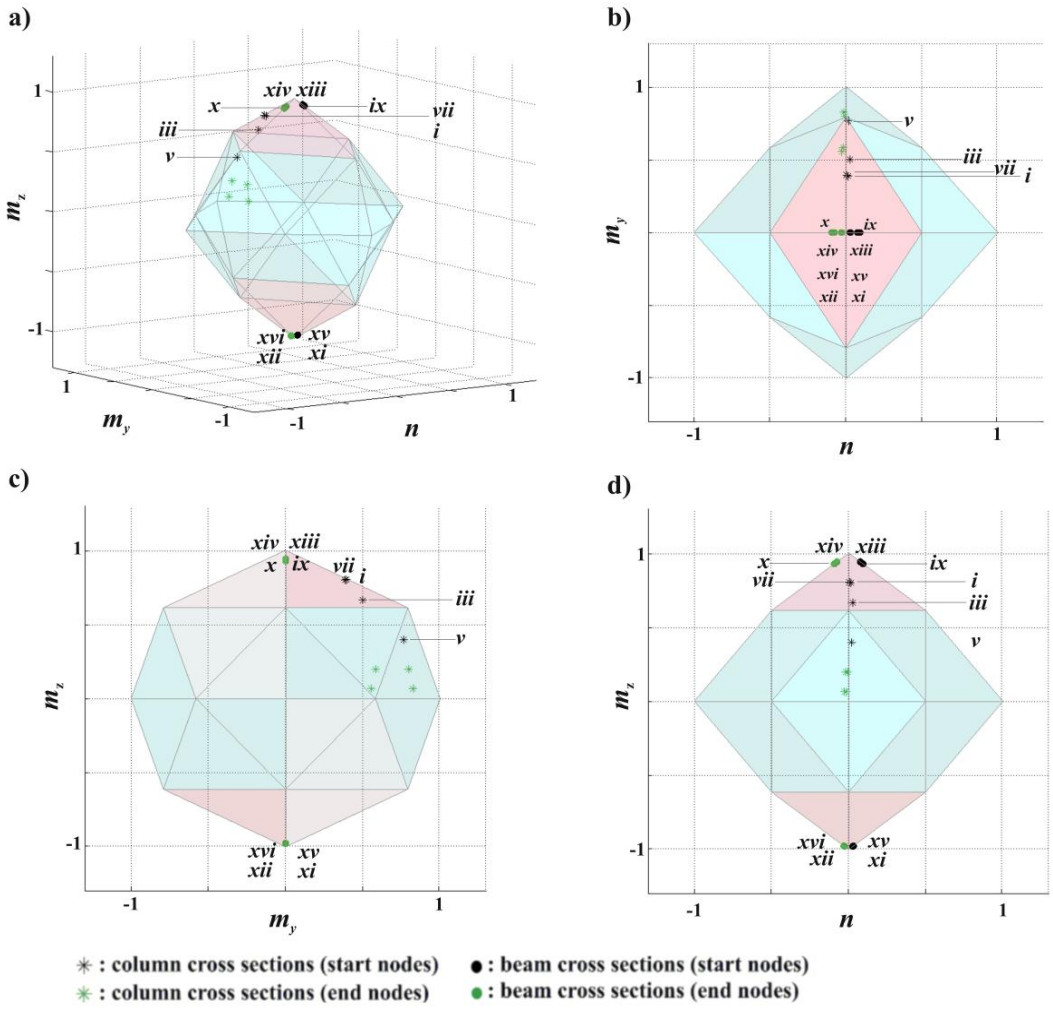

Fig. 6.8: Interaction diagram for case (a).

More specifically, the plastic hinge formation for rigid-perfectly plastic behavior (case a) is shown in Fig. 6.6. The results are verified by a step-by-step analysis using SAP2000 version 14, as shown in Fig. 6.7. The corresponding interaction diagram is presented in Fig. 6.8 designating the formatted plastic hinges with the number of the corresponding cross section. The role of bending moment along local z axis (strong axis) is dominant, the effect of bending moment along y axis is evident at column cross sections and the slight effect of axial force is presented mainly in beam cross sections.

The ultimate state for case (b) is shown in Fig. 6.9. Each plastic hinge is accompanied by a number indicating the corresponding hardening/softening segment. Plastic hinges at column bases lie on the second hardening segment presenting greater deformations compared to yielded beam cross sections. Results are verified using SAP2000 version 14 and the sequence of plastic hinge formation for step-by-step

analysis is shown in Fig. 6.10. The ultimate carrying load capacities in terms of base shear force are practically identical for both types of analysis, i.e. 180.18kN for step-by-step analysis and 180.27kN for limit load and deformation analysis with mathematical programming. The corresponding interaction diagram is presented in Fig. 6.11. Beam cross sections are stressed under the combined effect of bending moment (along the strong axis) and axial force, while the biaxial bending moment effect is evident at column cross sections.

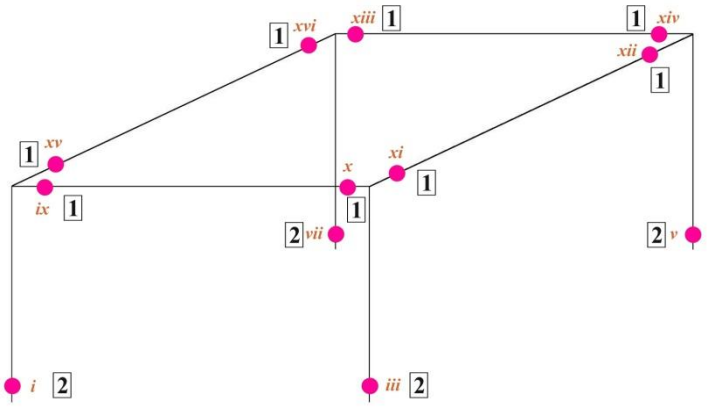

Fig. 6.9: Plastic hinge formation for case (b).

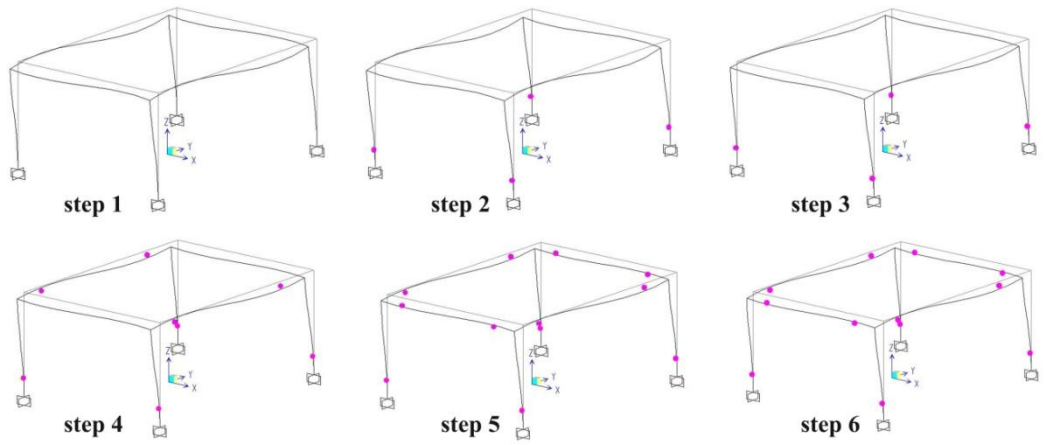

Fig. 6.10: Plastic hinge formation with step-by-step analysis for case (b).

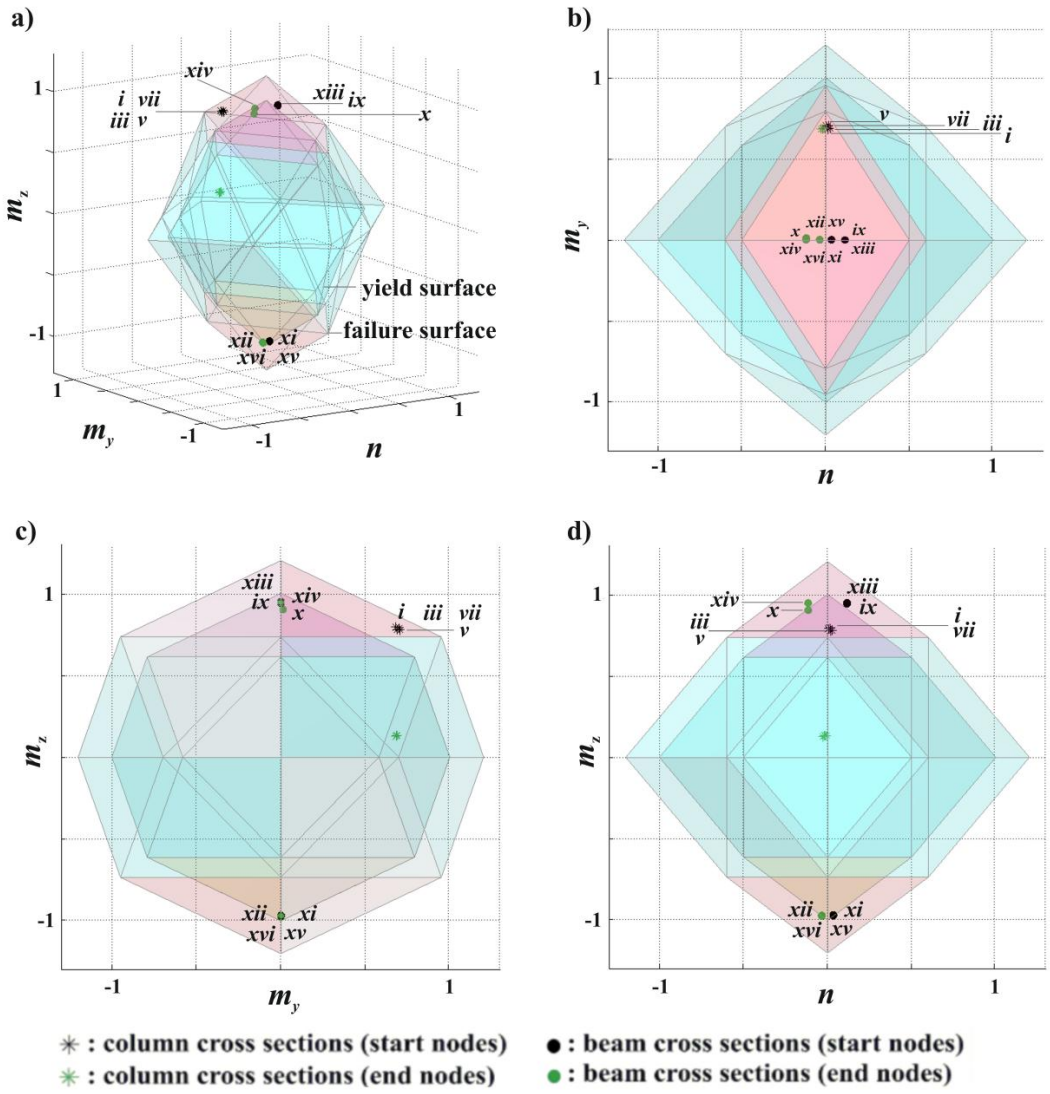

Fig. 6.11: Interaction diagram for case (b).

The plastic hinge pattern of the ultimate state for case (c) is shown in Fig. 6.12. The roman numbers designate the corresponding hardening/softening segment of each plastic hinge. The number and disposition of plastic hinges is the same as that of case (b). However, beam cross sections are more heavily stressed presenting deformations that correspond to the second (hardening) and the third (softening) segment. This is due to the local linearization of the yield surface allowing for greater and more accurate solutions. The corresponding interaction diagram is presented in Fig. 6.13. Bending moment along the strong axis is dominant, while the slight effect of axial force is evident at beam cross sections. Column cross sections are stressed under the biaxial bending moment effect with almost absent the role of axial force.

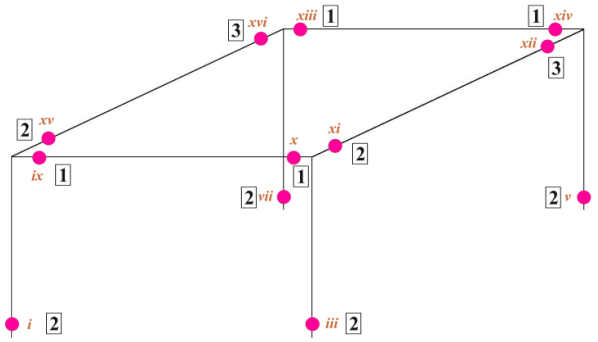

Fig. 6.12: Plastic hinge formation for case (c).

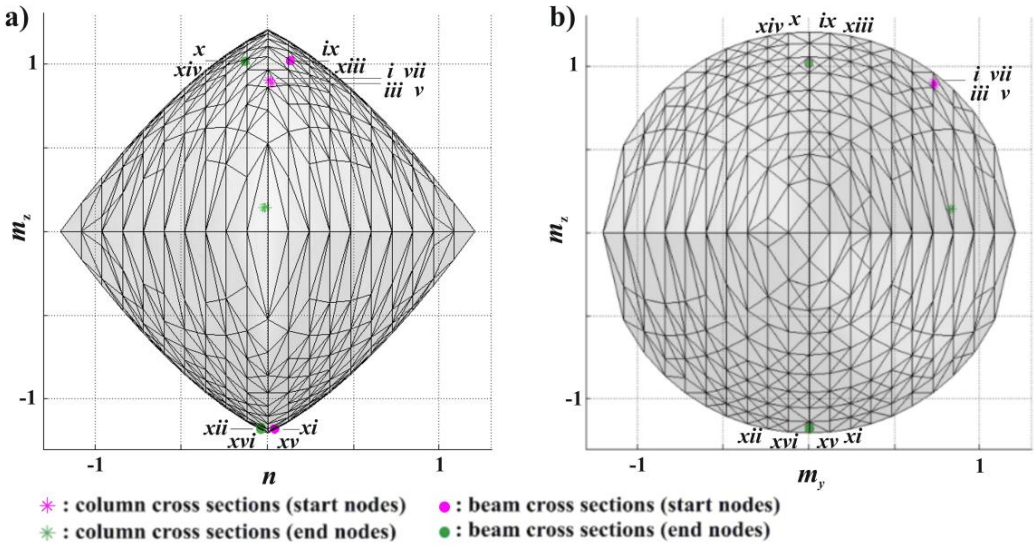

Fig. 6.13: Interaction diagram for case (c).

In Fig. 6.14 the ultimate state for case (d) is depicted, corresponding to a similar plastic hinge pattern to that of cases (b) and (c). The ultimate stress state of all cross sections is presented in Fig. 6.15. Beam cross sections are stressed under the combined effect of bending moment (along the strong axis) and axial force, while the biaxial bending moment effect is evident at column cross sections.

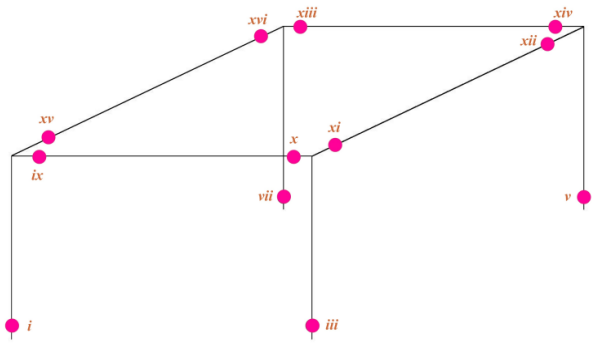

Fig. 6.14: Plastic hinge formation for case (d).

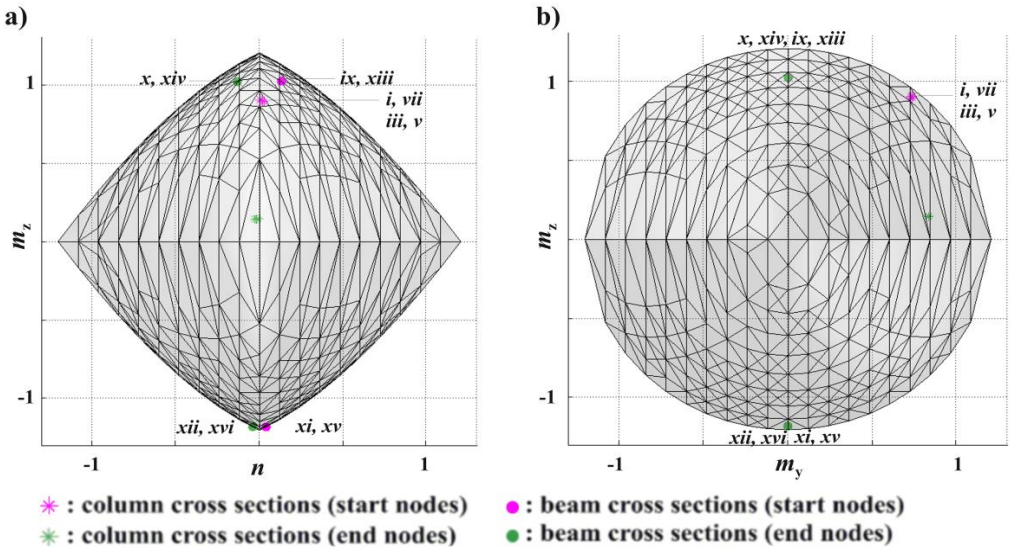

Fig. 6.15: Interaction diagram for case (d).

The computational performance for cases (b), (c) and (d) are presented in Fig. 6.16, 6.17 and 6.18, omitting initial iterations for demonstration purposes. Comparing cases (b) and (c) that concern the same structural behavior, it is observed that local linearization method requires more iterations (189 versus 90) and more computational time (186.06s versus 73.18s) until convergence. The sharp peaks that are presented for case (c) are due to the penalty parameter in the objective function that magnifies any divergence of the complementarity term. The computational performance of the algorithm requires 45 iterations and 37.3s for case (d) with the objective function attaining great values due to the penalty parameter.

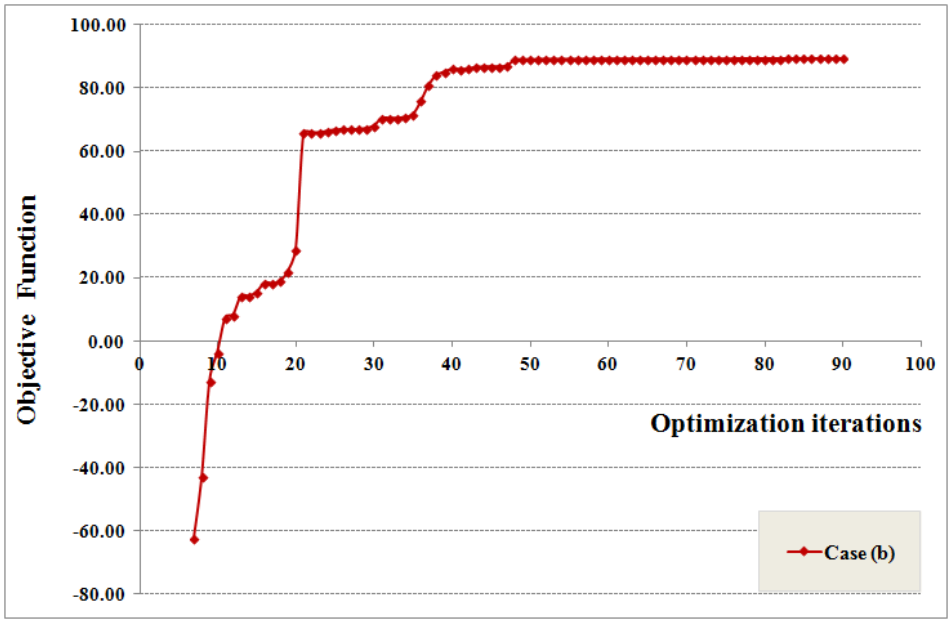

Fig. 6.16: Evolution of the optimization procedure of example #1 for case (b).

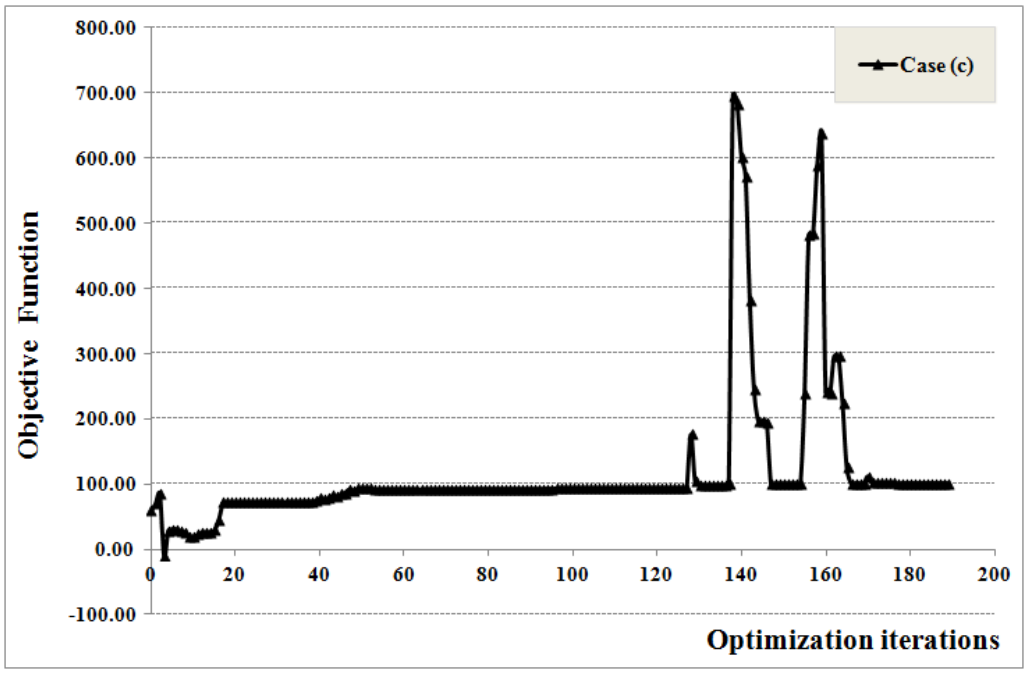

Fig. 6.17: Evolution of the optimization procedure of example #1 for case (c).

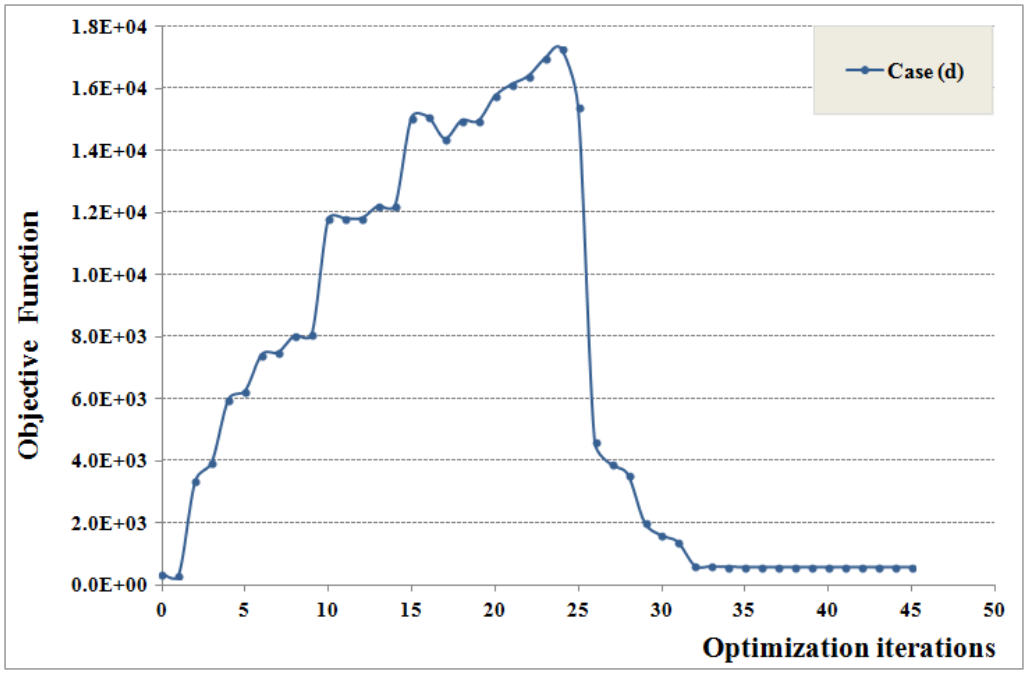

Fig. 6.18: Evolution of the optimization procedure of example #1 for case (d).

6.8.2. Example #2

The second example concerns the 3D frame shown in Fig. 6.19. It is subjected to increasing lateral loading along X axis, fixed lateral loading along Y axis and fixed vertical loading and it is discretized into 26 elements, 18 nodes and 72 degrees of freedom.

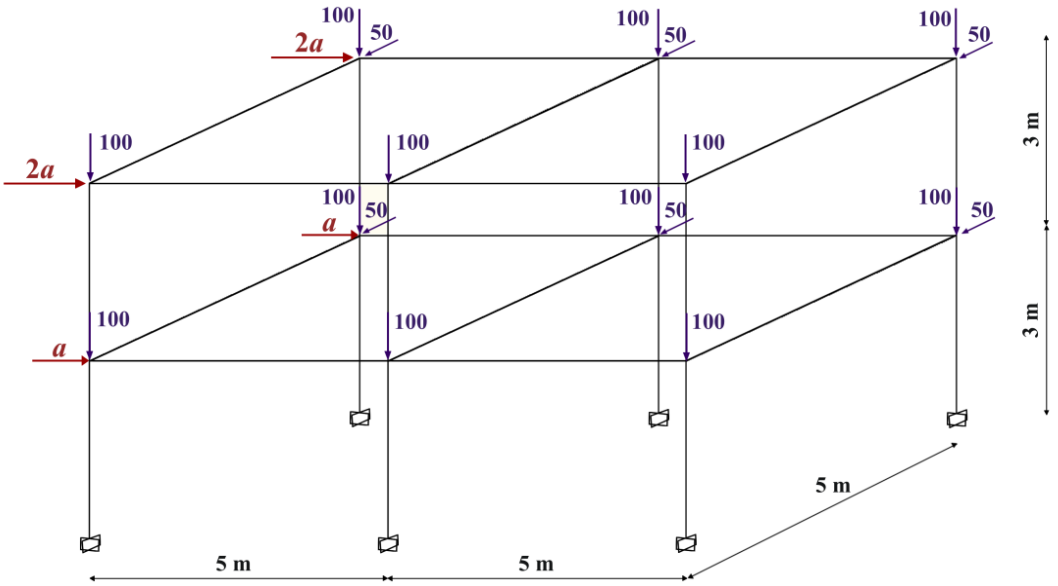

Fig. 6.19: Example #2.

The steel grade is S235 with $E=2\times10^8$kN/m^2. For all columns sections with $A=159\times10^{-4}m^2$, $I=45070\times10^{-8}m^4$ (strong axis), $I=8564\times10^{-8}m^4$ (weak axis), $I=189\times10^{-8}m^4$ (torsional), $s_{1y}=3736.5$ *kN*, $s_{2y}=301.6$ *kNm*, $s_{3y}=s_{5y}=205.1$ *kNm*, $s_{4y}=s_{6y}=602.1$*kNm* are used, while for all beams sections with $A=53.81\times10^{-4}m^2$, $I=8356\times10^{-8}m^4$ (strong axis), $I=603.8\times10^{-8}m^4$ (weak axis), $I=20.12\times10^{-8}m^4$ (torsional), $s_{1y}=1264.5$ *kN*, $s_{2y}=65.3$ *kNm*, $s_{3y}=s_{5y}=29.4$ *kNm*, $s_{4y}=s_{6y}=147.7$ *kNm*. The assumed multi-linear and the corresponding nonlinear hardening/softening behavior is shown in Fig. 6.20. More specifically, for columns $h_1=12041.4$ *kNm* $z_1=0.005$ $\lambda_1=1.1$, $h_2=6020.7$ *kNm* $z_2=0.015$ $\lambda_2=1.2$, $h_3=-6020.7$ *kNm* $z_3=0.05$ $\lambda_3=0.85$, $h_4=10^{-6}$ *kNm* $z_4=0.06$ $\lambda_4=0.85$, while for beam cross sections $h_1=1476.7$ *kNm* $z_1=0.005$ $\lambda_1=1.05$, $h_2=738.4$ *kNm* $z_2=0.015$ $\lambda_2=1.1$, $h_3=-1230.58$ *kNm* $z_3=0.05$ $\lambda_3=0.85$, $h_4=10^{-6}$ *kNm* $z_4=0.06$ $\lambda_4=0.85$, concerning the multi-linear behavior (Fig. 6.20a). The nonlinear structural behavior is described by a 4th degree polynomial line (Fig. 6.20b) based on data presented in Table 6.3. The values of z_4 constitute the upper bounds for column and beam cross sections respectively. The upper bound vector of all displacements is $u_u=10$ and the lower bound vector $u_l=-10$. For the penalty parameter ρ an updating rule of 10ρ is used until convergence is reached.

Table 6.3. Polynomial lines of structural behavior.

x	0.00	0.001	0.002	0.005	0.007	0.01	0.015	0.020	0.025	0.028	0.030	0.035	0.038	0.040	0.045	0.060
f(x)	1.00	1.05	1.10	1.15	1.18	1.20	1.18	1.15	1.12	1.10	1.05	1.02	1.00	0.95	0.90	0.85
Polynomial line for column cross sections								$f(x)=p_1\cdot x^4+p_2\cdot x^3+p_3\cdot x^2+p_4\cdot x+p_5$ $p_1=-1.83\cdot10^5, p_2=3.14\cdot10^4, p_3=-1817, p_4=32.54, p_5=1.02$								
x	0.00	0.0010	0.002	0.005	0.007	0.010	0.015	0.020	0.025	0.028	0.030	0.035	0.038	0.040	0.045	0.050
f(x)	1.00	1.00	1.008	1.05	1.08	1.10	1.08	1.05	1.03	1.008	0.96	0.94	0.92	0.87	0.825	0.80
Polynomial line for beam cross sections								$f(x)=p_1\cdot x^4+p_2\cdot x^3+p_3\cdot x^2+p_4\cdot x+p_5$ $p_1=-1.39\cdot10^4, p_2=1.02\cdot10^4, p_3=-901.3, p_4=17.84, p_5=0.99$								

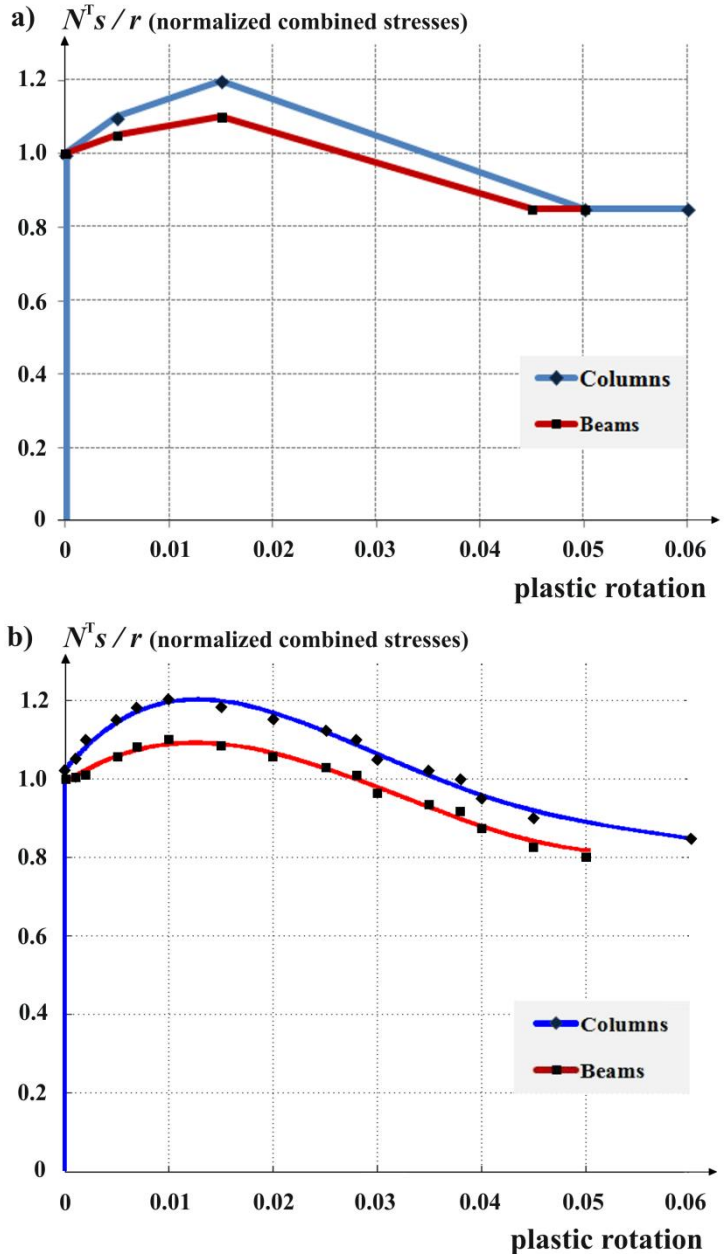

Fig. 6.20: a) Multi-linear and b) nonlinear hardening/softening structural behavior.

Table 6.4. Analysis results for all cases for example #2.

Cases	NMyMz rigid-p.plastic (a)	NMyMz PWL (b)	NMyMz NL-PWL (c)	NMyMz NL (d)
number of variables n_{var}	157	281		
number of equality constraints n_{eq}	72	228		
number of inequality constraints n_{inq}	1664	52		
maximum load factor a (kN)	188.50	204.13	211.98	215.07
number of plastic hinges	22	22	22	22
total computational time (s)	10.97	189.97	2953.38	2192.69
number of iterations	—	28	359	280
complementarity condition $\mathbf{w}^T\mathbf{z}$	—	4.74E-05	4.50E-12	3.04E-07
initial values of ρ	—	10^9	10^4	100

All analysis results are shown in Table 6.4. Case (a) corresponds to a LP problem that yields the smallest value of the maximum load factor a in the shortest computational time. The number of variables and equality constraints for rigid-perfectly plastic behavior is smaller compared to that of the NLP problem, but the number of inequalities is significantly larger since all yield planes are engaged. For cases (b), (c) and (d) the number of variables and constraints is the same regardless of the linearity or nonlinearity of the structural behavior and of the a priori or local linearization of the yield surface. Comparing cases (b) and (c) that correspond to the same multi-linear structural behavior, it is observed that the local linearization approach yields greater value of maximum load factor since the nonlinearity of the yield surface is retained. The number of plastic hinges and collapse mechanisms are identical for both cases. Comparing cases (c) and (d) that correspond to local linearization of the nonlinear yield surface, the value of the load factor is greater for case (d) since it corresponds to nonlinear structural behavior.

The plastic hinge pattern for rigid-perfectly plastic behavior is depicted in Fig. 6.20 and the results are verified by a step-by-step analysis using SAP2000 version 14, as shown in Fig. 6.21. The corresponding interaction diagram is presented in Fig. 6.22, where the role of bending moment along local z axis (strong axis) is dominant. Column cross sections are stressed also due to bending moment along local y axis, while the effect of axial force is presented mainly in beam cross sections.

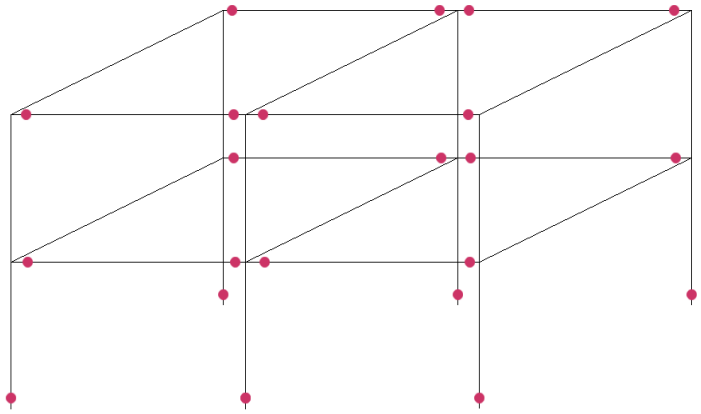

Fig. 6.21: Plastic hinge formation for case (a).

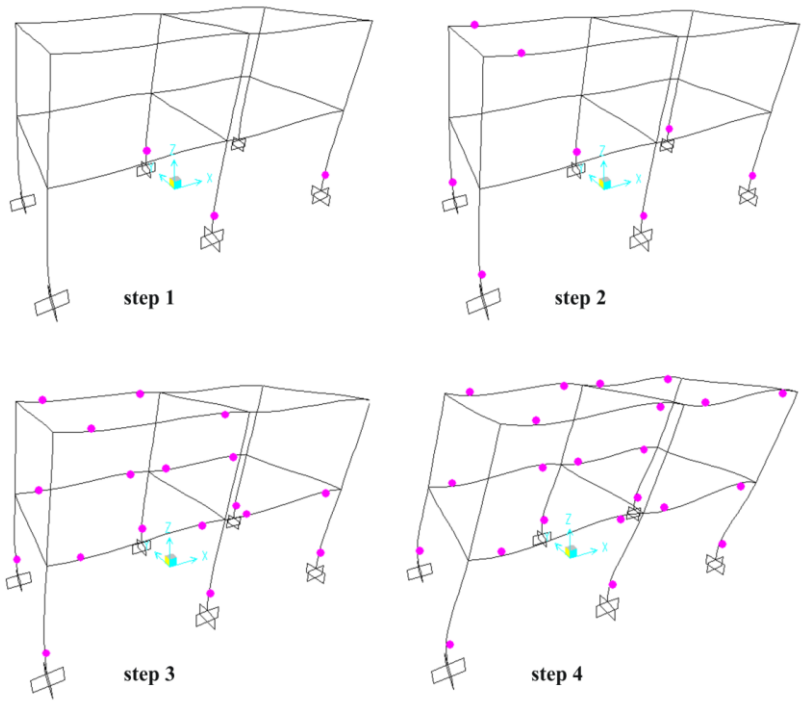

Fig. 6.22: Plastic hinge formation with step-by-step analysis for case (a).

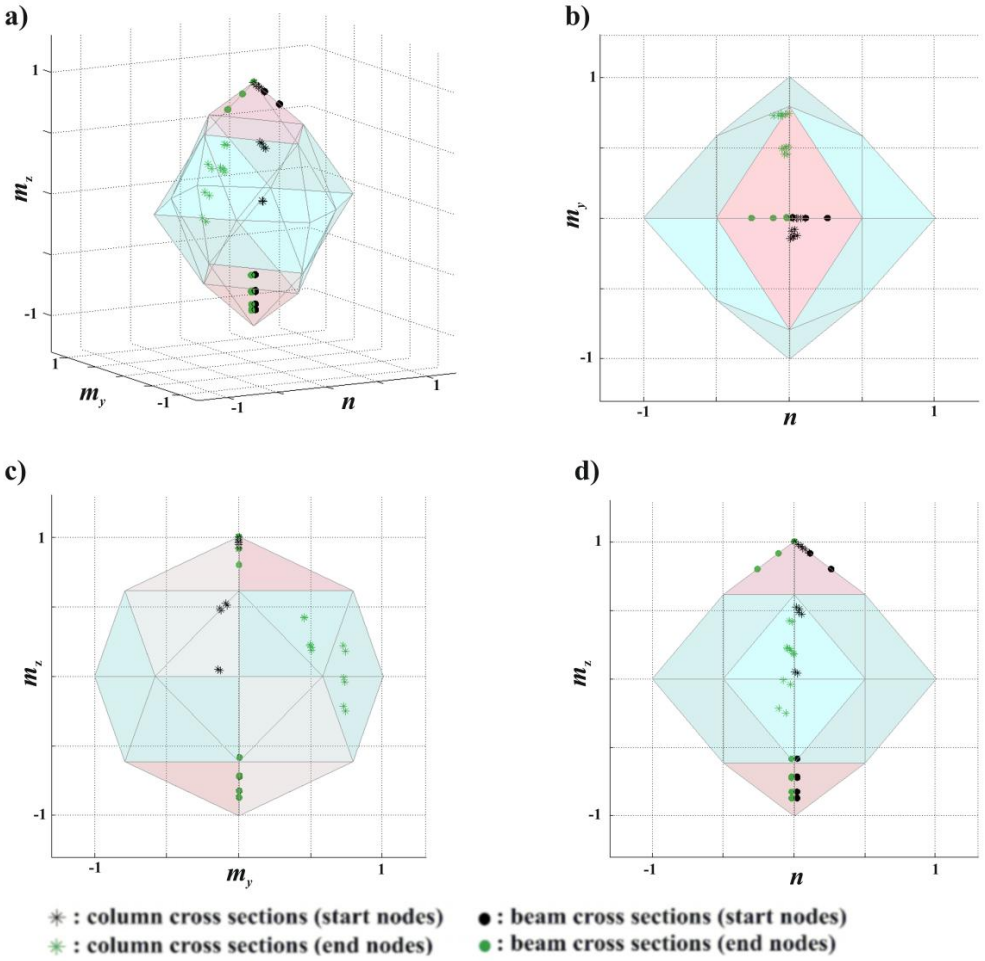

Fig. 6.23: Interaction diagram for case (a).

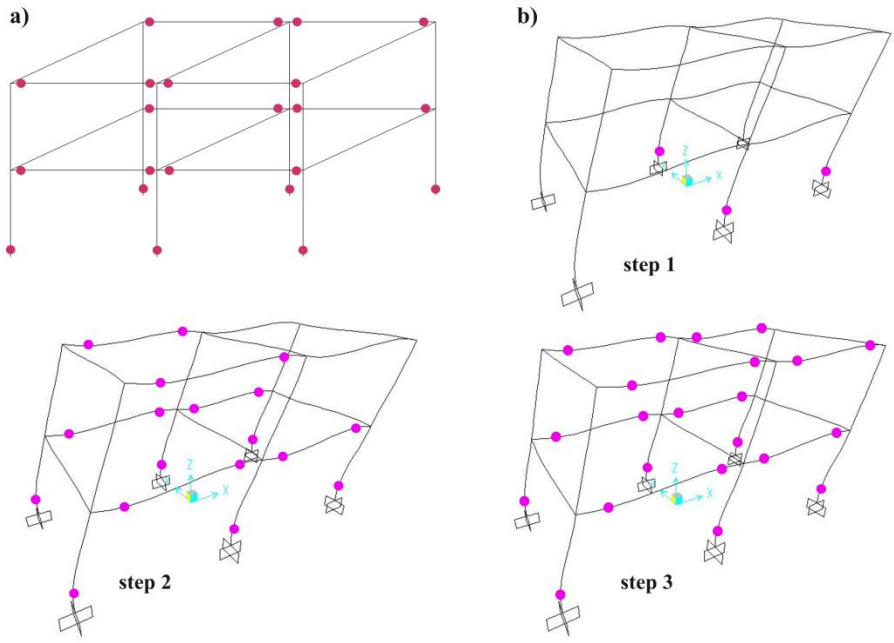

Fig. 6.24: Plastic hinge formation with a) limit and b) step-by-step analysis for case (b).

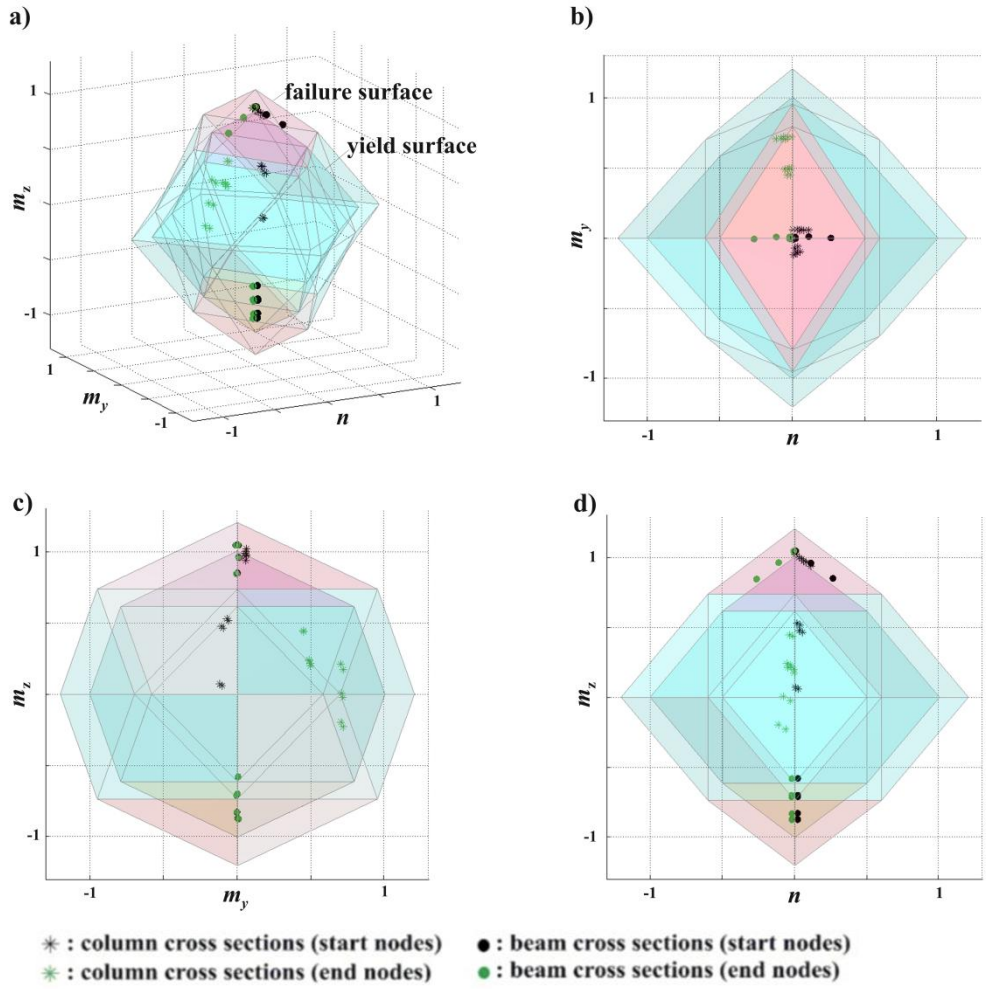

Fig. 6.25: Interaction diagram for case (b).

Analysis results for case (b) are presented in Figs. 6.24 and 6.25. In Fig. 6.24a, the plastic hinge pattern for limit load and deformation analysis is shown, while in Fig. 6.24b the collapse mechanism is verified by a step-by-step analysis with SAP2000 v.14. The stress state of all cross sections is depicted in Fig. 6.25, where it is concluded that the role of interaction is the same as that in case (a). The effect of bending moment along local z axis is prevailing for all cross sections. The role of bending moment along local y axis is evident mainly at column cross sections, while axial force affects mostly beam cross sections.

The plastic hinge pattern for case (c) is depicted in Fig. 6.26, where every plastic hinge is accompanied with a number that designates the corresponding hardening/softening segment. All yielded column cross sections lie on the second hardening segment (Fig. 6.28a), whereas most beam cross sections are on their softening branch (Fig. 6.28b). The interaction diagram is presented in Fig. 6.27. Beam

cross sections are stressed due to the combined effect of the axial force and the bending moment along local z axis (the effect of m_y is negligible), while the interaction of all stresses is evident in column cross sections. The same conclusions for the effect of combined stresses are reached for case (d), as presented in Fig. 6.30. The corresponding collapse mechanism is shown in Fig. 6.29, which is identical to that of other cases (number and disposition of plastic hinges).

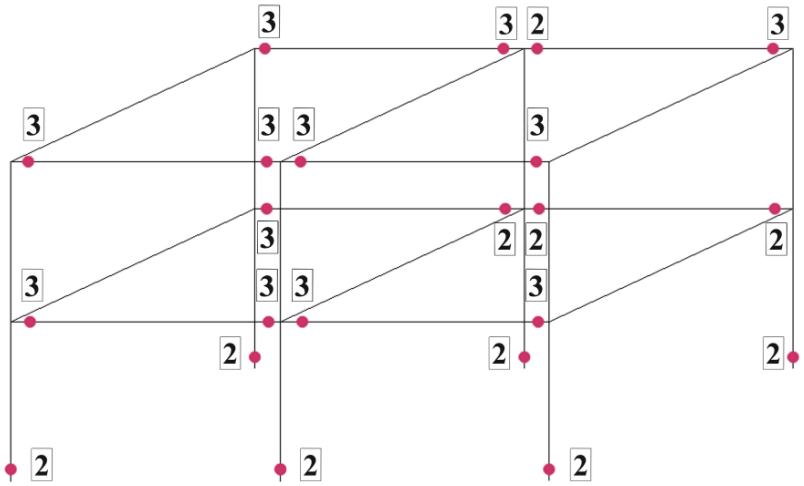

Fig. 6.26: Plastic hinge formation for case (c).

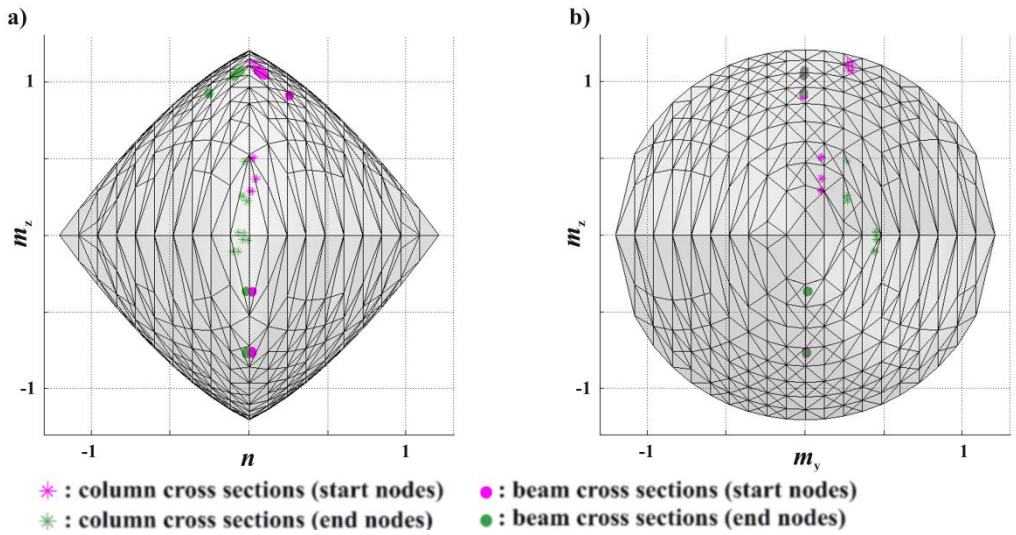

Fig. 6.27: Interaction diagram for case (c).

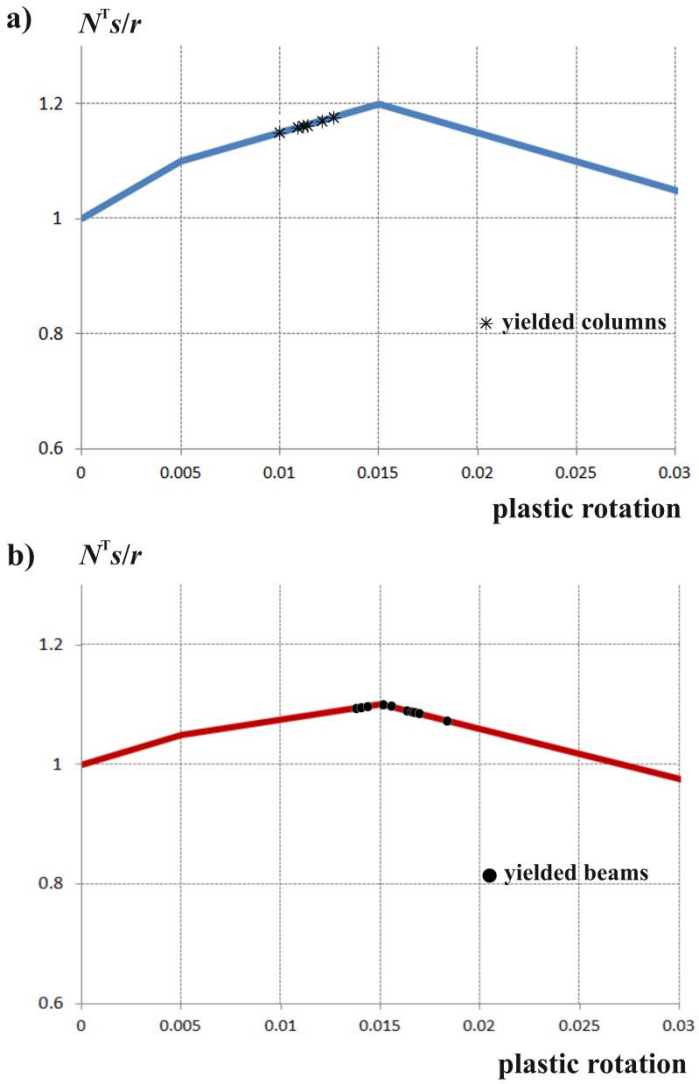

Fig. 6.28: Plastic hinge formation for case (c).

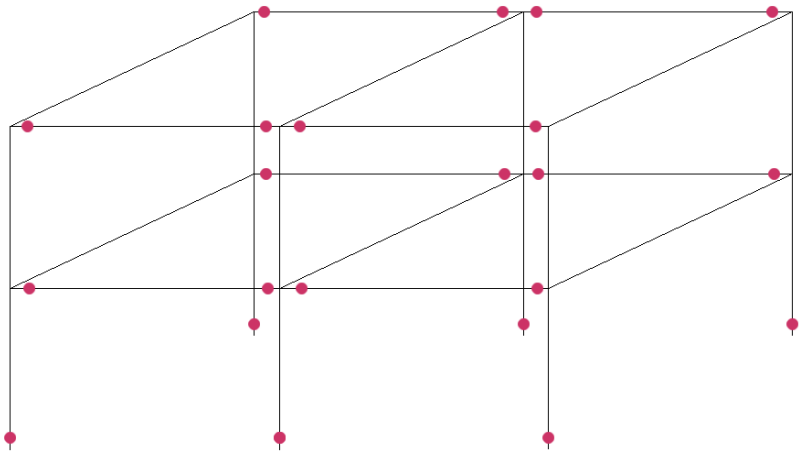

Fig. 6.29: Plastic hinge formation for case (d).

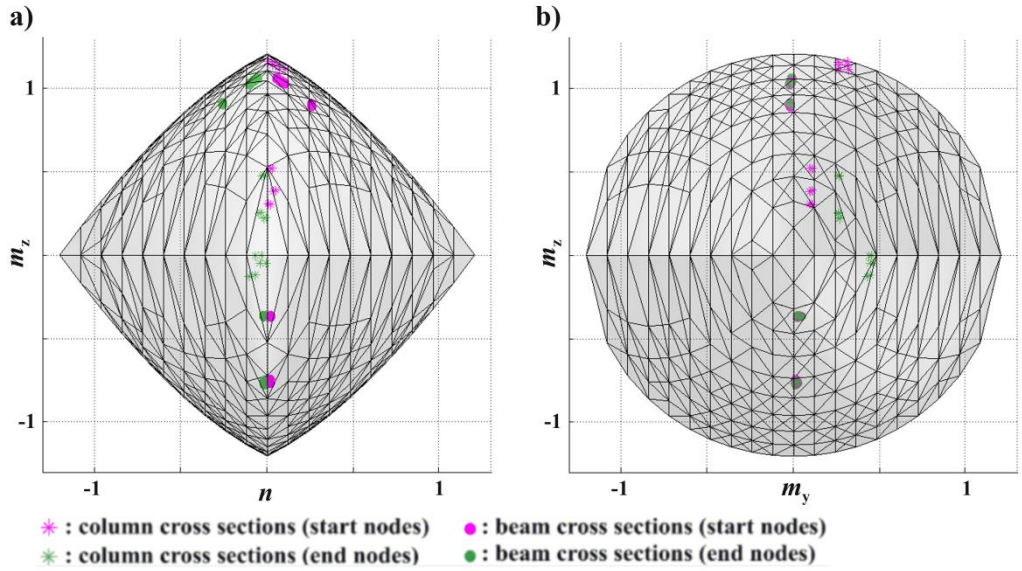

Fig. 6.30: Interaction diagram for case (d).

The computational performance of the algorithm for case (b) is depicted in Fig. 6.31. The convergence is achieved after 28 iterations and the required computational time is 189.97s. Note that the value of the objective function comes to -47145.83, while the value of the maximum load factor a is 204.13 kN. The significant difference between these two values is due to the great values of the penalty parameter ρ, which magnifies the tolerance of the complementarity term.

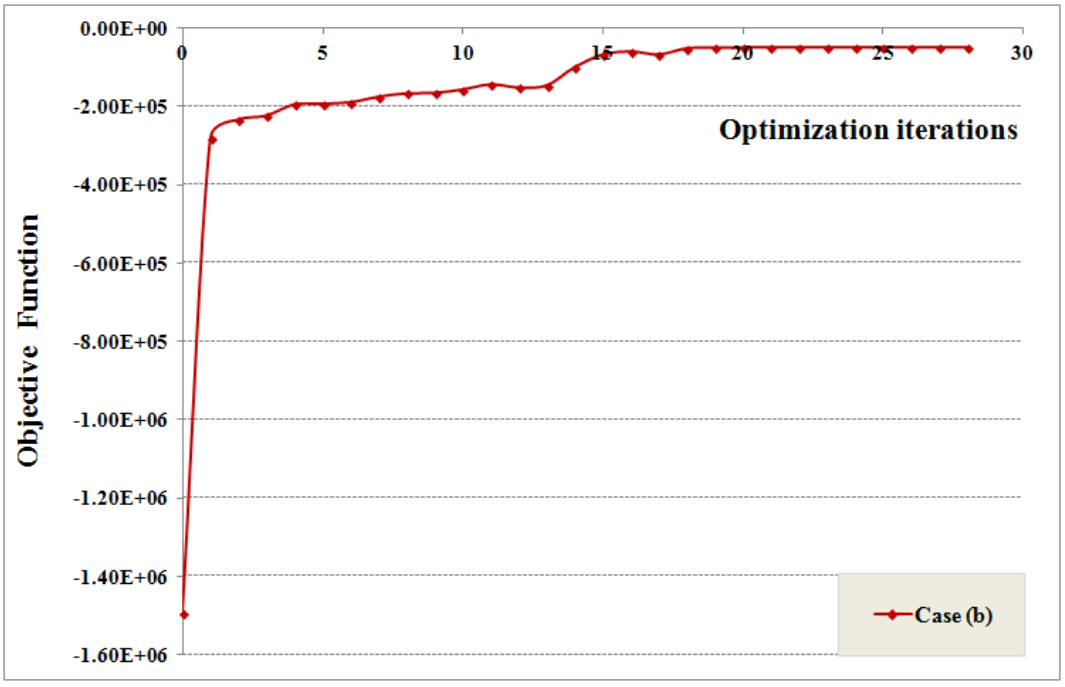

Fig. 6.31: Evolution of the optimization procedure of example #2 for case (b).

The evolution of the optimization process for case (c) is presented in Fig. 6.32 (Fig. 6.32b constitutes an enlargement of 6.32a omitting a few initial iterations). The algorithm converges after 359 iterations requiring 2953.38s. The smooth tendency of the objective function to attain greater values is distracted by some sharp peaks that are due to the penalized complementarity term.

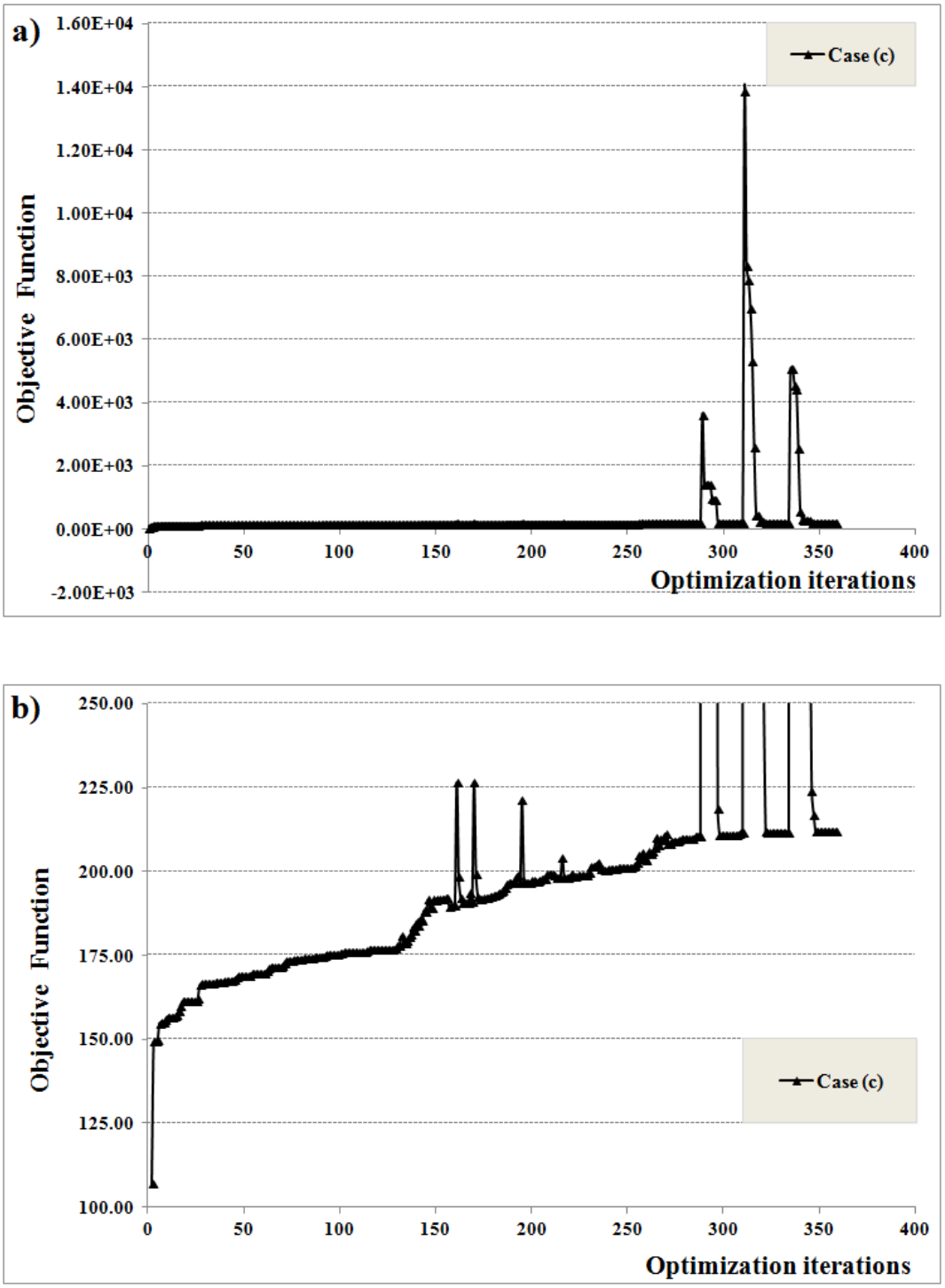

Fig. 6.32: Evolution of the optimization procedure of example #2 for case (c).

The observed behavior of the computational procedure for case (d) is presented in terms of objective function evolution in Fig. 6.33. The algorithm requires 280 iterations and 2192.69s until convergence, while its tendency is -comparatively to other cases- smoother.

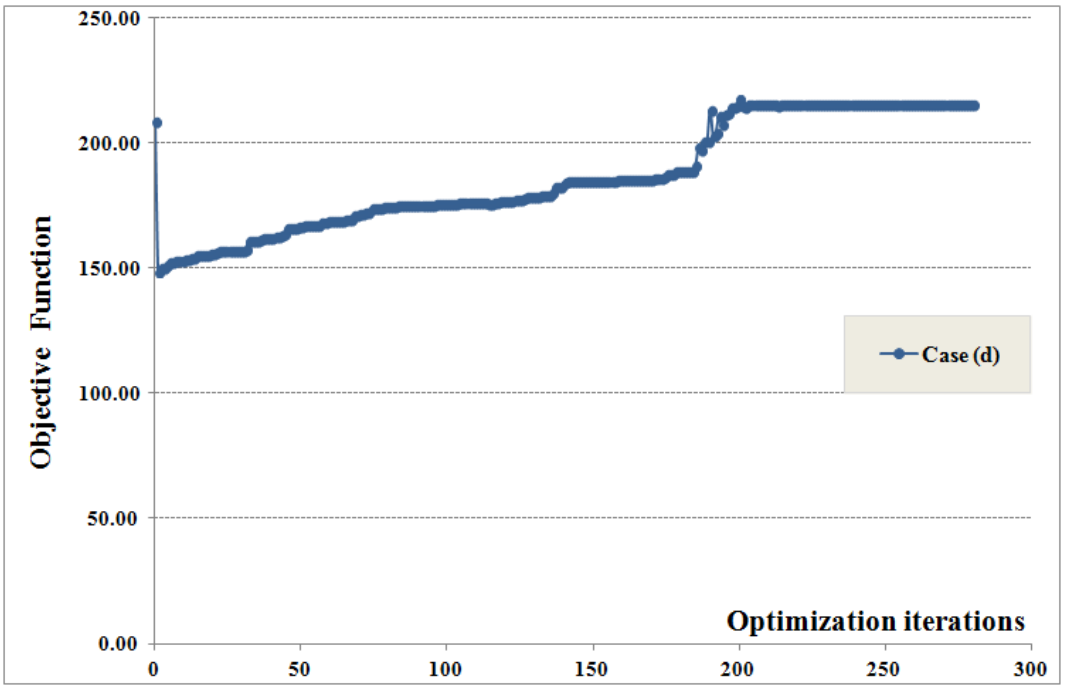

Fig. 6.33: Evolution of the optimization procedure of example #2 for case (d).

6.9. Concluding remarks

In this chapter the structural analysis in the framework of mathematical programming is extended to 3D steel frames. An optimization problem is formulated that aims at maximizing the load factor that the structure can sustain, subjected to constraints enforced by equilibrium, compatibility, yielding and complementarity conditions. The disjunctive nature of the latter constitutes the main source of numerical instabilities of the problem and thus it is appropriately treated using a penalty function formulation. The enforced NLP problem is sensitive to initial values and lower and upper bounds of variables. The yield condition is formulated following two different ways, i.e. either the a priori linearization or the local linearization technique, while the structural behavior is considered either multi-linear or nonlinear. From the presented examples, it turns out that the algorithm for the case of nonlinear yield condition (local linearization) and multi-linear hardening/softening behavior

performs in a more stable way compared to the case of nonlinear yield condition and structural behavior. However, the latter case, which addresses more accurately real structural response, is computationally more efficient since it requires fewer iterations and consequently less computational time until convergence.

Chapter 7

Concluding Remarks and Future Research

7.1. Summary and concluding remarks

The different methods of structural analysis constitute the basis of the engineering design of structures. They concern the determination of the effects of loads of all different kinds on structural systems and their components, involving mainly the fields of applied and computational mechanics, material science and applied mathematics. The aim is to evaluate structural response, i.e. deformations, internal forces, stresses, support reactions, accelerations and stability for actual or potential external loadings specified in the codes of practice. Among the existing methods, limit analysis aims at determining directly the ultimate capacity of frame, plate and other structures and possesses a central role in elastoplastic structural analysis. This objective is achieved at the cost of obtaining partial information, which though is sufficient to answer main design considerations. This "parachute launching" goal is driven by the power of optimization theory. The formulation of limit analysis in the context of mathematical programming enables further its straightforward application to large-scale problems.

In this dissertation, limit load and deformation analysis in combined form is addressed in the framework of mathematical programming for 2D and 3D frame structures. The formulation of the problem depends on structural behavior and additional list of demands such as ductility, specific design objectives etc. Classical limit analysis of structures depends on rigid-perfectly plastic behavior and thus with no considerations on plastic deformations. In this case, limit analysis is formulated as a Linear Programming - LP problem that aims at maximizing the load factor under equilibrium and yield constraints or in dual form minimizing the energy subject to compatibility and energy normalization constraints. The LP scheme is also capable of addressing indirectly isotropic hardening behavior focusing again only on the load axis, specifying the ultimate values as upper bounds, and disregarding deformation. If softening behavior and/or limited ductility are considered, the need for combined limit load and deformation analysis emerges, including constraints that prevent the simultaneous allowance of plastic deformation and strength reserves (complementarity condition). This case is addressed as a Mathematical Programming with Equilibrium Constraints (MPEC) problem, referring actually to the complementarity conditions. The aim is to maximize the load factor a subjected to constraints imposed by equilibrium, compatibility, yielding, complementarity and

lower and upper bounds for plastic deformations and displacements. This kind of problem is reformulated as a NonLinear Programming - NLP problem following different approaches among which smoothing techniques, penalty function formulation etc. The standard formulation is based on the piecewise linearization of yield condition and constitutive laws that enables their expression in a linear form. However, this approach interrelates the size of the problem with the refinement of discretization and may become prohibitive for large-scale problems. Additionally, the incorporation of multi-segmental constitutive behavior at critical sections leads to a combinatorial growth of the size of the problem engaging for every yield hyperplane all possible constitutive branches. This consideration renders the manipulation of hardening matrix almost impossible for the optimization process.

The objective of the present work was to highlight the inner structure and drawbacks of the existing formulation and propose new approaches that broaden the applicability of limit load and deformation analysis in the context of mathematical programming. In this dissertation a restructuring of the MPEC problem is achieved by avoiding unnecessary perplexities established for reasons of mathematical formalism and retaining strictly the physically-required information. In this respect, physical-based considerations are adopted for the formulation of yield condition and the incorporation of multi-linear or nonlinear constitutive behavior leading to the uncoupling of the size of the problem (number of design variables and number of constraints) from the type of discretization. This strict formulation, relieved from all the unnecessary information, results as computationally more efficient and robust compared to the standard one.

More specifically, in this work the yield condition is formulated following three different schemes: i) a convex hull formulation, ii) a cone identification approach and iii) a local linearization technique. Expressing the yield polyhedron on the basis of convex hull formulation, i.e. in the form of a linear combination of all vertices, leads to an expression of the yield condition with a set of equality and not inequality constraints. The number of these constraints depends on the dimensionality of interaction and results independent of the number of the yield hyperplanes. In this case though, the number of variables is increased as compared to the standard formulation due to a newly introduced set of nonnegative coefficients. This formulation favors computationally the conservative static theorem expressing advantageously the multi-component interaction, enabling also finer discretization of

the yield surface. The cone identification approach is based on the fact that every critical section, at any optimization iteration, belongs to a specific cone of the interaction diagram targeting only one yield hyperplane. Having this information, the yield condition is formed only for this specific hyperplane and not for all hyperplanes that form the piecewise linear (PWL) yield surface. This reduces the number of yield constraints to a minimum, decreasing the complexity of the problem, which becomes independent of the number of hyperplanes that approximate the nonlinear yield surface. Two simple and efficient processes concerning cone identification for 2D and 3D interaction are developed. Extending cone identification concept for the local linearization technique, the critical hyperplane for each cross section is not a priori defined, but it is determined at each optimization iteration for every stress point by locally linearizing the yield surface. This process provides accurate formulation of the yield condition, while the a priori linearization of the yield surface is avoided.

Multi-linear or nonlinear structural behavior is also efficiently embedded without affecting the size of the problem or the linearity of constraints. Having the critical yield hyperplane identified (either via the cone identification or the local linearization method), only one plastic multiplier is evaluated for each cross section. For multi-linear structural behavior, the linear hardening/softening segment that corresponds to this plastic multiplier is then identified and as a consequence, hardening matrices are formed for each cross section only for the specific segment of the constitutive relation. For nonlinear structural behavior, the evaluation of the extended/shrunk yield limit is directly based on the value of the plastic multiplier.

As a consequence of the aforementioned considerations on yield condition and structural behavior, the size of the complementarity condition, which is the main source of numerical instabilities, is also reduced to a minimum accelerating the convergence of the optimization algorithm.

Numerical results verify the applicability and the efficiency of the proposed approaches in 2D and 3D frames. It is also concluded that multi-component interaction affects the load carrying capacity and failure mechanisms of structures and therefore the role of combined stresses should be taken into account aiming at a safer structural design.

7.2. Future research

Engineering design standards tend to prioritize the displacement based or performance based design. Direct methods offer the means towards this direction, assessing the bearing capacity or ultimate load of structures and focusing on the ultimate deformations developed in structures. As mentioned before, yield condition and structural behavior are the main aspects that have been investigated and some new approaches have been proposed for their efficient formulation. Remaining strictly on the field of engineering, the following issues may constitute the central points of future research extending the results of the present work in the following directions:

- Geometrical nonlinearities can be incorporated, investigating their effect on the ultimate load and state of a structure.
- Nonholomic consideration may be addressed by using a stepwise holonomic approach incorporating linearized or nonlinear constitutive laws and yield criteria.
- Development of mathematical smoothening procedures that treat more efficiently the complementarity condition.
- Implementation of the proposed approaches in plane stress and plane strain problems, in fracture mechanics problems (crack tracking) and in soil mechanics applications (such as slope stability analysis, lateral earth pressures on rigid retaining structures etc.).

The combination of structural limit analysis with mathematical programming creates a promising field that treats limit state problems following a rather mathematical path with the physical constraints lying on the background. However, the presence of complementarity conditions, which are the source of numerical instabilities, has led to the development of diverse approaches and solution strategies, restricting the applicability of limit analysis with mathematical programming. As pointed out by G. Maier in 1984, the need for *a theory in the sense of the Greek etymology, i.e. a theoretical framework capable of providing a deeper insight, but also a versatile methodology for numerical solutions*, was and remains urgent for exploiting fully the potential of these methods.

Appendices

Appendix A. Linear programming.

I. Standard form of LP problem.

The standard form of a Linear Programming problem that is presented in equations (2.1) and (2.2) having *m* number of constraints and *n* number of variables. The main characteristics of the standard form are:

- Minimization problem
- Nonnegative vector ***b***
- Equality constraints
- Non-negative variables

The aforementioned characteristics should be met for any LP problem so that it is converted to one of standard form. Thus the following techniques may be followed:

1. Converting the **max**imization into **min**imization problem.

   The maximization problem is transformed to a minimization one by multiplying the objective function by minus unity.

2. Treatment of negative b_i (i=1…m).

   If there is a constraint i for which the value of b_i, it is multiplied by minus unity.

3. Converting inequality constraints into equalities.

   i) Converting a "≤" to equality constraint.

   An inequality of this form is transformed into equality by adding a slack variable, as shown below:

$$a_{i1}x_1 + a_{i2}x_2 + \cdots + a_{in}x_n \le b_i \Leftrightarrow$$

$$a_{i1}x_1 + a_{i2}x_2 + \cdots + a_{in}x_n + s_i = b_i, \quad where\ s_i \ge 0$$

   ii) Converting a "≥" to equality constraint.

   An inequality of this form is transformed into equality by adding a surplus variable, as shown below:

$$a_{i1}x_1 + a_{i2}x_2 + \cdots + a_{in}x_n \ge b_i \Leftrightarrow$$

$$a_{i1}x_1 + a_{i2}x_2 + \cdots + a_{in}x_n - s_i = b_i, \quad where\ s_i \ge 0$$

4. Converting all variables into nonnegative.

i) Negative variables

Every negative variable $x_j \leq 0$, (j=1…n) should be substituted by another variable $y_j = -x_j$, *where* $y_j \geq 0$. Then, the variable x_j is replaced by $-y_j$ in the LP problem.

ii) Free (unconstrained/unrestricted) variables

An unconstrained variable x_j may be treated in two different ways:

- Elimination of x_j using an equation in which it appears, for example:

$$a_{i1}x_1 + a_{i2}x_2 + \cdots + a_{ij}x_j + \ldots + a_{in}x_n + s_i = b_i \Leftrightarrow$$

$$x_j = \frac{1}{a_{ij}} \cdot \left(b_i - a_{i1}x_1 - a_{i2}x_2 - \ldots - a_{in}x_n - s_i\right)$$

  Then the variable x_j is substituted in all equations of the LP problem.

- Replacement of x_j with two nonnegative variables, i.e. $x_j = y_j - w_j$, *where* $y_j, w_j \geq 0$.

II. Primal-dual relations of LP.

In this section the definition of the dual program associated with a given LP program is discussed (Luenberger and Ye 2008). Duality relation may be presented in symmetric or asymmetric form depending on the kind of constraints. For the case that the primal program is expressed only in terms of inequality constraints, the duality relationship is symmetric and the primal and dual problems are given as:

$$\underbrace{\begin{array}{llll} min & \boldsymbol{c}^T\boldsymbol{x} & max & \boldsymbol{\lambda}^T\boldsymbol{b} \\ s.t. & \boldsymbol{A}\boldsymbol{x} \geq \boldsymbol{b} & s.t. & \boldsymbol{\lambda}^T\boldsymbol{A} \leq \boldsymbol{c}^T \\ & \boldsymbol{x} \geq \boldsymbol{0} & & \boldsymbol{\lambda} \geq \boldsymbol{0} \end{array}}_{symmetric\ form} \qquad \text{(A.1)}$$

The generation of the symmetric form of the dual problem depends on the change of minimization to maximization problem, the interchange of cost and constraint vectors, the transposition of coefficient matrix and the reversal of constraint inequalities. Based on the above formulation, the dual of any LP program can be enforced. For the case of a LP problem in the standard form, the duality relationship is asymmetric and the primal and dual problems are given following the next stages:

$$\underbrace{\left.\begin{array}{ll} min & \boldsymbol{c}^T\boldsymbol{x} \\ s.t. & \boldsymbol{A}\boldsymbol{x}=\boldsymbol{b} \\ & \boldsymbol{x}\geq\boldsymbol{0} \end{array}\right\} \Leftrightarrow \begin{array}{ll} min & \boldsymbol{c}^T\boldsymbol{x} \\ s.t. & \boldsymbol{A}\boldsymbol{x}\geq\boldsymbol{b} \\ & -\boldsymbol{A}\boldsymbol{x}\geq-\boldsymbol{b} \\ & \boldsymbol{x}\geq\boldsymbol{0} \end{array}}_{primal} \tag{A.2}$$

$$\underbrace{\left.\begin{array}{ll} max & \boldsymbol{u}^T\boldsymbol{b}-\boldsymbol{v}^T\boldsymbol{b} \\ s.t. & \boldsymbol{u}^T\boldsymbol{A}-\boldsymbol{v}^T\boldsymbol{A}\leq\boldsymbol{c}^T \\ & \boldsymbol{u}\geq\boldsymbol{0} \\ & \boldsymbol{v}\geq\boldsymbol{0} \end{array}\right\} \Leftrightarrow \begin{array}{ll} max & \boldsymbol{\lambda}^T\boldsymbol{b} \\ s.t. & \boldsymbol{\lambda}^T\boldsymbol{A}\leq\boldsymbol{c}^T \\ & \boldsymbol{\lambda}\ unrestricted \end{array}}_{dual}$$

The transformation of the standard primal problem to that of equation (A.1) depends on the replacement of the equality constraint $\boldsymbol{Ax}=\boldsymbol{b}$ with two inequalities $\boldsymbol{Ax}\leq\boldsymbol{b}$ and $-\boldsymbol{Ax}\geq-\boldsymbol{b}$. Moreover, the dual vector of variables consists of two nonnegative vectors, i.e. $\boldsymbol{u}$ and $\boldsymbol{v}$. Considering that $\boldsymbol{\lambda}=\boldsymbol{u}-\boldsymbol{v}$, the vector $\boldsymbol{\lambda}$ of variables becomes free (unrestricted) and the asymmetric form of the dual problem is given by the following relation:

$$\underbrace{\begin{array}{ll} min & \boldsymbol{c}^T\boldsymbol{x} \\ s.t. & \boldsymbol{A}\boldsymbol{x}=\boldsymbol{b} \\ & \boldsymbol{x}\geq 0 \end{array} \qquad \begin{array}{ll} max & \boldsymbol{\lambda}^T\boldsymbol{b} \\ s.t. & \boldsymbol{\lambda}^T\boldsymbol{A}\leq\boldsymbol{c}^T \\ & \boldsymbol{\lambda}\ unrestricted \end{array}}_{asymmetric\ form} \tag{A.3}$$

The equality constraints of the primal problem generate the corresponding free dual variables and vice versa. If some of the components of $\boldsymbol{x}$ in the primal problem are free, then the corresponding inequalities in $\boldsymbol{\lambda}^T\boldsymbol{A}\leq\boldsymbol{c}^T$ are turned into equalities.

Appendix B. Nonlinear programming-Interior point method.

I. Karush-Kuhn-Tucker conditions

Suppose that the objective function *f*, the inequality constraints *g* and the equality constraints *h* of the optimization problem (2.4) are continuously differentiable at point x^*. If point x^* is a local minimum provided that it satisfies the regularity conditions

mentioned in §2.2.2, it satisfies also the following Karush-Kuhn-Tucker (KKT) conditions:

- Stationarity condition

$$\nabla f(x^*) + \sum_{i=1}^{m} \lambda_{g,i} \nabla g_i(x^*) + \sum_{j=1}^{l} \lambda_{h,j} \nabla h_j(x^*) = 0, \quad \text{where } \lambda_{g,i} (i = 1...m) \text{ and } \lambda_{h,j} \ (j = 1...l) \text{ are KKT multipliers} \tag{B.1}$$

- Primal feasibility

$$g_i(x^*) \le 0, \quad \text{for all } i = 1...m \qquad h_j(x^*) \le 0, \quad \text{for all } j = 1...l \tag{B.2}$$

- Dual feasibility

$$\lambda_{g,i} \ge 0, \ \text{for all } i = 1...m \tag{B.3}$$

- Complementarity slackness

$$\lambda_{g,i} g_i(x^*) = 0, \ \text{for all } i = 1...m \tag{B.4}$$

The aforementioned necessary conditions are also sufficient for optimality when the objective function f is convex, the inequality constraints g are continuously differentiable convex functions and the equality constraints h are affine functions.

II. Interior-point method

The constrained optimization problem described in (2.4) is solved using a sequence of minimization problems. Adopting the logarithmic barrier function formulation, the problem becomes:

$$\begin{aligned} &\min_{x,s} f_\mu(x,s) = \min_{x,s} f(x) - \mu \sum_i ln(s_i) \\ &s.t. \qquad h(x) = 0 \\ &\qquad\quad g(x) + s = 0 \end{aligned} \tag{B.5}$$

where μ is a positive scalar and s_i is the slack variable corresponding to the i^{th} inequality constraint. The $ln(s_i)$ is bounded by the positive values of every s_i and as μ decreases to zero, the minimum value of $f_\mu(x,s)$ approaches to the minimum of f (Byrd, Hribar and Nocedal 1999). The algorithm that is incorporated in the herein adopted *fmincon* solver may use two types of step at each iteration, i.e. a direct step or a conjugate gradient (CG) step. According to the first one, the KKT conditions are solved for problem (B.5) via a linear approximation.

Appendix C. Equations of yield lines.

In this Appendix, the equations of the eight linear segments that approximate the yield surface are presented in detail. The adopted yield criterion is that of Gendy-Saleeb accounting for axial force-bending moment (NM) interaction. The coefficients of the yield lines form $\boldsymbol{N}$ matrix necessary for yield condition formulation. More specifically, for j element ends the equations are as follows:

$$
\begin{aligned}
&w_1 : tan\gamma_1 \cdot n^j + 1 \cdot m^j = tan\gamma_1 \Leftrightarrow \frac{tan\gamma_1}{s_{1y}^i} \cdot s_1^i + \frac{1}{s_{2y}^i} \cdot s_2^i = tan\gamma_1 \Leftrightarrow \\
&\quad A_1^j \cdot s_1^i + B_1^j \cdot s_2^i = C_1^j \\
&w_2 : tan\gamma_2 \cdot n^j + 1 \cdot m^j = 1 \Leftrightarrow \frac{tan\gamma_2}{s_{1y}^i} \cdot s_1^i + \frac{1}{s_{2y}^i} \cdot s_2^i = 1 \Leftrightarrow \\
&\quad A_2^j \cdot s_1^i + B_2^j \cdot s_2^i = C_2^j \\
&w_3 : -tan\gamma_2 \cdot n^j + 1 \cdot m^j = 1 \Leftrightarrow \frac{-tan\gamma_2}{s_{1y}^i} \cdot s_1^i + \frac{1}{s_{2y}^i} \cdot s_2^i = 1 \Leftrightarrow \\
&\quad A_3^j \cdot s_1^i + B_3^j \cdot s_2^i = C_3^j \\
&w_4 : -tan\gamma_1 \cdot n^j + 1 \cdot m^j = tan\gamma_1 \Leftrightarrow \frac{-tan\gamma_1}{s_{1y}^i} \cdot s_1^i + \frac{1}{s_{2y}^i} \cdot s_2^i = tan\gamma_1 \Leftrightarrow \\
&\quad A_4^j \cdot s_1^i + B_4^j \cdot s_2^i = C_4^j \\
&w_5 : -tan\gamma_1 \cdot n^j - 1 \cdot m^j = tan\gamma_1 \Leftrightarrow \frac{-tan\gamma_1}{s_{1y}^i} \cdot s_1^i - \frac{1}{s_{2y}^i} \cdot s_2^i = tan\gamma_1 \Leftrightarrow \\
&\quad A_5^j \cdot s_1^i + B_5^j \cdot s_2^i = C_5^j \\
&w_6 : -tan\gamma_2 \cdot n^j - 1 \cdot m^j = 1 \Leftrightarrow \frac{-tan\gamma_2}{s_{1y}^i} \cdot s_1^i - \frac{1}{s_{2y}^i} \cdot s_2^i = 1 \Leftrightarrow \\
&\quad A_6^j \cdot s_1^i + B_6^j \cdot s_2^i = C_6^j \\
&w_7 : tan\gamma_2 \cdot n^j - 1 \cdot m^j = 1 \Leftrightarrow \frac{tan\gamma_2}{s_{1y}^i} \cdot s_1^i - \frac{1}{s_{2y}^i} \cdot s_2^i = 1 \Leftrightarrow \\
&\quad A_7^j \cdot s_1^i + B_7^j \cdot s_2^i = C_7^j \\
&w_8 : tan\gamma_1 \cdot n^j - 1 \cdot m^j = tan\gamma_1 \Leftrightarrow \frac{tan\gamma_1}{s_{1y}^i} \cdot s_1^i - \frac{1}{s_{2y}^i} \cdot s_2^i = tan\gamma_1 \Leftrightarrow \\
&\quad A_8^j \cdot s_1^i + B_8^j \cdot s_2^i = C_8^j
\end{aligned}
\tag{C.1}
$$

For k element ends the corresponding equations of yield lines are given as:

$$
\begin{aligned}
&w_1 : tan\gamma_1 \cdot n^k + 1 \cdot m^k = tan\gamma_1 \Leftrightarrow \frac{-tan\gamma_1}{s_{1y}^i} \cdot s_1^i + \frac{1}{s_{3y}^i} \cdot s_3^i = tan\gamma_1 \Leftrightarrow \\
&\quad A_1^k \cdot s_1^i + B_1^k \cdot s_3^i = C_1^k \\
&w_2 : tan\gamma_2 \cdot n^k + 1 \cdot m^k = 1 \Leftrightarrow \frac{-tan\gamma_2}{s_{1y}^i} \cdot s_1^i + \frac{1}{s_{3y}^i} \cdot s_3^i = 1 \Leftrightarrow \\
&\quad A_2^k \cdot s_1^i + B_2^k \cdot s_3^i = C_2^k \\
&w_3 : -tan\gamma_2 \cdot n^k + 1 \cdot m^k = 1 \Leftrightarrow \frac{tan\gamma_2}{s_{1y}^i} \cdot s_1^i + \frac{1}{s_{3y}^i} \cdot s_3^i = 1 \Leftrightarrow \\
&\quad A_3^k \cdot s_1^i + B_3^k \cdot s_3^i = C_3^k \\
&w_4 : -tan\gamma_1 \cdot n^k + 1 \cdot m^k = tan\gamma_1 \Leftrightarrow \frac{tan\gamma_1}{s_{1y}^i} \cdot s_1^i + \frac{1}{s_{3y}^i} \cdot s_3^i = tan\gamma_1 \Leftrightarrow \\
&\quad A_4^k \cdot s_1^i + B_4^k \cdot s_3^i = C_4^k \\
&w_5 : -tan\gamma_1 \cdot n^k - 1 \cdot m^k = tan\gamma_1 \Leftrightarrow \frac{tan\gamma_1}{s_{1y}^i} \cdot s_1^i - \frac{1}{s_{3y}^i} \cdot s_3^i = tan\gamma_1 \Leftrightarrow \\
&\quad A_5^k \cdot s_1^i + B_5^k \cdot s_3^i = C_5^k \\
&w_6 : -tan\gamma_2 \cdot n^k - 1 \cdot m^k = 1 \Leftrightarrow \frac{tan\gamma_2}{s_{1y}^i} \cdot s_1^i - \frac{1}{s_{3y}^i} \cdot s_3^i = 1 \Leftrightarrow \\
&\quad A_6^k \cdot s_1^i + B_6^k \cdot s_3^i = C_6^k \\
&w_7 : tan\gamma_2 \cdot n^k - 1 \cdot m^k = 1 \Leftrightarrow \frac{-tan\gamma_2}{s_{1y}^i} \cdot s_1^i - \frac{1}{s_{3y}^i} \cdot s_3^i = 1 \Leftrightarrow \\
&\quad A_7^k \cdot s_1^i + B_7^k \cdot s_3^i = C_7^k \\
&w_8 : tan\gamma_1 \cdot n^k - 1 \cdot m^k = tan\gamma_1 \Leftrightarrow \frac{-tan\gamma_1}{s_{1y}^i} \cdot s_1^i - \frac{1}{s_{3y}^i} \cdot s_3^i = tan\gamma_1 \Leftrightarrow \\
&\quad A_8^k \cdot s_1^i + B_8^k \cdot s_3^i = C_8^k
\end{aligned}
\tag{C.2}
$$

The matrix $\boldsymbol{N}^i$ and the vector $\boldsymbol{r}^i$ of the element are given as:

$$
\boldsymbol{N}^i = \begin{bmatrix} A_1^j & \cdots & A_8^j & A_1^k & \cdots & A_8^k \\ B_1^j & \cdots & B_8^j & 0 & \cdots & 0 \\ 0 & \cdots & 0 & B_1^k & \cdots & B_8^k \end{bmatrix}
$$

$$
\boldsymbol{r}^{iT} = \begin{Bmatrix} C_1^j & \cdots & C_8^j & C_1^k & \cdots & C_8^k \end{Bmatrix}
\tag{C.3}
$$

Appendix D. Equations of planes.

In this Appendix, the equations of the plane triangles that approximate the yield surface are presented in detail. The adopted yield criterion is that of Gendy-Saleeb accounting for axial-shear force-bending moment (NQM) interaction. The coefficients of the yield lines form ***N*** matrix necessary for yield condition formulation. More specifically, for a plane triangle *p* and for start node *j* substituting the normalized quantities the following expression is obtained:

$$\begin{gathered}\tilde{A}_p^j n^j + \tilde{B}_p^j v^j + \tilde{C}_p^j m^j + \tilde{D}_p^j = 0 \Leftrightarrow \\ \tilde{A}_p^j \frac{s_1^i}{s_{1y}^i} + \tilde{B}_p^j \frac{s_2^i + s_3^i}{L^i v_y^i} + \tilde{C}_p^j \frac{s_2^i}{s_{2y}^i} + \tilde{D}_p^j = 0 \Leftrightarrow \\ \frac{\tilde{A}_p^j}{s_{1y}^i} s_1^i + \left(\frac{\tilde{B}_p^j}{L^i v_y^i} + \frac{\tilde{C}_p^j}{s_{2y}^i} \right) s_2^i + \frac{\tilde{B}_p^j}{L^i v_y^i} s_3^i = -\tilde{D}_p^j \Leftrightarrow \\ A_p^j s_1^i + B_p^j s_2^i + C_p^j s_3^i = D_p^j\end{gathered} \tag{D.1}$$

Similarly for end node *k*:

$$\begin{gathered}\tilde{A}_p^k n^k + \tilde{B}_p^k v^k + \tilde{C}_p^k m^k + \tilde{D}_p^k = 0 \Leftrightarrow \\ -\tilde{A}_p^k \frac{s_1^i}{s_{1y}^i} - \tilde{B}_p^k \frac{s_2^i + s_3^i}{L^i v_y^i} + \tilde{C}_p^k \frac{s_3^i}{s_{3y}^i} + \tilde{D}_p^k = 0 \Leftrightarrow \\ -\frac{\tilde{A}_p^k}{s_{1y}^i} s_1^i - \frac{\tilde{B}_p^k}{L^i v_y^i} s_2^i + \left(-\frac{\tilde{B}_p^k}{L^i v_y^i} + \frac{\tilde{C}_p^k}{s_{3y}^i} \right) s_3^i = -\tilde{D}_p^k \Leftrightarrow \\ A_p^k s_1^i + B_p^k s_2^i + C_p^k s_3^i = D_p^k\end{gathered} \tag{D.2}$$

The number of planes is 32 $\left(p = 1...32\right)$ and thus the matrix $\boldsymbol{N}^i$ and the vector $\boldsymbol{r}^i$ of the element are given as:

$$\begin{gathered}\boldsymbol{N}^i = \begin{bmatrix} A_1^j & \cdots & A_{32}^j & A_1^k & \cdots & A_{32}^k \\ B_1^j & \cdots & B_{32}^j & B_1^k & \cdots & B_{32}^k \\ C_1^j & \cdots & C_{32}^j & C_1^k & \cdots & C_{32}^k \end{bmatrix} \\ \boldsymbol{r}^{iT} = \begin{Bmatrix} D_1^j & \cdots & D_{32}^j & D_1^k & \cdots & D_{32}^k \end{Bmatrix}\end{gathered} \tag{D.3}$$

Appendix E. First-order optimality measure.

First-order optimality is measuring closeness of a point with respect to optimum. For a smooth constrained optimization problem with objective function $f(x)$ and $g(x)$ and $h(x)$ the vector functions representing all inequality and equality constraints respectively, the Lagrangian function $L(x,\lambda)$ is of the form:

$$L(x,\lambda) = f(x) + \sum \lambda_{g,i} \cdot g_i(x) + \sum \lambda_{h,i} \cdot h_i(x) \qquad \text{(E.1)}$$

where $\lambda_{g,i}$ is the Lagrange multiplier for the i^{th} inequality constraint $g(x)$ and $\lambda_{h,i}$ is the Lagrange multiplier for the i^{th} equality constraint $h(x)$. The vector λ, which contains all λ_g and λ_h, is the Lagrange multiplier vector of the problem and its length is the total number of constraints. The optimality measure associated with the stationarity condition (B.1) is given as:

$$\left\|\nabla_x L(x,\lambda)\right\| = \left\|\nabla f(x) + \sum \lambda_{g,i} \cdot \nabla g_i(x) + \sum \lambda_{h,i} \cdot \nabla h_i(x)\right\| \qquad \text{(E.2)}$$

The optimality measure associated with (B.4) is given as:

$$\left\|\overrightarrow{\lambda_g \cdot g(x)}\right\| \qquad \text{(E.3)}$$

where the infinity norm (maximum) is used for the vector $\overrightarrow{\lambda_g \cdot g(x)}$.The combined optimality measure is the maximum of the values calculated in (E.2) and (E.3), in which relations (B.2) and (B.3) are not directly considered.

References

Anderheggen, E. and Knöpfel, H. (1972) 'Finite element limit analysis using linear programming', *International Journal of Solids and Structures*, vol. 8, pp. 1413-1431.

Ardito, R., Cocchetti, G. and Maier, G. (2008) 'On structural safety assessment by load factor maximization in piecewise linear plasticity', *European Journal of Mechanics*, vol. 27, pp. 859-881.

Bertsekas, D. (1995) Nonlinear programming, Athena Scientific, Belmont, Massachusetts.

Bertsekas, D., Nedić, A. and Ozdaglar, A.E. (2003) Convex analysis and optimization, Athena Scientific, Belmont, Massachusetts.

Bisbos, C.D. and Pardalos, P.M. (2007) 'Second-order cone and semidefinite representations of material failure criteria', *Journal of Optimization Theory and Applications*, vol. 134, pp. 275-301.

Bleyer, J. and Buhan, P. (2013) 'Yield surface approximation for lower and upper bound yield design of 3D composite frame structures', *Computers and Structures*, vol. 129, pp. 86-98.

Boyd, S. and Vandenberghe, L. (2009) Convex Optimization, 7th ed., Cambridge University Press.

Bruneau, M., Uang, C-M. and Whittaker, A. (2011) Ductile Design of Steel Buildings, 2nd ed., Mc-Grow Hill.

Byrd, R., Hribar, M. and Nocedal, J. (1999) 'An Interior Point Algorithm for Large-Scale Nonlinear Programming', *SIAM Journal on Optimization*, vol. 9, no. 4, pp. 877–900.

Cannarozzi, A.A. (1980) 'A nontraditional linearizing procedure in limit analysis', *Journal of Structural Mechanics*, vol. 8, pp. 449-470.

Capurso, M. and Maier, G. (1970) 'Incremental elastoplastic analysis and quadratic optimization', *Meccanica*, vol. 4, no. 1, pp. 107-116.

Charnes, A. and Greenberg, H.J. (1951) 'Plastic collapse and linear programming', Bulletin of the American Mathematics Society, vol. 57, pp. 480.

Cocchetti, G. and Maier, G. (2003) 'Elastic–plastic and limit-state analyses of frames with softening plastic–hinge models by mathematical programming', *International Journal of Solids and Structures*, vol. 40, pp. 7219–44.

Cocchetti, G., Maier, G. and Shen, X.P. (2002) 'Piecewise linear models for interfaces and mixed mode cohesive cracks', *Computer Modeling in Engineering Sciences*, vol. 3, pp. 279-98.

Corradi, L. and Zavelani, A. (1974) 'A linear programming approach to shakedown analysis of structures', *Computer Methods in Applied Mechanics and Engineering*, vol. 3, pp. 37-53.

Cottle, R.W. (1972) 'Monotone solutions of the parametric linear complementarity problem', *Mathematical Programming*, vol. 3, pp. 210-224.

Dantzig, G.B (1947) 'Maximization of a linear function of variables subject to linear inequalities', Published in T.C. Koopmans (1951): *Activity Analysis of Production and Allocation*, New York-London: Wiley & Chapman-Hall, pp. 339–347.

Dirkse, S.P. and Ferris, M.C. (1995) 'The PATH solver: a non-monotone stabilization scheme for mixed complementarity problems', *Optimization Methods and Software*, vol. 5, pp. 123-156.

Donato, O.D. and Maier, G. (1972) 'Mathematical programming methods for the inelastic analysis of reinforced concrete frames allowing for limited rotation capacity', *International Journal for Numerical Methods in Engineering*, vol. 4, pp. 307–29.

Donato, O.D. and Maier, G. (1976) 'Historical deformation analysis of elastoplastic structures as a parametric linear complementarity problem', *Meccanica*, vol. 11, pp. 166-171.

Eriksson, A. (1992) 'On accurate descriptions for primary and secondary paths in equilibrium problems', *Computers and Structures*, vol. 44, pp. 229-242.

Facchinei, F., Jiang, H. and Qi, L. (1999) 'A smoothing method for mathematical programs with equilibrium constraints', *Mathematical Programming*, vol. 85, pp. 107-134.

Ferris, M.C. and Tin-Loi, F. (2001) 'Limit analysis of frictional block assemblies as a mathematical problem with complementarity constraints', *International Journal of Mechanical Sciences*, vol. 43, pp. 209-224.

Fletcher, R. and Leyffer, S. (2002) 'Nonlinear programming without a penalty function', *Mathematical programming*, vol. 9, pp. 239-269.

Fletcher, R., Leyffer, S., Ralph, D. and Scholtes, S. (2001) Local convergence of SQP methods for mathematical programs with equilibrium constraints, Numerical Analysis Report, Department of Mathematics, University of Dundee, Dundee, Scotland.

Franchi, A. (1977) STRUPL-ANALYSIS: structural plasticity by mathematical programming. Fundamentals for a general software, Ph.D. Thesis, University Waterloo.

Franchi, A. and Cohn, M.Z. (1980) 'Computer analysis of elastic-plastic structures', *Computer Methods in Applied Mechanics and Engineering*, vol. 21, pp. 271-294.

Franchi, A. and Genna, F. (1987) 'A numerical scheme for integrating the rate plasticity equations with an "a priori" error control', *Computer Methods in Applied Mechanics and Engineering*, vol. 60, pp. 317-342.

Fukushima, M. and Lin, G.H. (2004) 'Smoothing methods for Mathematical Programs with equilibrium constraints', 12th International Conference on Informatics Research for Development of Knowledge Society Infrastructure, IEEE.

Fukushima, M. and Tseng, P. (2002) ‘An implementable active-set algorithm for computing a B-stationary point of the mathematical program with linear complementarity constraints’, *SIAM Journal on Optimization*, vol. 12, pp. 724-739.

Gendy, A.S. and Saleeb, A.F. (1992) ‘Generalized yield surface representations in the elastoplastic three-dimensional analysis of frames’, *Computers and Structures*, vol. 49, pp. 351-362.

Greenberg, H.J. and Prager, W. (1951) ‘Limit design of beams and frames’, *Proceedings ASCE*, vol. 77 (59), pp. 1-12.

Greenwood, D.T. (2003) Advanced dynamics, Cambridge University Press.

Grierson, D.E. and Aly, A.A. (1980) ‘Plastic design under combined stresses’, *Journal of the Engineering Mechanics Division*, vol. 106, pp. 585-607.

Grüning, M. (1926) Die Tagfähigkeit statisch unbestimmter Tragwerke aus Stahl bei beliebig häufig widerholter Belastung, Julius Springer, Berlin.

Gvozdev, A. A. (1938) ‘Determination of the value of failure load for statically indeterminate systems subject to plastic deformations (in Russian)’, *Conference on Plastic Deformation 1936*, B.G. Galerkin (ed.), Akademia Nauk SSSR, Moscow and Leningrad, pp. 19-38.

Hadjidimos, A., Lapidakis, M. and Tzoumas, M. (2012) ‘On iterative solution for linear complementarity problem with an H+-matrix’, *SIAM Journal on Matrix Analysis and Applications*, vol. 33, no.1, pp. 97-110.

Hiriart-Urruty, J.B. and Lemaréchal, C. (1993) Convex analysis and minimization algorithms, Volume I: Fundamentals, Berlin: Springer-Verlag.

Hodge, P.G. (1977) ‘Automatic piecewise linearization in ideal plasticity’, *Computer Methods in Applied Mechanics and Engineering*, vol. 10, pp. 249–272.

Horne, M.R. (1949) ‘Fundamental propositions in the plastic theory of structures’, Journal of the Institute Civil Engineers (London), vol. 34, pp. 174-177.

Huang, X.X., Yang, X.Q. and Zhu, D.L. (2006) ‘A sequential smooth penalization approach to mathematical programs with complementarity constraints’, *Numerical Functional Analysis and Optimization*, vol. 27, pp. 71-98.

Jiang, H. and Ralph, D. (2000) ‘Smooth SQP methods for mathematical programs with nonlinear complementarity constraints’, *SIAM Journal on Optimization*, vol. 10, pp. 779-808.

Jiràsek, M. and Bažant, Z.P. (2002) Inelastic analysis of structures, Chichester: Wiley.

Kaneko, I. (1979) ‘Piecewise linear elastic-plastic analysis’, *International Journal for Numerical Methods in Engineering*, vol. 14, pp. 757-767.

Kaneko, I. and Maier, G. (1981) ‘Optimum design of plastic structures under displacement constraints’, *Computer Methods in Applied Mechanics and Engineering*, vol. 27, pp. 369-391.

Kantorovich, L.V. (1940) ‘ A new method of solving some classes of extremal problems’, Doklady Akad Sci USSR, vol. 28, pp. 211-214.

Karakostas, S.M. and Mistakidis, E.S. (2000) ‘Evaluation of the ductility features in steel structures with softening moment-rotation behavior based on a nonconvex optimization formulation’, *Engineering Computations*, vol. 17, pp. 573-592.

Karmarkar, N. K. (1984) ‘A New Polynomial Time Algorithm for Linear Programming’, *Combinatorica*, vol. 4, pp. 373–395.

Karush, W. (1939) Minima of Functions of Several Variables with Inequalities as Side Constraints, M.Sc. Dissertation, Dept. of Mathematics, Univ. of Chicago, Chicago, Illinois.

Kazinczy, G. V. (1914). Trials with fixed-end beams (in Hungarian), *Betonszemle*, vol. 2, pp. 68-71, 83–87 and 101–104.

Kist, N.C. (1917) ‘Does a stress analysis based on proportionality of force and deformation lead to a good design of steel bridges and buildings? (in Dutch)’, *De Ingenieur*, vol. 4, pp. 743.

Kist, N.C. (1920) ‘Die Zähligkeit des Materials als Grundlage für die Berechnung von Brücken, Hochbauten und ähnlichen Konstruktionen aus Flußeisen’, *Der Eisenbau*, vol. 11, pp. 425.

Lemke, C.E. (1965) ‘Bimatrix equilibrium points and mathematical programming’, Management Science, vol. 11, pp. 681-689.

Lin, G.H. and Fukushima, M. (2003) ‘New relaxation method for mathematical programs with complementarity constraints’, *Journal of Optimization Theory and Applications*, vol. 118, pp. 81-116.

Lin, G.H. and Fukushima, M. (2003) ‘Some exact penalty results for nonlinear programs and their applications to mathematical programs with equilibrium constraints’, *Journal of Optimization Theory and Applications*, vol. 118, pp. 67-80.

Lin, G.H. and Fukushima, M. (2005) ‘A modified relaxation scheme for mathematical programs with complementarity constraints’, *Annals of Operations Research*, vol. 133, pp. 63-84.

Liu, G.S. and Zhang, J.Z. (2002) ‘A new branch and bound algorithm for solving quadratic programs with linear complementarity constraints’, *Journal of Computational and Applied Mathematics*, vol. 146, pp. 77-87.

Liu, X. and Sun, J. (2004) ‘Generalized stationary points and an interior point method for mathematical programs with equilibrium constraints’, *Mathematical Programming*, vol. 101, pp. 231–261.

Lubliner, J. (2006) Plasticity theory, Revised Edition (PDF), University of California at Berkeley.

Luenberger, D. and Ye, Y. (2008) Linear and nonlinear programming, 3rd ed., New York: Springer Science+Business Media.

Luo, Z.Q., Pang, J.S. and Ralph, D. (1996) Mathematical programs with equilibrium constraint, Cambridge University Press.

Mahini, M.R., Moharrami, H. and Cocchetti G. (2013) 'A dissipated energy maximization approach to elastic-perfectly plastic analysis of planar frames', *Archives of Mechanics*, vol. 65, pp. 171-194.

Mahini, M.R., Moharrami, H. and Cocchetti, G. (2014) 'Elastoplastic analysis of frames composed of softening materials by restricted basis linear programming', *Computers and Structures*, vol. 131, pp. 98-108.

Maier, G. (1967) 'On elastic-plastic structures with associated stress-strain relations allowing for work softening', *Meccanica*, vol. 2, pp. 55-64.

Maier, G. (1968) 'A quadratic programming approach for certain classes of nonlinear structural problems', *Meccanica*, vol. 3, pp. 121-130.

Maier, G. (1970) 'A matrix structural theory of piecewise linear elastoplasticity with interacting yield planes', *Meccanica*, vol. 5, pp. 54-66.

Maier, G., Giacomini, S. and Paterlini, F. (1979) 'Combined elastoplastic and limit analysis via Restricted basis Linear Programming', *Computer Methods in Applied Mechanics and Engineering*, vol. 19, pp. 21-48.

Maier, G., Grierson, D.E. and Best, M.J. (1977) 'Mathematical programming methods for deformation analysis at plastic collapse', *Computers and Structures*, vol. 7, pp. 599-612.

Maier, G., Zavelani, A. and Dotreppe, J.C. (1973) 'Equilibrium branching due to flexural softening', *Journal of the Engineering Mechanics Division*, vol. 99, pp. 897-901.

Maier, G., Zavelani-Rossi, A. and Benedetti, D. (1972) 'A finite element approach to optimal design of plastic structures in plane stress', *International Journal for Numerical Methods in Engineering*, vol. 4, pp. 455-473.

Maier, G. (1984) 'Mathematical programming applications to structural mechanics: some introductory thoughts', *Engineering Structures*, vol. 6, pp. 2-5.

Manola, M.M.S. and Koumousis, V.K. (2014) 'Limit analysis of plane frames with piecewise linear hardening/softening behavior and axial-shear force-bending moment interaction', *Engineering Structures*, vol. 72, pp. 41-55.

Manola, M.M.S. and Koumousis, V.K. (2014) 'Ultimate state of plane frame structures with piecewise linear yield conditions and multi-linear behavior: A reduced complementarity approach', *Computer and Structures*, vol. 130, pp. 22-33.

Manola, M.M.S. and Koumousis, V.K. (2015) '*Limit analysis of structures: A convex hull formulation', Computers and Structures*, vol. 151, pp. 115-129.

Martin, C.M. and Makrodimopoulos, A. (2008) 'Finite-element limit analysis of Mohr-Coulomb materials in 3D using semidefinite programming', *Journal of Engineering Mechanics* (ASCE), vol. 134, pp. 339-347.

Massonet, C.E. and Save, M.A. (1965) Plastic analysis and design, New York: Blaisdell Pub. Co.

Mistakidis, E.S. and Stavroulakis, G.E. (1998) Nonconvex optimization in mechanics. Kluwer Academic Publishers.

Neal, B.G. (1977) The plastic methods of structural analysis, 3rd ed., New York:Wiley.

Nocedal, J. and Wright S. (1999) Numerical optimization, New York: Springer.

Oñate E. (2013) Structural Analysis with the Finite Element Method. Linear Statics. Volume 2. Beams, Plates and Shells, 1st ed., Barcelona: CIMNE.

Polizzotto C. (1975) 'Optimum plastic design of structures under combined stresses', *International Journal of Solids and Structures*, vol. 11, pp. 539-553.

Rao S. (2009) Engineering Optimization: theory and practice. 4th ed., New Jersey: John Wiley & Sons.

Shen, W.Q. (1995) 'Limit analyses of plane frames with a penalty linear programming method', *Computer and Structures*, vol. 56, pp. 287-295.

Simo, J.C., Hjelmstad, K.D. and Taylor, R.L. (1984) 'Numerical formulations of elasto-viscoplastic response of beams accounting for the effect of shear', *Computer Methods in Applied Mechanics and Engineering*, vol. 42, pp. 301-330.

Skordeli, M.A.A. and Bisbos, C.D. (2010) 'Limit and shakedown analysis of 3D steel frames via approximate ellipsoidal yield surfaces', *Engineering Structures*, vol. 32, pp. 1556-1567.

Spillers, W.R. and MacBain, K.M. (2009) Structural Optimization, New York: Springer Science+Business Media.

Tangaramvong, S. and Tin-Loi, F. (2007) 'A complementarity approach for elastoplastic analysis of strain softening frames under combined bending and axial force', *Engineering Structures*, vol. 29, pp. 742–53.

Tangaramvong, S. and Tin-Loi, F. (2008) 'Simultaneous ultimate load and deformation analysis of strain softening frames under combined stresses', *Engineering Structures*, vol. 30, pp. 664–674.

Tangaramvong, S. and Tin-Loi, F. (2010) 'A constrained non-linear system approach for the solution of an extended limit analysis problem', *International Journal for Numerical Methods in Engineering*, vol. 82, pp. 995-1021.

Tangaramvong, S. and Tin-Loi, F. (2010) 'The influence of geometric effects on the behavior of strain softening frames', *Computational Mechanics*, vol. 46, pp. 661-678.

Tangaramvong, S. and Tin-Loi, F. (2011) 'Collapse load evaluation of structures with frictional contact supports under combined stresses', *Computers and Structures*, vol. 89, pp. 1050-1058.

Tangaramvong, S. and Tin-Loi, F. (2011) 'Mathematical programming approaches for the safety assessment of semirigid elastoplastic frames', *International Journal of Solids and Structures*, vol. 48, pp. 1011-1023.

Tangaramvong, S. and Tin-Loi, F. (2012) 'An FE-MPEC approach for limit load evaluation in the presence of contact and displacement constraints', *International Journal of Solids and Structures*, vol. 49, pp. 1753-1763.

Tangaramvong, S., Tin-Loi, F. and Senjuntichai, T. (2011) 'An MPEC approach for the critical post-collapse behavior of rigid-plastic structures', *International Journal of Solids and Structures*, vol. 48, pp. 2732-2742.

Tin-Loi F. (1990) 'A yield surface linearization procedure in limit analysis', *Mechanics of Structures and Machines*, vol. 18, pp. 135-149.

Tin-Loi, F. (1990) 'On the optimal plastic synthesis of frames', *Engineering Optimization Journal*, vol. 16, pp. 91-108.

Tin-Loi, F. (1992) 'Optimal design of arches', *Computers and Structures*, vol. 43, pp. 675-679.

Tin-Loi, F. (1995) 'Plastic limit analysis of plane frames and grids using GAMS', *Computers and Structures*, vol. 54, pp. 15-25.

Tin-Loi, F. and Pang, J.S. (1993) 'Elastoplastic analysis of structures with nonlinear hardening: A nonlinear complementarity approach', *Computer Methods in Applied Mechanics and Engineering*, vol. 107, pp. 299–312.

Tin-Loi, F. and Tseng, P. (2003) 'Efficient computation of multiple solution in quasibrittle fracture analysis', *Computer Methods in Applied Mechanics and Engineering*, vol. 192, pp. 1377-1388.

Tin-Loi, F. and Xia, S.H. (2001) 'Holonomic softening: Models and analysis', *Mechanics of structures and machines*, vol. 29, pp. 65-84.

Wakefield, R. R. and Tin-Loi, F. (1990) 'Mathematical programming and uniqueness in nonholonomic plasticity', *Computers and Structures*, vol. 34, pp. 477-483.

Wong, M.B. (2009) Plastic analysis and design of steel structures, 1st ed., U.S.A.: Elsevier.

Wong, M.B. and Tin-Loi, F. (1987) 'Yield surface linearization in elastoplastic analysis', *Computers and Structures*, vol. 26, no. 6, pp. 951-956.

Yu, H. and Pu, D. (2011) ‘Smoothing Levenberg-Marquardt method for general nonlinear complementarity problems under local error bound’, *Applied Mathematical Modeling*, vol. 35, pp. 1337-1348.

Zavelani, A. (1973) ‘A compact linear programming procedure for optimal design in plane stress’, *Journal of Structural Mechanics*, vol. 2, no. 4, pp. 301-324.

Zavelani-Rossi, A. (1974) ‘Finite element techniques in plane limit problems’, *Meccanica*, vol. 9, no. 4, pp. 312-324.

*To **YOU**...for giving me the freedom to cry, the stimulation to fly and thousands of reasons to love...*